Biospectroscopy diagnosis of bacterial interaction with environmental molecules

An alternative format thesis submitted for the degree of Doctor of Philosophy in the Faculty of Science and Technology

Lancaster University

July 2018

Hanbing Li BSc

Lancaster Environment Centre

Declaration

I declare that this thesis is my work and has not been submitted for the award of a higher degree or qualification at this university or elsewhere.

Abstract

Aims: Bacteria are universal micro-organisms that can be found in almost all aquatic and terrestrial environments and strongly affect ecological systems at different spatial scales. The activities of bacteria are profound on the physicochemical features of natural environments, while natural environments shape bacterial behaviours through physical and chemical alterations. Different molecules present in the environment produce significant effects on bacteria. Therefore, it is required to study the rich and complementary interactions between bacteria and molecules. In this thesis, four research studies were conducted to investigate the interactions between bacteria and nanoparticles or carbonaceous substrates, deploying state-of-the-art techniques which can yield new insights.

Methods: Raman micro-spectroscopy was employed in this thesis as a diagnostic tool to detect the biochemical alterations of bacteria post-exposure to different chemical molecules. Unlike conventional methods, such as light/electron microscopy, molecular analysis techniques and bacterial behaviour assays, Raman spectroscopy provides detailed information of biological constituents of bacteria that interact with diverse molecules. In addition, computational analysis including principal component analysis and linear discriminant analysis (PCA and LDA) was used to process the Raman spectral data.

Results and Discussion: Raman spectra characterize the interaction between bacteria with different molecules. Spectral characterization showed the specific binding of nanoparticles with nucleic acids and amino acids in bacteria, and the different chemotactic behaviours of bacteria towards carbohydrates, organic acids and alkanes. Distinct spectral alterations allowed the evaluation of the alkane affinity in bacteria, and enabled quantification of the concentrations of glucose or organic acids in the

aquatic phase. Furthermore, computational analysis of spectral alterations illustrated the effects of nutrient cations on alkane affinity in bacteria, and indicated the selective affinity of bacteria towards different organic carbonaceous molecules in the mixture of carbonaceous substances. Findings from this thesis showed that Raman spectroscopy is a rapid, reliable and non-destructive approach to investigate the interaction of bacterial cells with diverse molecules, which implies techniques involved in Raman spectroscopy can diagnose subcellular changes both *in situ* and *in vivo* post-exposure to different natural conditions or chemical molecules.

Acknowledgements

I am extremely grateful to my supervisors Dayi Zhang and Frank Martin. During the whole course, Dayi not only gave me academic guides, but also offered me lots of valuable suggestions on many parts. Also, I need to give my special thanks to Frank, who helps me to finish my research experiments and offered me lots of help during my study.

I would like to give thanks to my friends and colleagues in Lancaster: Muren Zhang, Yanying Li, Jinyu Yang, Ying Zhu, Naifu Jin, Mary Paraskevaidi, and Shuang Wu. Additionally, I also need to deserve my thanks to the friends or collaborators in my department: Dr. Debra Hurst, Prof. Kevin Jones and Prof. Hao Zhang, for their great help during my research there.

Finally, I would like to give my deep and special thanks to my father, Prof. Guojun Li, and my mother, Dr. Qiuyan Chen, who funded my study and always stand a strong support for me. As well, great thanks to China Scholarship Council (CSC) which supports me during my PhD study.

List of Abbreviations

AgNPs: Silver Nanoparticles

Ag@MNPs: Silver Coated Magnetic Nanoparticles

ATP: Adenosine Triphosphate

BOD: Biochemical Oxygen Demand

CCD: Charged Couple Detector

CFU: Colony Forming Unit

CH_4: Methane

CO_2: Carbon Dioxide

D_I: Dispersion Indicator

DMSO: Dimethylsulfoxide

DNA: Deoxyribose Nucleic Acid

dNTPs: deoxynucleotide Triphosphate

FISH: Fluorescence in situ Hybridization

GC-FID: Gas Chromatography Flame Ionization Detector

GC-MS: Gas Chromatography Mass Spectrometry

HAP: Histidine-Aspartate Phosphrelay

H_2: Hydrogen Gas

IR: Infrared

LDA: Linear Discriminant Analysis

LSD: Least Significant Difference

MAHs: Monocyclic Aromatic Hydrocarbons

MCPs: Methyl-accepting Chemotaxis Proteins

MM: Minimal Medium

MNPs: Magnetic Nanoparticles

NADP: Nicotinamide Adenine Dinucleotide Phosphate

PAHs: Polycyclic Aromatic Hydrocarbons

PCA: Principal Component Analysis

PCR: Polymerase Chain Reaction

qPCR: quantitative Polymerase Chain Reaction

R6G: Rhodamine 6G

RNA: Ribose Nucleic Acid

rRNA: ribosomal Ribose Nucleic Acid

RRS: Resonant Raman Scattering

SEM: Scanning Electron Microscope

SERS: Surface-Enhanced Raman Scattering

SIP: Stable-Isotope Probing

SPME: Solid-Phase Microextraction

TCA: Tricarboxylic Acid

TEM: Transmission Electron Microscope

VSM: Vibrating Sample Magnetometer

XRD: X-ray Diffraction

List of Figures

Table of contents

General Introduction

1. Introduction

Bacteria are significant and necessary members of ecological systems and biogeochemical cycles. They are present in almost all aquatic and terrestrial environments and link with all plant and animal species. Together with fungi and protozoan, bacteria are categorized in the group of micro-organisms (Martiny et al., 2006). Although the microbial world is no longer so mysterious for the general public, the subject of microbiology (the study of microorganisms) was not developed until the late nineteenth and early twentieth centuries (Nester et al., 1978). Micro-organisms are typically between 1 and 100 μm in diameter, with bacterial sizes at the smaller end of this distribution. Bacteria occur in various shapes including spheres, rods and spirals (Young, 2003; Young, 2006). Due to the development of the polymerase chain reaction (PCR) technique, about 5000 bacterial species have been named (Staley, 2006; Martiny et al., 2006). However, the low recovery efficiencies of typical cultivation procedures mean that ~99% of bacterial species have not been properly investigated and characterised in environments (Staley and Konopka, 1985). Bacteria strongly affect and are affected by processing their pathogenic or symbiotic functions at different spatial scales. At the microbial scale, bacterial or fungal cells decompose non-living organic matter, making nutrients available for other organisms. The low concentrations of limiting substrates can result in competitions among bacterial species or among other microbes (Veldkamp et al., 1984). At the ecosystem scale, bacteria have specific interactions with plants or animals. Pathogenic bacteria generate adverse effects upon macro-organisms (Büttner and Bonas, 2003), while several bacterial species such as *Rhizobium* and *Frankia* form positive associations

with nodules on plant roots to fix nitrogen (N_2) into ammonium (NH_4^+) (Long, 1989; Chaia et al., 2010).

Bacteria physically operate as catalysts of biogeochemical cycles in which they mediate thermodynamically favourable reactions. Autotrophic bacterial species synthesise organic matter from inorganic and trace elements (Hankinson and Schmidt, 1984; Berman-Frank et al., 2003), and heterotrophic bacteria are responsible for catabolism of organic substrates to mineral forms for regeneration (Aksnes and Brekken, 1988; Berner, 1968). The effects of bacterial activities are profound on the physical and chemical features of ecosystems. On the contrary, ecosystem environments determine bacterial behaviour by physical and chemical alterations. Physical conditions including temperature, light and osmotic pressure impact bacterial diversities and function (Rosso et al., 1995; Csonka, 1989). Furthermore, a broad range of chemicals are present in micro-environments to interact with bacteria. Some of the chemicals are required nutrient resources, but others can be toxic compounds or chemical signals from other cells. To detect chemical cues of surrounding molecules, bacteria have developed chemotactic systems to follow concentration gradients and control their movement towards or away from stimulants (Kim et al., 2001; Sourjik and Berg, 2002). Bacteria uptake nutrient molecules around their surfaces, and transport molecules into the cell by membrane-bound permeases (Saurin et al., 1994). The rich and complementary interactions between bacteria and molecules produce significant effects on ecosystems and biogeochemical cycles, which need much further study.

Conventional technologies applied to study interactions of bacteria with molecules are often associated with the detection of bacteria or indirect genetic analysis. One of the simplest approaches to observe bacteria is the microscope, e.g. optical microscope and

electron microscope. The optical microscope is the popularized microscope that uses visible light and objective lenses to magnify images of bacterial cells (Murphy, 2002). This method is easy to operate, but the low resolution limits its application in the detection of detailed behaviours of bacteria (Courjon and Bulabois, 1979). As an alternative microscopic method, the electron microscope employs a beam of accelerated electrons as a source of illumination. Due to the shorter wavelength of electrons than that of visible light photons, the electron microscope possesses higher resolution than the optical microscope (Danilatos, 1990). However, samples must be hydrated and have to be viewed in high-vacuum mode, which affects the movement of bacteria, and causes inaccurate estimation of bacterial responses towards molecules (Bergmans et al., 2005). Polymerase chain reaction (PCR) techniques are molecular analysis tools used in exhibiting genetic expressions of bacteria under different environmental conditions. PCR is based on the isolation, amplification and quantification of a genome sequence containing a wealth of metabolic information (Mullis et al., 1986). Despite expensive consumables for sample preparation, this method only acquires indirect results from bacteria after a series of treatments. To understand in situ interactions between bacteria and molecules, there remain many requirements for the technique to simultaneously provide detailed bacterial behaviour and molecular information.

Raman spectroscopy is a powerful technique widely applied in biological research, offering information about the structure, functional groups, and environmental molecules presenting in biological samples (Feng et al., 2015; Nanda et al., 2016; Efrima and Zeiri, 2009). This spectroscopic technique is dependent on the Raman scattering process to measure the interaction when photons from a monochromatic light source (i.e., laser) encounters various chemical bonds in biomolecules. The

energy that photons gain from or lose to molecules consequently results in frequency shifts which are related to vibrational marks of specific molecules (Landsberg and Mandelstam, 1928). This enables Raman spectroscopy to analyze kinetic responses from bacterial cells towards different molecules. The enhanced improvements of Raman scattering with the use of metallic nanoparticles has lead to surface-enhanced Raman scattering (SERS) (Campion and Kambhampati, 1998). This is a rapid and highly sensitive tool to detect biological components in bacterial cells and provide chemical structure information of environmental molecules.

In this thesis, Raman microspectroscopy has been employed to establish a novel assay for the interaction of bacteria with diverse molecules. Research studies have been conducted to investigate the interaction between bacterial cells and nanoparticles or organic carbonaceous molecules. The specific main objectives were:

- To assess the capture efficiency of silver coated magnetic nanoparticles (Ag@MNPs) on two bacterial strains (*Acinetobacter baylyi* and *Escherichia coli*), and to evaluate the SERS enhancement of Ag@MNPs on Raman effects chemical (rhodamine 6G) and two aquatic pathogens (Chapter 2).
- To investigate and quantify the chemotaxis-related affinity and accumulation of *Acinetobacter baylyi* towards alkanes (dodecane and tetradecane), monocyclic aromatic hydrocarbons (toluene and xylene), polycyclic aromatic hydrocarbons (phenanthrene and naphthalene) and alkane mixtures (crude oil and mineral oil), and to study the effects of alkanes and alkane mixtures on *Pseudomonas* fluorescence (Chapter 3).
- To determine the impacts of nutrient cations (sodium, potassium, magnesium and calcium) on chemotactic behaviours of *Acinetobacter baylyi* towards pure alkanes

with carbon lengths of C10, C12, C14, C16, C19, C22 and C24, and alkane mixture (mineral oil) (Chapter 4).

- To identify chemotaxis-driven affinity and accumulation and competitive selection of four pure or mixed organic carbonaceous substances (glucose, succinate, acetate and salicylate) by three bacterial strains (*Acinetobacter baylyi*, *Pseudomonas fluorescence* and *Escherichia coli*) (Chapter 5).

2. The roles of bacteria in the environment

The term *bacteria* is the plural of *bacterium* which is originally from the Greek *bakterion*, meaning "staff and cane", because the first discovered bacteria were rod-shaped (White et al., 2007). Unlike eukaryotic cells, bacterial cells do not have a nucleus and possess membrane covered organelles. Traditionally, scientists believed that the word *bacteria* include all prokaryotes (Woese et al., 1990). Until 1990s, a report found that prokaryotes comprise two significantly different domains of organisms which are called *Bacteria* and *Archaea* (Woese et al., 1990). Therefore, current scientific classification of life consists of three domains: *Eukaryotes*, *Archaea* and *Bacteria*. Modern bacteria are believed to have evolved from unicellular microorganisms about 4 billion years ago. The first person who observed bacteria is Antonie van Leeuwenhoek in 1676, using a single-lens microscope of his own design (Gest, 2004). Because of technical limitations, bacteria were not classified until 1870 by Ferdinand Cohn who is said to be the founder of bacteriology (O'Malley, 2009). From the year of 1977, a major step was made to the study of bacteria, owing to the development of 16S ribosomal RNA sequencing (Staley and Konopka, 1985). Afterwards, a great number of studies related to the subject of bacteria have been published. As a consequence, diversities and functions of bacteria in ecosystems and their influence on biogeochemical cycles open up a new way for us to understand

deep secrets of life and broaden our eyes into microbial worlds of natural environments.

2.1 Bacteria in diverse ecosystems

Bacteria catalyze reactions involved in micro- and/or macro-environments, contributing to the dynamic equilibrium of biosphere. Several characteristics of bacteria distinguish them as significant units in natural environments. The small size of bacteria - ranging from 0.5 to 5 micrometres in length - results in wide distributions and extensive populations at different spatial scales (Nester et al., 1978). Large bacterial populations are also attributed to fast rates of growth and metabolism. The usual generation time of bacteria is 1-2 days in natural environments (Stotzky and Babich, 1986), and the time can be reduced to hours in laboratory conditions (Stotzky and Babich, 1986). The growth of individual bacterial cells is autocatalytic and they divide to form two cells for further growth. Hence, under favorable environmental conditions, the growth of bacteria exponentially increases to produce explosive number of cells over short periods of time. Because of their fast growth rate and small size, bacteria can travel for long distances through air or water and via animal transport (i.e. fecal transmission) (Tannock et al., 1990; Bovallius et al., 1978; Bovallius et al., 1980). One of the most important bacterial features is genetic flexibility. Different from some species of plants and animals, bacteria lack sexual recombination mechanisms to transfer genomes vertically. Nevertheless, bacteria are able to mediate vectorial gene transfer from donors to recipients, which is not limited within a species and may occur across phylogenetic boundaries (Thomas and Nielsen, 2005). The flexible gene transfer mechanism assists bacteria to evolve over a period of decades rather than millennia. In addition, evolution has occurred in several bacterial species when the environment condition is extreme.

Though bacteria are too small to be seen with naked eyes, they form biomass which is larger than that of all plants and animals (Lynch and Whipps, 1990; Michael et al., 2002). It is estimated that there are approximately 5×10^{30} bacterial cells on Earth (Michael et al., 2002). The concentration of bacterial cells in soil is 40 million per gram, and in fresh water is 1 million per milliliter (Vieira and Nahas, 2005; Csuros, 1999). The total amount of organic carbon conserved in Bacteria and Archaea is around $350 - 550 \times 10^8$ tonnes, equal to that in land plants (Schmidt and Schaechter, 2012). Population densities of bacteria in near-surface aquatic or soil environments are 1 or 2 orders of magnitude higher than in deep subsurface, but the major reservoir of bacterial life is harbored in the subsurface area (Fredrickson et al., 1989; Schmidt and Schaechter, 2012). Some bacterial species are adapted to grow in environments with extreme physical and/or chemical conditions that are too abnormal for plants and animals to live with. In the case of acid environments, sulfur-oxidizing bacterium *Acidithiobacillus* was the first acidophile to be isolated and characterized (Rawlings, 2005). This bacterium fixes carbon dioxide by oxidizing ferrous iron or reduced sulfur to synthesize organic matter (Rawlings, 2005). Bacteria found in high temperature environments are classified as thermophiles or hyperthermophiles. Photosynthetic cyanobacteria such as *Chloroflexus* and *Chromatium*, and spore-forming thermophiles including *Bacillus*, *Clostridium* and *Moorella* are found in geothermal environments (Gupta et al., 1999; Madigan, 2003; Matsumura and Aiba, 1985; Hyun et al., 1983; Drake and Daniel, 2004). In addition, bacteria exert strong effects on plants or animals via parasitism, mutualism or commensalism. The number of bacterial cells in human microbiota is about 39 trillion (Schmidt and Schaechter, 2012). The largest proportion is in gut flora, and the second largest is on the skin (Turnbaugh et al.,

2007). However, these microorganisms only account for less than 10^{-5} of microbial biomass on Earth (Turnbaugh et al., 2007).

Bacteria mediate diverse reactions to produce effects on the biosphere. The biosphere is a series of interlinked systems at different spatial scales as different habitats for bacteria. The diversities and numbers of different bacteria present in habitats are a signal of the abundance and amount of available nutrient resources. A majority of bacterial cells are in terrestrial soils where thousands of bacterial genomes per gram are found (Torsvik et al., 1990). However, bacteria only occupy less than 0.01% of the soil volume. In soil habitats, the convergence of water, nutrient and bacterial cells on a particle can cause a burst of bacterial events. Some terrestrial soil habitats that possess sufficient required resources for bacteria are responsible for the great bulk of primary production and available nutrient ions. The extracellular hydrolases of bacteria hydrolyze macromolecules to monomers which are for subsequent intracellular metabolism (Sánchez‐Porro et al., 2003). These bacterial metabolisms involve the oxidation of organic matter back to CO_2 and the transformation of organic nitrogen, sulfur and phosphorus (Lehmann et al., 2006; Eswaran et al., 1993; Robertson and Groffman, 2007; Stewart and Tiessen, 1987; Kopáček et al., 2013). When soil becomes the underlying matrix of aquatic environments, sedimentary environments are formed. Sediments are physically stabilized systems where mixing or convection is minimal and the niche is dominated by diffusion (Olsen et al., 1982; Mortimer, 1971). Biochemical consequences of bacterial metabolism in sediment habitats have to do with the solubility of key nutrients. Oxygen and organic matter are two key nutrients that are responsible for bacterial diversities in sediments. Bacterial activities in shallow water sediments are drastically different from those in deep water because of the availability of oxygen. Oxygen from photosynthesis in cyanobacteria

in overlying water leads to the internal production of organic carbon matter in shallow water sediments (Bernhard, 1989). On the contrary, photosynthate from surface water is nearly the only source of organic carbon for bacteria in deep water sediments (Revsbech et al., 1980). Therefore, biochemical processes can differ significantly from daytime to nighttime in shallow water sediments, which is rarely seen in deep water sediments.

Other major habitats of bacteria are water environments including oceans, lakes, ponds and streams. Apart from oceans, lakes, ponds, rivers and streams are typical freshwater environments which support large numbers of bacterial species and communities. Different characteristics such as temperature, nutrient composition, water potential and physical structure combine together to influence the types and numbers of bacteria in freshwater habitats (Covich et al., 2004). Phototrophic bacteria like cyanobacteria are predominant in oxic areas of most freshwater environments (Zurawell et al., 2005). They use energy from light to produce primary nutrient sources including oxygen and organic matter (Berman-Frank et al., 2003). Oxygen only occurs in the surface layer of a water environment, where the light is available. Unconsumed organic matter in surface layers sinks to the depths for subsequent decomposition by facultative bacteria species with dissolved oxygen, which results in the depletion of oxygen in the environment (Hobbie and Crawford, 1969). To measure the amount of oxygen-consuming organic material, biochemical oxygen demand (BOD) is determined. The determination of BOD is firstly taking a water sample, aerating it well, placing it in a sealed container, standing for usually 5 days at 20 ℃, and finally determining the residual oxygen in the water sample (Pasco et al., 2000). In ocean environments, salinity, average temperature and nutrient status make them different from freshwater environments for bacteria. Many bacteria in the top 300

meters (photic zone) in oceans are found to possess the visual pigment rhodopsin to transfer energy from light photons to cells (Cole et al., 1988; Béja et al., 2000). The number of bacteria decreases with depth. In the area between the photic zone and a depth of 1000 meter, chemoorganotrophic bacteria are responsible for considerable biochemical activities (Bruun, 1957). Below 1000 m, bacterial metabolism is relatively inactive due to environmental extremes (e.g. low temperature, high pressure and low nutrient levels).

2.2 Bacterial contributions for biogeochemical cycles

Bacterial activities influence not only the specific habitats, but also the global environments through biogeochemical cycles of nutrient elements including carbon, nitrogen, phosphorus, sulfur and other metal ions.

2.2.1 Carbon cycle

Carbon sources are primary and required nutrients for bacteria to survive in natural environments. Bacteria adopt different strategies to optimize their use of available carbon sources. Global carbon cycling involves CO_2 fixation, organic matter decomposition and oxidation (Figure 1). Major ways for the fixation of CO_2 and synthesis of new organic carbon are via photosynthesis and chemosynthesis (Vishniac and Trudinger, 1962; Stanier et al., 1959). Large amounts of organic carbon come from photosynthesis. As plants are dominant phototrophic organisms of terrestrial environments, phototrophic bacteria are therefore the basis for photosynthesis of aquatic environments. Phototrophic bacteria convert light energy into chemical energy by absorbing light photons into green chlorophyll pigments of specific proteins that are embedded in the plasma membrane (Das et al., 2011). Some energy from the light is used to strip electrons from suitable substances like water, which results in the

generation of oxygen gas (Borland et al., 1987). Hydrogen from the splitting water is carried into the creation of short-term energy compounds which are nicotinamide adenine dinucleotide phosphate ($NADP^+$) and adenosine triphosphate (ATP) (Bryant and Frigaard, 2006). ATP and NADPH is then used for further reduction of atmospheric CO_2 to long-term energy storage in the form of polysaccharides inside the cells of phototrophic bacteria (Bryant and Frigaard, 2006). Phototrophic bacteria also perform respiration in both daytime and nighttime. If the rate of photosynthesis exceeds the rate of respiration, organic carbon in phototrophic bacteria will become the starting material for other organisms and become the net balance for the whole carbon cycle.

To release the carbon trapped in organic matter, bacteria decompose polysaccharide from phototrophs. Decomposed organic carbon has two major oxidative states, methane (CH_4) and carbon dioxide. Bacterial respiration is one of the key ways to release energy from organic carbon to support essential activities. This process converts biochemical energy into ATP and produces CO_2 as waste products for some bacteria (Haddock and Jones, 1977; Richardson, 2000). The benefit of respiration is maximizing use of organic carbon. Glycolysis is the first step of bacterial respiration to break down organic matter to collect energy in cytoplasm (Haddock and Jones, 1977). The final product of glycolysis is pyruvate that can be broken down further to initiate two different processes, depending on the availability of oxygen. In aerobic bacterial cells, pyruvate is oxidized by oxygen in the citric acid cycle to generate ATP and CO_2 (Haddock and Jones, 1977). Without oxygen, pyruvate undergoes fermentation to generate some energy and waste products like alcohol, acetic acid or lactic acid that have to be removed from bacterial cells (Liu, 2003). Bacteria in some anoxic habitats carry out anaerobic respiration in which neither oxygen nor pyruvate

is the final electron acceptor (Coates et al., 2002). This bacterial activity is typically found in 'extreme' places, e.g. hydrothermal vents at oceanic bottom (Jannasch and Mottl, 1985). In some anoxic habitats, syntrophic bacteria and methanogens cooperate together to produce methane, which is of great importance to carbon flow in the whole global carbon cycle (Zeikus, 1977). Organic compounds are converted to CH_4 and CO_2 by the ecological interactions of several bacteria or archaea species (Hanson and Hanson, 1996).

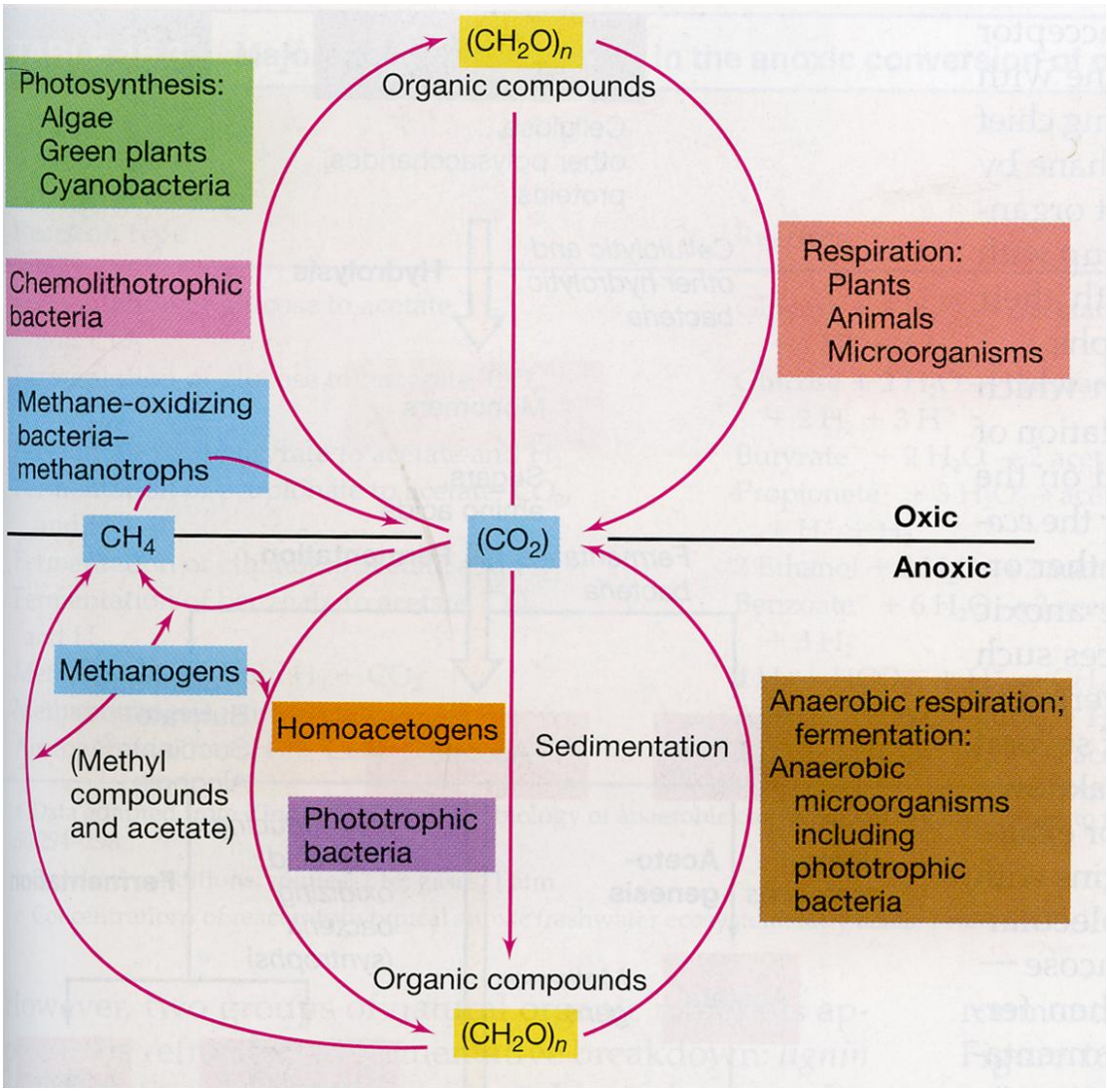

Figure 1. Biogeochemical cycle of carbon (From Michael et al., 2002).

2.2.2 Nitrogen cycle

The element nitrogen is essential for life and is a key constituent of proteins and nucleic acids (Munro and Fleck, 1969). Bacteria play a predominant role in diverse processes for the biological nitrogen cycle. Major processes involve nitrogen fixation, nitrification, denitrification and ammonification (Figure 2). Nitrogen fixation is significant in ecological systems because it provides a major source of available nitrogen for organisms (Burns and Hardy, 2012). Nitrogen gas is the most stable form of nitrogen that requires large amounts of energy for subsequent redox reactions. Nitrogenase is the enzyme used by some bacteria to catalyze the formation of ammonium (NH_4^+) and hydrogen gas (H_2) by reduction of nitrogen and proton (Burns and Hardy, 2012). The fixed nitrogen in the form of ammonium is essential to incorporate in nitrification. The whole nitrification process can be construed as the aerobic oxidation of ammonium. This process involves two classical steps. The first step is the oxidation of ammonium to nitrite via hydroxylamine by ammonia-oxidizing bacteria (Caffrey et al., 2007). The second step is carried out in nitrite oxidizing bacteria that convert nitrite to nitrate (Pollice et al., 2002). In the nitrogen cycle, nitrification is the process of nitrate production, and denitrification is the process of nitrate consumption. Gaseous nitrogen is biologically formed in this process. A series of reactions including respiration of nitrate, nitrite, nitric oxide and nitrous oxide catalyzed by corresponding reductase occur in denitrifying bacteria (Betlach and Tiedje, 1981). Because denitrification is usually oxygen-independent, its rate increases in anaerobic environments (Betlach and Tiedje, 1981). Contributions of bacteria to the biological nitrogen cycle balance the production and consumption of fixed nitrogen in environments.

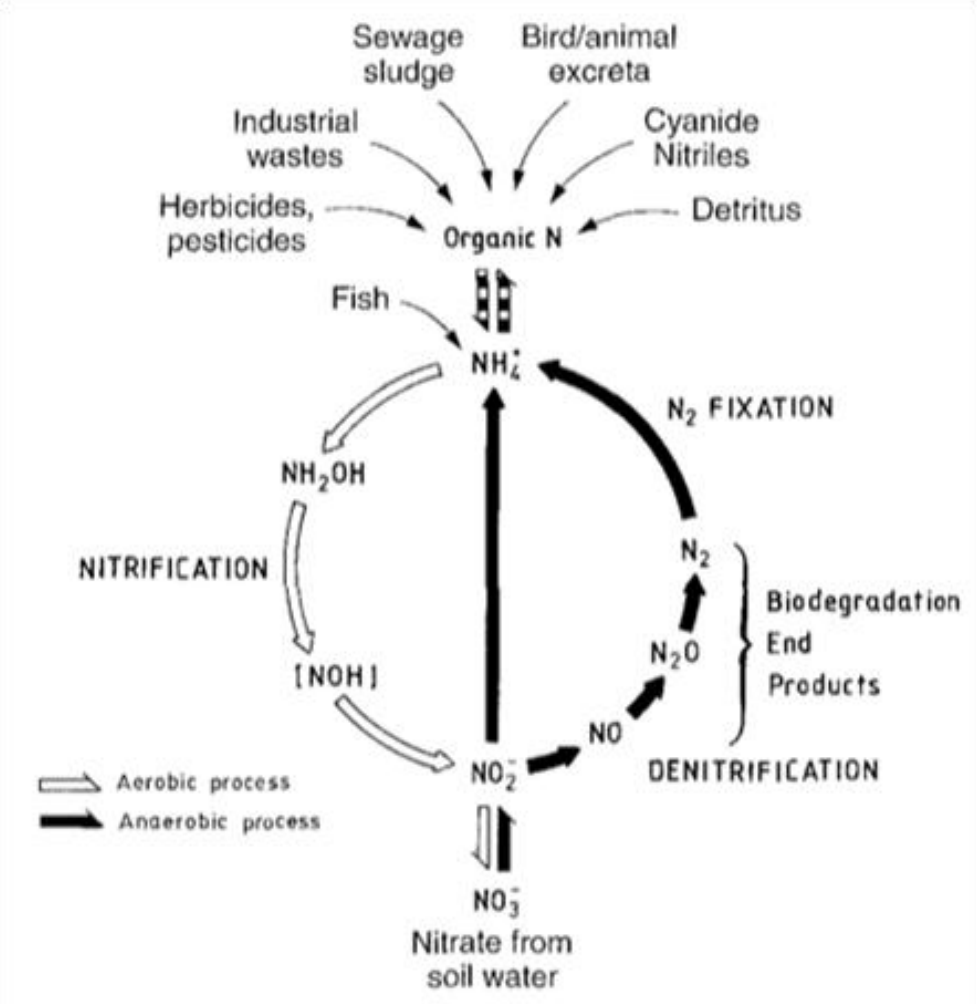

Figure 2. Biogeochemical cycle of nitrogen (From Nester et al., 1978)

2.2.3 Phosphorus cycle

Phosphorus is important for living organisms. Bacteria have a critical role in the global phosphorus cycle to forge a link between living and nonliving entities of phosphorus (Vadstein, 2000). The weathering, mineralization and solubilization process of non-available phosphorus is catalyzed by bacteria to produce available phosphorus for other organisms (Figure 3) (Vadstein, 2000). On the contrary, bacteria can immobilize phosphorus to diminish soluble and reactive phosphorus (Griffiths, 1986). Bacteria mediate the transformation of phosphorus by two weathering processes, mechanical weathering and chemical weathering. Bacteria contribute to the change in microenvironments at the surface of phosphorus containing materials by mechanical weathering, e.g. increasing the local humidity or forming biofilms on surfaces (Chen et al., 2000). The major bacterial weathering is classified as chemical processes such as hydrolysis, dissolution, hydration and redox reactions (Uroz et al., 2011). Chemical weathering processes alter the composition of the parent phosphorus material directly or indirectly. Bacteria perform phosphorus solubilization to provide available phosphorus for growth. The primary mechanism for phosphorus solubilization is acids production (Kucey, 1983). Chemoautotrophic bacteria generate biogenic acid to interact with phosphorus minerals for the formation of soluble phosphate (Kucey, 1983). Soluble phosphate is subsequently associated with the reduction of iron oxyhydroxides in ferric phosphate to generate bioavailable orthophosphate by sulfur-reducing bacteria (Alexander, 1961). Bacterial mineralization involves conversion of organic phosphorus into inorganic phosphate by a suite of cellular enzymes such as phytases and phosphatase (Alexander, 1961). The immobilization process involves the removal of phosphorus within living

bacterial cells and the generation of phosphorus containing minerals, which causes the loss of available phosphorus for organisms (Bond et al., 1995; Griffiths, 1986).

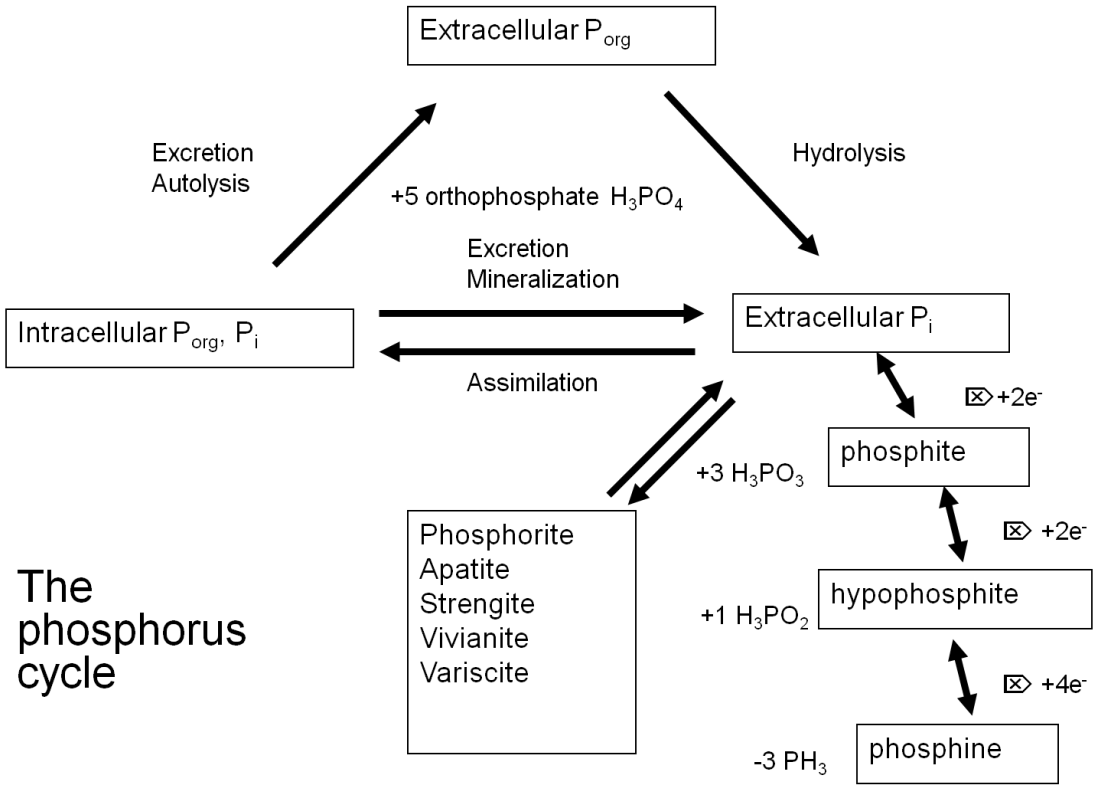

Figure 3. Biogeochemical cycle of phosphorus

2.2.4 Cycles of metal ions

In natural environments, bacteria are significantly involved in the transformation of metal ions. Under environmental conditions with rich metal ions, bacteria not only have to deal with the adverse effects, but also actively convert metal ions to shape the physical and chemical characteristics. As one of the most abundant elements in Earth's crust, iron exists naturally in two oxidation states, ferrous (Fe^{2+}) and ferric (Fe^{3+}) iron (Russo and Long, 2013). Large numbers of iron bacteria oxidize ferrous iron to form the precipitate ferric iron (Straub et al., 1996; Ehrenreich and Widdel, 1994; Widdel et al., 1993). Ferric iron interacts with organic constituents as a soluble and available electron acceptor for iron-reducing bacteria (Lovley and Phillips, 1986). Notable bacterial activities in the iron cycle involves acid mine drainage, where bacteria break down pyrite to form ferrous iron and sulfuric acid (Baker and Banfield, 2003). The extraction of metal ions from their ores is involved in bacterial leaching process (Lundgren and Silver, 1980). This process is useful for oxidation of copper sulfide ores by acidophilic chemolithotrophic bacteria to produce water-soluble copper sulfate which is significant in the copper cycle (Ehrlich and Fox, 1967). The leaching process is also important for the release of uranium and gold in their corresponding cycles. Ferric iron from bacterial oxidation oxidizes uranium ores (UO_2) to produce soluble uranium (UO_2SO_4) (Ganesh et al., 1997). Gold exists naturally with minerals containing arsenic and pyrite. In the leaching process of gold, bacteria attack and solubilize the arsenopyrite (FeAsS[Au]) to free the trapped gold (Attia and El-Zeky, 1989).

2.3 Behaviours and responses of bacteria in natural environments

In habitats with different physical and chemical conditions, it is vital for bacteria to direct chemical reactions and adapt to the changing environments. Environmental

characteristics shape the bacterial behaviour, and as a response, bacteria develop relevant functions to survive in the habitats where they live in. Physical factors such as light, temperature and pH are involved to interact with bacterial cells. Natural light is a portion of the electromagnetic radiation from the Sun, including infrared, visible and ultraviolet light (Davies and Evison, 1991). The light supports nearly all life on Earth. Autotrophs use the energy from light, cooperated with CO_2 and water, to produce organic matters. This process is known as photosynthesis and was discussed above in the carbon cycle. Photoautotrophic and photoheterotrophic bacteria play critical roles in this process, and heterotrophs consume the organic molecules from this process for energy supply (Armitage, 1997). Though light is beneficial to most bacterial species, this natural source can induce damage to photosensitive bacteria (Harrison Jr, 1967). The lag period of bacterial incubation is prolonged when growing in light (Harrison Jr, 1967). Intensive light can result in loss of colony formation or death of bacterial cells (Nitzan and Ashkenazi, 2001). Photolysis is a significant chemical reaction conducted by photons in light (Armitage, 1997). Photons with sufficient energy can affect the bonds of chemical molecules. Phototrophic bacteria involve photolysis as part of the light-dependent reactions. However, for non-phototrophic bacteria, photolysis is able to break down essential enzyme molecules in cells (Harrison Jr, 1967). Similar to light, temperature is a natural source resulted from the Sun. Temperature affects living bacterial cells in two opposing ways, cold or hot conditions. Under suitable temperature conditions, bacteria perform metabolic reactions at more rapid rates. Suitable temperature appears as a range and differs among different bacterial species (Zwietering et al., 1990). The optimum temperature for bacteria is always nearer the maximum temperature than the minimum (Michael et al., 2002). Above the maximum temperature, particular proteins

in bacterial cells may be irreversibly damaged. Bacteria whose growth temperature is above 45℃ are called thermophiles (Zeikus, 1979). The enzymes and proteins in thermophiles are more stable than those in mesophiles (Zeikus, 1979). Below minimum temperature, bacterial growth no longer occurs. Bacteria that can survive in cold environments are classified as psychrophiles (Gounot, 1991). Psychrophiles produce cold-active enzymes which are more flexible and enzymatically active than thermophiles (Gounot, 1991). In addition to light and temperature, bacteria have to deal with different pH values in natural environments. The neutral pH value is 7. Those pH values that are higher than 7 are alkaline, while pH values less than 7 are acidic (Speight, 2005). Bacteria that grow best at low pH are obligate acidophiles which require high concentrations of hydrogen ions for maintaining the stability of cytoplasmic membrane (Krulwich and Guffanti, 1983). A few bacterial species that grow in high pH environments are known as alkaliphiles (Krulwich and Guffanti, 1983). Alkaliphilic bacteria are usually found in soda lakes and high carbonate soils where they use sodium ions as energy suppliers for transport and motility (Ulukanli and Diğrak, 2002).

Apart from physical factors, bacteria have to interact with a broad suite of chemicals present in their surrounding environments. Some chemicals are required nutrient sources such as oxygen, organic carbon and inorganic ions. Bacteria use nutrient molecules for catabolic reactions. Two major mechanisms for energy conservation in catabolic reactions are respiration and fermentation. The achievement of each mechanism is the same, the synthesis of high-energy compound ATP (Haddock and Jones, 1977; Richardson, 2000; Liu, 2003). In respiration, a terminal electron acceptor like molecular oxygen is present for the oxidation of substrate molecules (Haddock and Jones, 1977). Aerobic respiration in aerobic and facultative anaerobic bacteria

involves the use of oxygen as the terminal electron acceptor for the oxidation of a compound. This catabolic pathway proceeds with the biochemical transformation of organic carbon to CO_2 and electron transfer for ATP synthesis (Hobbie and Crawford, 1969). Different from respiration, redox reactions of fermentation occur in the absence of usable electron acceptor (Müller, 2001). In fermentation, bacteria produce balanced oxidation-reduction reactions, and ATP is synthesized by the catabolism of an organic compound (Müller, 2001). Organic substances and oxygen support the growths of bacteria. However, bacteria have to deal with toxic chemicals. Heavy metals are well-studied toxic chemicals for bacteria. In the environment with accumulated concentrations of heavy metals such as mercury and chromium, several bacteria are able to transform the toxic form to non-toxic forms (Holm and Cox, 1975; Wang and Shen, 1995). For other heavy metal resistant bacteria, they have specific enzymes to pump out heavy metal ions including, arsenate and cadmium (Achour et al., 2007; Nies, 1992). The petroleum contaminated environments contribute to the increasing numbers of bacteria that use hydrocarbons as electron donor (Atlas, 1981). Hydrocarbon-oxidizing bacteria can attach to insoluble oil droplets, thereby oxidizing the oil to CO_2 (Leahy and Colwell, 1990). To sense chemical cues of either required or toxic molecules, bacteria have evolve a system known as chemotaxis to respond to the past chemical concentrations and control the movement of them, which is essential for survival in natural environments.

3. The movement of bacteria in a changing environment

In a changing environment, the bacterial cell is in a dynamic state and needs to adapt readily to shifts in environmental conditions. Bacteria have patterns of behavioral response to chemical cues that affect their growth. Chemical cues can be specific dissolved substances or signal molecules of living cells or nonliving particles.

Bacteria can sense changes in chemical concentration over time and respond by moving up or down the concentration gradient (Adler, 1966). The swimming behaviour or directions of bacteria are changed by environmental shifts. Some bacteria flail flagella in opposite directions to orient to a new direction, which is known as tumbling. The increasing concentration of an attractant contributes to the forward swimming, while decreasing concentration contributes to the tumbling. Conversely, an increase in concentration of a repellent chemical results in tumbling, and decreasing repellent concentration results in swimming forward. Motility allows bacteria to reach a new location in its environment for survival, resources and opportunities.

3.1 Required facilities for being motile

The motile function of bacteria is usually due to a special structure, the flagellum (plural flagella). The bacterial flagellum is a long, thin and lash-like appendage that protrudes from the cell body and free at the end (Figure 4) (Macnab, 1999). A single flagellum is too thin (about 20 nm in diameter) to be seen with the light microscope. After staining with special dyes, flagella are visible with a light microscope because of the increasing diameter (Heimbrook et al., 1989). The electron microscope is a powerful tool for the direct detection of bacterial flagella (Lowy and Hanson, 1965). The arrangement of flagella differs on different bacterial species. Two types of flagella are found for bacteria, polar flagellation and peritrichous flagellation (Leifson, 1951). Flagella of polar flagellation are attached at one or both ends of the cell (Leifson, 1951). A group of flagella may occasionally arise at one end of the cell, called lophotrichous flagella (Inoue et al., 1991). In peritrichous flagellation, flagella are at many places around the cell surface (Inoue et al., 1991). In addition to the usefulness in motility of these types of flagella, it is a feature that is responsible for

the classification of bacteria. A helically shaped hollow tube comprising the protein flagellin is the filament on a flagellum (Wilson and Beveridge, 1993). There is a constant distance between two contiguous curves on the filament, known as the wavelength (Wilson and Beveridge, 1993). The base of a flagellum is a wider region called the hook that connects the filament to the motor part of the flagellum (Macnab, 1999). The motor is a small central rod that passes through a system of rings in the cell wall and cell membrane (Inoue et al., 1991). The motor involves the rotary motion of the flagellum and requires the energy from bacterial cell. Flagella can increase or decrease the rotational speed to move bacteria at the speed of 60 cell lengths per second in a liquid medium (Michael et al., 2002).

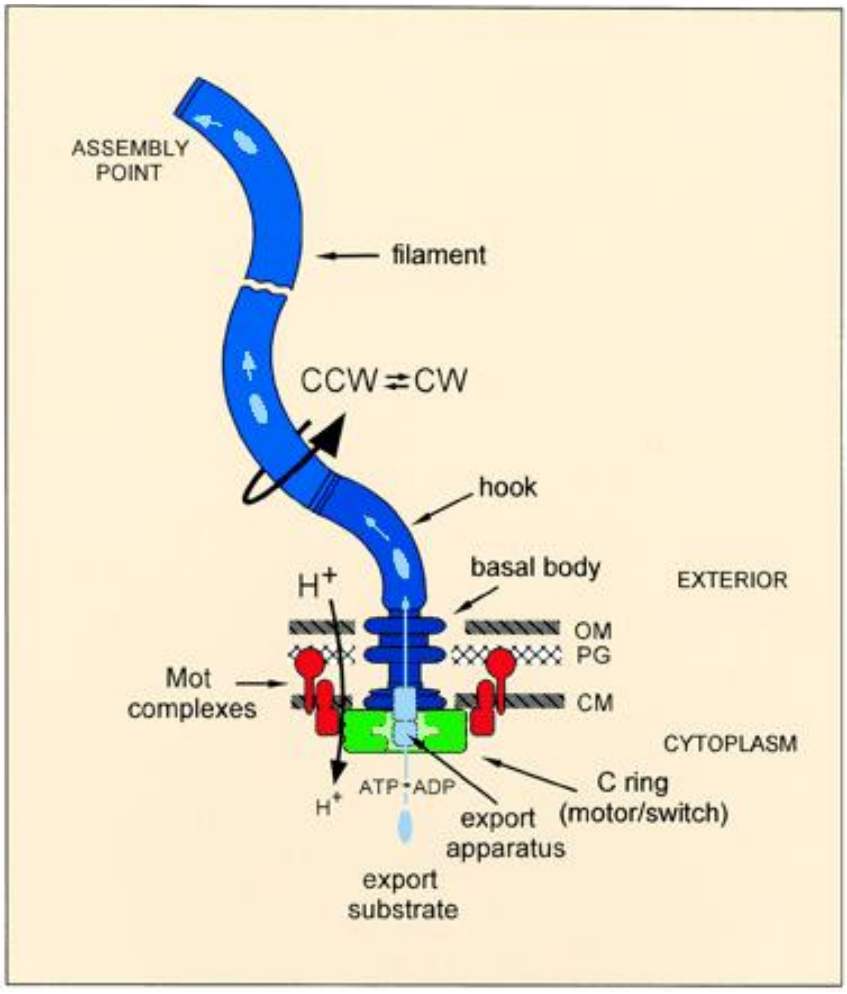

Figure 4. The structure of bacterial flagellum (From Macnab, 1999).

On the surface of many bacteria, a hair like appendage called a pilus is found (Latin for hair, plural for pili) (Figure 5). A pilus is typically 6 to 7 nm in diameter. Pili are structurally similar to flagella, but shorter and greater in numbers than flagella (Craig et al., 2004); they can be seen on bacteria with the electron microscope (Craig et al., 2006). Pili are antigenic receptors on which viruses or bacteriophages attached to initiate their reproductive cycle (Jacobson, 1972). Pili are involved in the process of conjugation and motile forces for several bacterial species (Ou and Anderson, 1970; Merz et al., 2000). In the process of bacterial conjugation, conjugative pili perform as the tube for the transfer of DNA between bacteria (Ou and Anderson, 1970). The donor bacterium uses a conjugative pilus to trap the recipient bacterium and pulls it in closer for the establishment of a mating bridge that forms a controlled pore to transfer DNA (Ou and Anderson, 1970). This process contributes to the dissemination of required genetic traits throughout a bacterial population. Though only some bacteria are able to form conjugative pili, bacterial conjugation can occur between different species (Christie and Vogel, 2000). Pili that generate motile force are called type IV pili (Merz et al., 2000). Type IV pili facilitated bacterial movement is typically jerky, so it is known as twitching motility (Ou and Anderson, 1970). During the process of horizontal genetic transfer, the protein of type IV pili mediates the specific recognition of DNA uptake sequences (Christie and Vogel, 2000). Therefore, pili are not only responsible for bacterial motility, but also mediate gene transfer between bacteria.

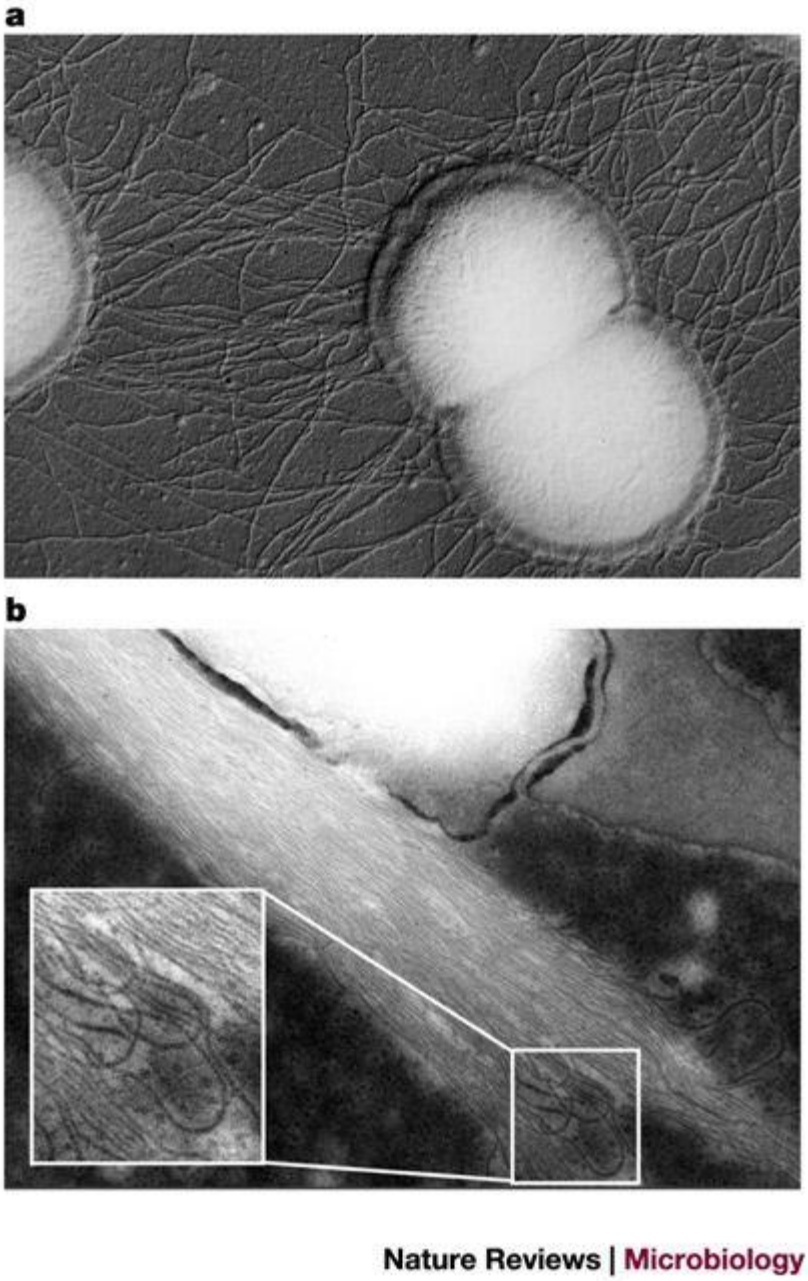

Figure 5. The image of pili on bacteria cells (From Craig et al., 2004)

3.2 Bacterial chemotaxis

Bacterial chemotaxis refers to the movement of cells towards attractant chemicals or away from repellents. In a stable environment, bacterial movement is in 'random walk' of straight-line and punctuated by short periods of reversal (Wadhams and Armitage,

2004). The probability of reversal is controlled by the chemotaxis system to randomize the direction of the next run of bacterial cells. Bacteria sense environmental cues, and subsequently modulate the probability of random changes in direction towards attractants or away from repellents (Adler, 1966). This mechanism is known as the 'biased random walk' that allows individual cells to determine whether to continue on a course or change direction (Hill and Häder, 1997). Bacteria are too small to have a sense of direction, but biased random walk enables bacteria to direct their motions. Due to the small size of bacteria, the chemotactic response of bacteria is dependent on a temporal mechanism rather than a spatial mechanism (Macnab and Koshland, 1972). By using this temporal sensing mechanism, bacterial movement does not rely on spatial gradients of attractants or repellents. As a consequence, when suddenly exposed to attractants or repellents, bacteria tend to suppress the motivation to change direction (Macnab and Koshland, 1972). A single bacterial cell is able to compare its present surrounding conditions to those it has experienced recently (Vladimirov and Sourjik, 2009). Favorable comparison leads to continuous movement, whereas unfavorable comparison leads to direction changes. This memory function of bacteria is related to their adaptation to new environment (Vladimirov and Sourjik, 2009). A bacterial cell that has adapted to the environment with a specific attractant finds that the direction to the environment lacking the attractant is unfavorable.

The bacterial response to chemical changes and adaptation to new environments is regulated by sensory pathways in chemotaxis systems. The common sensory pathways in most prokaryotes rely on a histine-aspartate phosphorelay (HAP) system (Wadhams and Armitage, 2004). The structure of this system requires at least two components: a dimetric histidine protein kinase and a response regulator (West and

Stock, 2001). More than 600 HAP systems have been identified in bacteria, and several bacterial species contain over 130 through genome sequencing (Ashby, 2004). Briefly, a residue of histidine auto-phosphorylate by the phosphoryl group of an ATP molecule, and then this phosphoryl group is transferred to an aspartate residue on a response regulator protein to activate sensory pathways and generate relevant response (Figure 6) (Stock et al., 2000; Inouye and Dutta, 2002). Chemotaxis is one of the pathways to regulate motile behaviour of bacteria. Bacterial chemotaxis is the biasing of movement towards regions with high concentrations of beneficial substrates, or low concentrations of hazardous chemicals. Chemotactic signals from the surrounding area are detected by transmembrane chemoreceptors — methyl-accepting proteins (MCPs), and a sensory domain of histidine protein kinase regulates the transcription of relevant chemotaxis genes (West and Stock, 2001; Wadhams and Armitage, 2004). CheW is an adaptor protein that assists the linkage of MCPs with cytoplasmic histidine protein kinase CheA (Wadhams and Armitage, 2004). Two response regulators, CheY and CheB, compete for binding to auto-phosphorylated CheA. The CheY is flagella-motor-binding protein that binds the switch protein to cause the motor rotation in phosphorylated form (Hess et al., 1988). The function of CheB is similar to methylesterase and controls the adaptation of MCPs (Anand et al., 1998). In an environment with increased concentration of attractant, the autophosphorylation of CheA is inhibited, thereby reducing the concentration of phosphorylated CheY (Adler, 1975). This contributes to a smooth swim in the positive direction for a longer time. The decreasing CheB phosphorylation allows the increasing concentration of constitutive methyltransferase CheR which is responsible for the methylation of MCPs (Djordjevic and Stock, 1998).

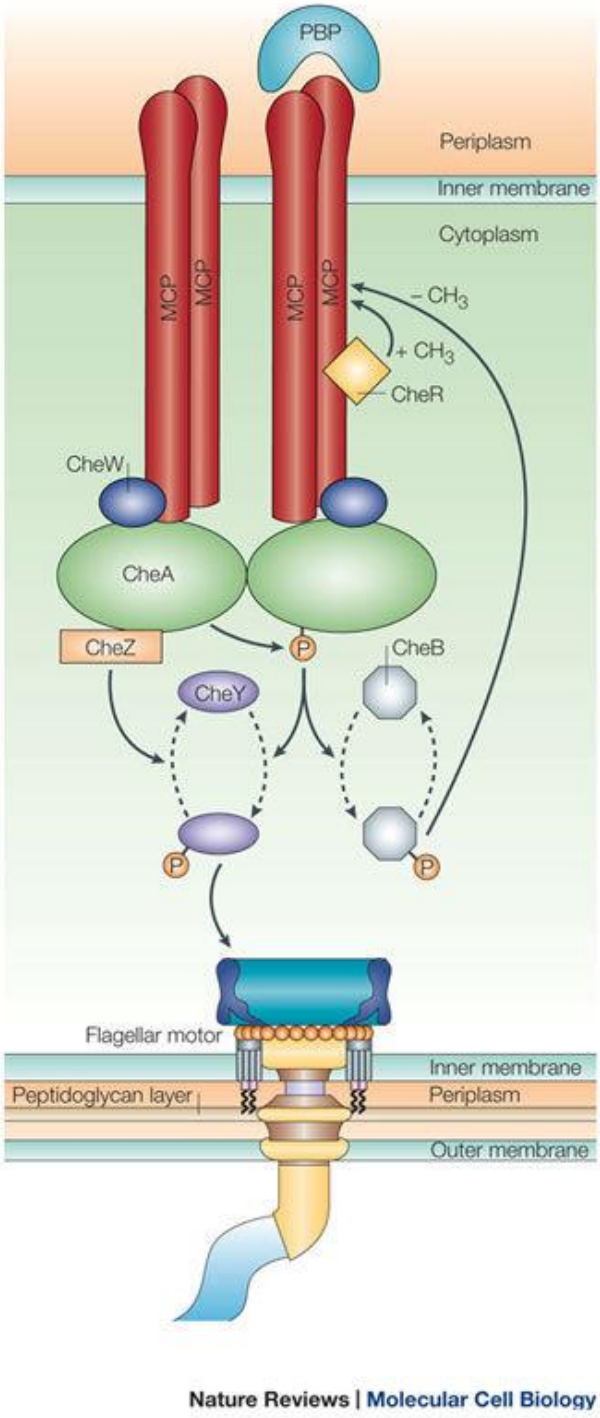

Figure 6. Schematic diagram of the chemosensory system in a bacterial cell (From Wadhams and Armitage, 2004)

Chemotactic genes in bacteria are categorized into two major groups, *cheA* and *cheB*, which are involved in the synthesis of protein CheA and CheB, respectively (Parkinson, 1976). The expression of CheA is regulated by two genes (*cheA* and *cheW*), while four genes (*cheR*, *cheB*, *cheY* and *cheZ*) are required for the expression of CheB (Smith and Parkinson, 1980; Parkinson, 1976). Mutant bacteria defective in *cheA*, *cheW*, *cheY* or *cheR* never change the motion directions (Parkinson et al., 2005). On the contrary, mutants with deficiencies in *cheB* and *cheZ* exhibit constant changing that is suppressed by additional attractants (Parkinson et al., 2005). Consequently, proteins CheA, CheW and CheY are essential for reversal excitation, whereas proteins CheB and CheR are required for motion adaptation. The function of individual Che genes is listed in Table1.

Motile bacteria that lack flagella are known as crawling bacteria which move across solid surfaces in the process called twitching motility (Merz et al., 2000). This movement uses type IV pili extended from the exterior cell membrane to attach on to solid substrates and retracts, thereby pulling bacterial cell forwards. The maximum speed of twitching motility is 10 μm per second which is slower than propulsion by flagella (Harshey, 2003). Proteins involved in twitching motility are similar to the flagella mediated chemotaxis system. The chemoreceptor PilJ is expected to sense environmental cues and initiate the signal transduction in twitching motility (Sampedro et al., 2015). Histidine kinase ChpA and two CheW homologues, PilI and ChpC, are suggested as signal transducers for twitching motility (Bertrand et al., 2010; Sampedro et al., 2015). The regulation of pili movement is likely related to PilG and PilH that are in homology with CheY (Bertrand et al., 2010). The mechanisms of twitching motility are based on model investigation, and further investigations are required for detailed information of this bacterial movement.

Table1 Function of Che genes

Gene	**Function**
cheA	Histidine kinase
cheY	Phosphorylation of CheY
cheR	Methylation of MCPs
cheB	Demethylation of MCPs
cheW	Coupling CheA to MCPs

3.3 Protein methylation and signal transduction in chemotaxis

From the study of bacterial chemotaxis on *E. coli*, methionine was found as a required substance for chemotaxis (Adler, 1975). Methionine is an essential amino acid for biological syntheses of proteins, and plays a critical role in bacterial metabolism (Aswad and Koshland, 1974). A methionine molecule comprises a protonated amino group, a deprotonated carboxylic group and an S-methyl thoether side chain (Aswad and Koshland, 1974). These functional groups of methionine allow it to be classified as a member of nonpolar and aliphatic amino acids. Bacteria defective in coding genes for methionine exhibit depressed chemotactic response to attractants, which is only discovered for methionine (Adler, 1975). Furthermore, a cell is unable to respond to the additional attractant when it is starved for methionine (Clark et al., 1980). It is suggested that the function of methionine in bacterial chemotaxis is related to the methylation of MCPs that is responsible for the detection of chemical cues and signal transduction. Relevant studies showed that methionine is the major component

for methylation of a wide range of biological macromolecules, including proteins, DNA and RNA (Adler, 1975; Aswad and Koshland, 1974; Clark et al., 1980).

The membrane MCPs require methionine as a methyl donor in the chemotaxis system. MCPs are transmembrane proteins that detect concentrations of attractants or repellents in extracellular environments. Diverse MCPs in bacteria are attributed to the diverse environmental conditions. For instance, five well-studied MCPs are found in *E. coli* (Parkinson, 2010). These five MCPs are Tar (taxis for aspartate and maltose, away from nickel and cobalt), Tsr (taxis for serine, away from leucine, indole and weak acids), Trg (taxis for galactose and ribose), Tap (taxis for dipeptides) and Aer (taxis for cellular redox potential) (Swain and Falke, 2007; Parkinson, 2010). MCPs have similar structure that consists of three MCP dimers (Chelsky and Dahlquist, 1980). This complex combines loosely with CheA and CheW into hexagonal lattices (Chelsky and Dahlquist, 1980). MCPs usually have two functional domains, sensing and signaling. Sensing domains contain an N-terminal signal peptide and a conserved periplasmic ligand-binding protein which directly binds ligands or interacts with corresponding proteins. The signaling domain is a highly conserved receptor that binds with CheA and CheW for signal transductions.

In the chemotaxis system, signal transduction is important to control the movement of bacteria. The CheA-CheW complexes are essential receptors that are involved in the initiation of signal transduction. The histidine kinase, CheA, can catalyze the phosphorylation of its own histidine residues, which is known as autophosphorylation (Bilwes et al., 1999). The rate of CheA autophosphorylation is dependent on the level of MCP methylations and binding ligands (Swanson et al., 1994). The signal from methylated MCPs is believed to be transmitted by CheW for the activation of CheA

autophosphorylation (Gegner et al., 1992). These receptor complexes support the signal integration and amplification.

The phosphoryl group from the phosphohistidine in CheA is transferred to CheY. The CheY is a monomeric enzyme that catalyzes the phosphorylation for its own aspartate residue to induce conformational change (Stock et al., 1989). The phosphorylated CheY binds to switching proteins in the motor of flagella for subsequent movement (Sanders et al., 1989). The dephosphorylation process of phosporylated CheY occurs spontaneously to terminate the chemotactic response, so that bacteria can swim smoothly for longer (Sanders et al., 1989). The CheB is a protein that acts competitively with CheY to bind with phosphoryl group from autophosphorylated CheA (Lupas and Stock, 1989). Phosphorylated CheB causes the increases in demethylation of MCPs, which results in the decrease in CheA autophosphorylation (Wadhams and Armitage, 2004). Consequently, the same mechanism produces a feedback control for bacterial adaptation.

4. Assessment of bacterial behaviours: techniques and challenges

Despite the fact that there have been numerous investigations of bacterial behaviour towards diverse chemical molecules, there is no method for the simultaneous characterization of bacterial cells and molecules. This is possibly due to that the physicochemical properties of chemical molecules are too diverse to be analysed by the same method. Several conventional methods are well-established to understand the behaviour of bacteria under different environmental conditions. Owing to the distinct target analytes, methods are usually grouped into three different types, bacteria detection methods, molecular analysis methods and bacterial chemotaxis assays. To detect bacterial cells directly, methods such as the light microscope, electron microscope and cultural methods are used for the observation of bacterial

movement or colony formation. Molecular analysis including polymerase chain reaction, immunological assay and fluorescence *in situ* hybridization provide the information of proteins and/or genomes that is related to particular bacterial behaviour or metabolisms. The specific chemotactic responses of bacteria are visualized by chemotaxis assays, e.g. swim agar, capillary assay, temporal stimulation of tethered cells and automated tracking of swimming cells.

4.1 Detection of bacteria

As the first equipment to observe bacteria, the light microscope is an important and universal method for the detection of bacteria. The light microscope is also known as the optical microscope that uses visible light and a system of lenses to magnify the observed image (Mertz, 2010). The oldest design of light microscope was possibly invented by the Dutch inventor Cornelius Drebbel in 17^{th} century, which is recorded in the description of the compound microscope (Mertz, 2010). In later centuries, complex designs were developed to improve resolution and sample contrast. The image from the light microscope is called a micrograph that is generated by photosensitive cameras (Mukamel, 1999). In the original light microscope, the micrograph was captured and produced by photographic film (Mukamel, 1999). The modern developments in charge-coupled devices and complementary metal-oxide-semiconductors enable the generation of digital micrographs from light microscopes (Wilson and Sheppard, 1984). Although the light microscope is now universal, its application to the detection of bacteria was not popularized until the 1850s. About 150 years after Antonie van Leeuwenhoek brought the microscope to the attention of biologists, the light microscope was used to investigate cholera and subsequently popularized for bacterial detection (Gest, 2004). The easy and simple operation of the light microscope makes it a general observation method for bacteria.

However, the low resolution limits this method from providing detailed behavioural information of bacteria under different environmental conditions (Mertz, 2010).

The electron microscope provides muchincreased magnification for the visualization of bacterial behaviour. The first electromagnetic lens was created by the physicist Ernst Ruska and the electrical engineer Mas Knoll in 1931 (Bozzola and Russell, 1999). The source of illumination in the electron microscope is a beam of accelerated electrons (Bozzola and Russell, 1999). The short wavelength of an electron results in high resolving power that can reveal the structure of smaller objects such as microorganisms, cells, metals and crystals (Egerton, 2005). The original form of electron microscope is the transmission electron microscope (TEM), in which a high voltage electron beam is generated to illuminate the specimen and produce an image (Williams and Carter, 1996). A TEM comprises several components, which includes an electron emission source for the generation of the electron beam, a vacuum system for electron travel, and a series of electromagnetic lenses and electrostatic plates for the guidance and manipulation of the electron beam. Though TEM has high resolution, it requires extremely thin sections of specimens (typically about 100 nm), which is technically challenging for sample preparation (Williams and Carter, 1996). Another type of electron microscope is the scanning electron microscope (SEM) that produces images by scanning across a rectangular area of specimens with a focused beam of electrons (Goldstein et al., 2017). The major advantage of SEM is that good-quality images of biological tissues and bacterial cells can be obtained with hydrated samples and in low vacuum gases (Danilatos and Robinson, 1979). However, the intact appearance of bacteria from SEM cannot distinguish if a cell is still alive, so the application of SEM is limited in the determination of the impacts of severe environmental conditions on bacteria (Goldstein et al., 2017).

Culture methods are one of the oldest ways to evaluate treatment effects, and they are still in use because they are simple operations and inexpensive (Rohde et al., 2017). Cultural methods are based on plate counting to estimate the ability of bacteria to give rise in colonies under specific conditions of nutrient medium, temperature and time (Reed and Reed, 1948). Different from microscopic detection - which counts all cells - living or the dead, cultural methods only count viable cells. Cultural methods distinguish viable and dead bacteria and are powerful tools for enumeration. Nevertheless, improvements are required to solve their drawbacks: there are difficulties to isolate the target bacteria from the bacterial community, long incubation and enrichment procedures, as well as high intensity of labour.

4.2 Molecular analysis for bacterial activities

The behaviour of bacteria under different environmental conditions is regulated by several proteins and genomes. Molecular analysis tools therefore play a significant role in unraveling the mechanisms that bacteria use to regulate their responses. Polymerase chain reaction (PCR) is a common and indispensable technique to isolate and sequence DNA segments from bacterial cells (Joshi and Deshpande, 2010). PCR is one of the most widely used techniques to investigate bacterial behaviour at the molecular level. The concept of PCR was firstly presented by Kjell Kleppe in 1971, although it did not receive much attention at that time (Kleppe et al., 1971). In 1983, Kary Mullis developed PCR as a promising technique for DNA amplifications through repeated cycles of duplication (Rabinow, 1996). Most PCR assays amplify specific DNA fragments of between 0.1 and 10 kilo base pairs (kbp). The basic requirements for PCR set-up often contain a DNA template that comprises: a target region for amplification; a DNA polymerase that synthesizes new DNA strands; two complementary DNA primers that initiate the complementary base pairing of specific

DNA segments; a mixture of deoxynucleotide triphosphate (dNTPs) that perform as the building blocks for the new DNA strand; and a buffer solution that provides a suitable chemical environment for reactions (Joshi and Deshpande, 2010). The major procedure of PCR is known as thermal cycling that consists of 20-40 repeated temperature changes. In each cycle, two or three discrete temperature steps are involved (Joshi and Deshpande, 2010). Most PCR protocols usually have 6 steps, initiation, denaturation, annealing, extension, final elongation and final hold. The principles and procedures of quantitative PCR (qPCR) are similar to that of normal PCR, except for fluorescent emission. Quantitative PCR involves the fluorescent emission through the attachment of a specific dye with the targeted amplicon to give fluorescence intensity that is proportional to the amount of amplified nucleic acid products (Wilhelm and Pingoud, 2003). Either PCR or quantitative PCR is less time-consuming, producing the results within 5 to 24 hours, and does not require previous enrichment steps (Joshi and Deshpande, 2010; Wilhelm and Pingoud, 2003). Apart from expensive consumables used in this method, PCR and qPCR is limited to discriminate viable and dead bacterial cells as DNA or RNA is always present (Lazcka et al., 2007). In addition, this nucleic based method cannot determine which environmental substrate or conditions cause the expression of specific genomes.

Immunological methods are established as molecular tools to analyze bacterial proteins or polysaccharides that bind with antibodies (Mine, 1997). Immunology is derived from the fields of epidemiology and medicine, and this subject focuses on the relationship between the body systems, pathogens and immunity. Therefore, immunological methods are based on the interaction between antibodies and antigens. In contrast to PCR and qPCR, the target molecules of immunological methods are usually not nucleic acids in bacterial cells, but proteins or polysaccharides that enable

them to distinguish between closely related serotypes (Rohde et al., 2017). There are different assays to implement immunological methods for the study of bacterial proteins. For instance, antibody coated magnetic beads are used in immunomagnetic assay to concentrate and separate target bacteria from a medium (Gu et al., 2006). In addition, enzyme linked immunosorbent assays are developed to conduct enzymatic readout reactions through the specific binding of antibody and antigen (Crowther, 1995). Although immunological methods are fast and easy, these methods only focus on the bacterial proteins or polysaccharides other than the behaviour from an intact bacterial cell. Also, similar to PCR and qPCR, immunological assays have the drawback that there is no discrimination of live or dead bacteria because target structures often remain unchanged after cell death.

Another molecular analysis tool is known as fluorescence in situ hybridization (FISH) that involves fluorescent probes binding with specific DNA or RNA sequences (Levsky and Singer, 2003). The FISH method was firstly developed in the 1980s to detect and localize the presence or absence of specific DNA sequences on chromosomes (Levsky and Singer, 2003). Most FISH methods are used to detect specific features in DNA for genetic characterization and species identification (Andreeff and Pinkel, 1999). This method can also provide the information of specific RNA targets such as messenger RNA, long on-coding RNA and micro RNA in bacterial cells (Levsky and Singer, 2003; Patterson et al., 1993). The spatial-temporal patterns of gene expression from bacteria can be defined by FISH. Owing to the development of stable-isotope probing (SIP), FISH become popularized for the examination of specific metabolic activities in bacterial cells from different environments (Wang et al., 2016). As combined with SIP, FISH is widely applied in the analysis of bacterial behaviour and responses to environmental molecules or

biological signals. However, the dependency of SIP-FISH on radioisotopes limited substrate labelling and applications.

4.3 Characterization of bacterial chemotaxis

Approaches used to characterize the bacterial chemotaxis include swarm plates, capillary assays, temporal stimulation of tethered cells, and automated tracking of swimming cells. Swarming agar is the method to investigate the movement of bacteria away from their initial locations (Henrichsen, 1972). The multicellular movement of bacteria across the agar surface *via* flagella rotation consequently forms a bacterial spot around specific chemicals (Henrichsen, 1972). In capillary assays, the motility of bacteria community was monitored. The flux of bacteria flows through a porous glass plate comprising a fused array of capillary tubes following chemicals gradients (Berg and Turner, 1990).

From the method of temporal stimulation of tethered cells, bacterial cells are tethered to glass and flushed by a medium containing chemoattractant. The changes in bias allow the evaluation of bacterial chemotaxis onto specific chemicals (Block et al., 1983). Another approach involves a real-time apparatus to track and trap swimming sperm in the digital computer at video rate (Shi et al., 2006). The chemotactic response and swimming speed of an individual bacterial cell is measured by this method (Shi et al., 2006). These approaches are versatile in testing the bacterial chemotaxis toward specific chemicals individually. However, approaches above are not able to detect the targeted molecules on/in bacterial cells in a mixture of a variety of chemicals, or to test the bacterial competitive selection of specific chemicals.

5. Raman spectroscopy

Raman spectroscopy is a fast, non-destructive and reliable technique that has been extensively applied in the real-time and in situ study of bacteria-molecule interactions. Raman spectroscopy, especially surface-enhanced Raman scattering (SERS), has attracted considerable attention in recent studies. This spectroscopy technique is traditionally used to identify the structure of unknown molecules. Because of the updated instruments, Raman spectroscopy is able to characterize biochemical components in complex biological samples, and it has been used as an essential method in biological research laboratories where bio-spectroscopy was pioneered. Bio-spectroscopy is a time- and labour-saving technique that provides a rapid and label-free analytical route for biological research.

5.1 Raman scattering

Raman scattering is the inelastic scattering of light that was predicted by Adolf Smekal in 1923 (Smekal, 1923). In 1928, a series of investigations about molecular diffraction of light were reported by Indian physicist C.V. Raman (Singh, 2002; Raman and Krishnan, 1928). This technique was not recognized as an analytical tool until 1998 (Singh, 2002). During the Raman scattering process, photons are able to gain energy from or lose energy to molecules, which contribute to the change in frequency of scattered photons (Landsberg and Mandelstam, 1928). Due to the energy of specific molecule vibrations, the scattered photons can shift in the frequency that is relative to the excitation photons (Kneipp et al., 2008). As a consequence, vibrational marks of a molecule from the scattering of diverse molecular vibrations finally generate a Raman spectrum. The energy of frequency-shifted scattered photons is determined by states of molecules they interact with. Based on the theories of Stokes and anti-Stokes scattering, photons firstly lose energy to excite vibrations to generate

lower frequency scattered light (Stokes scattering), and then the photons gain energy by interacting with molecules in excited vibrational state to provide higher frequency scattered light (anti-Stokes scattering) (Figure 7) (Kneipp et al., 2002).

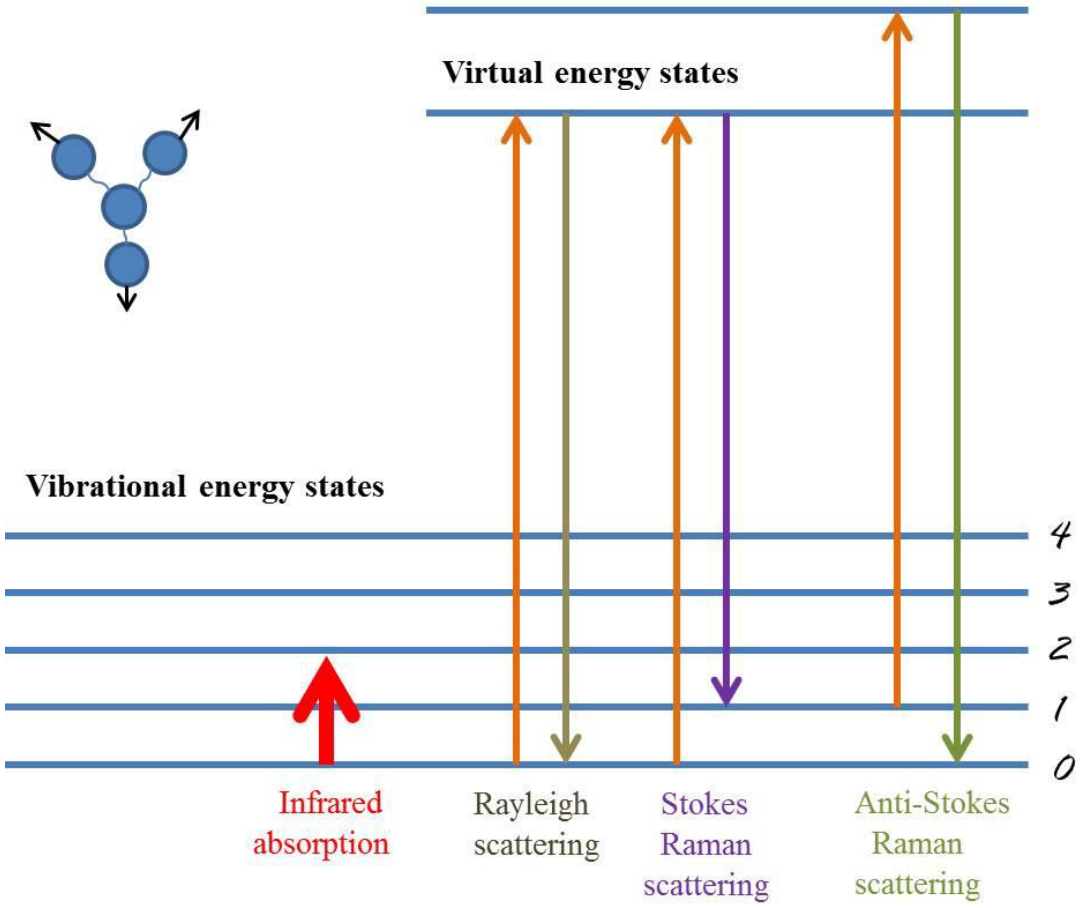

Figure 7. Brief description of the theory of Stokes and anti-Stokes scattering

The interaction of photons with molecules in the 'Raman Effect' is not caused by an absorption and emission process, but due to scattering. Theoretically, Raman scattering is a weak effect. Excited and/or scattered photons from the excitation light cannot match the related electronic transition in a molecule. In Raman scattering, the total Stokes Raman signal is proportional to the Raman cross section which is in the range from 10^{-30} cm^2 to 10^{-25} cm^2, while the cross section of fluorescence

spectroscopy is between 10^{-17} cm^2 and 10^{-16} cm^2 (Kneipp et al., 2008). Therefore, the small Raman cross section demands a large number of molecules to obtain adequate Raman photons from excitation laser photons. Consequently, Raman scattering is a tool for structural analysis, rather than a technique for ultra-sensitive trace measurement or even for single-molecular detection.

In the non-resonant Raman scattering process, the scattering signal favours the resonant Raman condition, which occurs only when the excitation light matches the related electronic transition energy in a molecule (Kneipp et al., 2008). Therefore, to meet this requirement, resonant Raman scattering (RRS) was invented. RRS not only has increased cross sections, but also has the advantage of higher specificity (McNay et al., 2011). Although the signal of Raman scattering can become stronger during the process of RRS, this technique is not powerful enough to cover up the influence of fluorescence (McCreery, 1996). Equipped with microscope, Raman spectroscopy is able to acquire a spectrum from a volume of sample that is smaller than 1 cubic micrometer, such as one bacterial cell (Li et al., 2012). Single-cell Raman spectroscopy enables the detection of different cell types and provides diverse signal information of bacterial species. Raman characterization can show changes in physiology and phenotype of one living single cell. However, because of the weak Raman signal, single-cell detection requires long acquisition time for the reliable spectrum of bacteria (van Manen et al., 2005). As a result, the discovery of surface-enhanced Raman scattering (SERS) attracts considerable attention.

5.2 Surface-enhanced Raman spectroscopy

Surface-enhanced Raman spectroscopy (SERS) enhances Raman scattering by molecules adsorbed on rough metal surfaces or by nanostructures. This sensitive technique was first discovered by Martin Fleischmann in 1973, using pyridine

adsorbed on silver to produce SERS signal (Fleischmann et al., 1974). It is reported that, from numerous studies on SERS, two theories are accepted to unravel the SERS signal. One is known as electromagnetic enhancement (Figure 8) (Campion and Kambhampati, 1998). This theory is arisen from the mechanism of Raman scattering. Based on the same mechanism of normal Raman scattering, the SERS signal is determined by excitation intensity and an effective SERS cross section, which is donated by electromagnetic enhancement depending on excitation and scattered field.

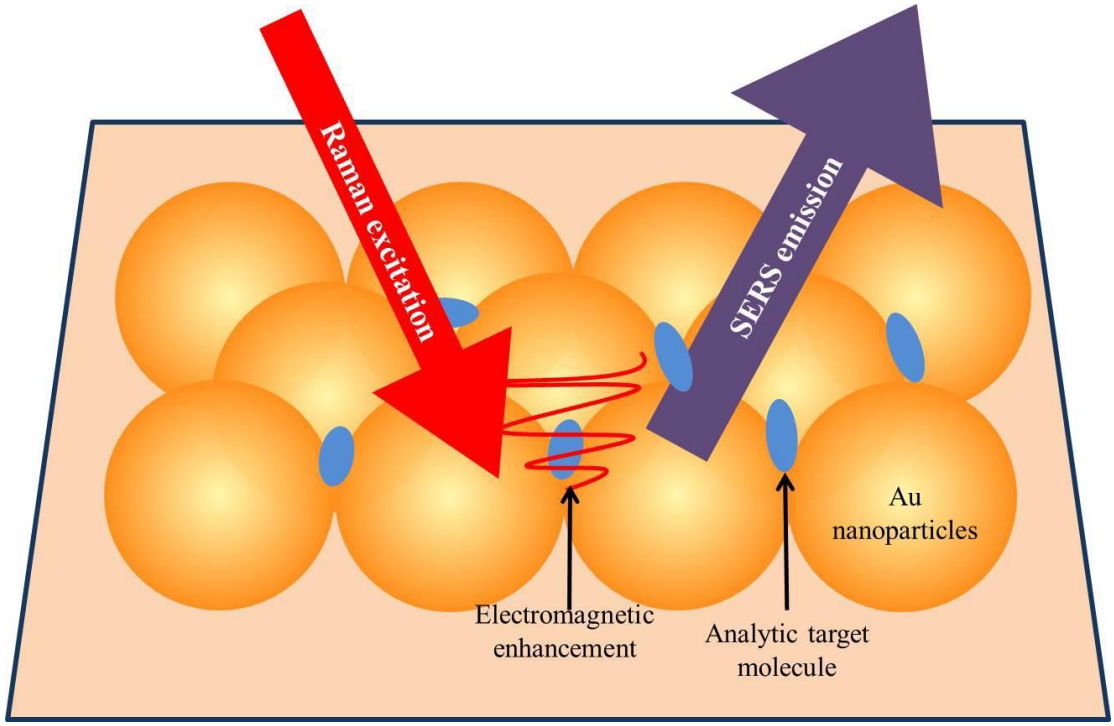

Figure 8. Electromagnetic mechanism of SERS

Plasmon energy arises when the surface bond to the plasmon is roughened enough to give a perpendicular component to the plasmon. Hence, the plasmon energy can contribute to the occurrence of the Raman process. The energy, gains from plasmon energy, of the analyte molecule can transfer back to the plasmon to achieve scattered radiation which is shifted into the frequency close to the nuclei in the Raman process,

and is finally detected by the Raman spectrometer. The second theory is called charge-transfer enhancement or chemical enhancement (Persson, 1981). Charge-transfer enhancement is related to an electronic coupling between the molecule and metal (Lombardi and Birke, 1986). During the process of charge-transfer enhancement, the analyte molecule is firstly bound to the metal surface to generate a charge-transfer complex. With the interaction between exciting radiation and the substrate metal, an electron-hole pair is formed to give a tunnel for transferring energy back to the bonds of the molecule and metal, which leads to the SERS signal. In addition, the complex of metal and molecule may increase the Raman cross section when compared to that of a free molecule, which strengthens the Raman signal (Lombardi and Birke, 1986). However, the chemical theory only explains for species that have formed a chemical bond with the surface metal, but not for all Raman signal enhancement. A study in 2016 reported that SERS can occur even when an excited molecule is relatively far from the metallic surface, which further supported the first theory, electromagnetic theory (Yang et al., 2016).

Due to the direct interaction of bacteria and AgNPs, label-free method can collect the intrinsic Raman signals of bacterial cells. To discriminately detect *Bacillus anthracis* spores from other *Bacillus* species, Farquharson *et al.* designed a SERS *B. anthracis* assay consisting of AgNPs functionalized peptides distributed throughout a porous glass structure to interact with bacteria samples (Farquharson et al., 2014). Rapid counting of live and dead *E. coli* was achieved through direct interaction of AgNPs with bacteria (Zhou et al., 2014). In a recent study, Wu *et al.* used vancomycin Ag nanorods to capture 27 different bacteria isolated from 12 species, and distinguish Gram-positive from Gram-negative bacteria with high sensitivity and specificity (Wu et al., 2015). An in situ and sensitive SERS fingerprinting approach has been

developed to study the antibacterial activity and mechanisms of AgNPs in different sizes, 18 (Ag18) and 80 nm (Ag80) (Cui et al., 2013). In the study of El-Zahry *et al.*, the antimicrobial effect of various shapes of AgNPs (spherical, hexagonal and triangular) against Gram-negative bacteria *Escherichia coli* was identified by SERS (El-Zahry et al., 2015). This study demonstrated similar changes in SERS peaks to the study stated above, indicating the inhibition of Ag NPs in protein synthesis, and the influences on the metabolic process of purine (El-Zahry et al., 2015).

Based on the enhancing silver or gold nanostructure, a key function from SERS in the field of bioanalytics is SERS labelling (Allain and Vo-Dinh, 2002; Cao et al., 2002). In order to detect particular molecules, especially biomolecules, a specific linker is used to functionalize SERS active substrate for SERS label. SERS active substrate with target molecules encapsulated in a glass shell can provide mechanically and chemically stable SERS label (Mulvaney et al., 2003). Because SERS is not controlled by the resonant system, the influences of photobleaching and self quenching on SERS detection can be removed. Additionally, with the non-resonant excitation radiation, SERS labels can work at the same excitation wavelength, which enables the real multiplexing capability for SERS labels, particularly in labelling and identifying various DNA strands (Faulds et al., 2004; Qin et al., 2007).

The fast and non-destructive properties allow *in situ* detection of molecular variations on bacteria cells, and identification of changes in biochemical substances in bacteria. By interrogating Raman spectroscopy, effects of nanomaterials on bacterial cells are evident, which is significant for bacterial detection. Raman spectroscopy has the potential to study bacterial behaviours including chemotaxis, accumulation and utilization towards diverse environmental molecules. In addition, it is possible to apply Raman spectroscopy for investigating the influences of nutrient ions on

bacterial response, which might lead to benefits and improvements of bioremediation technologies for environmental contamination.

6. Research aims and objectives

This thesis mainly focuses on the application of Raman microspectroscopy in the investigation of interactions of bacteria with different molecules, nanoparticles and organic carbonaceous substances. Four research projects are consisted in the thesis.

In Chapter 1, Raman scattering was performed to rapidly detect of bacteria. To improve the signal intensity, surface-enhanced Raman scattering (SERS) was developed and used in diagnosis of pathogens in drinking water. However, direct application of SERS requires the mixture and separation of bacterial cells with suspended silver (Ag) or gold (Au) nanoparticles. This approach also suffers from the difficulties in recovering Ag/Au nanoparticles from the samples, and faces the challenges that the low concentration of bacteria in water samples causes low capture efficiency of bacteria. Considering the high enrichment of magnetic nanoparticles (MNPs) for bacteria, surface modification has been applied for MNPs with Ag/Au coatings for bacterial collection and detection. A novel highly-sensitive screening method for rapid detection of pathogens in drinking water was developed with Ag coated MNPs (Ag@MNPs) by means of magnetic capturing and SERS diagnosis. The limit of detection for bacteria was significantly improved, attributed to the magnetic enrichment and SERS signal enhancement, which were simultaneously achieved by Ag@MNPs.

In Chapter 2, Raman spectroscopy was developed to identify bacterial chemotaxis towards hydrocarbons. The increasing usage of crude oil has been associated with the excess release of hydrocarbons into the environment. Because of that, alkanes are one of the most widespread contaminants in the natural environment. Chemical techniques

of alkane analysis include gravimetric (Kawahara, 1994), fluorophotometry (Zhou et al., 2013), infrared absorption (Lay-Ekuakille et al., 2013), and gas chromatography (Krupčík et al., 2013), but samples require pre-treatment using solvent extraction or solid-phase micro-extraction. Whole-cell bioreporters have been developed to evaluate bioavailability or bioaccessibility, and even applied in real-world cases. However, they suffer from relatively low reproducibility. Raman spectroscopy was therefore employed to identify bacterial chemotaxis-related affinity to alkanes, and to quantify alkane concentrations via spectral alterations.

In Chapter 3, the impacts of nutrient ions on alkane chemotaxis of *A. baylyi* were measured *via* Raman microspectroscopy. In real-world practice, the physicochemical conditions and soil nutrients may limit the bacterial chemotaxis, accumulation and utilization on alkane molecules (Annweiler et al., 2000). Thus, to study the effects of nutrient ions such as sodium, magnesium, potassium and calcium on the chemotactic response of bacteria towards alkane molecules, Raman microspectroscopy was used to study extra ionic influences. From the ion-alkane patterns, this work confirms that extra ions exhibit differential influences on bacterial chemotactic behaviours towards pure n-alkane molecules. By interrogating Raman spectra, the impacts of different extra ions on bacterial selection and accumulation towards alkane molecules in alkane mixture are measured. This is believed to be the first study exploring Raman spectral analysis in alkane chemotaxis-related affinity and accumulation of bacteria in diverse extra ions treatments. A new perspective has been found to uncover the bacterial chemotaxis associated degradation towards alkane molecules in natural environments. By using Raman microspectroscopy, it is confirmed that nutrient ions significantly affect the access to alkane droplets, change the accumulation priority in alkane mixture, and modify the degradation of alkane molecules by bacterial cells.

In Chapter 4, bacterial chemotactic behaviours towards organic carbonaceous substances and their competitive selections in the mixture of two different carbonaceous substances were studied by Raman spectral analysis. Organic carbonaceous substances, e.g., sugar, organic acids and polyols, are fundamental for bacterial growth. Bacteria exhibit positive chemotactic responses towards some specific carbonaceous substance molecules present in culture medium (Kirby, 2009). Glucose is a major carbonaceous substance molecule exhibiting high chemo-attraction to bacteria (Singh and Arora, 2001), and carbonaceous acids such as succinate and acetate can be used as chemo-attractant in bacterial chemotaxis assays (Dailey and Berg, 1993; Sampedro et al., 2015). Bacterial chemotaxis towards carbonaceous substances is vital for their survival in natural habitats as it assists them in accessing carbonaceous substances, and determines the accumulation and utilization of carbonaceous molecules in bacterial cells. In order to investigate the chemotaxis-driven affinity and accumulation of organic carbonaceous substances by bacteria, Raman microspectroscopy was applied on three model bacterial strains, *Acinetobacter baylyi*, *Pseudomonas fluorescence* and *Escherichia coli*. An additional study on bacterial chemotactic selection of carbonaceous substance mixtures suggests that Raman microspectroscopy can successfully investigate and distinguish different scenarios of bacterial competitive interactions with carbonaceous molecules.

Chapter 5 provides a summary, conclusions and recommendations for further work.

References

Achour, A. R., Bauda, P. & Billard, P. 2007. Diversity of arsenite transporter genes from arsenic-resistant soil bacteria. *Research in microbiology*, 158**,** 128-137.

Adler, J. 1966. Chemotaxis in Bacteria. *Science*, 153**,** 708-716.

Adler, J. 1975. Chemotaxis in bacteria. *Annual review of biochemistry*, 44**,** 341-356.

Aksnes, A. & Brekken, B. 1988. Tissue degradation, amino acid liberation and bacterial decomposition of bulk stored capelin. *Journal of the Science of Food and Agriculture,* 45**,** 53-60.

Alexander, M. 1961. Microbial transformation of phosphorus. *Introduction to soil microbiology*. John Wiley and Sons, Inc.

Allain, L. R. & Vo-Dinh, T. 2002. Surface-enhanced Raman scattering detection of the breast cancer susceptibility gene BRCA1 using a silver-coated microarray platform. *Anal. Chim. Acta,* 469**,** 149-154.

Anand, G. S., Goudreau, P. N. & Stock, A. M. 1998. Activation of methylesterase CheB: evidence of a dual role for the regulatory domain. *Biochemistry,* 37**,** 14038-14047.

Andreeff, M. & Pinkel, D. 1999. *Introduction to fluorescence in situ hybridization: principles and clinical applications,* Wiley-Liss.

Annweiler, E., Materna, A., Safinowski, M., Kappler, A., Richnow, H. H., Michaelis, W. & Meckenstock, R. U. 2000. Anaerobic degradation of 2-methylnaphthalene by a sulfate-reducing enrichment culture. *Applied and environmental microbiology,* 66**,** 5329-5333.

Armitage, J. P. 1997. Behavioural responses of bacteria to light and oxygen. *Archives of Microbiology,* 168**,** 249-261.

Ashby, M. K. 2004. Survey of the number of two-component response regulator genes in the complete and annotated genome sequences of prokaryotes. *FEMS microbiology letters,* 231**,** 277-281.

Aswad, D. & Koshland, D. 1974. Role of methionine in bacterial chemotaxis. *Journal of bacteriology,* 118**,** 640-645.

Atlas, R. M. 1981. Microbial degradation of petroleum hydrocarbons: an environmental perspective. *Microbiological reviews,* 45**,** 180.

Attia, Y. & El-Zeky, M. 1989. Bioleaching of gold pyrite tailings with adapted bacteria. *Hydrometallurgy,* 22**,** 291-300.

Béja, O., Aravind, L., Koonin, E. V., Suzuki, M. T., Hadd, A., Nguyen, L. P., Jovanovich, S. B., Gates, C. M., Feldman, R. A. & Spudich, J. L. 2000. Bacterial rhodopsin: evidence for a new type of phototrophy in the sea. *Science,* 289**,** 1902-1906.

Büttner, D. & Bonas, U. 2003. Common infection strategies of plant and animal pathogenic bacteria. *Current opinion in plant biology,* 6**,** 312-319.

Baker, B. J. & Banfield, J. F. 2003. Microbial communities in acid mine drainage. *FEMS microbiology ecology,* 44**,** 139-152.

Berg, H. C. & Turner, L. 1990. Chemotaxis of bacteria in glass capillary arrays. Escherichia coli, motility, microchannel plate, and light scattering. *Biophysical Journal,* 58**,** 919-930.

Bergmans, L., Moisiadis, P., Van Meerbeek, B., Quirynen, M. & Lambrechts, P. 2005. Microscopic observation of bacteria: review highlighting the use of environmental SEM. *International endodontic journal,* 38**,** 775-788.

Berman-Frank, I., Lundgren, P. & Falkowski, P. 2003. Nitrogen fixation and photosynthetic oxygen evolution in cyanobacteria. *Research in microbiology,* 154**,** 157-164.

Berner, R. A. 1968. Calcium carbonate concretions formed by the decomposition of organic matter. *Science,* 159**,** 195-197.

Bernhard, J. M. 1989. The distribution of benthic Foraminifera with respect to oxygen concentration and organic carbon levels in shallow-water Antarctic sediments. *Limnology and Oceanography,* 34**,** 1131-1141.

Bertrand, J. J., West, J. T. & Engel, J. N. 2010. Genetic analysis of the regulation of type IV pilus

function by the Chp chemosensory system of Pseudomonas aeruginosa. *Journal of bacteriology,* 192**,** 994-1010.

Betlach, M. R. & Tiedje, J. M. 1981. Kinetic explanation for accumulation of nitrite, nitric oxide, and nitrous oxide during bacterial denitrification. *Applied and Environmental Microbiology,* 42**,** 1074-1084.

Bilwes, A. M., Alex, L. A., Crane, B. R. & Simon, M. I. 1999. Structure of CheA, a signal-transducing histidine kinase. *Cell,* 96**,** 131-141.

Block, S. M., Segall, J. E. & Berg, H. C. 1983. Adaptation kinetics in bacterial chemotaxis. *Journal of bacteriology,* 154**,** 312-323.

Bond, P. L., Hugenholtz, P., Keller, J. & Blackall, L. L. 1995. Bacterial community structures of phosphate-removing and non-phosphate-removing activated sludges from sequencing batch reactors. *Applied and Environmental Microbiology,* 61**,** 1910-1916.

Borland, C., Mcgarvey, D., Truscott, T., Codgell, R. & Land, E. J. 1987. Photophysical studies of bacteriochlorophyll a and bacteriopheophytin a—singlet oxygen generation. *Journal of Photochemistry and Photobiology B: Biology,* 1**,** 93-101.

Bovallius, A., Bucht, B., Roffey, R. & Anäs, P. 1978. Long-range air transmission of bacteria. *Applied and Environmental Microbiology,* 35**,** 1231-1232.

Bovallius, , Roffey, R. & Henningson, E. 1980. Long-range transmission of bacteria. *Annals of the New York Academy of Sciences,* 353**,** 186-200.

Bozzola, J. J. & Russell, L. D. 1999. *Electron microscopy: principles and techniques for biologists,* Jones & Bartlett Learning.

Bruun, A. F. 1957. Deep sea and abyssal depths. *Geological Society of America Memoirs,* 67**,** 641-673.

Bryant, D. A. & Frigaard, N.-U. 2006. Prokaryotic photosynthesis and phototrophy illuminated. *Trends in microbiology,* 14**,** 488-496.

Burns, R. C. & Hardy, R. W. 2012. *Nitrogen fixation in bacteria and higher plants,* Springer Science & Business Media.

Caffrey, J. M., Bano, N., Kalanetra, K. & Hollibaugh, J. T. 2007. Ammonia oxidation and ammonia-oxidizing bacteria and archaea from estuaries with differing histories of hypoxia. *The ISME journal,* 1**,** 660.

Campion, A. & Kambhampati, P. 1998. Surface-enhanced Raman scattering. *Chem. Soc. Rev.*, 27**,** 241-250.

Cao, Y. W. C., Jin, R. C. & Mirkin, C. A. 2002. Nanoparticles with Raman spectroscopic fingerprint for DNA and RNA detection. *Science,* 297**,** 1536-1540.

Chaia, E. E., Wall, L. G. & Huss-Danell, K. 2010. Life in soil by the actinorhizal root nodule endophyte Frankia. A review. *Symbiosis,* 51**,** 201-226.

Chelsky, D. & Dahlquist, F. 1980. Structural studies of methyl-accepting chemotaxis proteins of Escherichia coli: evidence for multiple methylation sites. *Proceedings of the National Academy of Sciences,* 77**,** 2434-2438.

Chen, J., Blume, H.-P. & Beyer, L. 2000. Weathering of rocks induced by lichen colonization—a review. *Catena,* 39**,** 121-146.

Christie, P. J. & Vogel, J. P. 2000. Bacterial type IV secretion: conjugation systems adapted to deliver effector molecules to host cells. *Trends in microbiology,* 8**,** 354-360.

Clark, R., Szot, S., Venkatasubramanian, K. & Schiffmann, E. 1980. Chemotactic factor inactivation by myeloperoxidase-mediated oxidation of methionine. *The Journal of Immunology,* 124**,**

2020-2026.

Coates, J. D., Cole, K. A., Chakraborty, R., O'connor, S. M. & Achenbach, L. A. 2002. Diversity and ubiquity of bacteria capable of utilizing humic substances as electron donors for anaerobic respiration. *Applied and environmental microbiology,* 68**,** 2445-2452.

Cole, J. J., Findlay, S. & Pace, M. L. 1988. Bacterial production in fresh and saltwater ecosystems: a cross-system overview. *Marine ecology progress series. Oldendorf,* 43**,** 1-10.

Courjon, D. & Bulabois, J. 1979. Real time holographic microscopy using a peculiar holographic illuminating system and rotary shearing interferometer. *Journal of Optics,* 10**,** 125.

Covich, A. P., Austen, M. C., Bärlocher, F., Chauvet, E., Cardinale, B. J., Biles, C. L., Inchausti, P., Dangles, O., Solan, M. & Gessner, M. O. 2004. The role of biodiversity in the functioning of freshwater and marine benthic ecosystems. *AIBS Bulletin,* 54**,** 767-775.

Craig, L., Pique, M. E. & Tainer, J. A. 2004. Type IV pilus structure and bacterial pathogenicity. *Nature Reviews Microbiology,* 2**,** 363.

Craig, L., Volkmann, N., Arvai, A. S., Pique, M. E., Yeager, M., Egelman, E. H. & Tainer, J. A. 2006. Type IV pilus structure by cryo-electron microscopy and crystallography: implications for pilus assembly and functions. *Molecular cell,* 23**,** 651-662.

Crowther, J. 1995. ELISA. Theory and practice, Hamana Press. *Totowa, NJ*.

Csonka, L. N. 1989. Physiological and genetic responses of bacteria to osmotic stress. *Microbiological reviews,* 53**,** 121-147.

Csuros, M. 1999. *Microbiological examination of water and wastewater*, CRC Press.

Cui, L., Chen, P., Chen, S., Yuan, Z., Yu, C., Ren, B. & Zhang, K. 2013. In situ study of the antibacterial activity and mechanism of action of silver nanoparticles by surface-enhanced Raman spectroscopy. *Analytical chemistry,* 85**,** 5436-5443.

Dailey, F. E. & Berg, H. C. 1993. Change in direction of flagellar rotation in Escherichia coli mediated by acetate kinase. *Journal of bacteriology,* 175**,** 3236-3239.

Danilatos, G. D. 1990. Theory of the gaseous detector device in the environmental scanning electron microscope. *Advances in Electronics and Electron Physics.* Elsevier.

Danilatos, G. D. & Robinson, V. 1979. Principles of scanning electron microscopy at high specimen chamber pressures. *Scanning,* 2**,** 72-82.

Das, P., Lei, W., Aziz, S. S. & Obbard, J. P. 2011. Enhanced algae growth in both phototrophic and mixotrophic culture under blue light. *Bioresource Technology,* 102**,** 3883-3887.

Davies, C. M. & Evison, L. M. 1991. Sunlight and the survival of enteric bacteria in natural waters. *Journal of Applied Bacteriology,* 70**,** 265-274.

Djordjevic, S. & Stock, A. M. 1998. Chemotaxis receptor recognition by protein methyltransferase CheR. *Nature Structural and Molecular Biology,* 5**,** 446.

Drake, H. L. & Daniel, S. L. 2004. Physiology of the thermophilic acetogen Moorella thermoacetica. *Research in microbiology,* 155**,** 869-883.

Efrima, S. & Zeiri, L. 2009. Understanding SERS of bacteria. *Journal of Raman Spectroscopy,* 40**,** 277-288.

Egerton, R. F. 2005. *Physical principles of electron microscopy*, Springer.

Ehrenreich, A. & Widdel, F. 1994. Anaerobic oxidation of ferrous iron by purple bacteria, a new type of phototrophic metabolism. *Applied and environmental microbiology,* 60**,** 4517-4526.

Ehrlich, H. & Fox, S. I. 1967. Environmental effects on bacterial copper extraction from low-grade copper sulfide ores. *Biotechnology and Bioengineering,* 9**,** 471-485.

El-Zahry, M. R., Mahmoud, A., Refaat, I. H., Mohamed, H. A., Bohlmann, H. & Lendl, B. 2015. Antibacterial effect of various shapes of silver nanoparticles monitored by SERS. *Talanta,* 138**,** 183-189.

Eswaran, H., Van Den Berg, E. & Reich, P. 1993. Organic carbon in soils of the world. *Soil science society of America journal,* 57**,** 192-194.

Farquharson, S., Shende, C., Smith, W., Huang, H., Inscore, F., Sengupta, A., Sperry, J., Sickler, T., Prugh, A. & Guicheteau, J. 2014. Selective detection of 1000 B. anthracis spores within 15 minutes using a peptide functionalized SERS assay. *Analyst,* 139**,** 6366-6370.

Faulds, K., Smith, W. E. & Graham, D. 2004. Evaluation of surface-enhanced resonance raman scattering for quantitative DNA analysis. *Anal. Chem.,* 76**,** 412-417.

Feng, J., De La Fuente-Núñez, C., Trimble, M. J., Xu, J., Hancock, R. E. & Lu, X. 2015. An in situ Raman spectroscopy-based microfluidic "lab-on-a-chip" platform for non-destructive and continuous characterization of Pseudomonas aeruginosa biofilms. *Chemical Communications,* 51**,** 8966-8969.

Fleischmann, M., Hendra, P. J. & Mcquillan, A. J. 1974. Raman spectra of pyridine adsorbed at a silver electrode. *Chemical Physics Letters,* 26**,** 163-166.

Fredrickson, J., Garland, T., Hicks, R., Thomas, J., Li, S. & Mcfadden, K. 1989. Lithotrophic and heterotrophic bacteria in deep subsurface sediments and their relation to sediment properties. *Geomicrobiology Journal,* 7**,** 53-66.

Ganesh, R., Robinson, K. G., Reed, G. D. & Sayler, G. S. 1997. Reduction of hexavalent uranium from organic complexes by sulfate-and iron-reducing bacteria. *Applied and Environmental Microbiology,* 63**,** 4385-4391.

Gest, H. 2004. The discovery of microorganisms by Robert Hooke and Antoni Van Leeuwenhoek, fellows of the Royal Society. *Notes and Records of the Royal Society,* 58**,** 187-201.

Gegner, J. A., Graham, D. R., Roth, A. F. & Dahlquist, F. W. 1992. Assembly of an MCP receptor, CheW, and kinase CheA complex in the bacterial chemotaxis signal transduction pathway. *Cell,* 70**,** 975-982.

Goldstein, J. I., Newbury, D. E., Michael, J. R., Ritchie, N. W., Scott, J. H. J. & Joy, D. C. 2017. *Scanning electron microscopy and X-ray microanalysis*, Springer.

Gounot, A. M. 1991. Bacterial life at low temperature: physiological aspects and biotechnological implications. *Journal of Applied Bacteriology,* 71**,** 386-397.

Griffiths, B. 1986. Mineralization of nitrogen and phosphorus by mixed cultures of the ciliate protozoan Colpoda steinii, the nematode Rhabditis sp. and the bacterium Pseudomonas fluorescens. *Soil Biology and Biochemistry,* 18**,** 637-641.

Gu, H., Xu, K., Xu, C. & Xu, B. 2006. Biofunctional magnetic nanoparticles for protein separation and pathogen detection. *Chemical Communications***,** 941-949.

Gupta, R. S., Mukhtar, T. & Singh, B. 1999. Evolutionary relationships among photosynthetic prokaryotes (Heliobacterium chlorum, Chloroflexus aurantiacus, cyanobacteria, Chlorobium tepidum and proteobacteria): implications regarding the origin of photosynthesis. *Molecular microbiology,* 32**,** 893-906.

Haddock, B. A. & Jones, C. W. 1977. Bacterial respiration. *Bacteriological reviews,* 41**,** 47.

Hankinson, T. & Schmidt, E. 1984. Examination of an acid forest soil for ammonia-and nitrite-oxidizing autotrophic bacteria. *Canadian Journal of Microbiology,* 30**,** 1125-1132.

Hanson, R. S. & Hanson, T. E. 1996. Methanotrophic bacteria. *Microbiological reviews,* 60**,** 439-471.

Harrison Jr, A. P. 1967. Survival of Bacteria Harmful, Effects of Light, with some Comparisons with other Adverse Physical Agents. *Annual Reviews in Microbiology,* 21**,** 143-156.

Harshey, R. M. 2003. Bacterial motility on a surface: many ways to a common goal. *Annual Reviews in Microbiology,* 57**,** 249-273.

Heimbrook, M. E., Wang, W. & Campbell, G. 1989. Staining bacterial flagella easily. *Journal of clinical microbiology,* 27**,** 2612-2615.

Henrichsen, J. 1972. Bacterial surface translocation: a survey and a classification. *Bacteriological reviews,* 36**,** 478.

Hess, J. F., Oosawa, K., Kaplan, N. & Simon, M. I. 1988. Phosphorylation of three proteins in the signaling pathway of bacterial chemotaxis. *Cell,* 53**,** 79-87.

Hill, N. & Häder, D.-P. 1997. A biased random walk model for the trajectories of swimming micro-organisms. *Journal of Theoretical Biology,* 186**,** 503-526.

Hobbie, J. E. & Crawford, C. C. 1969. Respiration Corrections for Bacterial Uptake of Dissolved Organic Compounds in Natural WATERS1. *Limnology and Oceanography,* 14**,** 528-532.

Holm, H. W. & Cox, M. F. 1975. Transformation of elemental mercury by bacteria. *Applied microbiology,* 29**,** 491-494.

Hyun, H., Zeikus, J., Longin, R., Millet, J. & Ryter, A. 1983. Ultrastructure and extreme heat resistance of spores from thermophilic Clostridium species. *Journal of bacteriology,* 156**,** 1332-1337.

Inoue, K., Kosako, Y., Suzuki, K. & Shimada, T. 1991. Peritrichous flagellation in Plesiomonas shigelloides strains. *Japanese Journal of Medical Science and Biology,* 44**,** 141-146.

Inouye, M. & Dutta, R. 2002. *Histidine kinases in signal transduction*, Academic Press.

Jacobson, A. 1972. Role of F pili in the penetration of bacteriophage fl. *Journal of virology,* 10**,** 835-843.

Jannasch, H. W. & Mottl, M. J. 1985. Geomicrobiology of deep-sea hydrothermal vents. *Science,* 229**,** 717-725.

Joshi, M. & Deshpande, J. 2010. Polymerase chain reaction: methods, principles and application. *International Journal of Biomedical Research,* 2**,** 81-97.

Kawahara, F. K. 1994. Method for the gravimetric determination of oil and grease. Google Patents.

Kim, C., Jackson, M., Lux, R. & Khan, S. 2001. Determinants of chemotactic signal amplification in Escherichia coli1. *Journal of molecular biology,* 307**,** 119-135.

Kirby, J. R. 2009. Chemotaxis-like regulatory systems: unique roles in diverse bacteria. *Annu Rev Microbiol,* 63**,** 45-59.

Kleppe, K., Ohtsuka, E., Kleppe, R., Molineux, I. & Khorana, H. 1971. Studies on polynucleotides: XCVI. Repair replication of short synthetic DNA's as catalyzed by DNA polymerases. *Journal of molecular biology,* 56**,** 341-361.

Kneipp, J., Kneipp, H. & Kneipp, K. 2008. SERS--a single-molecule and nanoscale tool for bioanalytics. *Chem Soc Rev,* 37**,** 1052-60.

Kneipp, K., Kneipp, H., Itzkan, I., Dasari, R. R. & Feld, M. S. 2002. Surface-enhanced Raman scattering and biophysics. *Journal of Physics: Condensed Matter,* 14**,** R597-R624.

Kopáček, J., Cosby, B. J., Evans, C. D., Hruška, J., Moldan, F., Oulehle, F., Šantrůčková, H., Tahovská, K. & Wright, R. F. 2013. Nitrogen, organic carbon and sulphur cycling in terrestrial ecosystems: linking nitrogen saturation to carbon limitation of soil microbial processes. *Biogeochemistry,* 115**,** 33-51.

Krulwich, T. A. & Guffanti, A. A. 1983. Physiology of acidophilic and alkalophilic bacteria. *Advances*

in microbial physiology. Elsevier.

Krupčík, J., Gorovenko, R., Špánik, I., Bočková, I., Sandra, P. & Armstrong, D. W. 2013. On the use of ionic liquid capillary columns for analysis of aromatic hydrocarbons in low-boiling petrochemical products by one-dimensional and comprehensive two-dimensional gas chromatography. *Journal of Chromatography A,* 1301**,** 225-236.

Kucey, R. 1983. Phosphate-solubilizing bacteria and fungi in various cultivated and virgin Alberta soils. *Canadian Journal of Soil Science,* 63**,** 671-678.

Landsberg, G. & Mandelstam, L. 1928. Eine neue Erscheinung bei der Lichtzerstreuung in Krystallen. *Naturwissenschaften,* 16**,** 557-558.

Lay-Ekuakille, A., Palamara, I., Caratelli, D. & Morabito, F. 2013. Experimental infrared measurements for hydrocarbon pollutant determination in subterranean waters. *Review of Scientific Instruments,* 84**,** 015103.

Lazcka, O., Del Campo, F. J. & Munoz, F. X. 2007. Pathogen detection: A perspective of traditional methods and biosensors. *Biosensors and bioelectronics,* 22**,** 1205-1217.

Leahy, J. G. & Colwell, R. R. 1990. Microbial degradation of hydrocarbons in the environment. *Microbiological reviews,* 54**,** 305-315.

Lehmann, J., Gaunt, J. & Rondon, M. 2006. Bio-char sequestration in terrestrial ecosystems–a review. *Mitigation and adaptation strategies for global change,* 11**,** 403-427.

Leifson, E. 1951. Staining, shape, and arrangement of bacterial flagella. *Journal of bacteriology,* 62**,** 377.

Levsky, J. M. & Singer, R. H. 2003. Fluorescence in situ hybridization: past, present and future. *Journal of cell science,* 116**,** 2833-2838.

Li, M., Xu, J., Romero-Gonzalez, M., Banwart, S. A. & Huang, W. E. 2012. Single cell Raman spectroscopy for cell sorting and imaging. *Current opinion in biotechnology,* 23**,** 56-63.

Liu, S. Q. 2003. Practical implications of lactate and pyruvate metabolism by lactic acid bacteria in food and beverage fermentations. *International journal of food microbiology,* 83**,** 115-131.

Lombardi, J. R. & Birke, R. L. 1986. Charge-transfer theory of surface-enhanced Raman spectroscopy: Herzberg-Teller contributions. *J. Chem. Phys.,* 84**,** 4174-4180.

Long, S. R. 1989. Rhizobium-legume nodulation: life together in the underground. *Cell,* 56**,** 203-214.

Lovley, D. R. & Phillips, E. J. 1986. Organic matter mineralization with reduction of ferric iron in anaerobic sediments. *Applied and environmental microbiology,* 51**,** 683-689.

Lowy, J. & Hanson, J. 1965. Electron microscope studies of bacterial flagella. *Journal of molecular biology,* 11**,** 293-IN30.

Lundgren, D. & Silver, M. 1980. Ore leaching by bacteria. *Annual reviews in microbiology,* 34**,** 263-283.

Lupas, A. & Stock, J. 1989. Phosphorylation of an N-terminal regulatory domain activates the CheB methylesterase in bacterial chemotaxis. *Journal of Biological Chemistry,* 264**,** 17337-17342.

Lynch, J. & Whipps, J. 1990. Substrate flow in the rhizosphere. *Plant and soil,* 129**,** 1-10.

Müller, V. 2001. Bacterial fermentation. *Encylopedia of Life Sciences*.

Macnab, R. M. 1999. The bacterial flagellum: reversible rotary propellor and type III export apparatus. *Journal of bacteriology,* 181**,** 7149-7153.

Macnab, R. M. & Koshland, D. 1972. The gradient-sensing mechanism in bacterial chemotaxis. *Proceedings of the National Academy of Sciences,* 69**,** 2509-2512.

Madigan, M. T. 2003. Anoxygenic phototrophic bacteria from extreme environments. *Photosynthesis*

research, 76**,** 157-171.

Martiny, J. B. H., Bohannan, B. J., Brown, J. H., Colwell, R. K., Fuhrman, J. A., Green, J. L., Horner-Devine, M. C., Kane, M., Krumins, J. A. & Kuske, C. R. 2006. Microbial biogeography: putting microorganisms on the map. *Nature Reviews Microbiology,* 4**,** 102.

Matsumura, M. & Aiba, S. 1985. Screening for thermostable mutant of kanamycin nucleotidyltransferase by the use of a transformation system for a thermophile, Bacillus stearothermophilus. *Journal of Biological Chemistry,* 260**,** 15298-15303.

McCreery, R. L. 1996. *Modern Techniques in Raman Spectroscopy,* Chichester–New York–Brisbane–Toronto–Singapore.

Mcnay, G., Eustace, D., Smith, W. E., Faulds, K. & Graham, D. 2011. Surface-enhanced Raman scattering (SERS) and surface-enhanced resonance Raman scattering (SERRS): a review of applications. *Appl Spectrosc,* 65**,** 825-37.

Mertz, J. 2010. *Introduction to optical microscopy*, Roberts.

Merz, A. J., So, M. & Sheetz, M. P. 2000. Pilus retraction powers bacterial twitching motility. *Nature,* 407**,** 98.

Michael, T., John, M. & Jack, P. 2002. Brock microbiology of microorganism. *New Jersey. ISBN,* 10**,** 130662712.

Mine, Y. 1997. Separation of Salmonella enteritidis from experimentally contaminated liquid eggs using a hen IgY immobilized immunomagnetic separation system. *Journal of agricultural and food chemistry,* 45**,** 3723-3727.

Mortimer, C. H. 1971. Chemical exchanges between sediments and water in the great lakes-speculations on probable regulatory mechanisms 1. *Limnology and Oceanography,* 16**,** 387-404.

Mukamel, S. 1999. *Principles of nonlinear optical spectroscopy*, Oxford University Press on Demand.

Mullis, K., Faloona, F., Scharf, S., Saiki, R., Horn, G. & Erlich, H. Specific enzymatic amplification of DNA in vitro: the polymerase chain reaction. Cold Spring Harbor symposia on quantitative biology, 1986. Cold Spring Harbor Laboratory Press, 263-273.

Mulvaney, S. P., Musick, M. D., Keating, C. D. & Natan, M. J. 2003. Glass-coated, analyte-tagged nanoparticles: A new tagging system based on detection with surface-enhanced raman scattering. *Langmuir,* 19**,** 4784-4790.

Munro, H. & Fleck, A. 1969. Analysis of tissues and body fluids for nitrogenous constituents. *Mammalian protein metabolism,* 3**,** 423-525.

Murphy, D. B. 2002. *Fundamentals of light microscopy and electronic imaging*, John Wiley & Sons.

Nanda, S. S., Yi, D. K. & Kim, K. 2016. Study of antibacterial mechanism of graphene oxide using Raman spectroscopy. *Scientific reports,* 6.

Nester, E. W., Roberts, C. E., Pearsall, N. & Mccarthy, B. 1978. *Microbiology*, Holt, Rinehart and Winston.

Nies, D. H. 1992. Resistance to cadmium, cobalt, zinc, and nickel in microbes. *Plasmid,* 27**,** 17-28.

Nitzan, Y. & Ashkenazi, H. 2001. Photoinactivation of Acinetobacter baumannii and Escherichia coli B by a cationic hydrophilic porphyrin at various light wavelengths. *Current microbiology,* 42**,** 408-414.

O'Malley, M. A. 2009. What did Darwin say about microbes, and how did microbiology respond? *Trends in microbiology,* 17**,** 341-347.

Olsen, C. F., Cutshall, N. & Larsen, I. 1982. Pollutant—particle associations and dynamics in coastal

marine environments: a review. *Marine Chemistry,* 11**,** 501-533.

Ou, J. T. & Anderson, T. F. 1970. Role of pili in bacterial conjugation. *Journal of bacteriology,* 102**,** 648-654.

Parkinson, J. S. 1976. cheA, cheB, and cheC genes of Escherichia coli and their role in chemotaxis. *Journal of bacteriology,* 126**,** 758-770.

Parkinson, J. S. 2010. Signaling mechanisms of HAMP domains in chemoreceptors and sensor kinases. *Annual review of microbiology,* 64**,** 101-122.

Parkinson, J. S., Ames, P. & Studdert, C. A. 2005. Collaborative signaling by bacterial chemoreceptors. *Current opinion in microbiology,* 8**,** 116-121.

Pasco, N., Baronian, K., Jeffries, C. & Hay, J. 2000. Biochemical mediator demand–a novel rapid alternative for measuring biochemical oxygen demand. *Applied microbiology and biotechnology,* 53**,** 613-618.

Patterson, B. K., Till, M., Otto, P., Goolsby, C., Furtado, M. R., Mcbride, L. J. & Wolinsky, S. M. 1993. Detection of HIV-1 DNA and messenger RNA in individual cells by PCR-driven in situ hybridization and flow cytometry. *Science,* 260**,** 976-979.

Persson, B. N. 1981. On the theory of surface-enhanced Raman scattering. *Chem. Phys. Lett.,* 82**,** 561-565.

Pollice, A., Tandoi, V. & Lestingi, C. 2002. Influence of aeration and sludge retention time on ammonium oxidation to nitrite and nitrate. *Water research,* 36**,** 2541-2546.

Qin, L., Banholzer, M. J., Millstone, J. E. & Mirkin, C. A. 2007. Nanodisk codes. *Nano Letters,* 7 (12)**,** 3849-3853.

Rabinow, P. 1996. Making PCR: A Story of Biotechnology. Chicago: Univ. Chicago Press.

Raman, C. V. & Krishnan, K. S. 1928. A new type of second radiation. *Nature,* 121**,** 501-502.

Rawlings, D. E. 2005. Characteristics and adaptability of iron-and sulfur-oxidizing microorganisms used for the recovery of metals from minerals and their concentrates. *Microbial cell factories,* 4**,** 13.

Reed, R. & Reed, G. 1948. " Drop plate" method of counting viable bacteria. *Canadian Journal of Research,* 26**,** 317-326.

Revsbech, N. P., Sorensen, J., Blackburn, T. H. & Lomholt, J. P. 1980. Distribution of oxygen in marine sediments measured with microelectrodes 1. *Limnology and Oceanography,* 25**,** 403-411.

Richardson, D. J. 2000. Bacterial respiration: a flexible process for a changing environment. *Microbiology,* 146**,** 551-571.

Robertson, G. P. & Groffman, P. 2007. Nitrogen transformations. *Soil Microbiology, Ecology and Biochemistry (Third Edition)*. Elsevier.

Rohde, A., Hammerl, J. A., Boone, I., Jansen, W., Fohler, S., Klein, G., Dieckmann, R. & Al Dahouk, S. 2017. Overview of validated alternative methods for the detection of foodborne bacterial pathogens. *Trends in Food Science & Technology,* 62**,** 113-118.

Rosso, L., Lobry, J., Bajard, S. & Flandrois, J. 1995. Convenient model to describe the combined effects of temperature and pH on microbial growth. *Applied and environmental microbiology,* 61**,** 610-616.

Russo, U. & Long, G. J. 2013. Oxidation States of Iron. *Mössbauer Spectroscopy Applied to Inorganic Chemistry,* 3**,** 289.

Sánchez-Porro, C., Martin, S., Mellado, E. & Ventosa, A. 2003. Diversity of moderately halophilic

bacteria producing extracellular hydrolytic enzymes. *Journal of applied microbiology,* 94**,** 295-300.

Sampedro, I., Parales, R. E., Krell, T. & Hill, J. E. 2015. Pseudomonas chemotaxis. *FEMS Microbiol Rev,* 39**,** 17-46.

Sanders, D. A., Gillece-Castro, B., Stock, A., Burlingame, A. & Koshland, D. 1989. Identification of the site of phosphorylation of the chemotaxis response regulator protein, CheY. *Journal of Biological Chemistry,* 264**,** 21770-21778.

Saurin, W., Köster, W. & Dassai, E. 1994. Bacterial binding protein-dependent permeases: characterization of distinctive signatures for functionally related integral cytoplasmic membrane proteins. *Molecular microbiology,* 12**,** 993-1004.

Schmidt, T. & Schaechter, M. 2012. *Topics in ecological and environmental microbiology*, Elsevier.

Shi, L. Z., Nascimento, J., Chandsawangbhuwana, C., Berns, M. W. & Botvinick, E. L. 2006. Real-time automated tracking and trapping system for sperm. *Microsc Res Tech,* 69**,** 894-902.

Singh, R. 2002. CV Raman and the Discovery of the Raman Effect. *Physics in Perspective,* 4**,** 399-420.

Singh, T. & Arora, D. K. 2001. Motility and chemotactic response of Pseudomonas fluorescens toward chemoattractants present in the exudate of Macrophomina phaseolina. *Microbiol Res,* 156**,** 343-51.

Smekal, A. 1923. Zur quantentheorie der dispersion. *Naturwissenschaften,* 11**,** 873-875.

Smith, R. A. & Parkinson, J. S. 1980. Overlapping genes at the cheA locus of Escherichia coli. *Proceedings of the National Academy of Sciences,* 77**,** 5370-5374.

Sourjik, V. & Berg, H. C. 2002. Receptor sensitivity in bacterial chemotaxis. *Proceedings of the National Academy of Sciences,* 99**,** 123-127.

Speight, J. G. 2005. *Lange's handbook of chemistry*, McGraw-Hill New York.

Staley, J. T. 2006. The bacterial species dilemma and the genomic–phylogenetic species concept. *Philosophical Transactions of the Royal Society B: Biological Sciences,* 361**,** 1899-1909.

Staley, J. T. & Konopka, A. 1985. Measurement of in situ activities of nonphotosynthetic microorganisms in aquatic and terrestrial habitats. *Annual Reviews in Microbiology,* 39**,** 321-346.

Stanier, R., Doudoroff, M., Kunisawa, R. & Contopoulou, R. 1959. The role of organic substrates in bacterial photosynthesis. *Proceedings of the National Academy of Sciences,* 45**,** 1246-1260.

Stewart, J. & Tiessen, H. 1987. Dynamics of soil organic phosphorus. *Biogeochemistry,* 4**,** 41-60.

Stock, A. M., Mottonen, J. M., Stock, J. B. & Schutt, C. E. 1989. Three-dimensional structure of CheY, the response regulator of bacterial chemotaxis. *Nature,* 337**,** 745.

Stock, A. M., Robinson, V. L. & Goudreau, P. N. 2000. Two-component signal transduction. *Annual review of biochemistry,* 69**,** 183-215.

Stotzky, G. & Babich, H. 1986. Survival of, and genetic transfer by, genetically engineered bacteria in natural environments. *Adv. Appl. Microbiol,* 31**,** 93-138.

Straub, K. L., Benz, M., Schink, B. & Widdel, F. 1996. Anaerobic, nitrate-dependent microbial oxidation of ferrous iron. *Applied and environmental microbiology,* 62**,** 1458-1460.

Swain, K. E. & Falke, J. J. 2007. Structure of the conserved HAMP domain in an intact, membrane-bound chemoreceptor: a disulfide mapping study. *Biochemistry,* 46**,** 13684-13695.

Swanson, R. V., Alex, L. A. & Simon, M. I. 1994. Histidine and aspartate phosphorylation: two-component systems and the limits of homology. *Trends in biochemical sciences,* 19**,** 485-490.

Tannock, G. W., Fuller, R., Smith, S. & Hall, M. 1990. Plasmid profiling of members of the family Enterobacteriaceae, lactobacilli, and bifidobacteria to study the transmission of bacteria from mother to infant. *Journal of Clinical Microbiology,* 28**,** 1225-1228.

Thomas, C. M. & Nielsen, K. M. 2005. Mechanisms of, and barriers to, horizontal gene transfer between bacteria. *Nature reviews microbiology,* 3**,** 711.

Torsvik, V., Goksøyr, J. & Daae, F. L. 1990. High diversity in DNA of soil bacteria. *Applied and environmental microbiology,* 56**,** 782-787.

Turnbaugh, P. J., Ley, R. E., Hamady, M., Fraser-Liggett, C. M., Knight, R. & Gordon, J. I. 2007. The human microbiome project. *Nature,* 449**,** 804.

Ulukanli, Z. & Diğrak, M. 2002. Alkaliphilic micro-organisms and habitats. *Turkish Journal of Biology,* 26**,** 181-191.

Uroz, S., Oger, P., Lepleux, C., Collignon, C., Frey-Klett, P. & Turpault, M.-P. 2011. Bacterial weathering and its contribution to nutrient cycling in temperate forest ecosystems. *Research in microbiology,* 162**,** 820-831.

Vadstein, O. 2000. Heterotrophic, planktonic bacteria and cycling of phosphorus. *Advances in microbial ecology*. Springer.

Van Manen, H.-J., Kraan, Y. M., Roos, D. & Otto, C. 2005. Single-cell Raman and fluorescence microscopy reveal the association of lipid bodies with phagosomes in leukocytes. *Proceedings of the National Academy of Sciences of the United States of America,* 102**,** 10159-10164.

Veldkamp, H., Van Gemerden, H., Harder, W. & Laanbroek, H. 1984. Competition among bacteria: an overview. *Current perspectives in microbial ecology***,** 279-290.

Vieira, F. & Nahas, E. 2005. Comparison of microbial numbers in soils by using various culture media and temperatures. *Microbiological research,* 160**,** 197-202.

Vishniac, W. & Trudinger, P. A. 1962. V. Carbon Dioxide Fixation and Substrate Oxidation in the Chemosynthetic Sulfur and Hydrogen Bacteria. *Bacteriological reviews,* 26**,** 168.

Vladimirov, N. & Sourjik, V. 2009. Chemotaxis: how bacteria use memory. *Biological chemistry,* 390**,** 1097-1104.

Wadhams, G. H. & Armitage, J. P. 2004. Making sense of it all: bacterial chemotaxis. *Nature Reviews Molecular Cell Biology,* 5**,** 1024-1037.

Wang, Y., Huang, W. E., Cui, L. & Wagner, M. 2016. Single cell stable isotope probing in microbiology using Raman microspectroscopy. *Curr Opin Biotechnol,* 41**,** 34-42.

Wang, Y.-T. & Shen, H. 1995. Bacterial reduction of hexavalent chromium. *Journal of Industrial Microbiology,* 14**,** 159-163.

West, A. H. & Stock, A. M. 2001. Histidine kinases and response regulator proteins in two-component signaling systems. *Trends in biochemical sciences,* 26**,** 369-376.

White, D., Drummond, J. T. & Fuqua, C. 2007. *The physiology and biochemistry of prokaryotes*, Oxford University Press New York.

Widdel, F., Schnell, S., Heising, S., Ehrenreich, A., Assmus, B. & Schink, B. 1993. Ferrous iron oxidation by anoxygenic phototrophic bacteria. *Nature,* 362**,** 834.

Wilhelm, J. & Pingoud, A. 2003. Real-time polymerase chain reaction. *Chembiochem,* 4**,** 1120-1128.

Williams, D. B. & Carter, C. B. 1996. The transmission electron microscope. *Transmission electron microscopy*. Springer.

Wilson, D. R. & Beveridge, T. J. 1993. Bacterial flagellar filaments and their component flagellins. *Canadian journal of microbiology,* 39**,** 451-472.

Wilson, T. & Sheppard, C. 1984. *Theory and practice of scanning optical microscopy*, Academic Press London.

Woese, C. R., Kandler, O. & Wheelis, M. L. 1990. Towards a natural system of organisms: proposal for the domains Archaea, Bacteria, and Eucarya. *Proceedings of the National Academy of Sciences,* 87**,** 4576-4579.

Wu, X., Huang, Y.-W., Park, B., Tripp, R. A. & Zhao, Y. 2015. Differentiation and classification of bacteria using vancomycin functionalized silver nanorods array based surface-enhanced Raman spectroscopy and chemometric analysis. *Talanta,* 139**,** 96-103.

Yang, S., Dai, X., Stogin, B. B. & Wong, T.-S. 2016. Ultrasensitive surface-enhanced Raman scattering detection in common fluids. *Proceedings of the National Academy of Sciences,* 113**,** 268-273.

Young, K. D. 2003. Bacterial shape. *Molecular microbiology,* 49**,** 571-580.

Young, K. D. 2006. The selective value of bacterial shape. *Microbiology and molecular biology reviews,* 70**,** 660-703.

Zeikus, J. 1977. The biology of methanogenic bacteria. *Bacteriological reviews,* 41**,** 514.

Zeikus, J. 1979. Thermophilic bacteria: ecology, physiology and technology. *Enzyme and Microbial Technology,* 1**,** 243-252.

Zhou, H., Yang, D., Ivleva, N. P., Mircescu, N. E., Niessner, R. & Haisch, C. 2014. SERS detection of bacteria in water by in situ coating with Ag nanoparticles. *Analytical chemistry,* 86**,** 1525-1533.

Zhou, Z., Guo, L., Shiller, A. M., Lohrenz, S. E., Asper, V. L. & Osburn, C. L. 2013. Characterization of oil components from the Deepwater Horizon oil spill in the Gulf of Mexico using fluorescence EEM and PARAFAC techniques. *Marine Chemistry,* 148**,** 10-21.

Zurawell, R. W., Chen, H., Burke, J. M. & Prepas, E. E. 2005. Hepatotoxic cyanobacteria: a review of the biological importance of microcystins in freshwater environments. *Journal of Toxicology and Environmental Health, Part B,* 8**,** 1-37.

Zwietering, M., Jongenburger, I., Rombouts, F. & Van't Riet, K. 1990. Modeling of the bacterial growth curve. *Applied and environmental microbiology,* 56**,** 1875-1881.

Chapter 1

Diagnose Pathogens in Drinking Water via Magntic Surface-Enhanced Raman Scattering (SERS) Assay

Hanbing Li, Li Cui, Francis L. Martin, Dayi Zhang

Materials Today: Proceedings, 2017, 4, 25-31

Contribution:

- I prepared the samples required for the project;
- I processed and acquired all data and carried out computational analysis;
- I prepared the draft and figures of manuscript.

Available online at www.sciencedirect.com

ScienceDirect

Materials Today: Proceedings 4 (2017) 25–31

materialstoday: PROCEEDINGS

www.materialstoday.com/proceedings

Functional nanomaterials in Industrial Applications: Academic - Industry Meet

Diagnose Pathogens in Drinking Water via Magnetic Surface-Enhanced Raman Scattering (SERS) Assay

Hanbing Li[a], Cui Li[a,b], Francis L. Martin[a], Dayi Zhang[a,*]

[a]*Lancaster Environment Centre, Lancaster University, Lancaster LA1 2YQ, UK*
[b]*Key Laboratory of Urban Pollutant Conversion, Institute of Urban Environment, Chinese Academy of Sciences, Xiamen 361021, China*

Abstract

Rapid identification and diagnosis of bacteria and other microorganisms is a great challenge for drinking water safety due to the increasing frequency of pathogenic infections. Raman spectroscopy is a non-destructive tool to characterize the biochemical fingerprints of bacterial cells and its signal can be improved by surface-enhanced Raman scattering (SERS). Thus, Raman scattering has a huge potential in fast diagnosis of pathogens in drinking water, with low cost and high reproducibility. In this work, we developed a novel fast diagnosis method to detect aquatic pathogens via magnetic SERS assay. With chemical co-precipitation synthesis and surface glucose reduction, the silver-coated magnetic nanoparticles (Ag@MNPs) had a well-developed core-shell structure and high efficiency to capture bacterial cells. Ag@MNPs achieved 10^3 enhancement factor for rhodamine 6G and the limit of detection was 10^{-9} M. The magnetic SERS assay also successfully detected various bacteria (*A. baylyi* and *E. coli*) with high sensitivity (10^5 CFU/mL). This platform provided a promising and easy-operation approach for pathogen detection for food and drinking water safety.

Selection and Peer-review under responsibility of the Conference Committee Members of Functional Nanomaterials in Industrial Applications.

Keywords: magnetic nanoparticles (MNPs); silver-coated MNPs (Ag@MNPs); Raman spectroscopy; surface-enhanced Raman scattering (SERS)

* Corresponding author. Tel.: +44-152-451-0288; fax: +44-152-451-0082.
E-mail address: d.zhang@lancaster.ac.uk

Selection and Peer-review under responsibility of the Conference Committee Members of Functional Nanomaterials in Industrial Applications.

1. Introduction

Millions of cases of diseases are caused by pathogens in drinking water [1, 2], though they exist at low concentration and are hard to identify. Many diagnosis methods therefore are developed to rapidly detect these pathogens [3], as polymerase chain reaction (PCR) [4, 5], colony forming [6] and staining [7], but the majority of them are time-consuming and not suitable for worldwide application in practice. It raises great chances for novel technical development for water resource protection and water treatment to rapidly recognize aquatic pathogens addressing drinking water safety issues.

Magnetic nanoparticles (MNPs) have been widely applied in biological science for its affinity to biological molecules [8], such as bioenergy recovery [9], drug delivery [10] and drinking water purification [11]. In environmental science, most relative research has addressed the magnetisms improvement [12, 13] or surface modification to enhance bacteria capturing efficiency [14]. There is limited work on how to use MNPs as a diagnosis tool in quantifying pathogens in drinking water.

Raman microspectroscopy is a promising method for bacterial detection [15]. To improve the signal intensity, surface-enhanced Raman scattering (SERS) was developed [16] and used in diagnosis of pathogens in drinking water [17]. However, direct application of SERS requires the mixture and separation of bacterial cells with suspended Ag/Au nanoparticles [18] or bacteria capture on mesostructured materials supported with Ag/Au nanoparticles [19]. The former approach suffers from the difficulties in recovering Ag/Au nanoparticles from the samples, and the latter one faces the challenges that the low cell counts in water samples means the low capture efficiency. Considering the magnetic enrichment of MNPs and SERS active substrate Ag/Au, some surface modification has been applied to combine these two types of nanomaterials together in detecting pollutants [20], biomarkers [21] or pathogens [22].

Here, we developed a novel high-sensitive screening method for rapid detection of pathogens in drinking water with silver-coated MNPs (Ag@MNPs) by magnetic capturing and SERS diagnosis. The limit of detection for bacteria was significantly improved, attributing to the magnetic enrichment and SERS signal enhancement which were simultaneously achieved by Ag@MNPs.

2. Experimental Section

2.1. Synthesis of silver coated magnetic nanoparticles

The synthesis of MNPs followed chemical co-precipitation [23] and Ag surface coating was achieved by glucose reduction. Briefly, 1.0 M $FeCl_3$ (2.0 mL in 1.0 M HCl) and 2.0 M $FeCl_2$ (0.5 mL in 1.0 M HCl) were mixed and homologized, with 25 mL NaOH (2.5 M) dropwisely added until the appearance of dark iron oxide precipitates. With further 30 min vortex, the iron oxide suspension was separated by permanent magnet and washed by deionized water until neutral pH. The synthesized MNPs were further coated with silver as SERS active substrate by mixing 1 mL MNPs with a proper weight of Ag_2SO_4 to reach a 1:20 (MNPs:Ag_2SO_4) molar ratio. After adding 0.5 g glucose and sonicated for 15 min, the suspension was heated to 80ºC in a water bath and slowly stirred for 1 hour. The MNPs turned from dark into brownish colour, and the Ag@MNPs were further stirred for 30 minutes until room temperature. Separated by permanent magnet and washed by deionized water, Ag@MNPs were stored for further experiment and analysis.

2.2. Bacterial strains and cultivation

In this study, the two bacterial strains were *Acinetobacter baylyi* ADP1 and *Escherichia coli* JM109, with close phylotypic relationship to clinical pathogens *Acinetobacter baumannii* and *Escherichia coli* O157:H7. The strains were grown in sterile Lysogeny Broth medium for 16 hours, at 30°C for *A. baylyi* and 37°C for *E. coli*, respectively. The cell suspensions were further centrifuged at 4,000 rpm for 5 min and washed three times by sterile deionized water. Afterwards, the bacterial cells were serially diluted to 10^8 CFU/mL and 10^5 CFU/mL for Raman microspectroscopy analysis.

2.3. Bacteria capture and Raman microspectroscopy analysis

By adding the MNPs or Ag@MNPs suspension (5 μL) into diluted cell suspension or rhodamine 6G (R6G) samples (1 mL), the mixture was cultivated for 10 min and the magnetic pellets were harvested by permanent magnet. The pellet was then washed by deionized water and ethanol five times for Raman microspectroscopy analysis, obtained by InVia Raman microscopy (Horiba, UK) with 785-nm excitation laser (100% and 1% power for normal Raman and SERS spectrum respectively), 10 second exposure time and a 500-2000 cm^{-1} spectral range. For all the spectral measurement, at least twenty biological replicates were randomly selected and analysed.

2.4. Chemical and biological analysis

The phase identification of synthesized MNPs and Ag@MNPs nanocomposites was carried out by X-ray diffraction (XRD, D8-Advance, Bruker, UK). The magnetic properties were measured by a vibrating sample magnetometer (VSM, Lake Shore, 7304, USA) at 25°C and in a magnetic field varying from -1.7 T to +1.7 T. The Raman spectra were first subtracted by the IRootLab Matlab interface for spectra truncation between 500-2000 cm-1 and baseline correction (Martin et al., 2010). The Raman signal intensity of R6G was calculated at the bands of 1514, 1365, 1310, 1184, 774 and 614 cm^{-1}. To calculate the capture efficiency of MNPs and Ag@MNPs towards bacteria cells, the number of total and magnetic-free bacteria was determined by quantitative polymerase chain reaction (qPCR) respectively according to our previous study (Zhao et al., 2016). The 16S rRNA primer pair was 341F (5'-CCTACGGGNGGCWGCAG-3') and 802R (5'-TACNVGGGTATCTAATCC-3'). Each 10 μL qPCR reaction system contained 1 μL of each primer, 1 μL DNA template, 2 μL molecular water and 5 μL iTaq™ Universal SYBR® Green Supermix (BioRad, USA). The thermos cycling parameters followed: 94ºC for 3 min; 34 cycles of 94ºC for 45 s, 52ºC for 45 s, 72ºC for 45 s and 80ºC for 15 s for fluorescence data acquisition. Standard curves were obtained with serial dilutions of quantified plasmid DNA containing the fragment of 16S rRNA.

3. Results and Discussion

3.1. Characterization of silver-coated magnetic nanoparticles

The XRD pattern (Fig. 1a) identified the diffraction peaks of synthesized MNPs as 2θ=30.0°, 35.4°, 43.2°, 53.6°, 57.1° and 62.7°, indexed to (220), (311), (400), (422), (511) and (440) lattice planes [24]. For Ag@MNPs, the key diffraction peaks were 2θ = 38.1°, 44.3° and 64.4°, indexed to (111), (200) and (220) lattice planes [25]. The characteristic diffraction peaks of pure MNPs were significantly weakened and hardly distinguished on Ag@MNPs (black triangle in Fig. 1a). The results proved that Ag@MNPs nanocomposites had a well core-shell structure with fine Ag-coating on MNPs surface. Our magnetization test further illustrated that both the magnetization curves behaved the *S* shape (Figure 1b). The highest saturation magnetization of MNPs and Ag@MNPs was 44.3 emu/g and 37.9 emu/g respectively. It was worth mentioning that the magnetic separation of MNPs and Ag@MNPs were similar, and both supernatants were completely transparent. These results indicated limited magnetism loss after Ag-coating and the strong magnetic harvesting capacity of Ag@MNPs, suggesting that Ag@MNPs could be effectively controlled by magnetic field.

Ag@MNPs maintained high capture efficiency for bacterial cells (Fig. 2). From the results of qPCR, the original concentration of *E. coli* and *A. baylyi* suspension was 1.03×10^9 CFU/mL and 1.79×10^8 CFU/mL, respectively. After magnetic separation by MNPs and Ag@MNPs, the amount of magnetic-free bacteria in the supernatant was 5.0×10^4 CFU/mL (MNPs) and 17.6×10^4 CFU/mL (Ag@MNPs) for *E. coli*, and 4.6×10^4 CFU/mL (MNPs) and 2.8×10^4 CFU/mL (Ag@MNPs) for *A. baylyi*, respectively. The capture efficiency of MNPs and Ag@MNPs were both higher than 99.5% for *E. coli* and 99.9% for *A. baylyi*. Such similar capture efficiency indicated that: 1) Ag-coating showed limited impacts on the surface electrostatic properties of MNPs and the electrostatic attraction was attributed to the positively charged MNPs towards negative bacterial cells; 2) Ag@MNPs capturing was non-selective and could be used for various bacterial strains. Different from previous research which employed polymers to achieve high bacteria capture efficiency [8], our method directly coated Ag on naked MNPs and minimized the

disturbance of coating polymers on SERS signal. Besides, we did not introduce silicon dioxide shell for surface Ag- or Au-coating [26] and therefore maintained the high magnetism and strong affinity to bacteria of Ag@MNPs. Meanwhile, Ag@MNPs were not further functionalized with antibody conjugation to target specific bacteria as previous study [27, 28]. It broadened the application area of this magnetic assay for all types of pathogen detection in drinking water by direct electrostatic attraction. Given these advantages, the Ag@MNPs assay was therefore easy to be used for bacteria capture and magnetic enrichment for further SERS analysis.

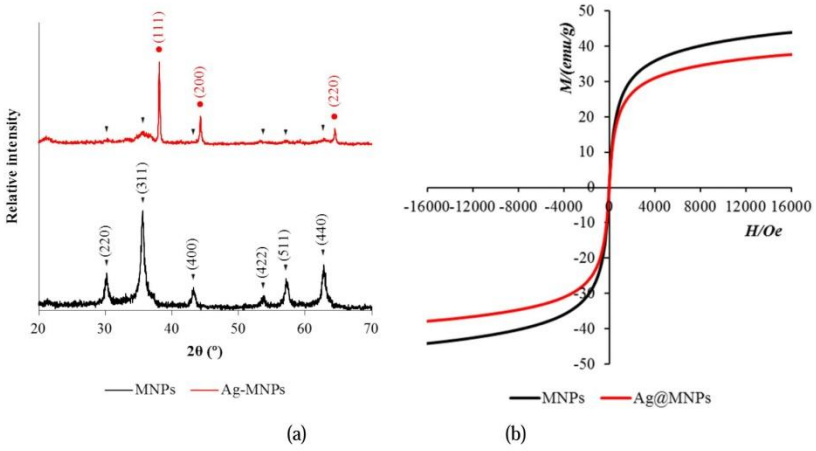

Fig. 1. The XRD pattern (a) and magnetization curve (b) of MNPs and Ag@MNPs nanocomposites.

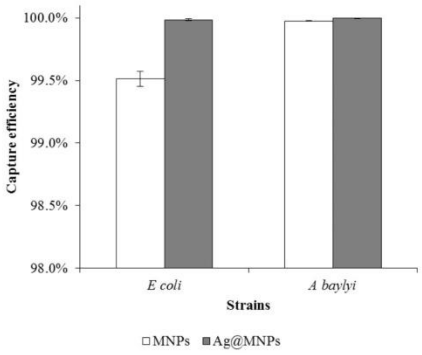

Fig. 2. Bacteria capture efficiency of MNPs and Ag@MNPs.

3.2. SERS enhancement of Ag@MNPs

Strong and stable SERS signal was obtained in the treatment of R6G with Ag@MNPs, proving the SERS enhancement by Ag@MNPs nanocomposite, as illustrated in Fig. 3a. Since R6G is a fluorescent xanthene derivative that possesses strong Raman effect when excitation laser emitting into its adsorption band [29], it was employed here to validate the enhancement of Ag@MNPs on Raman scattering. The predominant Raman shifts of R6G were at 1185,

1498, 1367 and 1310 cm^{-1} attributing to in-plane C-C stretch vibrations, 611 cm^{-1} for C-C-C ring in-plane bend vibrations, and 772 cm^{-1} for C-H out-of-plane bend vibrations [30]. The Raman spectra intensities of R6G characteristic peaks with 100% laser power excitation ranged from 1390.28 (611 cm^{-1}) to 4238.28 at (1365 cm^{-1}) when R6G concentration was 10^{-6} M. Treated with Ag@MNPs, strong SERS signals were identified with only 1% laser power. The six key Raman shift peaks included 611, 772, 1185, 1295, 1367 and 1498 cm^{-1}, similar to normal R6G Raman spectra. Different from conventional SERS analysis dropping R6G onto SERS active substrates [31], we directly mixed R6G with Ag@MNPs suspension and allowed their interaction in aquatic phase. The harvesting of Ag@MNPs via permanent magnet significantly concentrated R6G on the magnetic spot to achieve strong SERS signal. The Raman signal enhancement of Ag@MNPs was evaluated by the enhancement factor (EF), as calculated by Equation (1):

$$EF=I_{SERS}/I_{Normal} \quad (1)$$

where I_{SERS} is the Raman signal intensities of R6G with Ag@MNPs at 1% laser power; I_{Normal} is Raman signal intensities of 10^{-6} M pure R6G at 1% laser power.

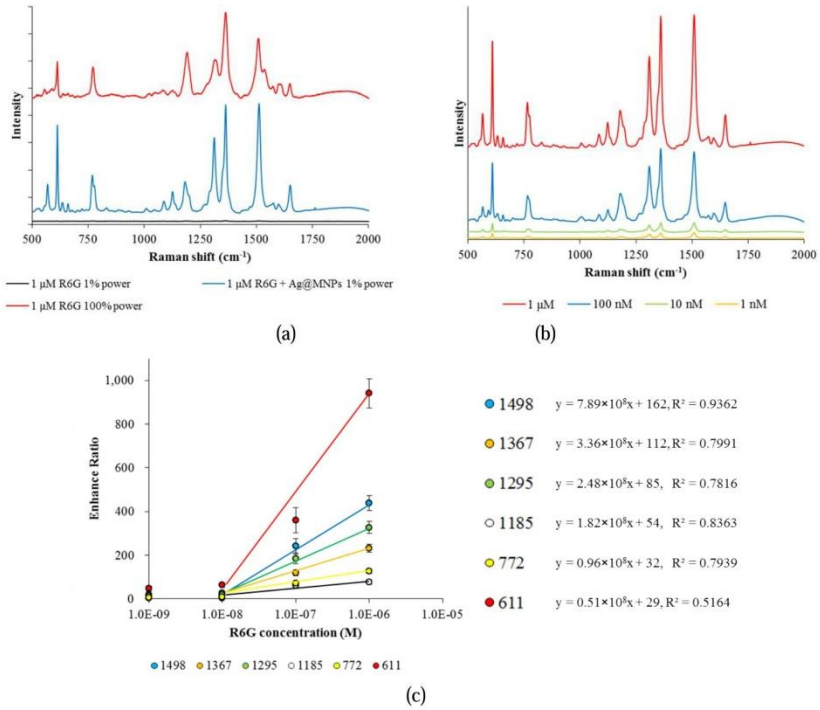

Fig. 3. R6G SERS spectra with Ag@MNPs. (a) Raman spectra of pure R6G and R6G with Ag@MNPs. (b) R6G SERS spectra of different concentrations. (c) Calibration curve of R6G SERS intensity.

For all the tested R6G concentrations (10^{-9} to 10^{-6} M), strong SERS signals were detected (Fig. 3b). For instance, the Raman intensity of 10^{-6} M R6G with Ag@MNPs with 1% laser power was about 1.5 times higher than that of 10^{-6} M pure R6G with 100% laser power. We therefore proved that Ag@MNPs were SERS active substrates. From

the calculation, the Raman signal of peak 611 cm^{-1} was enhanced nearly 10^3 times by Ag@MNPs when R6G concentration was 10^{-6} M, followed by 1498 cm^{-1} (439 times), 1295 cm^{-1} (327 times), 1367 cm^{-1} (232 times), 772 cm^{-1} (127 times) and 1185 cm^{-1} (77 times). As illustrated in Fig. 3c, the SERS intensity of each characteristic peak was positively correlated with the R6G concentrations, with a quantitative range from 10^{-8} M to 10^{-6} M. The limit of detection of R6G SERS with magnetic Ag@MNPs assay was 10^{-9} M, when the enhancement factor was 15 and distinguishable from the background, although the peaks of 772 cm^{-1} and 1185 cm^{-1} were non-detectable.

3.3. In situ bacteria detection by SERS

Different from conventional SERS detecting bacteria, we developed a magnetic SERS assay for the rapid screening of bacterial cells in aquatic phase. The Ag-coating did not affect the electrostatic interaction between MNPs and bacteria, allowing the non-selective capture and further enrichment by magnet. The bacteria were detected and quantified by the sensitive plasmonic Ag@MNPs SERS.

Bacterial SERS spectra varied from spot to spot due to the heterogeneous distribution of Ag@MNPs and bacterial cells at low concentration. The SERS spectra of individual cells were then randomly collected and the results demonstrated its high reproducibility. Fig. 4 showed the significant enhancement of Raman signal by Ag@MNPs assay. With 1% laser power, the enhancement factor of Ag@MNPs was similar for *E. coli* and *A. baylyi*, around 50-100 times compared to pure bacterial cells. It was significantly lower than that of R6G (10^2 to 10^3 as discussed above), attributing to the complicated structure and different functional groups of bacterial cell membrane. The main SERS shifts of *A. baylyi* and *E. coli* included 660, 731, 964, 1210, 1251, 1325 and 1584 cm^{-1}. The band with the highest SERS intensity was 731 cm^{-1}, explained by the ring breathing of adenine. The bands at 1210 and 1251 cm^{-1} were caused by Amide III of proteins [32]. The band at 1325 cm^{-1} was contributed not only from nucleic acid bases adenine and guanine, but also from aromatic amino acid tyrosine [33, 34]. Ring stretch vibration led to the band at 1584 cm^{-1} which was weaker than the other SERS peaks [35]. For the band at 964 cm^{-1}, previous studies tentatively assigned it to the C-N stretch [36]. Meanwhile, the band at 660 cm^{-1} is construed as a discriminative peak of guanosine in bacterial SERS spectra [34].

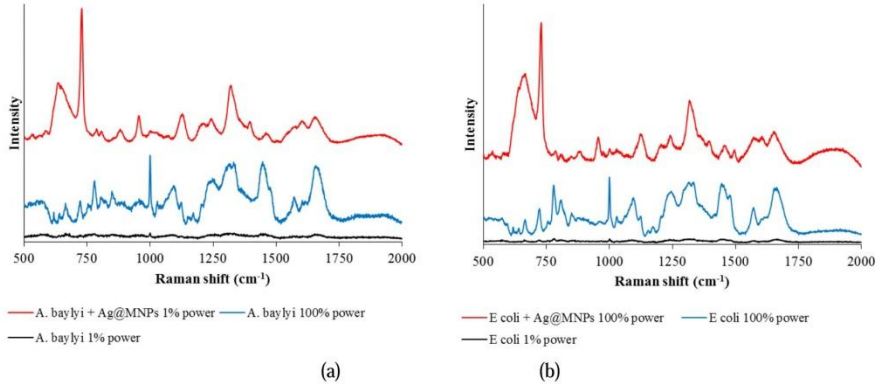

Fig. 4. Raman and SERS spectra of bacteria. (a) for *A. baylyi* and (b) for *E. coli.*

Compared to normal Raman spectra of *A. baylyi* and *E. coli*, we found different Raman spectra profiles of Ag@MNPs SERS. For instance, the most obvious band for normal Raman spectra of both bacteria was 1003 cm^{-1} attributing to polysaccharide [17], which was not enhanced by Ag@MNPs. It might be explained by the favourable binding of Ag@MNPs to some specific extracellular molecules [37], such as adenine and guanine. Meanwhile, the SERS spectra changed slightly at different bacterial concentration, explained by the change from sub-monolayer coverage to full monolayer coverage [38]. Thus, the SERS intensity and characteristic bands of bacteria via

Ag@MNPs might be used to quantify bacterial concentration. In the present work, the direct limited of bacteria detection via normal Raman in aquatic phase was 10^8 CFU/mL, while it was significantly improved to 10^5 CFU/mL when magnetically captured and enriched by Ag@MNPs.

4. Conclusion

For the first time in this study, we proposed and proved the novel concept of capturing bacteria from drinking water and fast detecting their concentration via SERS on magnetic-controllable Ag@MNPs. The results indicated that the bacterial cells were effectively captured by Ag@MNPs and then magnetically enriched for SERS analysis. The Raman intensity was enhanced 10^2 - 10^3 times when R6G was used as the standard chemical and the limit of detection was 10^{-9} M with SERS active substrate Ag@MNPs. This magnetic SERS assay achieved high sensitivity (10^5 CFU/mL) and rapid screening (<15 min) to diagnose bacteria in water samples. With further fabrication and instrumentation, this technique provides opportunities in diagnosing pathogens in other environmental or clinical samples.

Acknowledgement

The authors would like to thank National Natural Science Foundation of China (No. 41301331) for financial support. The authors are thankful to Chinese Scholarships Council (CSC) for providing studentship.

References

[1] U. Szewzyk, R. Szewzyk, W. Manz, K.H. Schleifer, Annu. Rev. Microbiol., 54 (2000) 81-127.
[2] World Health Organization. 2011. Guidelines for drinking-water quality. Fourth ed. WHO Library Cataloguing-in-Publication Data.
[3] A. Rompre, P. Servais, J. Baudart, M.R. de-Roubin, P. Laurent, J. Microbiol. Methods, 49 (2002) 31-54.
[4] A.M. Ibekwe, P.M. Watt, C.M. Grieve, V.K. Sharma, S.R. Lyons, Appl. Environ. Microbiol., 68 (2002) 4853-4862.
[5] U. Dharmasiri, M.A. Witek, A.A. Adams, J.K. Osiri, M.L. Hupert, T.S. Bianchi, D.L. Roelke, S.A. Soper, Anal. Chem.,82 (2010) 2844- 2849.
[6] V.T.C. Penna, S.A.M. Martins, P.G. Mazzola, BMC Public Health, 2 (2002).
[7] M.J. Lehtola, C.J. Loades, C.W. Keevil, J. Microbiol. Methods, 62 (2005) 211-219.
[8] Y.-F. Huang, Y.-F. Wang, X.-P. Yan, Environ. Sci. Technol., 44 (2010) 7908-7913.
[9] Z. Lin, Y. Xu, Z. Zhen, Y. Fu, Y. Liu, W. Li, C. Luo, A. Ding, D. Zhang, Bioresour. Technol., 190 (2015) 82-88.
[10] C. Sun, J.S.H. Lee, M. Zhang, Adv. Drug Delivery. Rev., 60 (2008) 1252-1265.
[11] Y. Xu, C. Li, X. Zhu, W.E. Huang, D. Zhang, Environ. Eng. Manage. J., 13 (2014) 2023-2029.
[12] I. Ennen, C. Albon, A. Weddemann, A. Auge, P. Hedwig, F. Wittbracht, A. Regtmeier, D. Akemeier, A. Dreyer, M. Peter, P. Jutzi, J. Mattay, N. Mitzel, N. Mill, A. Hutten, Acta Phys. Pol. *A*, 121 (2012) 420-425.
[13] C. Ozdemir, O. Akca, E.I. Medine, D.O. Demirkol, P. Unak, S. Timur, Food Anal. Meth., 5 (2012) 731-736.
[14] J. Luis Corchero, A. Villaverde, Trends Biotechnol., 27 (2009) 468-476.
[15] J.W. Chan, A.P. Esposito, C.E. Talley, C.W. Hollars, S.M. Lane, T. Huser, Anal. Chem., 76 (2004) 599-603.
[16] M.D. Porter, R.J. Lipert, L.M. Siperko, G. Wang, R. Narayanana, Chem. Soc. Rev., 37 (2008) 1001-1011.
[17] R.M. Jarvis, R. Goodacre, *Anal. Chem.*, 76 (2004) 40-47.
[18] A.E. Grow, L.L. Wood, J.L. Claycomb, P.A. Thompson, J. Microbiol. Methods, 53 (2003) 221-233.
[19] H. Wang, Y. Zhou, X. Jiang, B. Sun, Y. Zhu, H. Wang, Y. Su, Y. He, *Angew. Chem. Int. Edit.*, 54 (2015) 5132-5136.
[20] Q. An, P. Zhang, J.-M. Li, W.-F. Ma, J. Guo, J. Hu, C.-C. Wang, Nanoscale, 4 (2012) 5210-5216.
[21] T. Yang, X. Guo, H. Wang, S. Fu, Y. Wen, H. Yang, Biosens. Bioelectron., 68 (2015) 350-357.
[22] L. Zhang, J. Xu, L. Mi, H. Gong, S. Jiang, Q. Yu, Biosens. Bioelectron., 31 (2012) 130-136.
[23] D. Zhang, R.F. Fakhrullin, M. Ozmen, H. Wang, J. Wang, V.N. Paunov, G. Li, W.E. Huang, Microbial Biotech., 4 (2011) 89-97.
[24] X. Zhao, H. Li, A. Ding, G. Zhou, Y. Sun, D. Zhang, Mater. Lett., 163 (2016) 154-157.
[25] J.A. López Pérez, M.A. López Quintela, J. Mira, J. Rivas, S.W. Charles, J. Phy. Chem. *B*, 101 (1997) 8045-8047.
[26] J. Shen, Y. Zhu, X. Yang, J. Zong, C. Li, Langmuir, 29 (2013) 690-695.
[27] J. Joo, C. Yim, D. Kwon, J. Lee, H.H. Shin, H.J. Cha, S. Jeon, The Analyst, 137 (2012) 3609-3612.
[28] Y.W. Chu, D.A. Engebretson, J.R. Carey, J. Biomed. Nanotechnol., 9 (2013) 1951-1961.
[29] A.M. Michaels, M. Nirmal, L.E. Brus, J. Am. Chem. Soc., 121 (1999) 9932-9939.
[30] P. Hildebrandt, M. Stockburger, J. Phy. Chem., 88 (1984) 5935-5944.
[31] S. Nie, S.R. Emory, Science, 275 (1997) 1102-1106.
[32] H. Tian, G. Zhuang, A. Ma, C. Jing, J. Microbiol. Methods, 89 (2012) 153-158.
[33] E.C. López-Díez, R. Goodacre, Anal. Chem., 76 (2004) 585-591.
[34] L. Cui, P. Chen, B. Zhang, D. Zhang, J. Li, F.L. Martin, K. Zhang, Water Res., 87 (2015) 282-291.
[35] B. Giese, D. McNaughton, Phys. Chem. Chem. *Phys.*, 4 (2002) 5171-5182.
[36] L. Cui, P. Chen, S. Chen, Z. Yuan, C. Yu, B. Ren, K. Zhang, Anal. Chem., 85 (2013) 5436-43.
[37] M. Kahraman, K. Keseroglu, M. Culha, Appl. Spectrosc., 65 (2011) 500-506.
[38] H.W. Cheng, S.Y. Huan, R.Q. Yu, The Analyst, 137 (2012) 3601-8.

Chapter 2

Quantification of Chemotaxis-Related Alkane Accumulation in *Acinetobacter baylyi* Using Raman Microspectroscopy

Hanbing Li, Francis L. Martin, Dayi Zhang

Analytical Chemistry, 2017, 89, 3909-3918

Contribution:

- I prepared the samples required for the project;
- I processed and acquired all spectral data and carried out computational analysis;
- I prepared the first draft and figures of manuscript.

analytical chemistry

Article

pubs.acs.org/ac

Quantification of Chemotaxis-Related Alkane Accumulation in *Acinetobacter baylyi* Using Raman Microspectroscopy

Hanbing Li,[†] Francis Luke Martin,[†,‡] and Dayi Zhang*[,†]

[†]Lancaster Environment Centre, Lancaster University, Lancaster LA1 4YQ, U.K.

[‡]School of Pharmacy and Biomedical Sciences, University of Central Lancashire, Preston PR1 2HE, U.K.

Supporting Information

ABSTRACT: Alkanes are one of the most widespread contaminants in the natural environment, primarily as a consequence of biological synthesis and oil spills. Many indigenous microbes metabolize alkanes, and the chemotaxis and accumulation in some strains has been identified. For the first time, we apply Raman microspectroscopy to identify such chemotaxis-related affinity, and quantify the alkane concentrations via spectral alterations. Raman spectral alterations were only found for the alkane chemo-attractant bacteria *Acinetobacter baylyi* ADP1, not for *Pseudomonas fluorescence*, which exhibits limited chemotaxis toward alkane. The significant alterations were attributed to the strong chemotactic ability of *A. baylyi* enhancing the affinity and accumulation of alkane molecules on cell membranes or cellular internalization. Spectral fingerprints of *A. baylyi* significantly altered after 1-h exposure to pure alkanes (dodecane or tetradecane) and alkane mixtures (mineral oil or crude oil), but not monocyclic aromatic hydrocarbons (MAHs) or polycyclic aromatic hydrocarbons (PAHs). A semilog linear regression relationship between Raman spectral alterations and alkane concentrations showed its feasibility in quantifying alkane concentration in environmental samples. Pure alkanes or alkane mixtures exhibited different limits of detection and regression slopes, indicating that the chemotaxis-related alkane accumulation in *A. baylyi* is dependent on the carbon chain length. This work provides a novel biospectroscopy approach to characterize the chemotaxis-related alkane bioaccumulation, and has immense potential for fast and high-throughput screening bacterial chemotaxis.

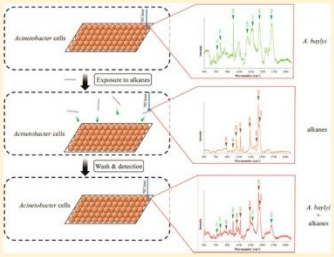

Many hazardous chemicals have been released into the environment through various industrial activities. Particularly, with industrial development and urbanization processes, the increasing usage of crude oil has consequently been associated with numerous oil spill accidents and contaminated sites. Since 1969, there have been >40 large oil spill incidents worldwide, including the Exxon Valdez oil spill in Prince William Sound in 1989,[1,2] the Deepwater Horizon oil spill in Gulf of Mexico,[3] and the Xingang oil spill in Dalian[4] in 2010. These incidents have resulted in large areas of oil-contaminated sites, damaged ecological systems, and threats to human health.[5,6] Chemical analysis of alkanes predominantly includes gravimetric,[7−9] fluorophotometry,[10,11] infrared (IR) absorption,[12] gas chromatography flame ionization detector (GC-FID),[13] or gas chromatography mass spectrometry (GC-MS) methods,[14] but samples require pretreatment using solvent extraction or solid-phase microextraction (SPME).[15] To evaluate alkane bioavailability or bioaccessibility, some whole-cell bioreporters have been developed[16] and even applied in real-world cases,[4,17] but they suffer from relatively low reproducibility. Considering the rapid response required for oil spill incidents, it is necessary to develop some real-time and nondestructive screening tools to achieve fast and reliable detection of crude oil contamination.

In the natural environment, alkanes are the main components of crude oil and carbon sources for many bacteria, and alkane chemotaxis has been found in some species.[18] Chemotaxis-related affinity to alkanes facilitates bacterial movement in alkane gradients and contributes to their elevated abilities to access and utilize alkane substrates.[19] In *Pseudomonas aeruginosa* PAO1, the *tlpS* gene, which is located downstream of the alkane monooxygenase *alkB1* gene, is believed to encode a methyl-accepting chemotaxis protein (MCP) that confers the chemotactic response to hexadecane.[20] Another *Pseudomonas* strain, *P. putida* GPo1, has the *alkN* gene encoding an MCP for alkane chemotaxis.[21] *Flavimonas oryzihabitans* is reported to exhibit weak chemotactic responses to hexadecane, but its mechanisms remain unknown.[22] The alkane chemotaxis machinery of marine alkane degrader *Alcanivorax dieselolei* consists of eight cytoplasmic chemotaxis proteins, including MCP and flagellar proteins.[23] *Acinetobacter baylyi* is the bacterial species with the strongest alkane chemotaxis and accumulation.[16,24−26] In *A. baylyi*, the putative gene encoding an MCP is *chpA*, which has high similarity to

Received: June 13, 2016
Accepted: March 3, 2017
Published: March 3, 2017

DOI: 10.1021/acs.analchem.6b02297
Anal. Chem. 2017, 89, 3909−3918

cheY (fused chemotactic sensory histidine kinase) and *ompR* (two-component response regulator) in *Escherichia coli*, suggesting potentially similar chemotaxis machinery. *A. baylyi* cells have high affinity only to alkane droplets, but not to other hydrophobic molecules,[16] suggesting that the MCP has high recognition specificity to linear alkanes. Meanwhile, alkane chemotaxis further helps microbial accumulation, internalization, and degradation of alkanes by providing enhanced opportunities to seek out linear alkanes. The fimbriae on the surface of *Acinetobacter* cells are postulated to drive the access to alkane droplets for cellular uptake.[27−29] Trapped alkane droplets on the cell surface are subsequently transported into bacterial cells after being emulsified by biosurfactant mediation.[30−32]

Raman microspectroscopy has been widely applied in biological molecule detection, as a fast, reproducible, and nondestructive approach generating a chemical fingerprint.[33] It has been well developed to identify bacteria and study their responses to their environment.[34−37] Most spectrally identified biological molecules are well characterized, such as purine, pyrimidine, amino acids, and proteins.[38−42] Though many approaches, such as swarm plates,[43] capillary assays,[44] temporal stimulation of tethered cells,[45] and automated tracking of swimming cells,[46] have been applied to test the bacterial chemotaxis toward specific chemicals, there is still no study exploring Raman spectral alterations during chemotaxis-related affinity and bioaccumulation processes. The chemotactic behavior of alkanes hints at the possibility that alkane molecules will accumulate on the membrane and/or in the cytoplasm of bacterial cells, potentially allowing them to be identified in Raman spectra.

In the present study, we used Raman microspectroscopy to distinguish the spectral alterations and quantify alkane concentrations based on the chemotaxis-related alkane accumulation of *A. baylyi*. For the first time, we demonstrate that chemotaxis-related alkane affinity and accumulation is measurable by Raman microspectroscopy and the MCP of *A. baylyi* is highly specific to alkane molecules, instead of monocyclic aromatic hydrocarbons (MAHs) or polycyclic aromatic hydrocarbons (PAHs). Not only contributing to fast quantification of aqueous alkane concentrations, this method also has the potential as a screening tool in characterizing chemotaxis-related affinity and accumulation toward various chemicals.

■ EXPERIMENTAL SECTION

Strains and Growth Conditions. The two bacterial strains used in this study were the alkane chemotactic *Acinetobacter baylyi* ADP1 and chemotaxis-negative *Pseudomonas fluorescence*. Both strains were grown in minimal medium with 20 mM sodium succinate as the sole carbon source, at 30 °C and 150 rpm for 16 h. The 1.0 L minimal medium contained 1.0 g of $(NH_4)_2SO_4$, 2.5 g of KH_2PO_4, 0.1 g of $MgSO_4{\cdot}7H_2O$, 0.005 g of $FeSO_4{\cdot}7H_2O$, 0.25 g of nitrilotriacetic acid (NTA), 0.55 g of NaOH, and 1 mL of Bauchop and Elsden solution. Strains were further centrifuged at 4,000 rpm for 5 min and washed three times using sterile deionized water, and finally suspended in minimal medium for further experimentation.

Hydrocarbon Exposure. Unless specifically stated otherwise, all chemicals in this study were of analytical grade and purchased from Sigma-Aldrich (UK). The hydrocarbons included six pure chemicals: dodecane, tetradecane, toluene, xylene, phenanthrene, and naphthalene, and two hydrocarbon mixtures, crude oil and mineral oil. They were dissolved in dimethyl sulfoxide (DMSO) to prepare the 10 g/L stock solution, and serially diluted to 0.1−5.0 g/L. The hydrocarbon stock solution was separately mixed with bacterial suspensions (1:100, v/v) to reach a final concentration of 100 mg/L. After 1-h exposure at 30 °C, the medium was removed by 5 min centrifugation at 5,000 rpm, and the cell pellets were resuspended in deionized water and washed twice.

The time-dependence of chemotaxis-related chemo-association was measured by exposing *A. baylyi* suspensions to dodecane, tetradecane, crude oil, or mineral oil for 0.5, 1, 3, and 5 h at 30 °C, respectively. The final alkane concentrations were 100 mg/L. The cells were further centrifuged at 5,000 rpm for 7 min, and washed twice with deionized water.

To establish the dose response of alkane accumulation, different volumes of dodecane, tetradecane, crude oil, or mineral oil stock solution were added to 1 mL of washed *A. baylyi* suspensions. The final concentrations were: 1, 2, 5, 10, 20, 50, and 100 mg/L. After 1-h exposure at 30 °C, the mixtures were centrifuged at 5,000 rpm for 7 min, and washed twice with deionized water.

Hydrocarbon Chemotaxis Capillary Test. To validate chemotaxis effects, conventional capillary tests were applied according to Alder's protocol[47] with some modifications. Briefly, the capillary tubes (internal diameter of 0.2 mm and length of 10 cm) were plunged into 1 mL of chemotaxis medium with attractant (alkanes, PAHs, MAHs, and oils). After approximately 10 min, the liquid was drawn up to approximately 1 cm of the length of the tube; the capillary was then inserted (without rinsing) into the bacterial suspension (*A. baylyi* or *P. fluorescence*) and incubated for 1 h at 30 °C. To test the time-dependency of chemotaxis, the capillary tubes with tetradecane or crude oil attractants were incubated within the *A. baylyi* suspension for 0.5, 1, 3, or 5 h at 30 °C, similar to the hydrocarbon exposure experiment described above.

Instead of plate counting, we used a quantitative polymerase chain reaction (qPCR) to quantify the 16S rRNA copy numbers of chemotactic bacteria in duplicate. After 1-h of incubation, the capillary tube was removed and the exterior of the open end was directly plunged into qPCR buffer. The 10 μL of qPCR buffer consisted of 1 μL of primer 341F (5′-CCTACGGGNGGCWGCAG-3′), 1 μL of primer 802R (5′-TACNVGGGTATCTAATCC-3′), 3 μL of molecular water, and 5 μL of iTaq Universal SYBR Green Supermix (BioRad, USA). The thermos cycling program was: initial denaturation at 94 °C for 3 min; 34 amplification cycles of 94 °C for 45 s, 52 °C for 45 s, 72 °C for 45 s, and fluorescence data acquisition at 80 °C for 15 s. Standard curves were obtained with serial dilutions of quantified plasmid DNA (via nanodrop) containing the fragment of 16S rRNA, as described previously.[48]

Chemical Analysis of Hydrocarbons. After exposing chemotactic *A. baylyi* suspensions to hydrocarbon solutions, the determination of residual hydrocarbons at different time points was achieved by following the hexane extraction method.[48] At 0, 0.5, 1, 3, or 5 h, the 50 mL cell-hydrocarbon suspensions were added with 50 mL of hexane and subsequently ultrasonically homologized for 2 min (40 kHz). The supernatant was fractionalized by column chromatography, in which the hexane supernatant was loaded onto a glass column (Φ10 mm × 100 mm, consisting of 2 cm anhydrous Al_2O_3 and 0.3 cm anhydrous Na_2SO_4 from the bottom to the top) and washed with 50 mL of hexane. The elution was evaporated in 40 °C

DOI: 10.1021/acs.analchem.6b02297
Anal. Chem. 2017, 89, 3909−3918

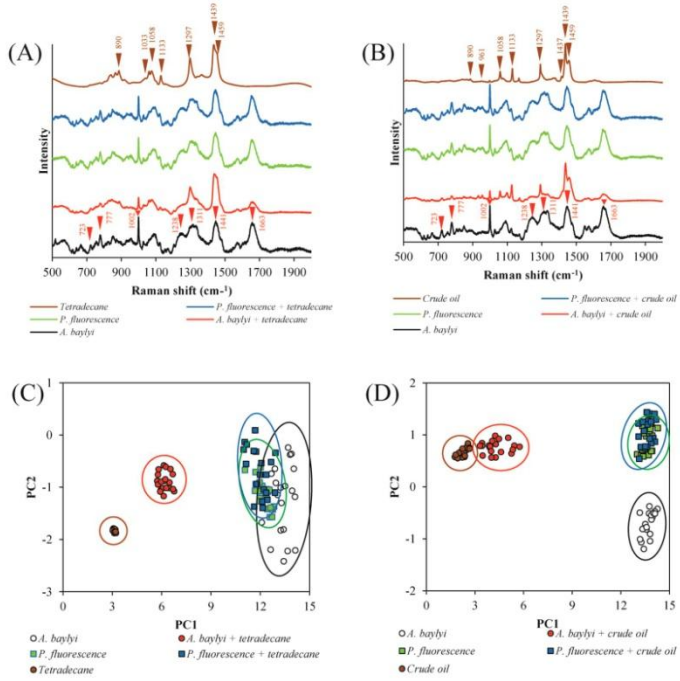

Figure 1. Raman spectra of *A. baylyi* and *P. fluorescence*, pre- and postexposure to 100 mg/L tetradecane (A) or crude oil (B). PCA of Raman spectra shows the significant segregation of *A. baylyi* categories when exposed to 100 mg/L tetradecane (C) or crude oil (D) due to chemotaxis-related alkane affinity and accumulation, but not *P. fluorescence*. Twenty Raman spectra were randomly obtained per treatment.

water bath, and the hydrocarbons were measured by the gravimetric method.

Raman Microspectroscopy Analysis. Ten microliters of washed cells were transferred onto a slide covered with aluminum foil and air-dried before Raman microspectroscopy analysis.[49] Raman spectra were obtained using an InVia confocal micro-Raman system (Renishaw, Gloucestershire, UK) equipped with a 100 mW 785 nm laser diode with a Rayleigh holographic edge filter. The spectrometer's entrance slit of 50 μm combined with a 1200 lines per mm (1 cm^{-1} spatial resolution) diffraction grating allowed dispersion of Raman signals onto a Master Renishaw Pelletier cooled charged couple detector (CCD). A white light camera mounted on the microscope allowed the use of dark-field images to visualize locations for spectral acquisition. An attached microscope (Leica Microsystems, Milton Keynes, UK) with ×50 objective (0.75 numerical aperture; ≈1 μm spatial resolution) was utilized for sample detection and acquisition. All sample spectra were obtained using 100% laser power (26 mW at sample), 15 s acquisition time, and one accumulation within a spectral range from 500 to 2000 cm^{-1}. The Renishaw system was calibrated with a Renishaw silicon calibration source for wavenumber shifts. All the treatments were carried out in triplicates, and at least 20 biological replicates were performed and analyzed for each sample.

Raman Spectra Analysis. Unless otherwise stated, all data were normalized and analyzed using the IRootLab toolbox for Matlab (version R2013b, MathWorks, USA).[50] Principal component analysis (PCA) was carried out to reduce the dimensionality of the multivariate data and allow visualization of the natural variance within the data set.[51] Postexposure to different alkane or oil concentrations, the distance of individual Raman spectra to that of comparator negative controls (alkane/oil concentration = 0 mg/L) was calculated based on the values of principal component (PC) 1 (PC1) and PC2. The dispersions of individual group to negative control and pure alkane/oil groups were evaluated by output data derived from PCA and linear discriminant analysis (LDA) and were visualized as dispersion indicator (D_I) scores plots, in which increasing D_I between two categories is proportional to dissimilarity [for details see the Supporting Information (SI)]. The statistical significance of differences and variance analysis (P-value < 0.05) of LDA among the different treatments was performed using a one-way ANOVA and least significant difference (LSD) test.

DOI: 10.1021/acs.analchem.6b02297
Anal. Chem. 2017, 89, 3909−3918

Table 1. Variations and Assignments of Raman Bands of Alkanes and *A. baylyi* before and after Exposure[a]

Band (cm^{-1})	Tentative bands assignment	Origin	Alkane	*A. baylyi*	Alkane + *A. baylyi*
890	Terminal methyl CH_3 rock	Dodecane, tetradecane, mineral oil	++	-	+ ↑
961	CH_2 rock	Dodecane	++	-	+ ↑
1033	CH_2 rock	Dodecane	+	-	-
1058	C-C stretch	Mineral oil	++	+	+
1133	C-C asymmetric stretch and CH_2 wag	Dodecane, tetradecane, crude oil, mineral oil	+++	+	+
1297	CH_2 twist	Dodecane, tetradecane, crude oil	+++	+	+++ ↑
1437	Symmetric CH_2 scissors vibration	Crude oil	+++	-	+++ ↑
1439	CH_2 bend	Dodecane, tetradecane, mineral oil	+++	+++	+++ ↑
1459	Antisymmetric CH_2 scissors vibration	Crude oil	+++	-	+++ ↑
723	Ring breathing vibration	Bacterial nucleic acids	-	++	+ ↓
777	Ring breathing vibration	Bacterial nucleic acids	-	++	+ ↓
1002	Benzene ring breathing	Bacterial phenylalanine	-	+++	++ ↓
1238	/	Bacterial amino acids	-	+	- ↓
1311	/	Bacterial amino acids	-	+	- ↓
1441	Deformations of CH_2	Bacterial glycine	-	+++	+++ ↑
1663	C=C stretching	Bacterial proteins	-	+++	+++

[a]"–" represents no peak identified; "+" represents weak peak; "++" represents medium peak; "+++" represents strong peak. Brown or green symbols indicate characteristic peaks belonging to alkanes and *A. baylyi*, respectively. Red or blue arrows represent the increases or decreases in the respective Raman intensity of *A. baylyi* postexposure to alkanes.

RESULTS AND DISCUSSION

Raman Spectral Characterization of *A. Baylyi* Exposed to Alkanes. Exposed to alkanes or oil droplets, *A. baylyi* bacterial cells were predominantly found on the oil–water interface and could emulsify hydrocarbons into small droplets (see SI Figure S1). The majority of *A. baylyi* cells were found at the alkane–water interface, not in the aqueous phase, demonstrating their high affinity to alkane droplets. In contrast, the strains negative for or with minor alkane chemotactic properties, such as *P. fluorescence*, exhibited a very weak oil droplets affinity, and most bacterial cells remained in the water phase (see SI Figure S1). Similarly, the droplets of alkane mixtures (mineral oil) or hydrocarbon mixtures (crude oil) also showed strong attraction to *A. baylyi*, but no adhesion with *P. fluorescence*. *A. baylyi* ADP1 has been reported with high affinity to alkane droplets,[16] explained as alkane chemotaxis.[43,52] From the results of the hydrocarbon capillary assay (Figure 2A), we confirmed the chemotaxis-related affinity of *A. baylyi* to alkanes. The accumulation of 16S rRNA copies of *A. baylyi* in capillaries in oil mixture and pure alkane treatments ranged from 3.9×10^8 to 1.07×10^9 per capillary, significantly higher than those in PAHs and MAHs treatments (8.7×10^5 to 3.6×10^7 16S rRNA copies per capillary). In contrast, the low 16S rRNA copy numbers of *P. fluorescence* in capillary tubes postexposure to oil mixtures and pure alkanes (2.9×10^4 to 9.7×10^6 16S rRNA copies per capillary) suggested that *P. fluorescence* is not an alkane chemotactic strain.

The hydrocarbon capillary assay proves that *A. baylyi* ADP1 cells can swim down the attractant gradient toward alkanes. From another perspective, MCP on the cell membranes of *A. baylyi* ADP1 effectively recognizes and binds the alkane molecules, eventually trapping and accumulating the soluble fraction of alkane molecules in the aqueous phase. Considering the low solubility of alkane in water, it generates the alkane gradient and contributes to the access of *A. baylyi* ADP1 cells to alkane molecules. This is strongly suggested by the significant accumulation of *A. baylyi* cells in capillaries following exposure to alkane mixtures or pure alkanes (Figure 2A). Alkane chemotaxis significantly helps the internalization and utilization of the insoluble alkanes by *A. baylyi* ADP1.[16] The accumulation of alkane molecules either on cell membranes or internalized within cells provides the opportunity to employ Raman microspectroscopy to investigate the chemotaxis-related affinity and accumulation of alkanes.

Since dodecane and tetradecane are both linear alkane molecules with carbon chain lengths of 12 and 14, respectively, their Raman spectra are similar (Figure 1A and Table 1; see SI Figure S2A). The predominant bands include 890 cm^{-1} (terminal methyl CH_3 rock), 1133 cm^{-1} (C–C asymmetric stretch and CH_2 wag), 1297 cm^{-1} (CH_2 twist), and 1439 cm^{-1} (CH_2 bend).[53] The only difference between dodecane and tetradecane is the bands at 961 and 1033 cm^{-1} in dodecane, which are attributed to CH_2 rock.[54] As the distillation product of crude oil, the Raman spectra of mineral oil (see SI Figure S2C) show distinct peaks at bands 1058 and 890 cm^{-1}, assigned

DOI: 10.1021/acs.analchem.6b02297
Anal. Chem. 2017, 89, 3909–3918

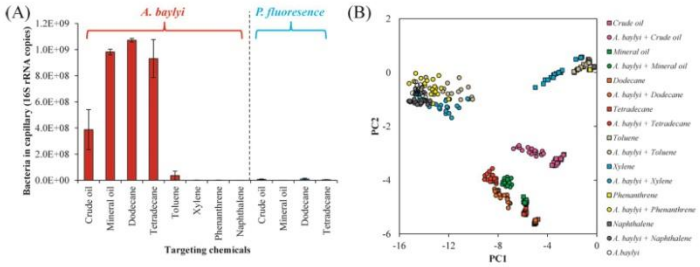

Figure 2. (A) Validation of alkane chemotaxis via capillary assay. A high amount of bacterial 16S rRNA in a capillary indicates significant chemotaxis of *A. baylyi* (red bar) toward dodecane, tetradecane, mineral oil, or crude oil, whereas *P. fluorescence* (blue bar) does not show chemotaxis to these hydrocarbons. (B) Raman spectral segregation by PCA of *A. baylyi* exposed to different hydrocarbons. The tested chemicals with the alkane-chemotaxis effect include: dodecane, tetradecane, mineral oil, or crude oil. The tested chemicals without the chemotaxis effect were: monocyclic aromatic hydrocarbons (toluene or xylene) and polycyclic aromatic hydrocarbons (naphthalene or phenanthrene). Twenty Raman spectra were randomly obtained per treatment.

to CH_2 twist-rock and C−C stretch, respectively.[55] Although the CH_2 twist peak at 1297 cm^{-1} is observed for both crude oil and mineral oil, crude oil also contains MAHs and PAHs, and therefore possesses three unique peaks (Figure 1B): the benzene ring breathing band at 1060 cm^{-1}, and symmetric and antisymmetric CH_2 scissors vibration bands at 1437 and 1459 cm^{-1}.[56]

The Raman spectra of the original *A. baylyi* and *P. fluorescence* cells are similar, due to their close relationship to the order *Pseudomonadales* from genomic and proteomic analyses.[25,26,57] From Figure 1A, 1B and Table 1, both 777 and 723 cm^{-1} bands refer to nucleic acids.[58] The band at 1441 cm^{-1} is assigned to glycine in bacterial cells.[40] Amino acid bands are also observed in the Raman spectra at 1238 and 1311 cm^{-1}.[58] The 1663 cm^{-1} band represents protein, and the 1002 cm^{-1} band points to phenylalanine. Postexposure to tetradecane or crude oil, entirely different Raman spectra are identified for the two strains. The Raman spectra of *P. fluorescence* remain unchanged, which is explained by the fact that alkanes exhibit no chemo-attraction and are not accumulated in *P. fluorescence*. Accordingly, all the *P. fluorescence* cells fall into one category after PCA (Figure 1C and 1D) and are indistinguishable pre- and postexposure to tetradecane or crude oil. The Raman spectra of *A. baylyi* exhibit significant alterations postexposure to alkanes (Figure 1A, 1B and Table 1). Postexposure bacterial spectra are coupled with some key alkane bands. Two strong alkane bands, 1297 cm^{-1} (CH_2 twist) and 1439 cm^{-1} (CH_2 bend), are observed in all Raman spectra of *A. baylyi* exposed to tetradecane or crude oil.

In dodecane treatment, the specific 961 and 1033 cm^{-1} bands are attributed to CH_2 rock (Table 1). The bands 1058 cm^{-1} (CH_2 twist-rock) and 890 cm^{-1} (C−C stretch) only appear in *A. baylyi* treated with mineral oil (see SI Figure S2D), and the bands 1060 cm^{-1} (ring breathing of benzene) and 1430−1470 cm^{-1} (symmetric and antisymmetric CH_2 scissors vibrations) are found in the spectra of *A. baylyi* exposed to crude oil (Figure 1B). It is worth noting that both chemotaxis-related affinity and accumulation of alkane might contribute to the appearance of alkane characteristic bands, where alkane affinity significantly accelerates the access, accumulation, and potential internalization of alkanes by *A. baylyi* and enhances Raman signals. PCA of Raman spectra (Figure 1C and 1D) further proves that alkane affinity and accumulation result in the significant differentiation of *A. baylyi* postexposure to tetradecane or crude oil. The category comprising *A. baylyi* treated with tetradecane is very close to that of pure tetradecane, whereas the crude oil exposure leads to similarity between *A. baylyi* and crude oil. They are both significantly separated from the original *A. baylyi* group. The results show that the significant Raman spectral alterations are caused by the alkane affinity and accumulation of *A. baylyi*. Moreover, the strong terminal methyl CH_3 rock (890 cm^{-1}) is only found in *A. baylyi* spectra postexposed to tetradecane, readily discriminated from those in the crude oil treatment. Therefore, our findings reveal that chemotaxis-related alkane affinity contributes to the adhesion of alkane molecules onto the membrane of *A. baylyi* cells, allowing further alkane accumulation or cellular internalization. Raman spectral alterations highlight such chemotaxis-related affinity and accumulation, and even distinguish the different chemo-attracted molecules quickly and with high reproducibility.

Specific Chemotaxis-Related Alkane Affinity and Accumulation in *A. Baylyi*. To test the specificity of the hydrocarbons affinity and accumulation in *A. baylyi*, various hydrocarbon molecules were tested, including pure alkanes (dodecane or tetradecane), alkane mixtures (mineral oil or crude oil), MAHs (toluene or xylene), and PAHs (naphthalene or phenanthrene). Raman spectral alterations are only found for pure alkanes or alkane mixtures (Figure 2B; see SI Figure S2). PCA differentiation illustrates that the categories for postexposure to MAHs or PAHs cocluster due to significant Raman bands for benzene ring breathing peaks at 1001 and 1027 cm^{-1} for toluene or xylene, 760 cm^{-1} for naphthalene, and 705 cm^{-1} for phenanthrene (see SI Figure S2).[59−61] The category for crude oil is located between pure alkanes and MAHs/PAHs, because it consists of various hydrocarbons, including alkanes, MAHs, and PAHs. As a byproduct from crude oil distillation, mineral oil is a mixture of *n*-alkanes and located very close to the category for pure alkanes.[62] Postexposure to MAHs (toluene, xylene) or PAHs (phenanthrene and naphthalene), PCA of *A. baylyi* fails to segregate these categories from unexposed comparator cells. The results were consistent with hydrocarbon capillary assay (Figure 2A), in which the accumulated 16S rRNA copy numbers of *A. baylyi*

DOI: 10.1021/acs.analchem.6b02297
Anal. Chem. 2017, 89, 3909−3918

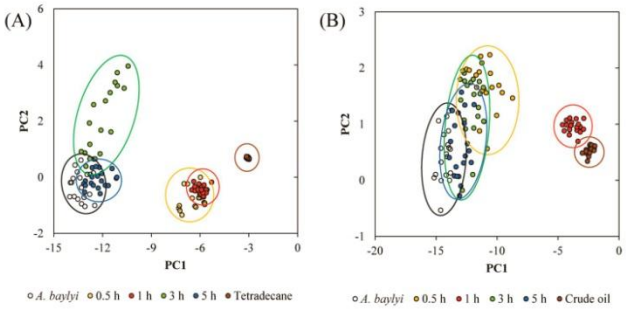

Figure 3. PCA segregation of *A. baylyi* Raman spectra against exposure time in tetradecane (A) and crude oil (B) treatments. Twenty Raman spectra were randomly obtained per treatment.

were much higher in oil mixtures and pure alkanes treatments than those in PAHs and MAHs treatments, indicating that *A. baylyi* has chemo-attraction toward neither MAHs nor PAHs, which has been proved previously.[16,24] After PCA, the categories for *A. baylyi* exposed to pure alkane or alkane mixtures cocluster with those of the pure chemicals respectively, and are completely separated from the unexposed comparator cells. These results prove that the chemotactic association between alkane and *A. baylyi* is the key factor in altering Raman spectra. Such chemotaxis-related affinity is specific to alkanes and helps further alkane accumulation or internalization within *A. baylyi* cells, resulting in significant spectral alterations compared to those induced by other hydrophobic molecules (MAHs or PAHs). Thus, we conclude from the Raman spectral discrimination that the alterations in *A. baylyi* exposed to mineral oil or crude oil are attributable to chemotaxis-related affinity toward alkanes; these are the main components of mineral oil and crude oil.

Previous research has examined the mechanisms of alkane chemotaxis. In the presence of alkanes, OmpS is most likely the first sensor protein to transmit signals back to bacterial cells.[63] The chemotactic signals are stimulated by a complex protein system that is comprised of coupling CheW and methyl-accepting chemotaxis protein (MCP) to the histidine kinase CheA.[64−66] It is also reported that the MCP is captured firmly in this protein complex, whereas a substantial part of CheW and CheA is free in cells.[67] The signals from OmsP are likely received by the MCP embedded on the CheW/CheA complex. The coupling protein CheW2 is found in *Alcanivorax dieselolei* as the chemotaxis complex only induced by long-chain alkanes.[68−71] Hence, bacterial chemotaxis toward alkanes is hypothesized to exhibit high specificity, and the chemotaxis-related alkane affinity and accumulation therefore follow the same behavior. Our results provide direct evidence that Raman spectral alterations of *A. baylyi* are only observed for linear *n*-alkanes, not MAHs or PAHs.

Time-Dependent Raman Spectra Alteration. To identify the optimal exposure time of *A. baylyi* to alkanes, bacterial cells were treated with 100 mg/L tetradecane or crude oil for 0.5, 1.0, 3.0, or 5.0 h. The results from PCA (Figure 3) indicate that the Raman spectral alterations of *A. baylyi* alkane association are time-dependent. With the sensitive chemotactic affinity of *A. baylyi* toward alkanes, significant spectral alterations are observed within 0.5 h for both tetradecane and crude oil, and the most discrimination is at 1.0 h. Interestingly, after 0.5 h exposure, the cluster of *A. baylyi* cells treated with tetradecane exhibits the most discrimination compared to the untreated category (Figure 3A) versus cells exposed to crude oil (Figure 3B). Thus, the affinity of tetradecane appears stronger than that of crude oil. This is very likely explained by the complex composition of crude oil, which consists of alkanes, MAHs, and PAHs. On the surface of crude oil droplets, all these molecules are evenly distributed, leaving fewer active sites of chemo-attractive alkanes for the effective recognition by the MCP of *A. baylyi*. The diverse hydrophobic components in crude oil droplets reduce alkanes bioavailability, challenge the access of bacteria to alkane molecules,[72] and slow down alkanes utilization by *A. baylyi*.[73] The accessibility of *A. baylyi* to tetradecane is therefore faster, and such stronger adhesion to pure alkane droplets has been reported.[74−76]

A. baylyi has the alkane monooxygenese encoding *alkM* gene and can metabolize *n*-alkanes.[16] The activation of *alkM* is reported to occur within 30 min postexposure to alkanes, when significant alkane degradation occurs.[66,74] The alkane molecules accumulated on the cell membrane or internalized inside *A. baylyi* cells are therefore hypothesized to be rapidly consumed. Our test on residual hydrocarbon concentrations (see SI Figure S3) proves this hypothesis that the dramatic alkane degradation was only observed within the first 1 h and its concentration remained stable thereafter. Thus, the amount of alkanes captured and accumulated by *A. baylyi* cells peaked at 1 h and resulted in the most discrimination in Raman spectral fingerprints (Figure 3). This explains the diminishing spectral alterations after 1-h exposure. As a consequence, the Raman spectral categories of 0.5, 3, and 5 h exposure are clustered close to the original *A. baylyi* category in either tetradecane or crude oil treatments (Figure 3, see SI Figure S4). Thus, the highest alkane affinity and accumulation of alkanes was at 1.0 h, at which time the strongest spectral alterations are found. Therefore, 1-h exposure was applied for all the subsequent experiments. Compared to the conventional hydrocarbon chemotaxis capillary assay (see SI Figure S5), in which the maximum bacterial enrichment was 0.5 h for crude oil and 3 h for tetradecane, our Raman assay had a different response time (1.0 h for both crude oil and tetradecane). It might be explained by the different chemotaxis-related behavior quantified by the two methods. The chemotaxis capillary assay measures the chemotaxis-driven bacterial migration in

DOI: 10.1021/acs.analchem.6b02297
Anal. Chem. 2017, 89, 3909−3918

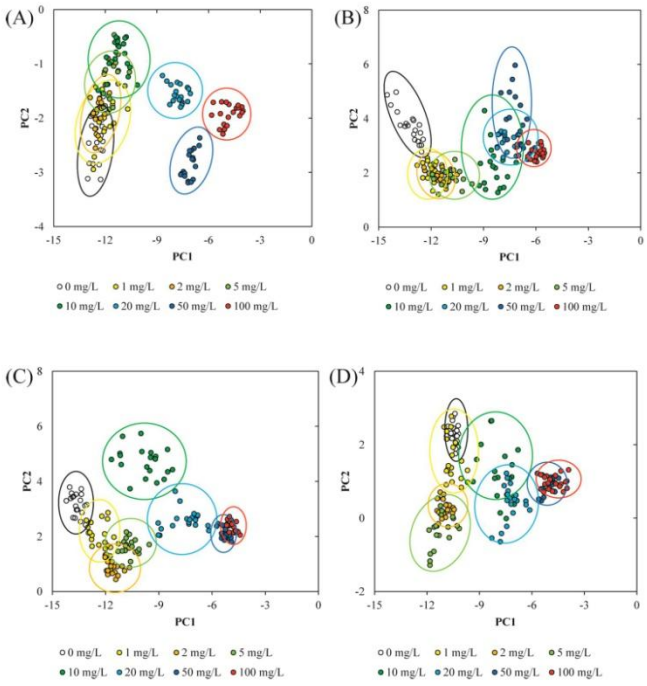

Figure 4. PCA segregation of *A. baylyi* Raman spectra at different concentrations of dodecane (A), tetradecane (B), mineral oil (C), or crude oil (D). For each treatment, 20 replicates were performed.

alkane gradients, whereas the Raman spectral alteration represents the chemotaxis-related affinity and accumulation of alkane molecules on *A. baylyi* cells. It is worth highlighting that the Raman assay is a faster and higher throughput interrogation of specific chemical affinity and accumulation than the conventional capillary assay. Though the chemotactic response is around 1 h in both methods, the Raman assay takes only 20 min for wash/dry and 1−2 min spectral measurement, much less than that required in determining bacterial enrichment by the capillary assay (3−4 h by qPCR or 18 h by plate counting). Additionally, the attractant only needs to be mixed together with targeting bacterial suspension, easier than the plunge and transfer of attractant medium in numerous capillaries in the conventional assay, allowing high-throughput detection for many chemicals in 96-well plates.

Quantification of Alkane Affinity and Accumulation by Raman Spectral Alterations. Raman spectral alterations of *A. baylyi* chemotaxis-related affinity and accumulation toward alkane allow evaluation of the sensitivity of alkane affinity and quantification of alkane concentration in the aquatic phase. Figure 4 illustrates the PCA categorization of *A. baylyi* Raman spectra following different exposures (1, 2, 5, 10, 20, 50, and 100 mg/L) of dodecane, tetradecane, mineral oil, or crude oil, respectively. After 1-h exposure to the targeted alkane molecules or mixtures, all the characteristic peaks of *A. baylyi* remained the same, and the new altered peaks originated from alkanes (see SI Figure S6). The intensity of alkane characteristic peaks increased with increasing dodecane (or tetradecane) exposure, especially for the band at 1297 cm^{-1}, which is annotated to CH_2 twist and dominates in alkane molecules. The Raman peak of the CH_2 bend at 1493 cm^{-1} was positively related to the alkane concentrations. The terminal methyl CH_3 Raman signal of alkane at 890 cm^{-1} was detected when the concentrations of dodecane and tetradecane were 20 mg/L or higher. Besides pure alkanes, similar Raman spectral alterations were found for treatments with alkane mixtures (mineral oil or crude oil; Figure 4C and 4D). Spectral alternations of *A. baylyi* are separated postexposure to different concentrations of mineral oil or crude oil. The key altered peaks of mineral oil and crude oil include the 1297 and 1439 cm^{-1} bands representing the CH_2 twist and bend, respectively (see SI Figure S7). The consistent alterations (1297 and 1439 cm^{-1}) in all bacterial spectra exposed to alkanes and alkane mixtures prove that *A. baylyi* has specific affinity toward alkane molecules.[16,77]

The results of LDA and dispersion indicator (D_I) scores plots show the specific chemotaxis-related affinity and accumulation of *A. baylyi* toward different alkanes (Figure 5). There is no significant discrimination between the categories of *A. baylyi* exposed to 0, 1, or 2 mg/L dodecane (Figure 5A), while

DOI: 10.1021/acs.analchem.6b02297
Anal. Chem. 2017, 89, 3909−3918

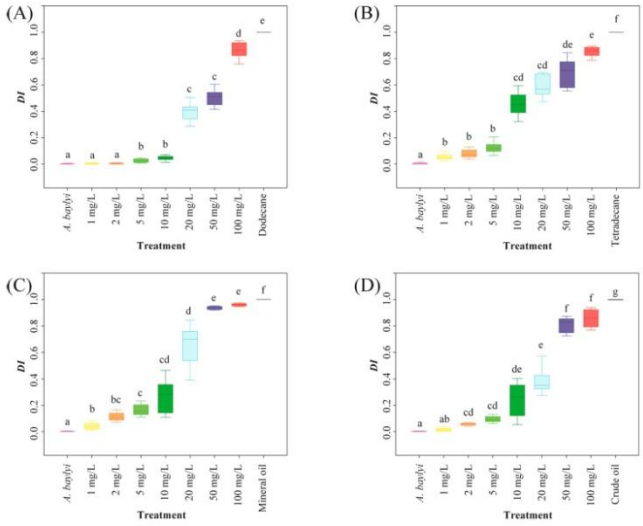

Figure 5. D_I scores plots of *A. baylyi* Raman spectra following different concentrations of dodecane (A), tetradecane (B), mineral oil (C), or crude oil (D). For each treatment, 20 replicates were performed. Boxes with different letters indicated a significant difference based on LSD (*P*-value < 0.05).

A. baylyi treated with 1 mg/L tetradecane is completely segregated from the negative control (0 mg/L, Figure 5B). This indicates that the limit of alkane detection via Raman microspectroscopy is 5 mg/L for dodecane and 1 mg/L for tetradecane. Although *A. baylyi* can respond to alkane levels as low as 0.1 mg/L by bioreporter data,[16] the lower sensitivity of Raman spectra is possibly attributed to the weak signal of accumulated or internalized alkane molecules. At low alkane concentrations, only partial MCP recognizes and captures alkane molecules. Similar behavior is observed for alkane mixtures, with a limit of detection of 1 mg/L for mineral oil and 2 mg/L for crude oil.

With increasing alkane levels, more alkane molecules accumulate on or inside *A. baylyi* cells, consequently resulting in increasing alkane characteristic peaks and more significant Raman spectral alterations. Above the limit of detection, all the alkanes or alkane mixtures gave rise to a semilog linear regression relationship with D_I (see SI Figure S8). The semilog linear slope of pure alkanes and alkane mixtures followed the order: mineral oil (0.583) > crude oil (0.532) > tetradecane (0.478) > dodecane (0.399). The quantification range was from 1 mg/L to 100 mg/L for tetradecane and mineral oil, 2 mg/L to 100 mg/L for crude oil, and 5 mg/L to 100 mg/L for dodecane. The values of semilog linear slopes were consistent with the limits of detection for all the pure alkanes and alkane mixtures. This indicates that the selectivity of alkane affinity and accumulation in *A. baylyi* varies with different carbon chain lengths. For instance, the *cheY1* and *cheY2* genes in *Alcanivorax dieselolei* are triggered by C_8–C_{24} *n*-alkanes and alkanes longer than C_{24}, respectively.[71] In this study, *A. baylyi* had higher affinity toward and subsequent accumulation of tetradecane than dodecane, due to a lower limit of detection (1 mg/L vs 5 mg/L) and higher slopes (0.478 vs 0.399). The expression of genes related to alkane affinity and internalization in *A. baylyi* is therefore dependent on alkane carbon chain length, and it can be evaluated and quantified by Raman spectra.

The differing spectral alteration in mineral oil and crude oil treatments suggests that *A. baylyi* exhibits the stronger sensitivity of chemotaxis-related affinity and accumulation for mineral oil than crude oil. Considering the composition of the two alkane mixtures, mineral oil is fully composed of alkanes with different carbon chain lengths, whereas alkanes only account for 20–25% of the total weight of crude oil. Not all the molecules of crude oil can be chemotactically sensed by *A. baylyi* cells, consequently resulting in the lowest affinity and accumulation. More interestingly from linear slopes, both tetradecane and dodecane have lower affinity than mineral oil and crude oil. From the discussion above, the MCP recognition and expression is dependent on the carbon chain length of alkanes. For instance, the expression of the *alkM* alkane monooxygenese gene in *A. baylyi* is more highly induced by dodecane than tetradecane, suggesting that the *alkR* encoding AraC-XylS-like transcriptional regulators have unique sensitivity toward alkanes with different carbon chain lengths.[29,36,75,78] Thus, *A. baylyi* is hypothesized to have higher affinity toward some other alkane molecules with different carbon chain lengths in mineral oil or crude oil, and Raman spectral alterations of *A. baylyi* are enhanced postexposure to mineral oil and crude oil.

Though the current detection limit of the Raman assay is still above the natural hydrocarbon contamination level (0.1–1 mg/L) and does not meet with the monitoring requirement for environmental hydrocarbons, it can be improved by optimizing the attractant medium, such as pH and ionic strength.

DOI: 10.1021/acs.analchem.6b02297
Anal. Chem. 2017, 89, 3909–3918

Meanwhile, alkane affinity and accumulation have been extensively investigated, but there is a lack of effective approaches to quantify its sensitivity, which is one of the restriction factors in bioremediation at oil contaminated sites. Our results successfully prove the concept that Raman spectral alterations provide a rapid, nondestructive tool toward understanding alkane affinity and accumulation. More research is required to address the mechanisms of chemotaxis-related alkane affinity and accumulation to a wider range of alkanes with differing carbon chain lengths.

■ CONCLUSION

Herein, we developed a novel alkane quantification method based on chemotaxis-related alkane affinity and accumulation of *A. baylyi* and Raman spectral alterations. To the best of our knowledge, this is the first study to show that Raman microspectroscopy can be used to identify and quantify the microbial chemotaxis-related affinity and accumulation of alkanes. It opens up new possibilities for the rapid biological detection of aquatic alkane concentrations with natural microorganisms, instead of gene-modified bioreporters. Importantly, alkane chemo-affinity facilitates bacterial access to alkanes, and internalization determines alkane metabolism inside bacterial cells, both playing a key role in alkane degradation in the natural environment. The effective quantification of alkane affinity and accumulation via Raman spectra contribute to new insights into the microbial utilization of alkanes. This technique is also feasible to identify and characterize bacterial affinity and accumulation toward other molecules.

■ ASSOCIATED CONTENT

Supporting Information

The Supporting Information is available free of charge on the ACS Publications website at DOI: 10.1021/acs.analchem.6b02297.

Dispersion indicator model; Chemotaxis of *A. baylyi* and *P. fluorescence* to mineral oil, tetradecane, xylene, and phenanthrene (Figure S1); Raman spectra of *A. baylyi* exposure to different hydrocarbons (Figure S2); Relationship between dispersion indicator of Raman spectra and residual hydrocarbon contents (Figure S3); Raman spectra of *A. baylyi* against exposure time (Figure S4); Alkane chemotaxis against time via chemotaxis capillary assay (Figure S5); Raman spectra of *A. baylyi* exposure to different concentrations of dodecane and tetradecane (Figure S6); Raman spectra of *A. baylyi* exposure to different concentrations of mineral oil and crude oil (Figure S7); Semilog linear regression of the *n*-alkane concentrations and dispersion indicator within the quantification range (Figure S8) (PDF)

■ AUTHOR INFORMATION

Corresponding Author

*Tel.: +44(0)1524510288; Fax: +44(0)1524510082; E-mail: d.zhang@lancaster.ac.uk.

ORCID

Francis Luke Martin: 0000-0001-8562-4944

Dayi Zhang: 0000-0002-4175-5982

Notes

The authors declare no competing financial interest.

■ ACKNOWLEDGMENTS

The authors would like to thank National Natural Science Foundation of China (No. 41301331) and Lancaster University FST research grant for financial support. H.L. is supported by China Scholarship Council (CSC).

■ REFERENCES

(1) Bence, A. E.; Kvenvolden, K. A.; Kennicutt, M. C. *Org. Geochem.* **1996**, *24*, 7−42.

(2) Bragg, J. R.; Prince, R. C.; Harner, E. J.; Atlas, R. M. *Nature* **1994**, *368*, 413−418.

(3) Camilli, R.; Reddy, C. M.; Yoerger, D. R.; Van Mooy, B. A. S.; Jakuba, M. V.; Kinsey, J. C.; McIntyre, C. P.; Sylva, S. P.; Maloney, J. V. *Science* **2010**, *330*, 201−204.

(4) Zhang, D.; Ding, A.; Cui, S.; Hu, C.; Thornton, S. F.; Dou, J.; Sun, Y.; Huang, W. E. *Water Res.* **2013**, *47*, 1191−1200.

(5) Peterson, C. H.; Rice, S. D.; Short, J. W.; Esler, D.; Bodkin, J. L.; Ballachey, B. E.; Irons, D. B. *Science* **2003**, *302*, 2082−2086.

(6) Piatt, J. F.; Lensink, C. J.; Butler, W.; Kendziorek, M.; Nysewander, D. R. *Auk* **1990**, *107*, 387−397.

(7) USEPA Method 9071A, Oil & Grease - Extraction for Sludge & Sediment. 1998.

(8) USEPA Method 9071B, n-Hexane Extractable Material (HEM) for Sludge, Sediment, and Solid Samples. 1998.

(9) N-Hexane Extractable Material (HEM; Oil and Grease) and Silica Gel Treated N-Hexane Extractable Material (SGT-HEM; Non-Polar Material) by Extraction and Gravimetry. 1999.

(10) Zhou, Z.; Guo, L.; Shiller, A. M.; Lohrenz, S. E.; Asper, V. L.; Osburn, C. L. *Mar. Chem.* **2013**, *148*, 10−21.

(11) Wang, C.; Shi, X.; Li, W.; Wang, L.; Zhang, J.; Yang, C.; Wang, Z. *Mar. Pollut. Bull.* **2016**, *104*, 322−328.

(12) Lay-Ekuakille, A.; Palamara, I.; Caratelli, D.; Morabito, F. C. *Rev. Sci. Instrum.* **2013**, *84*, 015103.

(13) Krupcik, J.; Gorovenko, R.; Spanik, I.; Bockova, I.; Sandra, P.; Armstrong, D. W. *J. Chromatogr. A* **2013**, *1301*, 225−236.

(14) Liu, W.; Chen, J.; Lin, X.; Fan, Y.; Tao, S. *Environ. Pollut.* **2007**, *146*, 470−477.

(15) D'Auria, M.; Racioppi, R.; Velluzzi, V. *J. Chromatogr. Sci.* **2008**, *46*, 339−344.

(16) Zhang, D.; He, Y.; Wang, Y.; Wang, H.; Wu, L.; Aries, E.; Huang, W. E. *Microb. Biotechnol.* **2012**, *5*, 87−97.

(17) Sticher, P.; Jaspers, M. C. M.; Stemmler, K.; Harms, H.; Zehnder, A. J. B.; vanderMeer, J. R. *Appl. Environ. Microbiol.* **1997**, *63*, 4053−4060.

(18) Wang, W.; Shao, Z. *Front. Microbiol.* **2013**, *4*. 116.

(19) Parales, R. E.; Harwood, C. S. *Curr. Opin. Microbiol.* **2002**, *5*, 266−273.

(20) Smits, T. H. M.; Witholt, B.; van Beilen, J. B. *Antonie van Leeuwenhoek* **2003**, *84*, 193−200.

(21) van Beilen, J. B.; Panke, S.; Lucchini, S.; Franchini, A. G.; Rothlisberger, M.; Witholt, B. *Microbiology* **2001**, *147*, 1621−1630.

(22) Lanfranconi, M. P.; Alvarex, H. M.; Studdert, C. A. *Environ. Microbiol.* **2003**, *5*, 1002−1008.

(23) Lai, Q.; Li, W.; Shao, Z. *J. Bacteriol.* **2012**, *194*, 6674−6674.

(24) Huang, W. E.; Singer, A. C.; Spiers, A. J.; Preston, G. M.; Whiteley, A. S. *Environ. Microbiol.* **2008**, *10*, 1668−1680.

(25) Vaneechoutte, M.; Young, D. M.; Ornston, L. N.; De Baere, T.; Nemec, A.; Van Der Reijden, T.; Carr, E.; Tjernberg, I.; Dijkshoorn, L. *Appl. Environ. Microbiol.* **2006**, *72*, 932−936.

(26) Young, D. M.; Parke, D.; Ornston, L. N. *Annu. Rev. Microbiol.* **2005**, *59*, 519−551.

(27) Foster, J. *Oxygenases*; Academic: New York, 1962; pp 241−261.

(28) Rosenberg, E. *Trends Biotechnol.* **1993**, *11*, 419−424.

(29) Wentzel, A.; Ellingsen, T. E.; Kotlar, H.-K.; Zotchev, S. B.; Throne-Holst, M. *Appl. Microbiol. Biotechnol.* **2007**, *76*, 1209−1221.

(30) Boulton, C.; Ratledge, C. *Top. Enzyme Ferment. Biotechnol.* **1984**, *9*, 11−77.

DOI: 10.1021/acs.analchem.6b02297
Anal. Chem. 2017, 89, 3909−3918

(31) Haferburg, D.; Hommel, R.; Claus, R.; Kleber, H.-P. *Bioproducts*; Springer: 1986; pp 53−93.
(32) Singer, M.; Finnerty, W. 1984, http://agris.fao.org/agris-search/search.do?recordID=US8605568.
(33) Efrima, S.; Zeiri, L. *J. Raman Spectrosc.* **2009**, *40*, 277−288.
(34) Efrima, S.; Bronk, B. *J. Phys. Chem. B* **1998**, *102*, 5947−5950.
(35) Guzelian, A. A.; Sylvia, J. M.; Janni, J. A.; Clauson, S. L.; Spencer, K. M. In *Environmental and Industrial Sensing*; International Society for Optics and Photonics: 2002; pp 182−192.
(36) Wang, Y.; Ravindranath, S.; Irudayaraj, J. *Anal. Bioanal. Chem.* **2011**, *399*, 1271−1278.
(37) Zhou, H.; Yang, D.; Ivleva, N. P.; Mircescu, N. E.; Schubert, S. r.; Niessner, R.; Wieser, A.; Haisch, C. *Anal. Chem.* **2015**, *87*, 6553−6561.
(38) Cheng, H.-W.; Huan, S.-Y.; Yu, R.-Q. *Analyst* **2012**, *137*, 3601−3608.
(39) Cheng, H.-W.; Luo, W.-Q.; Wen, G.-L.; Huan, S.-Y.; Shen, G.-L.; Yu, R.-Q. *Analyst* **2010**, *135*, 2993−3001.
(40) Cui, L.; Chen, P.; Chen, S.; Yuan, Z.; Yu, C.; Ren, B.; Zhang, K. *Anal. Chem.* **2013**, *85*, 5436−5443.
(41) Liu, Y.; He, L.; Mustapha, A.; Li, H.; Hu, Z.; Lin, M. *J. Appl. Microbiol.* **2009**, *107*, 1193−1201.
(42) Schuster, K. C.; Reese, I.; Urlaub, E.; Gapes, J. R.; Lendl, B. *Anal. Chem.* **2000**, *72*, 5529−5534.
(43) Kearns, D. B. *Nat. Rev. Microbiol.* **2010**, *8*, 634−644.
(44) Berg, H. C.; Turner, L. *Biophys. J.* **1990**, *58*, 919−930.
(45) Block, S. M.; Segall, J. E.; Berg, H. C. *J. Bacteriol.* **1983**, *154*, 312−323.
(46) Shi, L. Z.; Nascimento, J.; Chandsawangbhuwana, C.; Berns, M. W.; Botvinick, E. L. *Microsc. Res. Tech.* **2006**, *69*, 894−902.
(47) Adler, J. *J. Gen. Microbiol.* **1973**, *74*, 77−91.
(48) Wang, X.; Zhao, X.; Li, H.; Jia, J.; Liu, Y.; Ejenavi, O.; Ding, A.; Sun, Y.; Zhang, D. *Res. Microbiol.* **2016**, *167*, 731−744.
(49) Cui, L.; Butler, H. J.; Martin-Hirsch, P. L.; Martin, F. L. *Anal. Methods* **2016**, *8*, 481−487.
(50) Trevisan, J.; Angelov, P. P.; Scott, A. D.; Carmichael, P. L.; Martin, F. L. *Bioinformatics* **2013**, *29*, 1095−1097.
(51) Butler, H. J.; Ashton, L.; Bird, B.; Cinque, G.; Curtis, K.; Dorney, J.; Esmonde-White, K.; Fullwood, N. J.; Gardner, B.; Martin-Hirsch, P. L.; Walsh, M. J.; McAinsh, M. R.; Stone, N.; Martin, F. L. *Nat. Protoc.* **2016**, *11*, 664−687.
(52) Mao, H.; Cremer, P. S.; Manson, M. D. *Proc. Natl. Acad. Sci. U. S. A.* **2003**, *100*, 5449−5454.
(53) Mizushima, S.-i.; Simanouti, T. *J. Am. Chem. Soc.* **1949**, *71*, 1320−1324.
(54) Kalyanasundaram, K.; Thomas, J. *J. Phys. Chem.* **1976**, *80*, 1462−1473.
(55) Graham, S. F.; Haughey, S. A.; Ervin, R. M.; Cancouët, E.; Bell, S.; Elliott, C. T. *Food Chem.* **2012**, *132*, 1614−1619.
(56) Orange, D.; Knittle, E.; Farber, D.; Williams, Q. *Geol. Soc. Spec. Pub.* **1996**, *5*, 65−81.
(57) Barbe, V.; Vallenet, D.; Fonknechten, N.; Kreimeyer, A.; Oztas, S.; Labarre, L.; Cruveiller, S.; Robert, C.; Duprat, S.; Wincker, P. *Nucleic Acids Res.* **2004**, *32*, 5766−5779.
(58) De Gelder, J.; De Gussem, K.; Vandenabeele, P.; Moens, L. *J. Raman Spectrosc.* **2007**, *38*, 1133−1147.
(59) Cloutis, E.; Szymanski, P.; Applin, D.; Goltz, D. *Icarus* **2016**, *274*, 211−230.
(60) Konradi, J.; Singh, A. K.; Materny, A. *Phys. Chem. Chem. Phys.* **2005**, *7*, 3574−3579.
(61) Biedermann, M.; Grob, K. *J. Chromatogr. A* **2012**, *1255*, 56−75.
(62) Tarnow, P.; Hutzler, C.; Grabiger, S.; Schon, K.; Tralau, T.; Luch, A. *PLoS One* **2016**, *11*, e0147239.
(63) Wang, S.-K.; Wang, F.; Hu, Y.-R.; Stiles, A. R.; Guo, C.; Liu, C.-Z. *ACS Appl. Mater. Interfaces* **2014**, *6*, 109−115.
(64) Briegel, A.; Li, X.; Bilwes, A. M.; Hughes, K. T.; Jensen, G. J.; Crane, B. R. *Proc. Natl. Acad. Sci. U. S. A.* **2012**, *109*, 3766−3771.
(65) Hazelbauer, G. L.; Falke, J. J.; Parkinson, J. S. *Trends Biochem. Sci.* **2008**, *33*, 9−19.
(66) Xu, L.; Guo, C.; Wang, F.; Zheng, S.; Liu, C.-Z. *Bioresour. Technol.* **2011**, *102*, 10047−10051.
(67) Liu, J.; Hu, B.; Morado, D. R.; Jani, S.; Manson, M. D.; Margolin, W. *Proc. Natl. Acad. Sci. U. S. A.* **2012**, *109*, E1481−8.
(68) Lanfranconi, M. P.; Alvarez, H. M.; Studdert, C. A. *Environ. Microbiol.* **2003**, *5*, 1002−1008.
(69) Smits, T. H.; Witholt, B.; van Beilen, J. B. *Antonie van Leeuwenhoek* **2003**, *84*, 193−200.
(70) Sourjik, V.; Armitage, J. P. *EMBO J.* **2010**, *29*, 2724−2733.
(71) Wang, W.; Shao, Z. *Nat. Commun.* 2014, *5*.
(72) Prince, R. C.; McFarlin, K. M.; Butler, J. D.; Febbo, E. J.; Wang, F. C.; Nedwed, T. J. *Chemosphere* **2013**, *90*, 521−526.
(73) Lal, B.; Khanna, S. *J. Appl. Microbiol.* **1996**, *81*, 355−362.
(74) Maeng, J. H.; Sakai, Y.; Tani, Y.; Kato, N. *J. Bacteriol.* **1996**, *178*, 3695−3700.
(75) Ratajczak, A.; Geißdörfer, W.; Hillen, W. *J. Bacteriol.* **1998**, *180*, 5822−5827.
(76) Throne-Holst, M.; Wentzel, A.; Ellingsen, T. E.; Kotlar, H.-K.; Zotchev, S. B. *Appl. Environ. Microbiol.* **2007**, *73*, 3327−3332.
(77) Tanaka, D.; Takashima, M.; Mizuta, A.; Tanaka, S.; Sakatoku, A.; Nishikawa, A.; Osawa, T.; Noguchi, M.; Aizawa, S.-I.; Nakamura, S. *Curr. Microbiol.* **2010**, *60*, 203−209.
(78) Wang, X. B.; Nie, Y.; Tang, Y. Q.; Wu, G.; Wu, X. L. *Appl. Environ. Microbiol.* **2013**, *79*, 400−402.

DOI: 10.1021/acs.analchem.6b02297
Anal. Chem. 2017, 89, 3909−3918

Electronic Supporting Information

Quantification of alkane chemotaxis and accumulation in *Acinetobacter baylyi* using Raman microspectroscopy

Hanbing Li[a], Francis Luke Martin[a,b], Dayi Zhang[a,*]

[a] Lancaster Environment Centre, Lancaster University, Lancaster, LA1 4YQ, UK

[b] School of Pharmacy and Biomedical Sciences, University of Central Lancashire, Preston PR1 2HE, UK

No. of Pages = 11

No. of Figures = 8

Dispersion indicator model

The initial spectral dataset is an ensemble of multivariate observations partitioned into M distinct groups (different microbiota composition in this study). For the n_m observation in each group (m runs from 1 to M and refers to the m^{th} group). The multivariate observation vectors can be written as n_{mi} where i is the i^{th} observation. To search for the linear combination in linear discriminant analysis (LDA) that optimally separates our multivariate observation into M groups (Ami et al., 2013a), the linear transformation of y_{mi} is written as z_{mi}:

$$z_{mi} = w^T y_{mi} \tag{1}$$

Here, w^T represents the linear transformation matrix, and the mean of the m^{th} group of the transformed data ($\langle z_m \rangle$) is:

$$\langle z_m \rangle = w^T \langle y_m \rangle \tag{2}$$

where y_m is the mean of the observations within a group and defined as:

$$\langle y_m \rangle = \sum_{j=1}^{n_m} y_{mj} / n_m \tag{3}$$

The dispersion among groups (B) and within groups (E) are defined in the following equations:

$$B_y = \sum_{m=1}^{G} n_m (\langle y_{mi} \rangle - \langle y \rangle)(\langle y_{mi} \rangle - \langle y \rangle)^T \tag{4}$$

$$E_y = \sum_{m=1}^{G} n_g \sum_{j=1}^{n_m} (\langle y_{mi} \rangle - \langle y_m \rangle)(\langle y_{mi} \rangle - \langle y_m \rangle)^T \tag{5}$$

where $\langle y \rangle = \frac{1}{M} \sum_{m=1}^{G} \frac{1}{n_m} \sum_{j=1}^{n_m} y_{mj}$ is the total average of the dataset. Using Fisher's linear discriminant, the optimal linear regression in PCA-LDA is to find the vector w maximizing λ (the rate of between-groups sum of squares to within-groups sum of squares):

$$\lambda = \frac{w^T B_y w}{w^T E_y w} \tag{6}$$

The solutions of Equation (6) are the eigenvalues $|\lambda|$, which are associated to the eigenvectors $|w|$. In the most cases, the first two ranked λ_1 and λ_2 account for the most of $|\lambda|$, and the discriminant functions are obtained as LD1 ($z_1 = w_1^T Y$) and LD2

($z_2 = w_2^T Y$) to represent the spectra variables of each community.

The dispersions of the among groups (B) and within groups (E) (Fig. 2B) are defined in the following equations:

$$O_{y,q}|(q = 0,1) = w^T B'_{y,q} w = w^T \left\{ \sum_{i=1}^{M} \sum_{j=1}^{M} n_m \left(\langle y_{mi} \rangle - \langle y_{qj} \rangle \right) \left(\langle y_{mi} \rangle - \right.\right.$$

yqjTw=i=1Mj=1MngwTymi−wTyqjwTymi−wTyqjT=i=1Mj=1Mngzmi−zqizmi−zqiT (7)

$$T_y = w^T E'_y w = \sum_{q=0,1} \sum_{i=1}^{M} \sum_{j=1}^{M} n_g \left(\langle z_{mi} \rangle - \langle z_{qj} \rangle \right) \left(\langle z_{gi} \rangle - \langle z_{qj} \rangle \right)^T \quad (8)$$

Here we introduce the dispersion indicator (D_I) to calculate the spectra dissimilarity of targeting groups to negative control (alkane/oil concentration = 0 mg/L, $q = 0$) and pure alkane/oil groups ($q = 1$), defined as:

$$D_I = \frac{O_{y,0}}{T_y} \quad (9)$$

$$\sum_{q=0}^{1} D_{I,q} = \frac{O_{y,q}}{T_y} = 100\% \quad (10)$$

Reference

(1) Ami, D.; Mereghetti, P.; Doglia, S. M. *Multivariate analysis for Fourier transform infrared spectra of complex biological systems and processes*; INTECH Open Access Publisher, 2013.

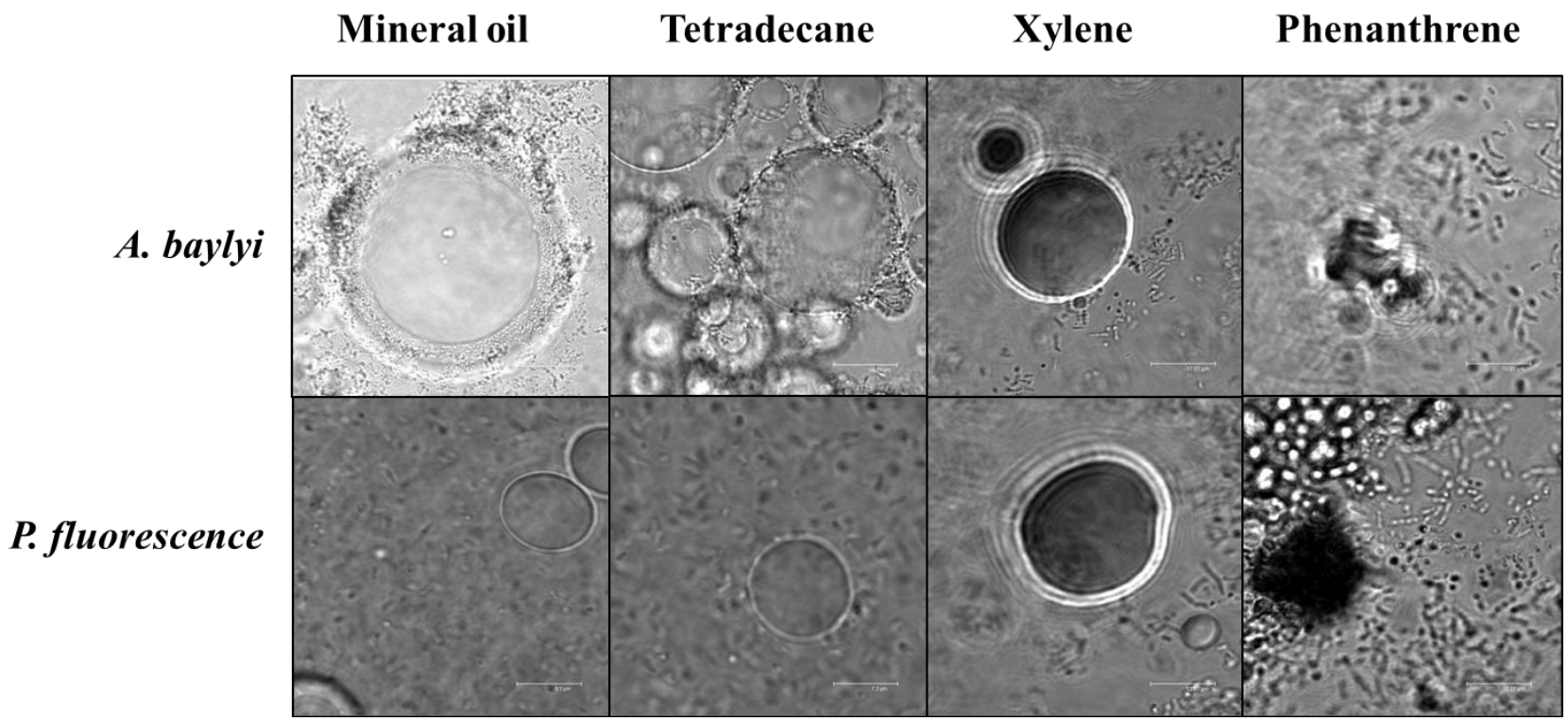

Figure S1 Chemotaxis of *A. baylyi* and *P. fluorescence* to mineral oil, tetradecane, xylene and phenanthrene.

.

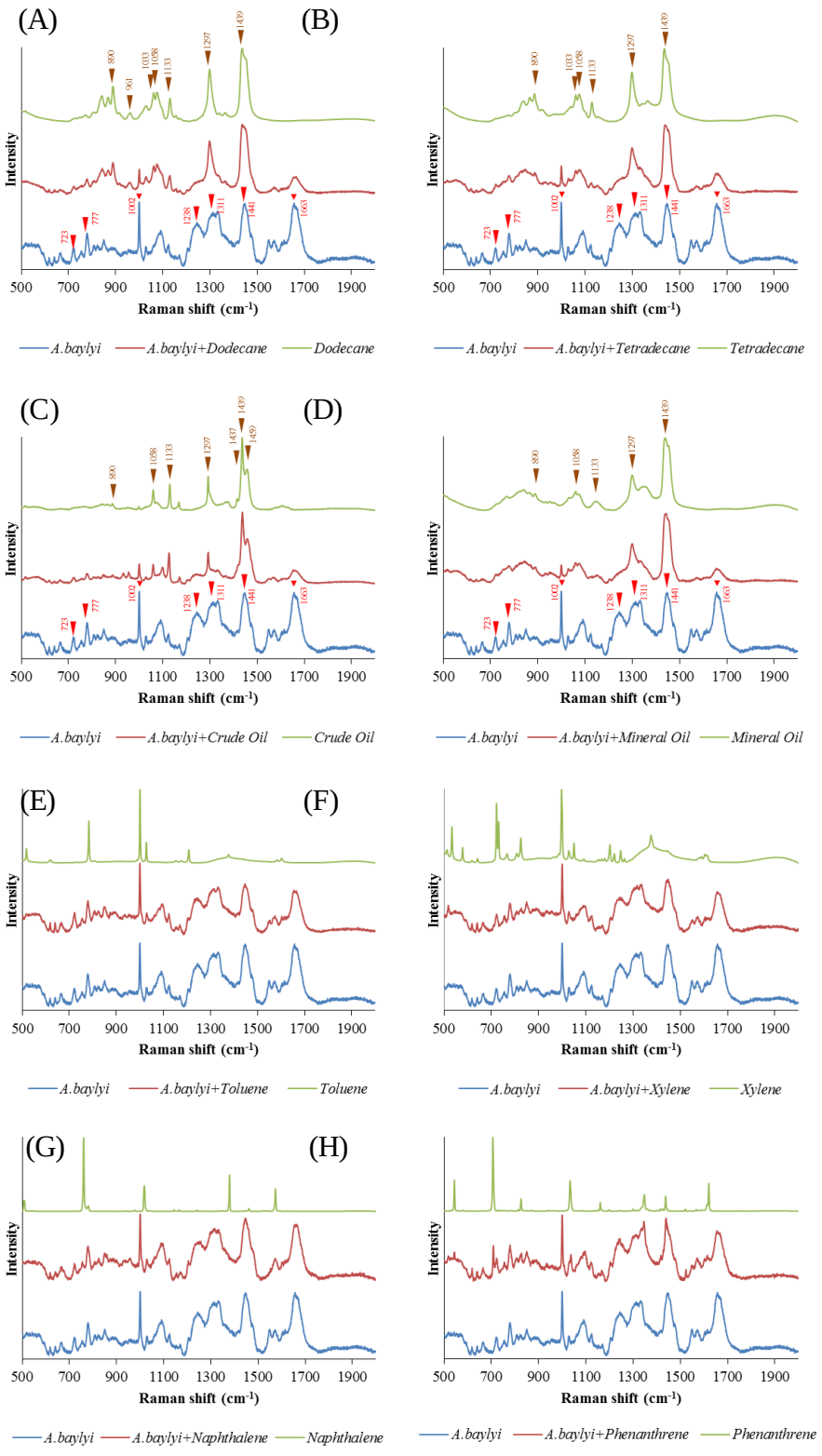

Figure S2 Raman spectra of *A. baylyi* exposure to different hydrocarbons. The chemicals with alkane-chemotaxis effect include: dodecane (A), tetradecane (B), mineral oil (C) and crude oil (D). The chemicals without chemotaxis effect include: monocyclic aromatic hydrocarbons [toluene (E) or xylene (F)] and polycyclic

aromatic hydrocarbons [naphthalene (G) or phenanthrene (H)].

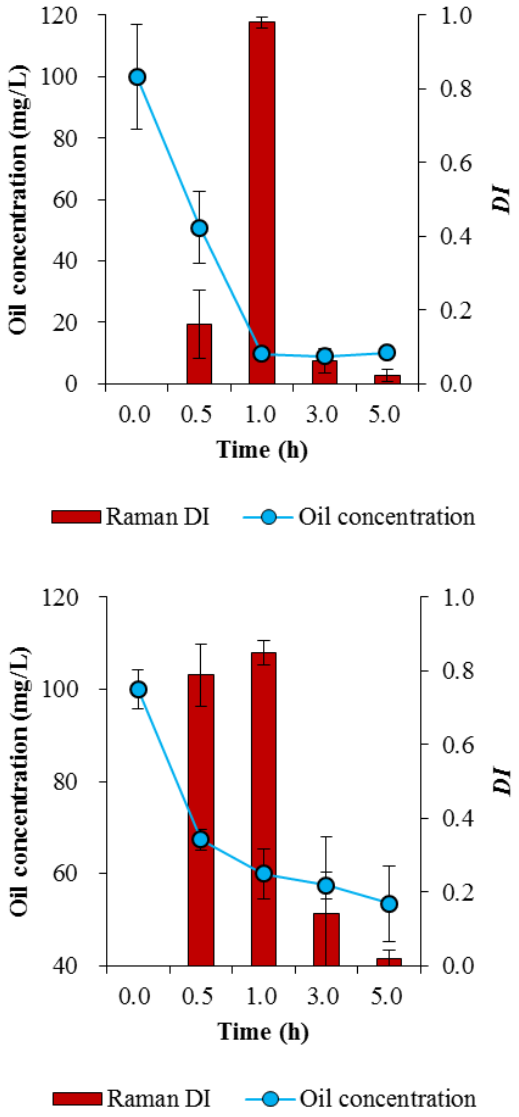

Figure S3. Relationship between dispersion indicator (*DI*) of Raman spectra and residual hydrocarbon contents. (A) for crude oil and (B) for tetradecane.

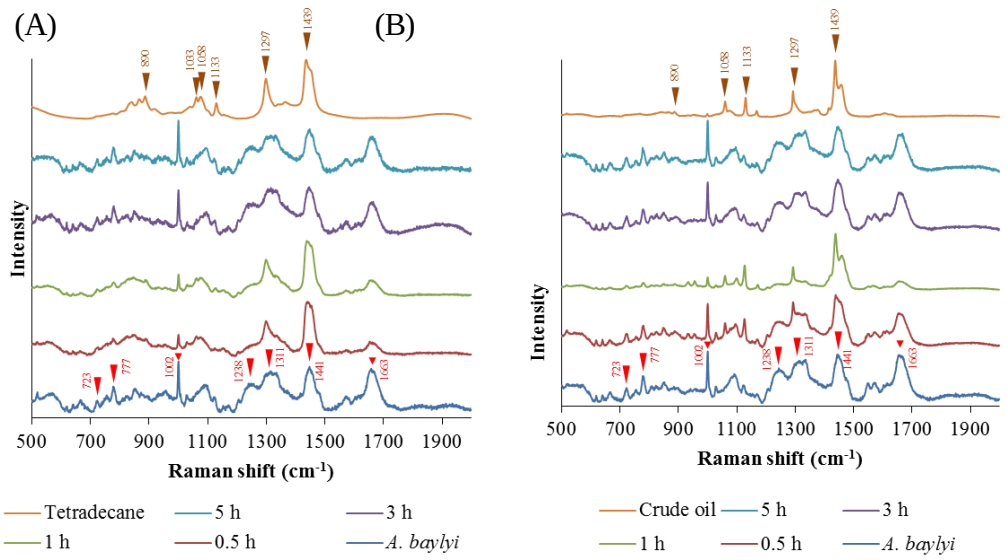

Figure S4. Raman spectra of *A. baylyi* against exposure time in tetradecane (A) and crude oil (B) treatments. Twenty Raman spectra were randomly obtained per treatment.

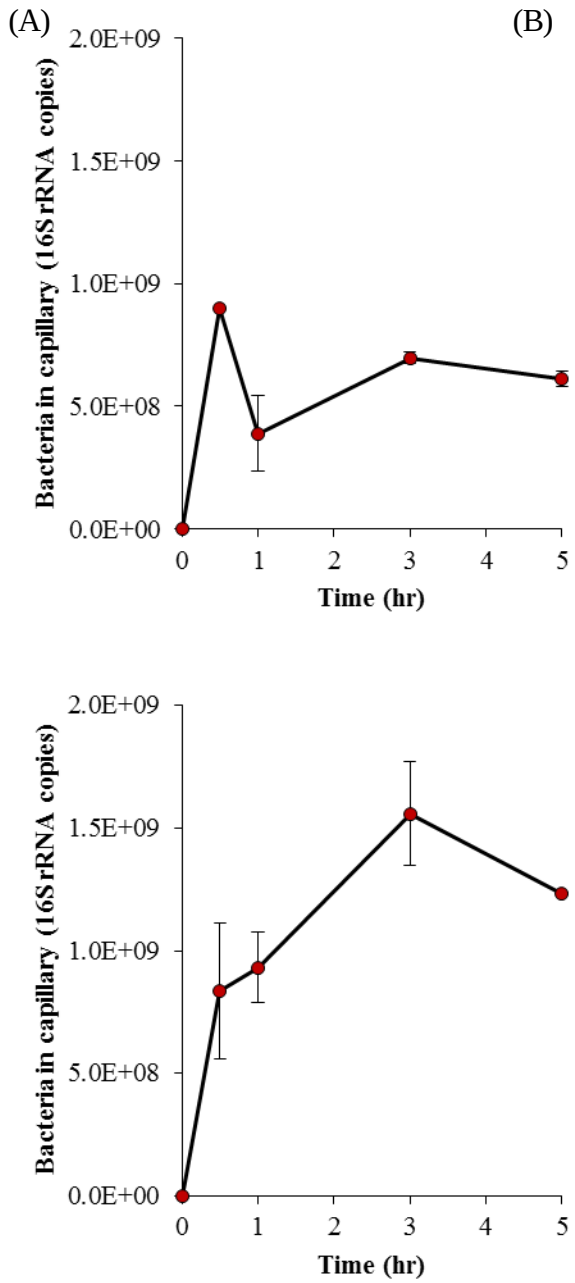

Figure S5. Alkane chemotaxis against time via chemotaxis capillary assay. (A) for crude oil and (B) for tetradecane.

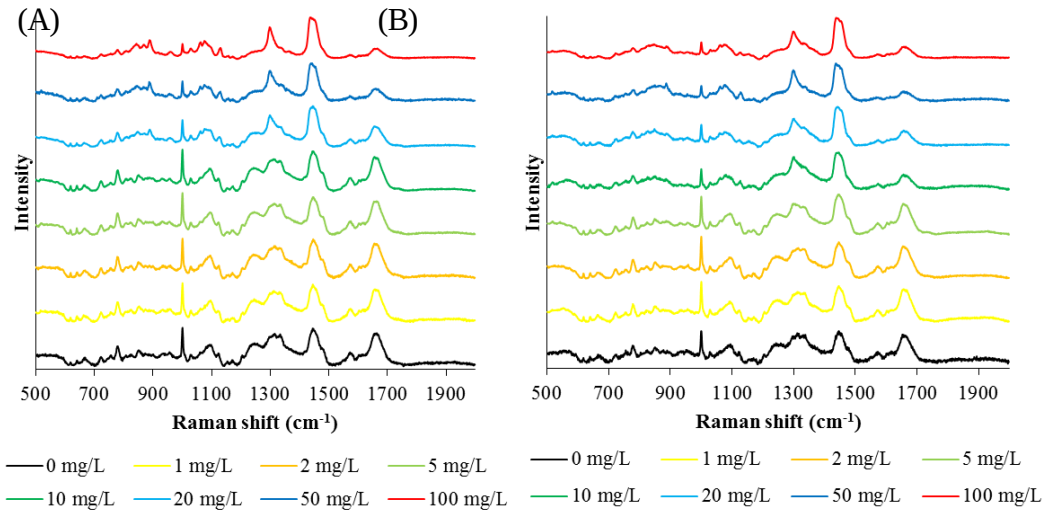

Figure S6. Raman spectra of *A. baylyi* exposure to different concentrations of dodecane (A) and tetradecane (B). Twenty Raman spectra were randomly obtained per treatment.

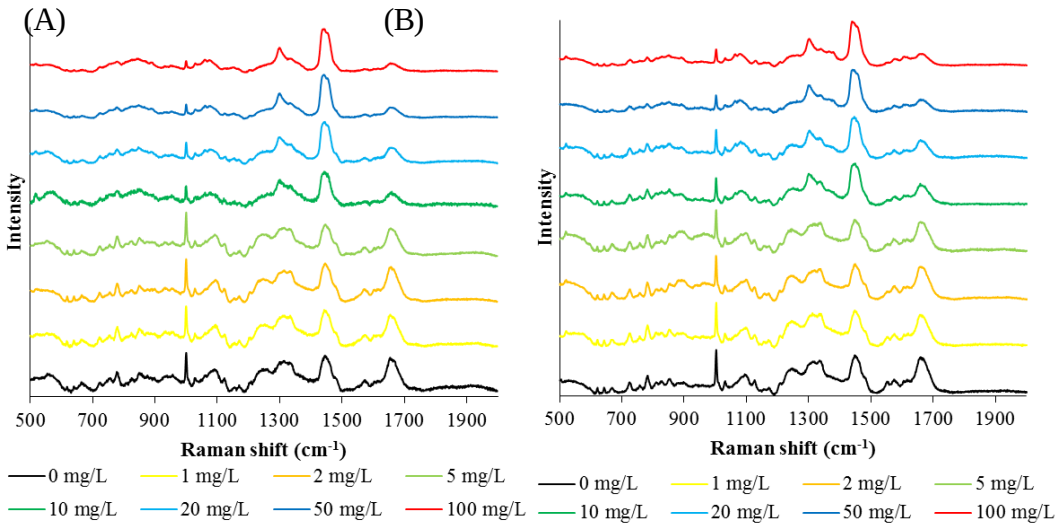

Figure S7. Raman spectra of *A. baylyi* exposure to different concentrations of mineral oil (A) and crude oil (B). Twenty Raman spectra were randomly obtained per treatment.

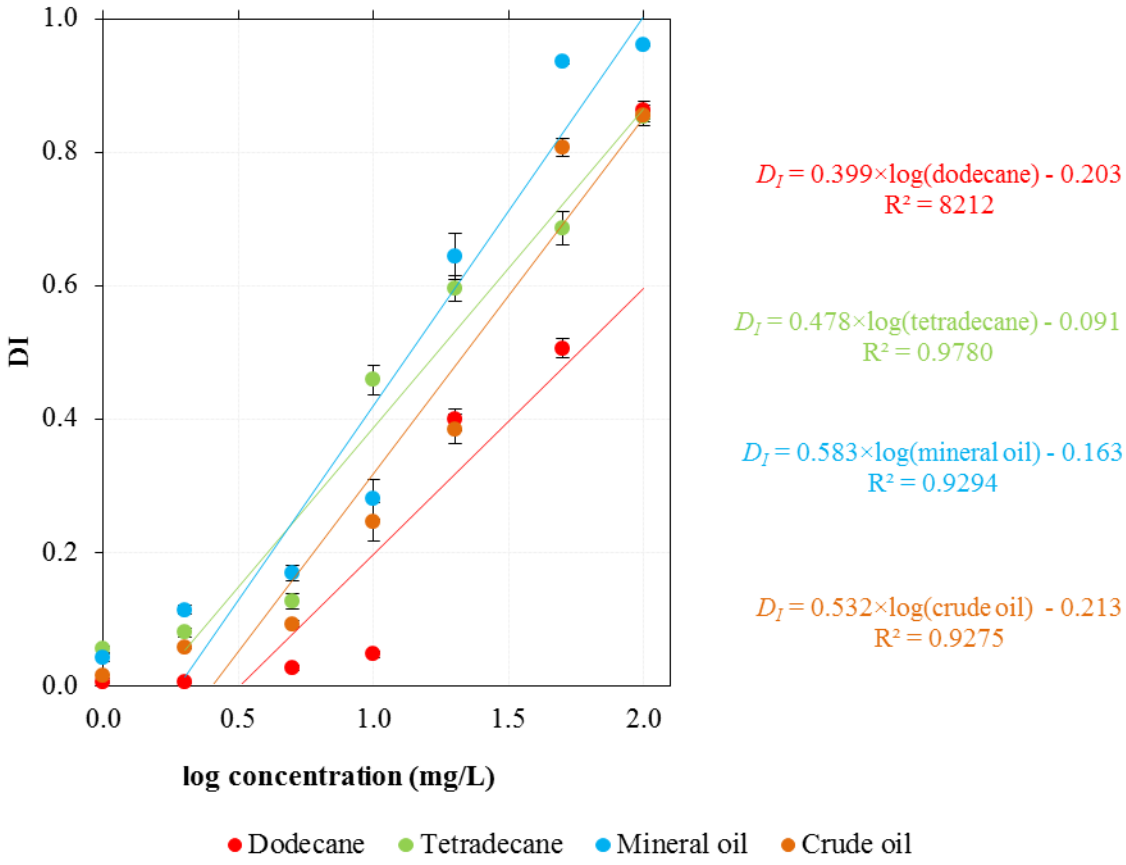

Figure S8. Semi-log linear regression of the n-alkane concentrations and dispersion indicator (D_I) within the quantification range (2 mg/L to 100 mg/L for tetradecane, mineral oil and crude oil; 10 mg/L to 50 mg/L for dodecane).

Chapter 3

Investigating Impacts of Nutrient Cations on Alkane Chemotaxis-Related Affinity and Accumulation of *Acinetobacter baylyi* ADP1 *via* Raman Microspectroscopy

Hanbing Li, Francis L. Martin, Dayi Zhang

Manuscript for submission

Contribution:

- I prepared the samples required for the project;
- I processed and acquired all spectral data and carried out computational analysis;
- I prepared the first draft and figures of manuscript.

Investigating the impacts of nutrient cations on alkane chemotaxis-related affinity and accumulation of *Acinetobacter baylyi* ADP1 *via* Raman microspectroscopy

Hanbing Li[a], Francis L Martin[b], Dayi Zhang[c,a,*]

[a] Lancaster Environment Centre, Lancaster University, Lancaster LA1 4YQ, UK

[b] School of Pharmacy and Biomedical Sciences, University of Central Lancashire, Preston PR1 2HE, UK

[c] School of Environment, Tsinghua University, Beijing, 100086, PR China

***Corresponding author**

Dr Dayi Zhang

School of Environment, Tsinghua University, Beijing, 100086, PR China

Lancaster Environment Centre, Lancaster University, Lancaster LA1 4YQ, UK

Tel.: +44(0)1524510288; Fax: +44(0)1524510082; Email: d.zhang@lancaster.ac.uk

Abstract

Crude oil contamination has attracted substantial attentions due to its extensive damage to ecological system, and potential threats to human health. On alkane contaminated sites, many indigenous bacteria can degrade alkanes, and some of them have been reported to possess the abilities of alkane chemotaxis and accumulate. To remediate alkane contaminations, several alkane-degrading bacterial strains have been studied. However, the physicochemical properties and nutrient ions of the environment reduce the efficiency of such bioremediation. It is required to identify the influences of nutrient cations on alkane affinity and accumulation in bacterial cells. In present study, we apply Raman microspectroscopy to study how the extra cations affected chemotaxis-related affinity and accumulation of *Acinetobacter baylyi* ADP1 towards pure alkanes and their mixture. After being treated with four extra nutrient cations (Na^+, K^+, Mg^{2+} and Ca^{2+}), *A. baylyi* ADP1 were exposed to pure n-alkane molecules in different carbon lengths (decane, dodecane, tetradecane, hexadecane, nonadecane, eicosane and tetracosane), and alkane mixture (mineral oil). Our Raman spectral alterations from multivariate analysis indicated that chemotaxis-related affinity and accumulation was dependent on the carbon chain lengths and the extra cations altered the pattern of bacterial affinity to n-alkane molecules. Sodium significantly increased the bacterial affinity towards short-chain alkanes (decane and dodecane), whereas potassium and magnesium enhanced that towards medium-chain alkanes (tetradecane and hexadecane). On the contrast, the bacterial chemotactic response towards alkanes was inhibited by calcium. As for the alkane mixture (mineral oil), the bacterial chemotactic behaviours under different cation conditions were well explained by their change of pure alkanes. Our work used a new tool of Raman spectroscopy to offer a deep insight into how the nutrient cations affect bacterial affinity and accumulation towards alkanes, suggesting the chemotaxis associated alkane degradation of bacteria relies on extra nutrient cations present in natural environment.

Introduction

Due to the rapid industrial development and intensive urbanization processes, the usage of hydrocarbon-based chemicals such as crude oil and mineral oil is increasing in the world. The release of hydrocarbons from anthropogenic activities into the environment is a major cause for environmental pollution. Hence, oil spill accidents and contaminated sites have received considerable attention for decades. From the year of 1969, more than 40 large oil spill incidents have been reported, e.g. the Deepwater Horizon oil spill in Gulf of Mexico, the Xingang oil spill in Dalian, and the Exxon Valdez oil spill in Prince William Sound (Bence et al., 1996; Bragg et al., 1994; Camilli et al., 2010; Zhang et al., 2013). Oil spill can cause adverse effects on human healths and ecological systems, and result in extensive damages to marine and terrestrial living organisms (Wang et al., 2016; Peterson et al., 2003; Piatt et al., 1990; Wang and Fingas, 2003). In order to monitor and remediate oil spill contaminations, bacteria, as the possible strategy for hydrocarbon pollution, have attracted considerable research interests (Sticher et al., 1997; Van Beilen et al., 2003; Van Beilen and Funhoff, 2007; Wentzel et al., 2007; Zhang et al., 2012). Whole-cell bioreporters have been used for the evaluation of alkane bioavailability and bioaccessibility, some even applied in practical field, but the low reproducibility limits them for alkane monitoring (Zhang et al., 2013; Zhang et al., 2012). Hydrocarbon-degrading bacteria, which play a major role in bioremediation technologies for oil pollutant removal, are ubiquitous in soils (Leahy and Colwell, 1990; Yakimov et al., 2007). However, the physicochemical conditions and nutrient limitations of soil reduce the efficiency of bioremediation on hydrocarbon contaminated sites (Annweiler et al., 2000; de la Cueva et al., 2016). Prior to utilize alkane molecules, sensing and uptake are involved in initial steps for bacterial cells towards such chemicals (Shao and Wang, 2013). Therefore, it is required to uncover the influences of nutrient ions on bacterial chemotaxis-related affinity and accumulation towards alkanes.

In natural environment, a number of bacteria species are highly specialized to utilize alkanes as carbon sources, and some have shown positive chemotactic behaviours towards alkane molecules (Shao and Wang, 2013). Alkane chemotaxis affinity assists bacterial cells swimming down the concentration gradient to accumulate and utilize alkanes (Parales and Harwood, 2002). Bacterial chemotaxis system is associated with

methyl-accepting chemotaxis proteins (MCP), histine kinase (CheA) and signal transduction protein (CheW) (Wang and Shao, 2014). Several alkane degrading bacterial strains possess specific MCP-encoding genes. In *Pseudomonas putida* GPo1, *alkN* gene has been found to encode an MCP for alkane chemotaxis (van Beilen et al., 2001). The *tlpS* gene, situated in the downstream of *alkB1*, is believed to encode chemotaxis protein MCP for hexadecane chemotaxis in *Pseudomonas aeruginosa* PAO1 (Smits et al., 2003). In *Acinetobacter baylyi* ADP1, the transcriptional activator *alkR* gene is required for the expression of alkane hydroxylase *alkM* (Ratajczak et al., 1998). Though the chemotaxis mechanisms remain unknown in *A. baylyi*, this bacteria exhibits sensitive specificity to alkane molecules (Huang et al., 2008; Vaneechoutte et al., 2006; Young et al., 2005). Putative chemotaxis systems in *Acinetobacter* drive the fimbriae on cell membrane to access alkane droplets (Foster, 1962; Rosenberg, 1993). When attaching on alkane droplets, *Acinetobacter* produces a biosurfactant to emulsify alkanes. This biosurfactant is known as emulsan which is encoded in a gene cluster, termed *wee*, consisting of 20 open reading frames in *Acinetobacter* (Kothari et al., 2016). After being emulsified, alkane droplets are subsequently transported into bacterial cells for further utilization.

In previous studies, conventional methods including swarm plates (Kearns, 2010), capillary assays (Berg and Turner, 1990), temporal stimulation of tethered cells (Block et al., 1983), and automated tracking of swimming cells (Shi et al., 2006) have been performed to test the chemotaxis affinity of bacterial cells. Although these methods successfully confirm the chemotactic movement of bacterial cells towards specific chemical molecules, they fail in showing the impacts of different ions on bacterial chemotactic behaviours. In nature environments, the influences of nutrient ions are inevitable for the access and uptake of alkane molecules in bacterial cells. There is no study using Raman microspectroscopy to explore such influences on alkane chemotaxis-related affinity and bioaccumulation. The applications of Raman microspectroscopy in biological studies are well-documented (Efrima and Zeiri, 2009; Guzelian et al., 2002; Wang et al., 2011; Zhou et al., 2015). This fast, reproducible and non-destructive approach can provide vibrational information of the chemical collected by bacteria. It has been well developed to determine interactions of bacteria with alkane molecules (Li et al., 2017c). The analysis of differential alterations in Raman spectra allows the measurement of chemotactic behaviours of *A. baylyi*

towards alkane molecules with different extra ions, and characterizes the bacterial selection in alkane mixture.

In this study, we used Raman microspectroscopy to identify the impacts of four different nutrient ions (sodium, potassium, magnesium and calcium) on alkane affinity and accumulation in *A. baylyi*. Raman spectra reveal the patterns of ion-alkane relationships, in which sodium increases chemotaxis sensitivities towards short carbon length alkanes (decane and dodecane), potassium and magnesium enhances the bacterial affinity towards medium carbon length alkanes (tetradecane and hexadecane), while calcium inhibits bacterial movements towards alkane molecules. In addition, we confirm the changes of alkane molecules selected by *A. baylyi* in alkane mixture vary directly with extra nutrient ions. This study provides a novel insight into selective strategies of bacteria towards various hydrocarbon molecules in natural environments, which is potential to improve the efficiency of bioremediation techniques for hydrocarbon pollutions.

Materials and methods

Bacterial Strain and Growths Conditions

In this study, we used the alkane chemotactic *Acinetobacter baylyi* ADP1 for all treatments. Bacterial cells were incubated in minimal medium (MM) with 20 mM sodium succinate as the sole carbon source, shaking at 150 rpm and 30 ℃ for 16 h. Briefly, to prepare 1.0 L mineral medium, 1.0 g of $(NH_4)_2SO_4$, 2.5 g of KH_2PO_4, 0.1 g of $MgSO_4 \cdot 7H_2O$, 0.005 g of $FeSO_4 \cdot 7H_2O$, 0.25 g of nitrilotriacetic acid, 0.55 g of NaOH and 1 mL of Bauchop and Elsden solution were mixed well in 1.0 L deionized water and autoclaved (Jia et al., 2016). Strains were harvested by centrifugation at 4000 rpm for 4 min and washed three times using sterile deionized water. Afterwards, bacterial cells were suspended in fresh mineral medium to reach an average concentration of 10^7 CFU/mL for further experimentation.

Hydrocarbon exposure with four extra ions

Unless specifically stated otherwise, all chemicals in this study were of analytical grade and purchased from Sigma Aldrich (UK). To investigate the impacts of Na^+, K^+, Mg^{2+} and Ca^{2+} on bacterial chemotactic affinity towards alkanes, four chemicals (NaCl, KCl, $MgCl_2$ and $CaCl_2$) were used in this study. Chemicals were first dissolved

in mineral medium to prepare 100 mM ion stock solution, respectively. A certain volume of ion stock solution was mixed with bacterial suspensions to reach a final ionic concentration of 10 mM.

For hydrocarbon exposure, we used seven pure hydrocarbon chemicals: decane, dodecane, tetradecane, hexadecane, nonadecane, eicosane and tetracosane; and one hydrocarbon mixture: mineral oil. All hydrocarbon chemicals were dissolved in dimethyl sulfoxide (DMSO) to prepare the 10 g/L stock solution. The hydrocarbon stock solution was mixed with bacterial suspensions with/-out extra ions to reach a final concentration of 100 mg/L. A volume of 10 μL DMSO was mixed with bacteria suspensions as the control sample. All samples were incubated at 30 ℃ for 1 h, and further centrifuged at 5000 rpm for 5 min. The purpose of changes in centrifugation speed (from 4000 to 5000 rpm) and time (from 4 to 5 min) was to concentrate bacterial cells and to remove the medium. The cell pellets were resuspended in deionized water and washed twice.

Capillary test of hydrocarbon exposure with four different ions

To confirm the impacts of extra ions on bacterial chemotaxis, capillary assay were performed based on the protocol of Li et al. with some modifications (Li et al., 2017c). Capillary tubes (internal diameter of 0.2 mm and length of 10 cm) were immersed into 1 mL of chemotaxis attractant stock solution (alkanes or mineral oil) for 10 min until the liquid was drawn up to approximately 1 cm of the length of the tube. The capillary was then inserted into the bacterial suspensions with different extra ions, respectively, and incubated for 1 h at 30 ℃.

Quantitative polymerase chain reaction (qPCR) was introduced to quantify the 16S rRNA copy numbers of chemotactic bacteria in triplicate. After 1-h incubation, the capillary tube was removed and the 1-cm exterior from the open end was directly plunged into qPCR buffer. The 10 μL qPCR buffer included 1 μL of primer 314F (5'-CCTACGGGNGGCWGCAG-3'), 1 μL of primer 802R (5'-TACNVGGGTATCTAATCC-3'), 3 μL molecular water and 5 μL iTaq™ Universal SYBR® Green Supermix (BioRad, USA). The qPCR thermos cycling program of 16S rRNA was: initial denaturation at 94 ℃ for 3 min; 34 amplification cycles of 94 ℃ for 45 s, 52 ℃ for 45 s, 72 ℃ for 45 s, and fluorescence data acquisition at 80 ℃ for 15 s. The standard curves of were obtained with serial dilutions

of quantified plasmid DNA containing the fragment of 16S rRNA (Li et al., 2017a).

Raman microspectroscopy measurement

Prior to Raman microspectroscopy measurement, ten microliters of washed cell pellets were transferred onto a slide covered with aluminium foil and air-dried over night. Raman spectra of all samples were obtained using an InVia confocal micro-Raman system (Renishaw, Gloucestershire, UK). This system was equipped with a 100 mW 785 nm excitation laser diode. The entrance slit of the spectrometer is 50 μm combined with a 1200 lines per mm (1 cm^{-1} spatial resolution) diffraction grating, allowing the dispersion of Raman signals onto a Master Renishaw Pelletier cooled charged couple detector (CCD). Locations of sample detection were visualized via an attached microscope (Leica Microsystems, Milton Keynes, UK) with ×50 objective (0.75 numerical aperture; ≈1 μm spatial resolution). The Raman system was calibrated using a Renishwa silicon calibration source for wavenumber shifts before sample analysis. All sample spectra were obtained using 50% laser power (13 mW at sample), 10 s acquisition time, and one accumulation within a spectral range from 500 to 2000 cm^{-1}. All treatments were carried out in triplicates, and at least twenty replicates were performed and analysed for each sample.

Computational analysis of Raman spectra

Unless specifically stated otherwise, all Raman spectral data were normalized and analyzed using the IRootLab toolbox for MatLab (version R2013b, MathWorks, USA) (Trevisan et al., 2013). Baseline correction and vector normalization is essential for Raman spectra before principal component analysis (PCA) and linear discriminant analysis (LDA). PCA was employed to reduce the dimensionality of the multivariate data and allow visualization of the natural variance within the data set. To accomplish inter-class separation and minimize intra-class differences, LDA was used to extract inter-category discriminating features. The separation of individual spectral categories from negative control and pure alkane classes was measured by exporting PCA-derived data. Post-exposure to different types of alkanes or treated with different extra ions, the dispersion of individual Raman spectra to that of negative controls (no alkanes and no extra ions added) and pure alkane was calculated on the values of principal component (PC) 1 and PC2, and visualized as dispersion indicator (D_I) score plots. In D_I score plots, the increasing D_I value between two categories is proportional

to dissimilarity.

Results and discussion

Raman spectral characterization of alkane exposed *A. baylyi*

Before using Raman spectra to characterize the alkane or alkane mixture exposed bacterial cells, we first performed Raman microspectroscopy to measure the spectra of pure alkanes and alkane mixture to investigate the differences among those alkanes. Since decane, dodecane, tetradecane, hexadecane, nonadecane, eicosane and tetracosane are all belong to the categorization of linear alkane molecules, several Raman peaks in their Raman spectra are assigned to similar energy shifts (Figure1). Owing to the dominant structures of methyl (CH_3) and methylene (CH_2) in alkane molecules, Raman peaks generated from CH_3 and CH_2 are obvious in Raman spectra. The dominant peaks observed in all Raman spectra of n-alkane molecules include 890 cm^{-1} (CH_3 rock), 1060 cm^{-1} (C–C symmetric stretching), 1079 cm^{-1} (C–C stretching), 1136 cm^{-1} (CH_2 stretching), 1296 cm^{-1} (CH_2 twisting) and 1436 cm^{-1} (CH_2 bending) (Mizushima and Simanouti, 1949). Although Raman spectra of pure n-alkane molecules are similar, the spectra of decane and hexadecane show specific peaks at 1535 cm^{-1}, might attributed to the linkages of carbon and hydrogen deformation (Figure 1A) (Sheppard and Simpson, 1953). In the spectrum of dodecane, two distinct peaks are 961 and 1033 cm^{-1}, assigned to CH_2 rock (Figure 1B) (Kalyanasundaram and Thomas, 1976). Because of the solid state of nonadecane, eicosane and tetracosane, CH_2 bending band shifts to 1440 and 1463 cm^{-1}, indicating a increase in intermolecular interactions and vibrational motion (Figure 1E, 1F and 1G) (Corsetti et al., 2017). As the mixture of alkanes, the Raman spectra of mineral oil show similar peaks at 890, 1060, 1136 and 1436 cm^{-1} (Figure 1H).

To study the spectral alterations of post-exposed bacteria, Raman spectra of original *A. baylyi* were measured as control. From the results of Figure 1, Raman peaks at 1238 and 1311 cm^{-1} are assigned to amino acids, and the one at the 1441 cm^{-1} band is generated from the glycine in bacterial cells (Cui et al., 2013). In addition, the band at 1002 cm^{-1} represents phenylalanine, and 1663 cm^{-1} contributes to protein (De Gelder et al., 2007). *Acinetobacter baylyi* ADP1 are ubiquitous bacteria observed in natural soil environment that are frequently found to be able to utilize alkanes with carbon lengths ranging from 12 up to 36 (Zhang et al., 2012). Previous study has proved the

strong chemotactic affinity and accumulation of *A. baylyi* towards dodecane and tetradecane (Li et al., 2017b). As a consequence, Raman microspectroscopy is able to test the chemotaxis-related affinity of *A. baylyi* towards short, medium and long carbon chain length n-alkane molecules.

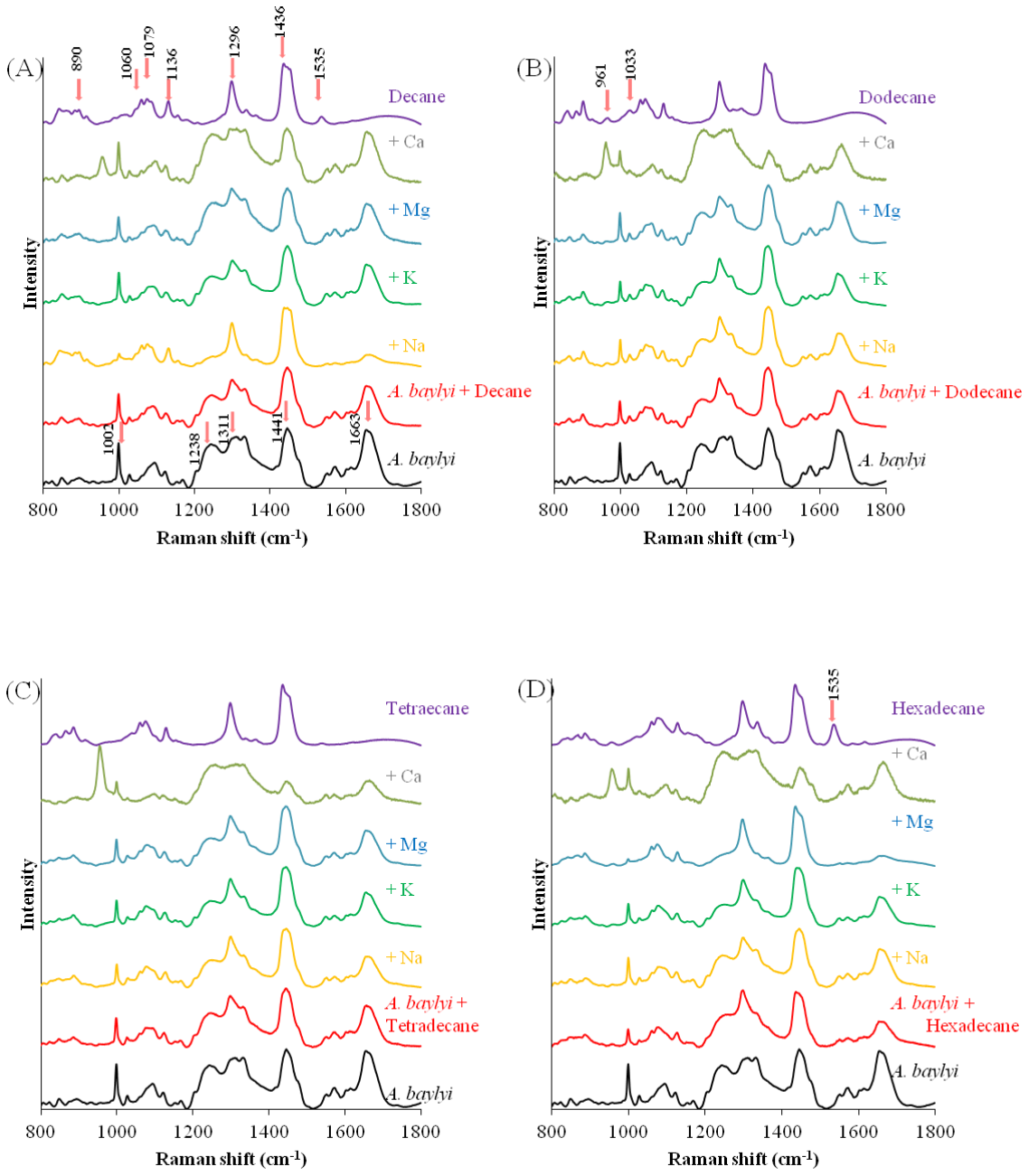
(A)
890
1060
1079
1136
1296
1436
1535
Decane
+ Ca
+ Mg
+ K
+ Na
A. baylyi + Decane
1003
1238
1311
1441
1663
A. baylyi
Intensity
800
1000
1200
1400
1600
1800
Raman shift (cm-1)
(B)
961
1033
Dodecane
+ Ca
+ Mg
+ K
+ Na
A. baylyi + Dodecane
A. baylyi
Intensity
800
1000
1200
1400
1600
1800
Raman shift (cm-1)
(C)
Tetraecane
+ Ca
+ Mg
+ K
+ Na
A. baylyi +
Tetradecane
A. baylyi
Intensity
800
1000
1200
1400
1600
1800
Raman shift (cm-1)
(D)
1535
Hexadecane
+ Ca
+ Mg
+ K
+ Na
A. baylyi +
Hexadecane
A. baylyi
Intensity
800
1000
1200
1400
1600
1800
Raman shift (cm-1)

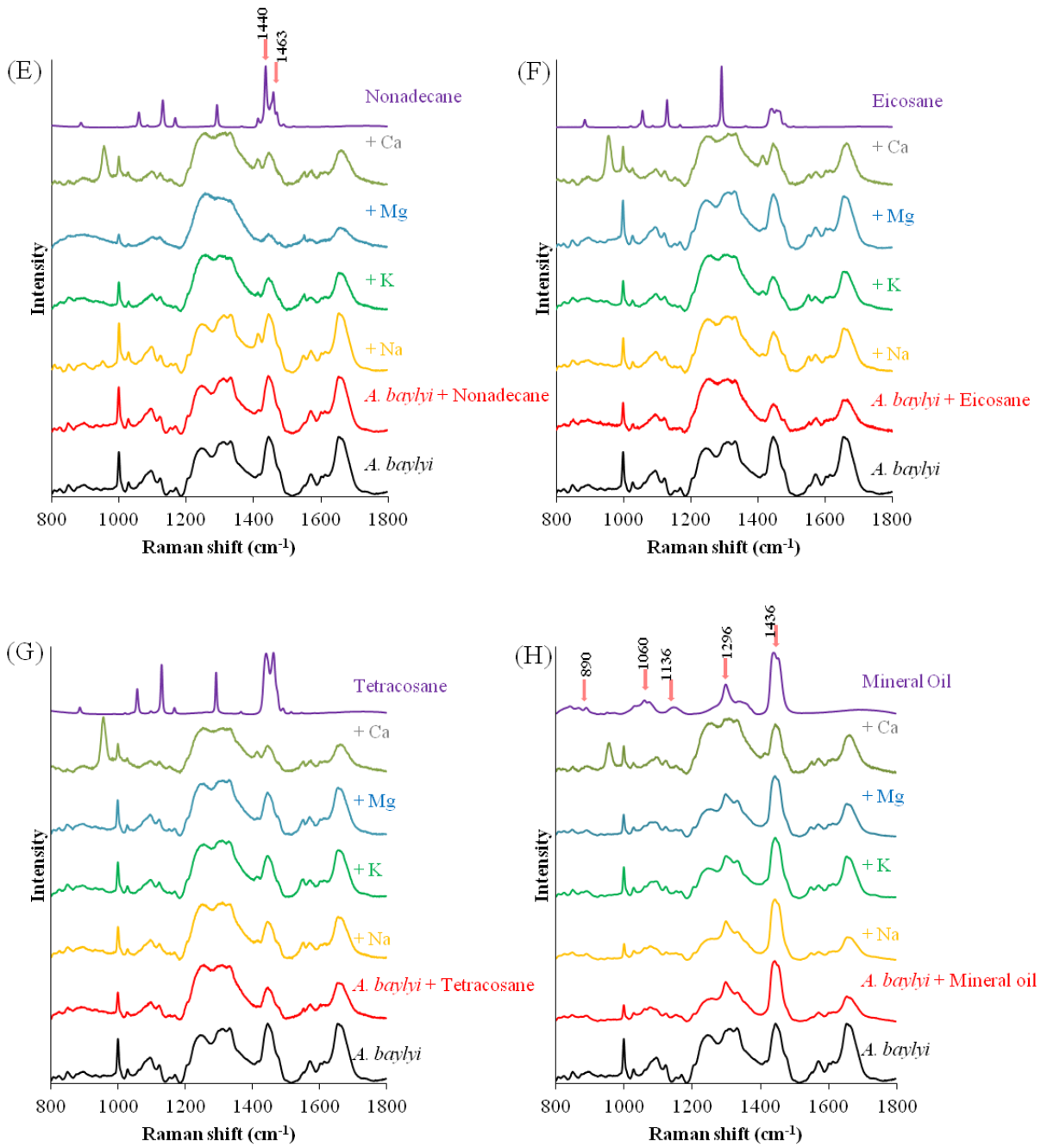

Figure 1. Raman spectra of *A. baylyi* towards decane (A), dodecane (B), tetradecane (C), hexadecane (D), nonadecane (E), eicosane (F), tetracosane (G), and mineral oil (H) with/-out different extra nutrient cations

To characterize the chemotaxis-related affinity of *A. baylyi* towards different n-alkanes, Raman microspectroscopy detected the samples of bacteria exposed to 7 linear alkane molecules and 1 alkane mixture, respectively. Post-exposed to decane, dodecane, tetradecane, hexadecane and mineral oil, alterations at 1296 and 1436 cm^{-1} generated from methylene twisting and bending indicates the chemotactic accumulations of alkane molecules around bacterial cells. However, after the exposure to nonadecane, eicosane or tetracosane, the Raman spectra are similar to that of original *A. baylyi*, and show no significant alterations from alkane molecules. From the results of Raman spectral alterations, the linear alkanes with carbon lengths of C10 (decane), C12 (dodecane), C14 (tetradecane) and C16 (hexadecane) are strong attractants to *A. baylyi* in normal mineral medium, whereas the alkane molecules with carbon lengths of C19 (nonadecane), C20 (eicosane) and C24 (tetracosane) are less attractive. The significant alterations of C10, C12, C14 and C16 are attributed to the strong affinity of *A. baylyi* (Li et al., 2017b). It is evident that *Acinetobacter* is capable of swimming down towards the area where alkane molecules are adequate (Wentzel et al., 2007). Captured alkane droplets on cell surfaces are therefore bioaccumulated after being emulsified (Boulton and Ratledge, 1984; Haferburg et al., 1986; Singer and Finnerty, 1984), allowing Raman spectroscopy to characterize the bacterial affinity towards alkanes.

The hydrocarbon capillary assay proves the different chemotactic sensitivities of *A. baylyi* towards various linear alkanes. In Figure S1, the accumulation of 16S rRNA copies in capillary tubes of the alkanes with carbon chain length less than 19 are ranging from 8.8×10^9 to 2.33×10^{11} copies per capillary, significantly higher than those in treatments of long carbon length alkanes (nonadecane, eicosane and tetracosane). High 16S rRNA copy numbers of *A. baylyi* in capillary tubes postexposure to decane, dodecane, tetradecane and hexadecane indicates that *A. baylyi* possesses more sensitive affinity towards short and medium carbon length alkanes than towards long carbon length alkanes. Because alkane molecules are hydrophobic substances in mineral medium, the soluble fraction generates concentration gradients for bacteria to access alkane molecules (Li et al., 2017c). Hence, the strong chemotaxis-related affinity towards alkane assists the uptake and internalization of insoluble alkane molecules by *A. baylyi*, which is shown as the accumulation of bacterial cells in capillary tubes following exposure to highly attractive alkanes. These results are

consistent with Raman spectral alterations, suggesting the feasibility of Raman spectroscopy to investigate the alkane affinity of *A. baylyi* with various conditions.

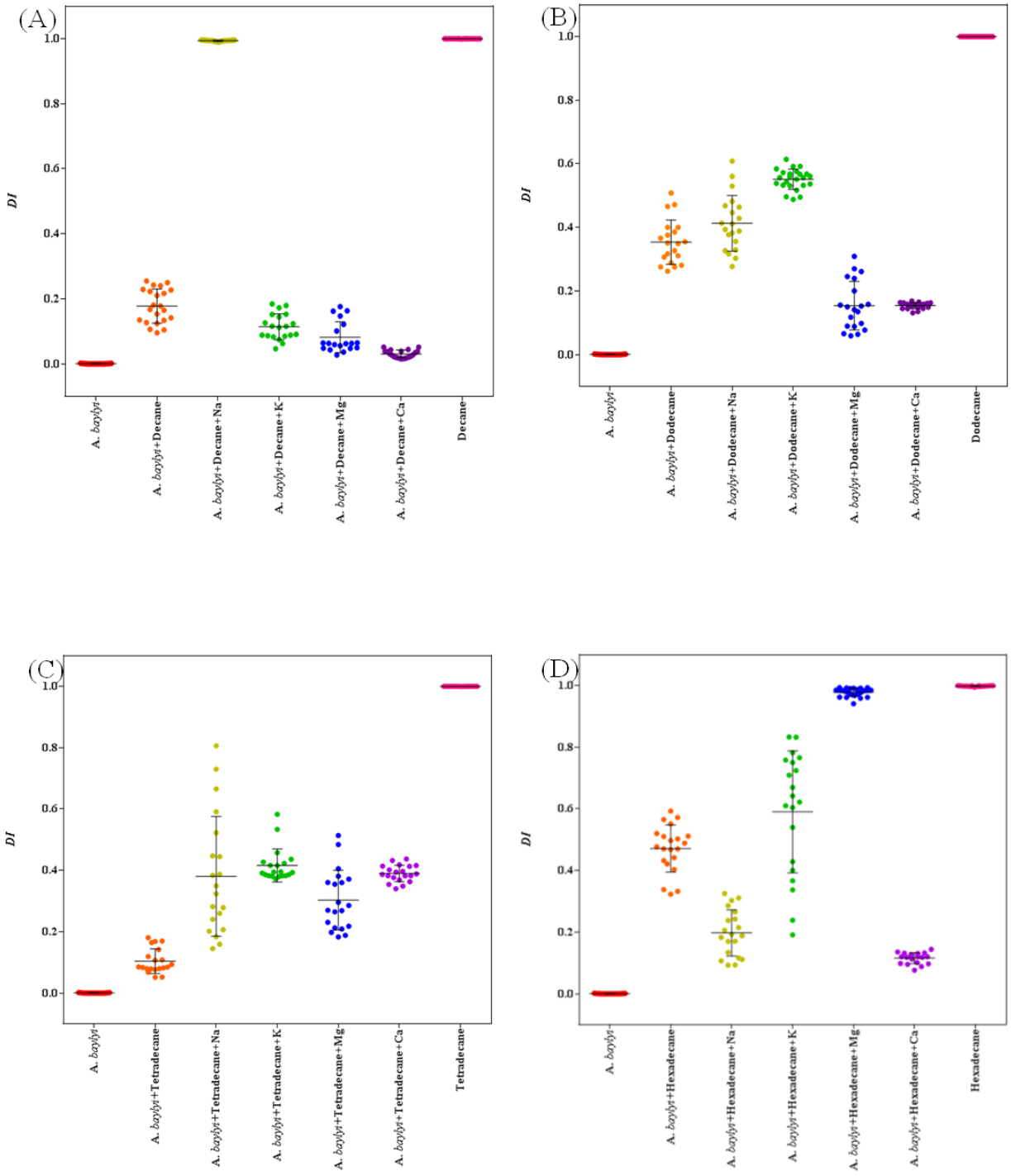

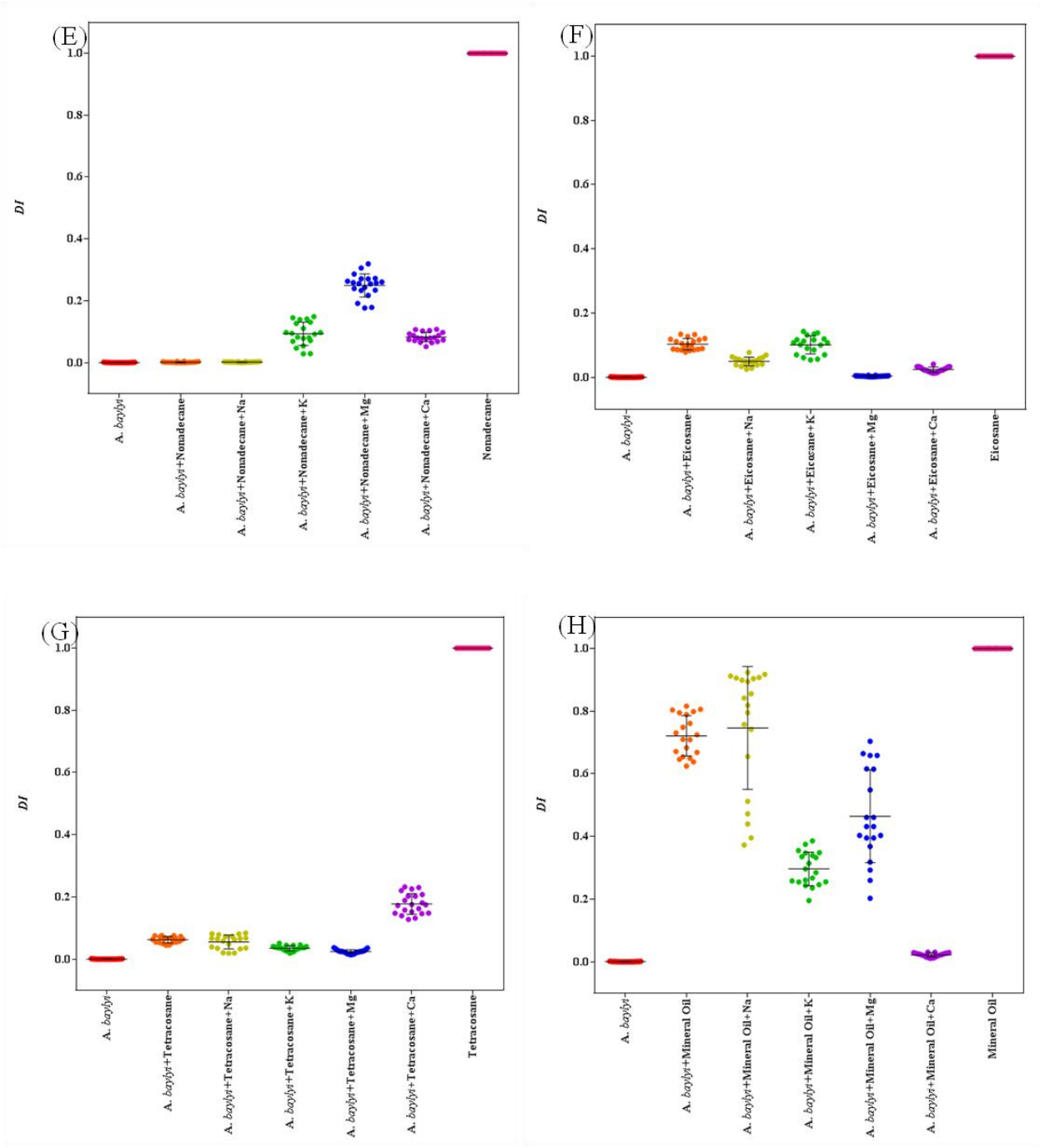

Figure 2. D_I scores of extra ionic effects on chemotaxis-related affinity and accumulation of A. baylyi towards decane (A), dodecane (B), tetradecane (C), hexadecane (D), nonadecane (E), eicosane (F), tetracosane (G), and mineral oil (H)

Distinct ionic effects on alkane chemotaxis-related affinity and accumulation of *A. baylyi*

To test different ionic impacts on alkane chemotaxis-related affinity and accumulation of *A. baylyi*, bacterial cells were exposed to 100 mg/L alkane or alkane mixture for 1 hour with 10 mM different extra ions including Na^+, K^+, Mg^{2+} and Ca^{2+}, respectively. In contrast with the low solubility of alkane molecules, nutrient ions are perfectly soluble in mineral medium. This may imply that nutrient ions only affect the affinity and accumulation of bacteria towards alkanes, but do not have serious impacts on the chemotactic attractiveness of alkane molecules. Extra nutrient ion at a concentration of 10 mM in mineral medium is not enough to alter the cell structure, so no further influences on Raman spectra of *A. baylyi* after being washed twice by deionized water. As a consequence, Raman spectra of pure *A. baylyi* cells are useable as the negative control for D_I calculation. The D_I results demonstrate the Raman spectral alterations of alkane association in *A. baylyi* bacteria are varied in different ions. Hence, D_I scores allow the quantifiable evaluation of the alkane chemotactic affinity in *A. baylyi* bacteria treated with different ions. Ions performed differential impacts on the sensitivities of bacterial chemotaxis-related affinity and accumulation towards alkanes in varying carbon lengths, contributing to observed increase or decrease in D_I values. Post-exposed to decane in original medium or with different extra ions, their Raman spectra show distinguishable peak alterations from each other, resulting in the strong differences in D_I score plots (Figure 2A). Excluded the extra ionic effects, the 0.177 D_I value indicates the moderate chemotactic affinity towards decane molecules of *A. baylyi*. After treated with Na^+, the remarkable D_I values are close to that of pure decane molecules, demonstrating the strong enhancement of Na^+ in decane affinity of *A. baylyi*. In the treatments of other ions, however, the influences of extra ions might decrease the decane affinity, which is also confirmed by the low D_I values (0.114 for K^+, 0.066 for Mg^{2+} and 0.012 for Ca^{2+}). Though decane molecules are not perfect carbon sources for *A. baylyi* to degrade, their chemotactic attractions are captured by bacterial cells to generate the spectral alterations in Figure 1A. In previous study, similar results demonstrated that the outer-membrane protein OmpS is responsible for the signal transport of short carbon alkane such as octane, nonane and decane in bacterial cells (Wang and Shao, 2014). In Figure 2B, post-exposed to dodecane molecules, the D_I values of bacterial cells in the treatments of Na^+ (0.501) and K^+

(0.583) are higher than those in original mineral medium (0.423), indicating the increment in dodecane chemotactic affinity and accumulation, while the low D_I scores show that Mg^{2+} and Ca^{2+} reduce the attractiveness of dodecane to *A. baylyi*. It is reported that *A. baylyi* is able to grow when dodecane is the sole carbon source in a medium (Zheng et al., 2012). The strong dodecane affinity cause faster movement of *A. baylyi* to accumulate molecules in mineral medium measured by Raman microspectroscopy was well-documented (Li et al., 2017c). From the genetic evidence, alkane degradation genomes are significantly dependent on the chemotaxis genome, proving that bacterial sensing, chemotaxis and accumulation is critical for the degradation of dodecane in *Acinetobacter* bacteria (Wang and Shao, 2014; Kothari et al., 2016). Our results from Raman spectral analysis also confirm the sensitive chemotactic response of *A. baylyi* to dodecane, and such chemotactic response can be regulated by extra ions.

Although tetradecane Raman peaks are observed in spectra of normal medium treatment (Figure 1C), the average D_I score is close to that of original bacterial cells (Figure 2C). This indicates the weak tetradeccane affinity and accumulation of *A. baylyi*. In contrast, from results in Figure 2C, higher D_I values indicate that all tested nutrient ions are able to improve the bacterial affinity and accumulations towards tetradecane. The peak alterations observed in Raman spectra also prove the chemotactic attraction of tetradecane for *A. baylyi*, which is similar to previous spectral results (Figure 1C) (Li et al., 2017c). In *Acinetobacter* bacteria, the alkane signal transmitter protein, OmpS, and the alkane uptake protein, OmpW, is both essential for alkane access and accumulation (Wang and Shao, 2014; Jung et al., 2015). From the results of Raman spectra, extra ions might be able to enhance upregulations of these two proteins when exposed to tetradecane. Different from tetradecane, the D_I value of hexadecane exposed bacterial cells in normal mineral medium is 0.547, significantly higher than that of original bacterial cells (Figure 2D). Post-exposed to hexadecane, the D_I values of different ions treatments are in the order of: Mg^{2+} (0.991) > K^+ (0.788) > Na^+ (0.272) > Ca^{2+} (0.133), where the hexadecane chemotaxis-related affinity of *A. baylyi* is increased by K^+ and Mg^{2+} increases, but decreased by Na^+ and Ca^{2+}, compared to that without extra ions (Figure 2D). It is postulated that several proteins are responsible for the regulation of hexadecane bioaccumulation in *Acinetobacter* (Rosenberg et al., 1982; Geißdörfer et al., 1999).

We deduce that different extra nutrient ions might contribute to the differentiated synthesis of chemotaxis-related proteins for alkane uptake and utilization in bacteria (Wang and Shao, 2012). In addition, the large variations in D_I plots of hexadecane-K^+ or tetradecane-Na^+ exposed bacteria are attributed to the dissimilar intensity of alkane peaks in bacteria spectra. The extra potassium and sodium might enhance the alkane affinity, so that partial bacterial cells can assess and accumulate more alkane molecules in medium and reduce the available alkane molecules for the rest of bacteria. This uneven distribution of alkane molecules collected by bacterial cells leads to the significant differences in alkane peaks intensity, and causes noticeable variations in D_I values.

In normal mineral medium or treated with extra Na^+, nonadecane shows limited chemotactic attractions to *A. baylyi*, proved by the extremely low D_I values (0.001 for normal medium and 0.002 for Na^+) in Figure 2E. From the results of D_I scores, the scores of nonadecane exposed bacterial cells treated with extra K^+, Mg^{2+} and Ca^{2+} (0.130, 0.287 and 0.098) demonstrate the slight, but not enough increase in bioaccumulation of nonadecane to generate obvious Raman alterations (Figure 1E and 2E). Since eicosane and tetracosane are both long carbon chain alkane molecules with carbon lengths of 20 and 24, respectively, their D_I values of bacterial cells in normal medium are similar (Figure 2F and 2G). Furthermore, in the treatments with extra Na^+, K^+ and Mg^{2+}, the D_I scores of eicosane or tetracosane exposed bacterial cells are all smaller than those in normal medium treatment (0.102 for eicosane and 0.062 for tetracosane), indicating the low chemotactic sensitivities towards eicosane and tetracosane of *A. baylyi*. Pre- and post-exposed to eicosane or tetracosane, the unaltered Raman spectra also prove the weak chemotactic responses from bacterial cells (Figure 1F and 1G). The bacterial degradation and uptake of long carbon n-alkanes in *Acinetobacter* is well-documented (Sakai et al., 1996), while the mechanisms of bacterial access, detection and chemotaxis are unravelled. It is reported that one signal transmitter protein can straightforward initiate the alkane transport from outer bacterial membrane for utilization without triggering at the chemotaxis protein (Wang and Shao, 2014), contributing to the reduced chemotaxis attractions. The mechanism of gene expression is required to uncover the effects of extra ions on eicosane and tetracosane chemotaxis-related affinity of *A. baylyi*. Exposed to pure alkane molecules, bacterial cells in the medium with extra ions

exhibit various chemotactic responses. From the results of Raman spectral alterations and D_I score plots, bacterial chemotaxis behaviours towards specific alkane molecules are sensitive to the extra ions, illustrating that Raman spectra are essential to uncover the impacts of extra ions on pure alkane chemotaxis association of *A. baylyi*.

By interrogating Raman microspectroscopy, the influences of extra ions on bacterial selections towards different alkane molecules in alkane mixture are uncovered. We used mineral oil as the alkane mixture chemical to investigate the chemotactic selections of *A. baylyi*. Post-exposed to mineral oil, similar D_I values of normal or Na^+ added treatment demonstrate the insignificant changes in mineral oil affinity of *A. baylyi* with extra Na^+ (Figure 2H). The average D_I scores of mineral oil exposed bacterial cells with extra K^+ or Mg^{2+} are 0.296 and 0.464, respectively, smaller than that in normal medium treatment (Figure 2H). It is worth noting that, post exposure to mineral oil, the variations in D_I plots of Na^+ or Mg^{2+} treatments are associated with the Raman intensity of mineral oil in bacteria spectra. We speculate that sodium and magnesium ions may increase the affinity and accumulation of *A. baylyi* towards one specific type of alkane in alkane mixture. Therefore, alkane molecules selected by bacterial cells are not perfectly identical, contributing to the differentiated alterations in Raman spectra and large variations in D_I plots. Though extra sodium, potassium and magnesium show similar or decreased mineral oil chemotactic sensitivities in *A. baylyi* bacteria, Raman bands of mineral oil are detectable in bacterial spectra. The specific peak at 1296 cm^{-1} assigned to CH_2 twisting indicates that the extra ions do not greatly affect the *A. baylyi* affinity and accumulation towards mineral oil (Figure 1H). The lowest D_I value of mineral oil exposed bacterial cells is found in the treatment with extra Ca^{2+}, leading to the unchanged bacterial Raman spectra pre- and post-exposed to mineral oil (Figure 1H and 2H). In normal medium, bacterial cells can detect and accumulate various alkane molecules in mineral oil to generate peak alterations in Raman spectra. When treated with extra ions, the influences of ionic strengths might change the bacterial selection towards alkane molecules in varying carbon lengths in mineral oil, contributing to the accumulation of specific alkane molecules around bacterial cells in an alkane mixture. The different D_I values of mineral oil exposure also prove that the change in bacterial chemotaxis association with mineral oil is mainly from the different influences of extra ions. Therefore, the spectral alterations and analysis allow Raman microspectroscopy to detect the impacts

of extra ions on alkane mixture chemotactic sensitivities of *A. baylyi*.

Alkane patterns with/-out different extra ions

Raman spectral analysis provides the patterns of n-alkane affinity in *A. baylyi* cells in the original or extra ionic treated medium. Post-exposed to different alkanes in the medium with or without extra ions, respectively, the changes in Raman spectral alterations result in the differences in D_I score plot. The results of D_I scores in Figure3 illustrate the enhancement of extra ions on the bacterial chemotactic ability towards n-alkane is varying in carbon lengths. From the alkane pattern of each ion, the extra ions exhibit differential influences on short carbon length (decane and dodecane), medium carbon length (tetradecane, hexadecane and nonadecane), and long carbon length alkane (eicosane and tetracosane). In Figure 3A, higher D_I values of dodecane (0.423) and hexadecane (0.547) indicate the stronger chemotactic attractions than that of decane, tetradecane, eicosane and tetracosane on *A. baylyi* cells without extra ions. Raman spectral alterations also confirm the strong dodecane and hexadecane chemotaxis-related affinity. In normal medium, the Raman signal of CH_3 methyl rock at 890 cm^{-1} was detected post-exposed to dodecane, and two peaks at 1060 and 1079 cm^{-1} was observed in hexadecane exposure. This is suggested that the bioaccumulation of dodecane or hexadecane molecules in *A. baylyi* is stronger than being exposed to other alkanes. It has been earlier shown that *Acinetobacter venetianus* produces emulsan when grown in dodecane and hexadecane. Emulsan is able to emulsify alkanes thereby increasing the bacterial uptake and accumulation (Kothari et al., 2016; Rosenberg et al., 1979). Homologous to *A. venetianus*, *A. baylyi* is hypothesized to produce similar emulsan towards dodecane and hexadecane.

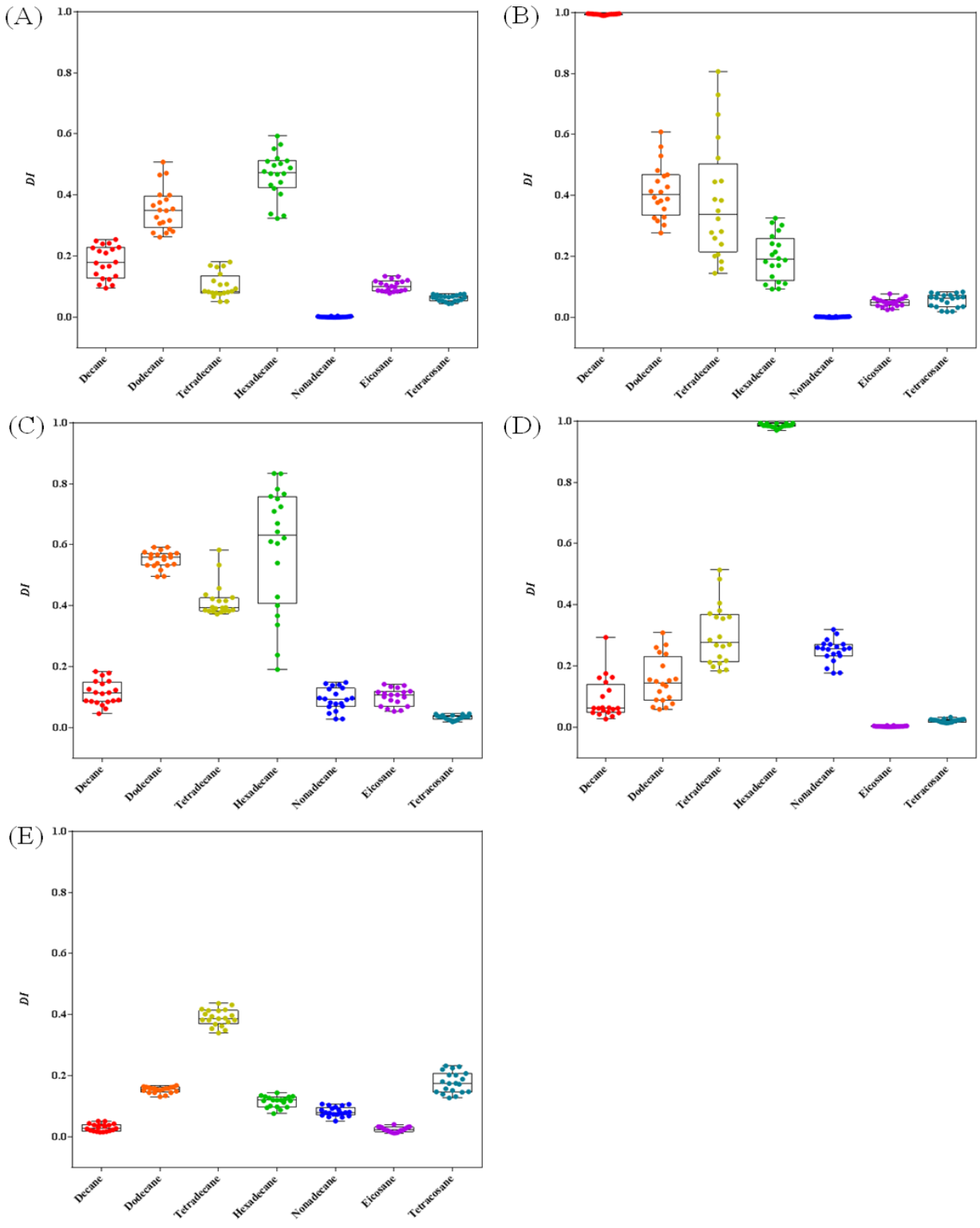

Figure 3. Alkane patterns of *A. baylyi* with no extra ion (A), sodium (B), potassium (C), magnesium (D), and calcium (E)

In the medium with extra 10 mM Na+, the highest D_I value (0.994) is found for decane exposed bacterial cells, and value of 0.501 and 0.380 is for dodecane and tetradecane, respectively. These D_I values represent that the added sodium in medium strengthen the affinity and accumulation of *A. baylyi* towards decane, dodecane and tetradecane (Figure 3B). The significant Raman peak of CH_2 twist and CH_2 bend at 1296 and 1436 cm^{-1} of decane, together with other Raman signals of alkane molecules at 890, 1060, 1079 and 1136 cm^{-1}, illustrates the strong decane affinity in *A. baylyi*. The enhancement for chemotactic attractions of dodecane and tetradecane indicates that Na^+ is useful for bacterial uptake and accumulation towards short carbon alkane molecules. The external sodium improves the alkane adherence and emulsification on cell membranes, and further increases their bioaccumulation (Fernandez-Linares et al., 1996). Post-exposed to long carbon chain alkanes, extra Na^+ shows no assistance on the affinity of *A. baylyi* towards nonadecane, eicosane and tetracosane according to low D_I scores. Consequently, owing to the halotolerant feature of *A. baylyi*, we believe that this bacterial strain might possess such ability to utilize outer Na^+ to accumulate short carbon n-alkanes (Jia et al., 2016).

In the treatment with extra K^+, bacterial cells exhibit sensitive chemotactic responses to dodecane, tetradecane and hexadecane, contributing to the high D_I values of 0.583, 0.416 and 0.788, respectively (Figure 3C). From the Raman spectra, peak alterations at 890 cm^{-1} (CH_3 rock) and 1296 cm^{-1} (CH_2 twist) found in bacterial cells post-exposed to dodecane, tetradecane and hexadecane demonstrate that extra K^+ strengthened the chemotactic attractions of medium carbon length alkane molecules in *A. baylyi*. Since the movement of fimbriae is sensitive with the potassium concentrations, the chemotactic behaviours of bacterial cells might be influenced when swimming down to specific molecules in a medium (Lu et al., 2013). It is reported that extracellular K^+ is important in the communications among bacterial cells, and can direct cell mobility in a biofilm (Humphries et al., 2017). Because of these two features of external K^+ operated on bacterial cells, the high D_I results we collected from Raman spectroscopy in dodecane and hexadecane exposed bacterial cells might attribute to the promoted chemotactic signals of alkane molecules among bacterial cells. We therefore believe that K^+ has the ability to increase the *A. baylyi* chemotaxis-related affinity and accumulation towards short and medium carbon length n-alkanes.

The alkane pattern of extra magnesium treatment illustrates that Mg^{2+} is positively corresponded to the chemotaxis-related affinity of *A. baylyi* towards medium carbon length alkanes (Figure 3D). The highest D_I score of hexadecane exposed bacteria is generated from the noticeable alterations in Raman spectra (Figure 1D). Our D_I score plot also demonstrate that tetradecane and nonadecane both exhibit vigorous chemotactic attractions to *A. baylyi* bacteria when extra Mg^{2+} presents (Figure 3D). It was reported that magnesium can stabilize the phosphorylation of CheY to initiate the chemotactic movement of bacteria (Welch et al., 1993; Stock et al., 1993). The differentiated D_I scores believe this Mg^{2+} stabilization is not uniform among various alkanes. Hence, it is hypothesized that, post-exposed to different alkanes, CheY is not the exclusive chemotaxis-related protein to interact with magnesium. We speculated that the extra intracellular Mg^{2+} transported from outer membrane combines with chemotaxis-related proteins to provide the stable chemotactic movement towards tetradecane, hexadecane and nonadecane.

The extra Ca^{2+} in bacterial medium only exhibit slightly positive influences on tetradecane exposed bacterial cells (Figure 3E). Post-exposed to other alkane molecules, the low D_I values indicate weak chemotactic responses of *A. baylyi*. Furthermore, the limited chemotactic behaviours towards alkane molecules result in undistinguished Raman spectra. The concentration of extracellular calcium higher than 100 nM cause tumbling in bacterial cells, followed by the inhibition of bacterial movement (Ordal, 1977). Successful bacterial chemotaxis requires the movement towards specific molecules other than staying tumbling. As a consequence, *A. baylyi* with extra calcium may lose the ability of chemotaxis-related movement towards alkanes. A previous study reported that calcium might promote bacterial aggregation by interacting with the anionic from bacterial cells (Rose et al., 1993). In this study, from the results of Raman spectral analysis, we deduce that Ca^{2+} may block the chemotactic channels in bacterial cells towards alkane molecules, and increase the trend to aggregate in *A. baylyi* bacteria. Hence, it is essential to uncover the blocking mechanisms in future study.

In the treatments with/without different extra ions, the chemotactic behaviours of bacterial cells towards n-alkane molecules are distinguishable. Using the Rama spectral analysis, we confirm the alkane chemotaxis-related affinity and accumulation in *A. baylyi*. Our results successfully observed the distinct chemotactic response to

alkane molecules in varying carbon lengths in each extra ionic treatment. Extracellular sodium can increase the bacterial chemotaxis accumulation towards decane, dodecane and tetradecane. Bacterial chemotactic sensitivities for dodecane, tetradecane and hexadecane are stronger when extra potassium presents. Extra magnesium exhibits the enhancement on chemotactic attractions of tetradecane, hexadecane and nonadecane in *A. baylyi*, whereas calcium inhibits the bacterial chemotaxis towards alkane molecules. By interrogating Raman microspectroscopy, we detected the ion-alkane patterns from differential bacterial chemotactic behaviours on various n-alkane molecules.

Ionic influences in bacterial selection in alkane mixture

The impacts of extra ions on the chemotactic affinity and accumulation towards pure n-alkane molecules of *A. baylyi* are stated as above. To detect the chemotactic selection of bacterial cells towards various alkane molecules in alkane mixture, *A. baylyi* were exposed to alkane mixture, mineral oil, in the normal mineral medium or extra ions treated medium, compared with bacterial cells exposed to pure alkane molecules. PCA-LDA performed to determine the Raman spectral similarity of alkane and mineral oil exposed bacterial cells in each extra ion treatment *via* Raman microspectroscopy. In normal mineral medium, the LDA group of mineral oil exposed bacterial cells are separated from those exposed to pure alkane, indicating that the alkane molecules selected and accumulated on/inside *A. baylyi* in mineral oil are various (Figure 4A). Namely, alkane affinity of *A. baylyi* is not highly specific in mineral oil, and each bacterial cell may select different types of alkane molecules from others. The main components observed in mineral oil are saturated alkane molecules in carbon lengths from C_{10} to C_{35} (Moret et al., 2016). Post-exposed to mineral oil or C10, C12, C14 and C16, similar LD1 values show that *A. baylyi* is likely to select short and medium carbon length alkane molecules in mineral oil. In contrast, other types of alkane molecules selected by *A. baylyi* in mineral oil contribute to segregations in LD2. Since LD1 is more noted than LD2 in class separation of bacterial spectra, the Raman alterations of mineral oil has proximity to those of short and medium carbon length alkanes. Therefore, the priority chemotactic selection of *A. baylyi* is for short and medium carbon length alkane molecules in mineral oil.

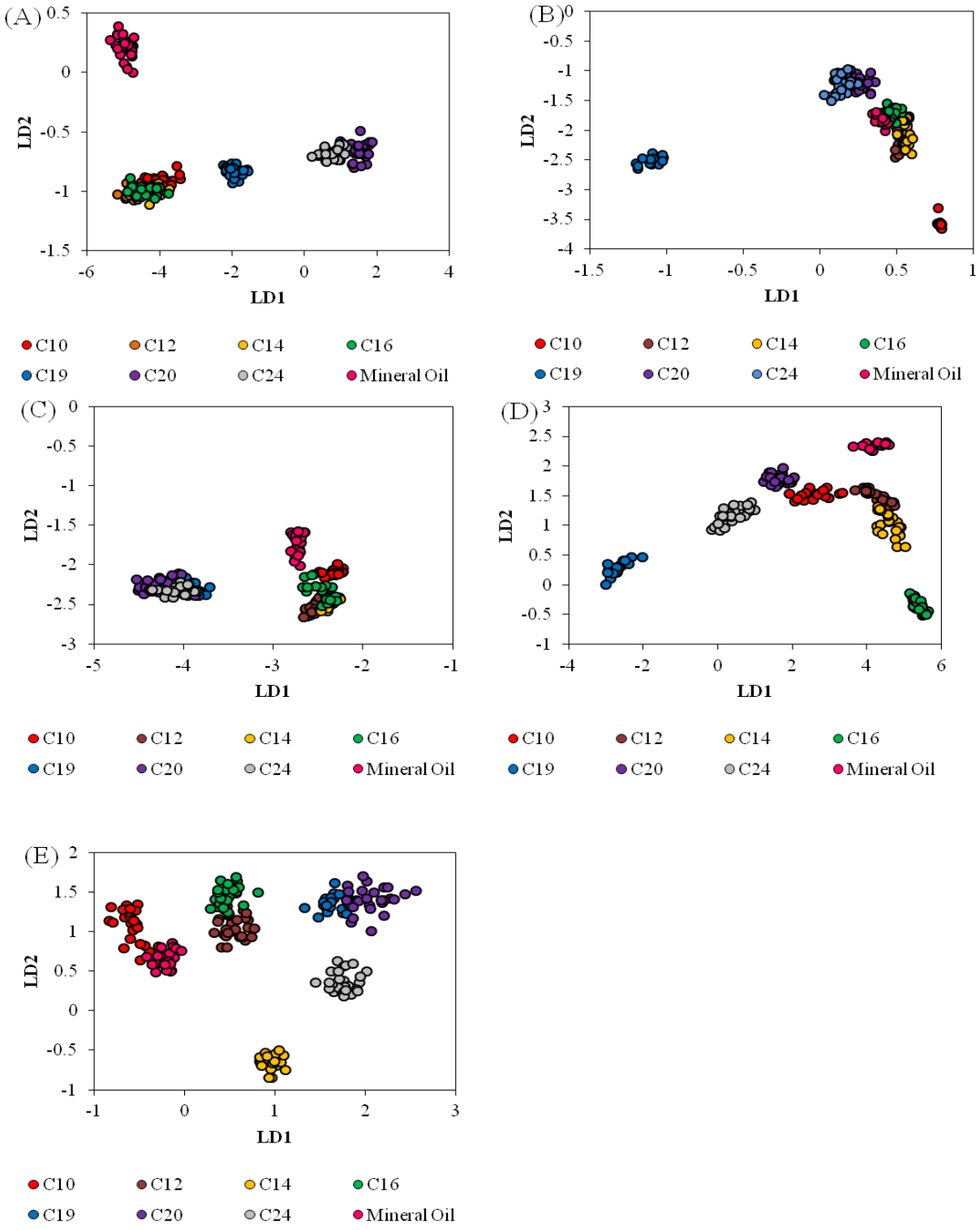

Figure 4. LDA plots of alkane chemotactic selection of A. baylyi in alkane mixture (mineral oil) with no extra ions (A), sodium (B), potassium (C), magnesium (D), and calcium (E)

When treated with extra sodium in a medium, the LDA categorisation of *A. baylyi* exposed to mineral oil is close to that of exposed to dodecane, tetradecane and

hexadecane (Figure 4B). The strong Raman spectral alterations observed in decane exposed bacterial cells increase the distance in LDA to those exposed to mineral oil (Figure 1A and 4B). This demonstrates that the concentration of decane in mineral oil is not enough to generate significant spectral alterations, so that bacterial cells mainly select dodecane, tetradecane and hexadecane. The external sodium can enhance the emulsification process of bacterial cells to accumulate more alkane molecules on cell membrane (Fernandez-Linares et al., 1996). The upregulations of chemotaxis genes in short and medium carbon lengths alkanes also facilitate the chemotactic selection towards dodecane, tetradecane and hexadecane of *A. baylyi* (Kothari et al., 2016; Rosenberg et al., 1982). The alkane signal transmitter protein, OmpS, assist a small amount of long carbon lengths alkane molecules such as eicosane and tetracosane accumulated on/inside bacterial cells (Wang et al., 2013). Consistent with D_I scores, LDA confirm that the extra Na^+ may prompt the bacterial selection towards n-alkane molecules in carbon lengths of 12, 14 and 16.

Post-exposed to mineral oil, LDA results show the close relationship to pure alkane exposed bacterial cells in the extra potassium treatment (Figure 4C). The similar LD1 values of dodecane, hexadecane and mineral oil exposed *A. baylyi* indicates that the dominant alkane molecules selected and accumulated in bacterial cells are hexadecane in mineral oil. Decane, dodeccane and tetradecane also exhibit strong chemotactic attractions to *A. baylyi* in the alkane mixture. The extracellular K^+ is important for the movement of bacterial cells in a medium (Lu et al., 2013). Hence, in mineral oil, potassium may enhance the movement of *A. baylyi* towards short and medium carbon length alkane molecules. The bacterial accumulation of long carbon length alkane molecules in mineral oil might be limited when extra potassium presents. In *A. baylyi*, we prove that K^+ can increase the bacterial chemotaxis-related selection towards the alkane molecules with carbon lengths of 12 and 16.

In the treatment with extra magnesium, the LDA group of mineral oil exposed bacterial cells are separated from that of pure alkane exposed bacteria, showing the similar amount of alkanes in varying carbon lengths selected and accumulated on/inside bacterial cells (Figure 4D). However, post-exposed to dodecane and mineral oil, the close distance between these two LDA groups indicates a number of dodecane molecules accumulated by *A. baylyi* in mineral oil (Figure 4D). The inadequate hexadecane molecules in mineral oil cannot allow bacterial cells to produce

remarkable Raman spectral alterations, contributing to the large LDA distance between mineral oil and pure hexadecane exposed *A. baylyi* with extra magnesium (Figure 1D and 4D). Since extra magnesium is able to stabilize the phosphorylated CheY which is essential for directing flagella for bacterial movement, Mg^{2+} can assist bacterial cells to access chemical molecules faster (Stock et al., 1993). From the results of LDA, we also found out that extra Mg^{2+} alter the bacterial behaviours towards alkane molecules in mineral oil.

From the LDA results in Figure 4E, extra calcium in mineral oil exposed bacterial cells only exhibit similar influences to that in decane exposed bacterial. Unlike the LDA plot of normal medium treatment in Figure 4A, the categorisations of different pure alkane exposed *A. baylyi* are separated in Figure 4E. The D_I scores prove that the alkane chemotaxis-related affinity is blocked for bacterial cells (Figure 4E). Raman spectra also confirm the inhibited chemotactic accumulation of *A. baylyi* towards mineral oil and pure alkane molecules. Because of extra calcium, bacterial chemotaxis is limited (Rose et al., 1993). In mineral oil, it is believed that extra calcium may reduce the chemotactic responses of *A. baylyi* towards alkane molecules.

Mineral oil is complex alkane mixture comprising saturated n-alkanes and aromatic hydrocarbons (Moret et al., 2016). Diverse hydrophobic components in the droplet of mineral oil challenges the bacterial access to alkane molecules, and reduces the utilization of alkanes in *A. baylyi* (Lal and Khanna, 1996; Prince et al., 2013). Therefore, due to various extra ions present in nature environment, ionic strengths need considerable attention for the study of bacterial detection, chemotaxis and utilization towards alkane molecules in hydrocarbon contaminated sites. We investigated how individual nutrient ion affects alkane affinity, but the combination of various ions is important for bacterial movement in natural environment. From the results in this study, the combination of ions may increase or decrease more significantly than single ion does. This still requires further investigations. As it is reported that Raman microspectroscopy performed successfully to measure bacterial chemotactic behaviours towards hydrocarbons (Li et al., 2017c), we used this technique in this study to investigate the extra ionic influences on alkane chemotaxis-related affinity and accumulation of *A. baylyi* in mineral oil. Compared to Raman spectra of pure alkane exposed bacterial cells, our results confirm that the extra ion can change the chemotactic selection of bacteria to alkane molecules in

mineral oil, thereby leading to the change in alkane degradation in real hydrocarbon contaminated environment. Therefore, in impacts of extra ions on the chemotaxis directed bacterial degradation in alkane mixture should be carried out in further study.

Conclusion

Our results prove the extra ions can improve the alkane chemotaxis-related affinity and accumulation of *A. baylyi*. From the ion-alkane patterns, we confirm that extra ions exhibit differential influences on bacterial chemotactic behaviours towards pure n-alkane molecules. By interrogating Raman spectra, the impacts of different extra ions on bacterial selection and accumulation towards alkane molecules in alkane mixture are measured. Compared with nature environment, the concentrations of ions used in this study cannot represent the real concentration in bacterial habitats. Therefore, nutrient ions at different concentration are required to understand their influences on bacterial movement. To the best our knowledge, this is the first study exploring Raman spectral analysis in alkane chemotaxis-related affinity and accumulation of bacteria in diverse extra ions treatments. A new perspective has been found to uncover the bacterial chemotaxis associated degradation towards alkane molecules in natural environments. By using Raman microspectroscopy, we confirm that nutrient ions significantly affect the access to alkane droplets, change the accumulation priority in alkane mixture, and modify the degradation of alkane molecules of bacterial cells.

References

Annweiler, E., Materna, A., Safinowski, M., Kappler, A., Richnow, H. H., Michaelis, W. & Meckenstock, R. U. 2000. Anaerobic degradation of 2-methylnaphthalene by a sulfate-reducing enrichment culture. *Applied and environmental microbiology,* 66**,** 5329-5333.

Bence, A., Kvenvolden, K. & Kennicutt, M. 1996. Organic geochemistry applied to environmental assessments of Prince William Sound, Alaska, after the Exxon Valdez oil spill—a review. *Organic geochemistry,* 24**,** 7-42.

Berg, H. C. & Turner, L. 1990. Chemotaxis of bacteria in glass capillary arrays. Escherichia coli, motility, microchannel plate, and light scattering. *Biophysical Journal,* 58**,** 919-930.

Block, S. M., Segall, J. E. & Berg, H. C. 1983. Adaptation kinetics in bacterial chemotaxis. *Journal of bacteriology,* 154**,** 312-323.

Boulton, C. & Ratledge, C. 1984. The physiology of hydrocarbon-utilizing microorganisms.

Topics in enzyme and fermentation biotechnology, 9**,** 11-77.

Bragg, J. R., Prince, R. C., Harner, E. J. & Atlas, R. M. 1994. Effectiveness of bioremediation for the Exxon Valdez oil spill. *Nature,* 368**,** 413-418.

Camilli, R., Reddy, C. M., Yoerger, D. R., Van Mooy, B. A., Jakuba, M. V., Kinsey, J. C., Mcintyre, C. P., Sylva, S. P. & Maloney, J. V. 2010. Tracking hydrocarbon plume transport and biodegradation at Deepwater Horizon. *Science,* 330**,** 201-204.

Corsetti, S., Rabl, T., Mcgloin, D. & Kiefer, J. 2017. Intermediate phases during solid to liquid transitions in long-chain n-alkanes. *Physical Chemistry Chemical Physics,* 19**,** 13941-13950.

Cui, L., Chen, P., Chen, S., Yuan, Z., Yu, C., Ren, B. & Zhang, K. 2013. In situ study of the antibacterial activity and mechanism of action of silver nanoparticles by surface-enhanced Raman spectroscopy. *Analytical chemistry,* 85**,** 5436-5443.

De Gelder, J., De Gussem, K., Vandenabeele, P. & Moens, L. 2007. Reference database of Raman spectra of biological molecules. *Journal of Raman Spectroscopy,* 38**,** 1133-1147.

De La Cueva, S. C., Rodr ́guez, C. H., Cruz, N. O. S., Contreras, J. a. R. & Miranda, J. L. 2016. Changes in bacterial populations during bioremediation of soil contaminated with petroleum hydrocarbons. *Water, Air, & Soil Pollution,* 227**,** 91.

Efrima, S. & Zeiri, L. 2009. Understanding SERS of bacteria. *Journal of Raman Spectroscopy,* 40**,** 277-288.

Fernandez-Linares, L., Acquaviva, M., Bertrand, J.-C. & Gauthier, M. 1996. Effect of sodium chloride concentration on growth and degradation of eicosane by the marine halotolerant bacterium Marinobacter hydrocarbonoclasticus. *Systematic and Applied Microbiology,* 19**,** 113-121.

Foster, J. 1962. Bacterial oxidation of hydrocarbons. *Oxygenases. Academic, New York***,** 241-261.

Geißdörfer, W., Kok, R. G., Ratajczak, A., Hellingwerf, K. J. & Hillen, W. 1999. The genes rubA and rubB for alkane degradation in Acinetobacter sp. strain ADP1 are in an operon with estB, encoding an esterase, andoxyR. *Journal of bacteriology,* 181**,** 4292-4298.

Guzelian, A. A., Sylvia, J. M., Janni, J. A., Clauson, S. L. & Spencer, K. M. SERS of whole-cell bacteria and trace levels of biological molecules. Environmental and Industrial Sensing, 2002. International Society for Optics and Photonics, 182-192.

Haferburg, D., Hommel, R., Claus, R. & Kleber, H.-P. 1986. Extracellular microbial lipids as biosurfactants. *Bioproducts.* Springer.

Huang, W. E., Singer, A. C., Spiers, A. J., Preston, G. M. & Whiteley, A. S. 2008. Characterizing the regulation of the Pu promoter in Acinetobacter baylyi ADP1. *Environmental microbiology,* 10**,** 1668-1680.

Humphries, J., Xiong, L., Liu, J., Prindle, A., Yuan, F., Arjes, H. A., Tsimring, L. & Suel, G. M. 2017. Species-Independent Attraction to Biofilms through Electrical Signaling. *Cell,* 168**,** 200-209 e12.

Jia, J., Li, H., Zong, S., Jiang, B., Li, G., Ejenavi, O., Zhu, J. & Zhang, D. 2016. Magnet bioreporter device for ecological toxicity assessment on heavy metal contamination of coal cinder sites. *Sensors and Actuators B: Chemical,* 222**,** 290-299.

Jung, J., Jang, I.-A., Ahn, S., Shin, B., Kim, J., Park, C., Jee, S. C., Sung, J.-S. & Park, W. 2015. Molecular mechanisms of enhanced bacterial growth on hexadecane with red clay. *Microbial ecology,* 70**,** 912-921.

Kalyanasundaram, K. & Thomas, J. 1976. The conformational state of surfactants in the solid state and in micellar form. A laser-excited Raman scattering study. *The Journal of Physical Chemistry,* 80**,** 1462-1473.

Kearns, D. B. 2010. A field guide to bacterial swarming motility. *Nat Rev Microbiol,* 8**,** 634-44.

Kothari, A., Charrier, M., Wu, Y.-W., Malfatti, S., Zhou, C. E., Singer, S. W., Dugan, L. & Mukhopadhyay, A. 2016. Transcriptomic analysis of the highly efficient oil-degrading bacterium Acinetobacter venetianus RAG-1 reveals genes important in dodecane uptake and utilization. *FEMS microbiology letters,* 363.

Lal, B. & Khanna, S. 1996. Degradation of crude oil by Acinetobacter calcoaceticus and Alcaligenes odorans. *Journal of Applied Microbiology,* 81**,** 355-362.

Leahy, J. G. & Colwell, R. R. 1990. Microbial degradation of hydrocarbons in the environment. *Microbiological reviews,* 54**,** 305-315.

Li, H., Li, C., Martin, F. L. & Zhang, D. 2017a. Diagnose Pathogens in Drinking Water via Magnetic Surface-Enhanced Raman Scattering (SERS) Assay. *Materials Today: Proceedings,* 4**,** 25-31.

Li, H., Martin, F. L. & Zhang, D. 2017b. Quantification of chemotaxis-related alkane accumulation in Acinetobacter baylyi using Raman microspectroscopy. *Analytical Chemistry,* 89**,** 3909-3918.

Li, H., Martin, F. L. & Zhang, D. 2017c. Quantification of Chemotaxis-Related Alkane Accumulation in Acinetobacter baylyi Using Raman Microspectroscopy. *Anal Chem,* 89**,** 3909-3918.

Lu, N., Bevard, T., Massoudieh, A., Zhang, C., Dohnalkova, A. C., Zilles, J. L. & Nguyen, T. H. 2013. Flagella-mediated differences in deposition dynamics for Azotobacter vinelandii in porous media. *Environ Sci Technol,* 47**,** 5162-70.

Mizushima, S.-I. & Simanouti, T. 1949. Raman frequencies of n-paraffin molecules. *Journal of the American Chemical Society,* 71**,** 1320-1324.

Moret, S., Scolaro, M., Barp, L., Purcaro, G. & Conte, L. S. 2016. Microwave assisted saponification (MAS) followed by on-line liquid chromatography (LC)-gas chromatography (GC) for high-throughput and high-sensitivity determination of mineral oil in different cereal-based foodstuffs. *Food Chem,* 196**,** 50-7.

Ordal, G. W. 1977. Calcium ion regulates chemotactic behaviour in bacteria. *Nature,* 270**,** 66-67.

Parales, R. E. & Harwood, C. S. 2002. Bacterial chemotaxis to pollutants and plant-derived aromatic molecules. *Current opinion in microbiology,* 5**,** 266-273.

Peterson, C. H., Rice, S. D., Short, J. W., Esler, D., Bodkin, J. L., Ballachey, B. E. & Irons, D. B. 2003. Long-term ecosystem response to the Exxon Valdez oil spill. *Science,* 302**,** 2082-2086.

Piatt, J. F., Lensink, C. J., Butler, W., Kendziorek, M. & Nysewander, D. R. 1990. Immediate impact of the'Exxon Valdez'oil spill on marine birds. *The Auk***,** 387-397.

Prince, R. C., Mcfarlin, K. M., Butler, J. D., Febbo, E. J., Wang, F. C. & Nedwed, T. J. 2013. The primary biodegradation of dispersed crude oil in the sea. *Chemosphere,* 90**,** 521-526.

Ratajczak, A., Geißdörfer, W. & Hillen, W. 1998. Expression of Alkane Hydroxylase fromAcinetobacter sp. Strain ADP1 Is Induced by a Broad Range of n-Alkanes and Requires the Transcriptional Activator AlkR. *Journal of bacteriology,* 180**,** 5822-5827.

Rose, R., Dibdin, G. & Shellis, R. 1993. A quantitative study of calcium binding and aggregation

in selected oral bacteria. *Journal of dental research,* 72**,** 78-84.

Rosenberg, E. 1993. Exploiting microbial growth on hydrocarbons—new markets. *Trends in Biotechnology,* 11**,** 419-424.

Rosenberg, E., Zuckerberg, A., Rubinovitz, C. & Gutnick, D. 1979. Emulsifier of Arthrobacter RAG-1: isolation and emulsifying properties. *Applied and Environmental Microbiology,* 37**,** 402-408.

Rosenberg, M., Bayer, E. A., Delarea, J. & Rosenberg, E. 1982. Role of thin fimbriae in adherence and growth of Acinetobacter calcoaceticus RAG-1 on hexadecane. *Applied and Environmental Microbiology,* 44**,** 929-937.

Sakai, Y., Maeng, J. H., Kubota, S., Tani, A., Tani, Y. & Kato, N. 1996. A non-conventional dissimilation pathway for long chain n-alkanes in Acinetobacter sp. M-1 that starts with a dioxygenase reaction. *Journal of fermentation and bioengineering,* 81**,** 286-291.

Shao, Z. & Wang, W. 2013. Enzymes and genes involved in aerobic alkane degradation. *Frontiers in microbiology,* 4**,** 116.

Sheppard, N. & Simpson, D. M. 1953. The infra-red and Raman spectra of hydrocarbons. Part II. Paraffins. *Quarterly Reviews, Chemical Society,* 7**,** 19-55.

Shi, L. Z., Nascimento, J., Chandsawangbhuwana, C., Berns, M. W. & Botvinick, E. L. 2006. Real-time automated tracking and trapping system for sperm. *Microsc Res Tech,* 69**,** 894-902.

Singer, M. & Finnerty, W. 1984. Microbial metabolism of straight-chain and branched alkanes.

Smits, T. H., Witholt, B. & Van Beilen, J. B. 2003. Functional characterization of genes involved in alkane oxidation by Pseudomonas aeruginosa. *Antonie Van Leeuwenhoek,* 84**,** 193-200.

Sticher, P., Jaspers, M., Stemmler, K., Harms, H., Zehnder, A. & Van Der Meer, J. R. 1997. Development and characterization of a whole-cell bioluminescent sensor for bioavailable middle-chain alkanes in contaminated groundwater samples. *Applied and environmental microbiology,* 63**,** 4053-4060.

Stock, A. M., Martinez-Hackert, E., Rasmussen, B. F., West, A. H., Stock, J. B., Ringe, D. & Petsko, G. A. 1993. Structure of the magnesium-bound form of CheY and mechanism of phosphoryl transfer in bacterial chemotaxis. *Biochemistry,* 32**,** 13375-13380.

Trevisan, J., Angelov, P. P., Scott, A. D., Carmichael, P. L. & Martin, F. L. 2013. IRootLab: a free and open-source MATLAB toolbox for vibrational biospectroscopy data analysis. *Bioinformatics,* 29**,** 1095-1097.

Van Beilen, J., Li, Z., Duetz, W., Smits, T. & Witholt, B. 2003. Diversity of alkane hydroxylase systems in the environment. *Oil & gas science and technology,* 58**,** 427-440.

Van Beilen, J. B. & Funhoff, E. G. 2007. Alkane hydroxylases involved in microbial alkane degradation. *Applied microbiology and biotechnology,* 74**,** 13-21.

Van Beilen, J. B., Panke, S., Lucchini, S., Franchini, A. G., Röthlisberger, M. & Witholt, B. 2001. Analysis of Pseudomonas putida alkane-degradation gene clusters and flanking insertion sequences: evolution and regulation of the alk genes. *Microbiology,* 147**,** 1621-1630.

Vaneechoutte, M., Young, D. M., Ornston, L. N., De Baere, T., Nemec, A., Van Der Reijden, T., Carr, E., Tjernberg, I. & Dijkshoorn, L. 2006. Naturally transformable Acinetobacter sp. strain ADP1 belongs to the newly described species Acinetobacter baylyi. *Applied and environmental microbiology,* 72**,** 932-936.

Wang, C., Shi, X., Li, W., Wang, L., Zhang, J., Yang, C. & Wang, Z. 2016. Oil species

identification technique developed by Gabor wavelet analysis and support vector machine based on concentration-synchronous-matrix-fluorescence spectroscopy. *Mar Pollut Bull.*

Wang, S.-K., Wang, F., Hu, Y.-R., Stiles, A. R., Guo, C. & Liu, C.-Z. 2013. Magnetic flocculant for high efficiency harvesting of microalgal cells. *ACS applied materials & interfaces,* 6**,** 109-115.

Wang, W. & Shao, Z. 2012. Diversity of flavin-binding monooxygenase genes (almA) in marine bacteria capable of degradation long-chain alkanes. *FEMS microbiology ecology,* 80**,** 523-533.

Wang, W. & Shao, Z. 2014. The long-chain alkane metabolism network of Alcanivorax dieselolei. *Nat Commun,* 5**,** 5755.

Wang, Y., Ravindranath, S. & Irudayaraj, J. 2011. Separation and detection of multiple pathogens in a food matrix by magnetic SERS nanoprobes. *Analytical and bioanalytical chemistry,* 399**,** 1271-1278.

Wang, Z. & Fingas, M. F. 2003. Development of oil hydrocarbon fingerprinting and identification techniques. *Marine pollution bulletin,* 47**,** 423-452.

Welch, M., Oosawa, K., Aizawa, S.-L. & Eisenbach, M. 1993. Phosphorylation-dependent binding of a signal molecule to the flagellar switch of bacteria. *Proceedings of the National Academy of Sciences,* 90**,** 8787-8791.

Wentzel, A., Ellingsen, T. E., Kotlar, H.-K., Zotchev, S. B. & Throne-Holst, M. 2007. Bacterial metabolism of long-chain n-alkanes. *Applied microbiology and biotechnology,* 76**,** 1209-1221.

Yakimov, M. M., Timmis, K. N. & Golyshin, P. N. 2007. Obligate oil-degrading marine bacteria. *Current opinion in biotechnology,* 18**,** 257-266.

Young, D. M., Parke, D. & Ornston, L. N. 2005. Opportunities for genetic investigation afforded by Acinetobacter baylyi, a nutritionally versatile bacterial species that is highly competent for natural transformation. *Annu. Rev. Microbiol.,* 59**,** 519-551.

Zhang, D., Ding, A., Cui, S., Hu, C., Thornton, S. F., Dou, J., Sun, Y. & Huang, W. E. 2013. Whole cell bioreporter application for rapid detection and evaluation of crude oil spill in seawater caused by Dalian oil tank explosion. *Water research,* 47**,** 1191-1200.

Zhang, D., He, Y., Wang, Y., Wang, H., Wu, L., Aries, E. & Huang, W. E. 2012. Whole-cell bacterial bioreporter for actively searching and sensing of alkanes and oil spills. *Microbial biotechnology,* 5**,** 87-97.

Zheng, Y., Li, L., Liu, Q., Qin, W., Yang, J., Cao, Y., Jiang, X., Zhao, G. & Xian, M. 2012. Boosting the free fatty acid synthesis of Escherichia coli by expression of a cytosolic Acinetobacter baylyi thioesterase. *Biotechnology for biofuels,* 5**,** 76.

Zhou, H., Yang, D., Ivleva, N. P., Mircescu, N. E., Schubert, S. R., Niessner, R., Wieser, A. & Haisch, C. 2015. Label-free in situ discrimination of live and dead bacteria by surface-enhanced Raman scattering. *Analytical chemistry,* 87**,** 6553-6561.

Electronic Supporting Information

Investigating impacts of nutrient cations on alkane chemotaxis-related affinity and accumulation of *Acinetobacter baylyi* ADP1 *via* Raman microspectroscopy

Hanbing Li[a], Francis L. Martin[b], Dayi Zhang [c,a,*]

[a] Lancaster Environment Centre, Lancaster University, Lancaster, LA1 4YQ, UK

[b] School of Pharmacy and Biomedical Sciences, University of Central Lancashire, Preston PR1 2HE, UK

[c] School of Environment, Tsinghua University, Beijing, 100086, PR China

***Corresponding author**

Dr Dayi Zhang

School of Environment, Tsinghua University, Beijing, 100086, PR China

Lancaster Environment Centre, Lancaster University, Lancaster, LA1 4YQ, UK

Tel.: +44(0)1524510288; Fax: +44(0)1524510082; Email: d.zhang@lancaster.ac.uk

No. of Pages = 1

No. of Figures = 1

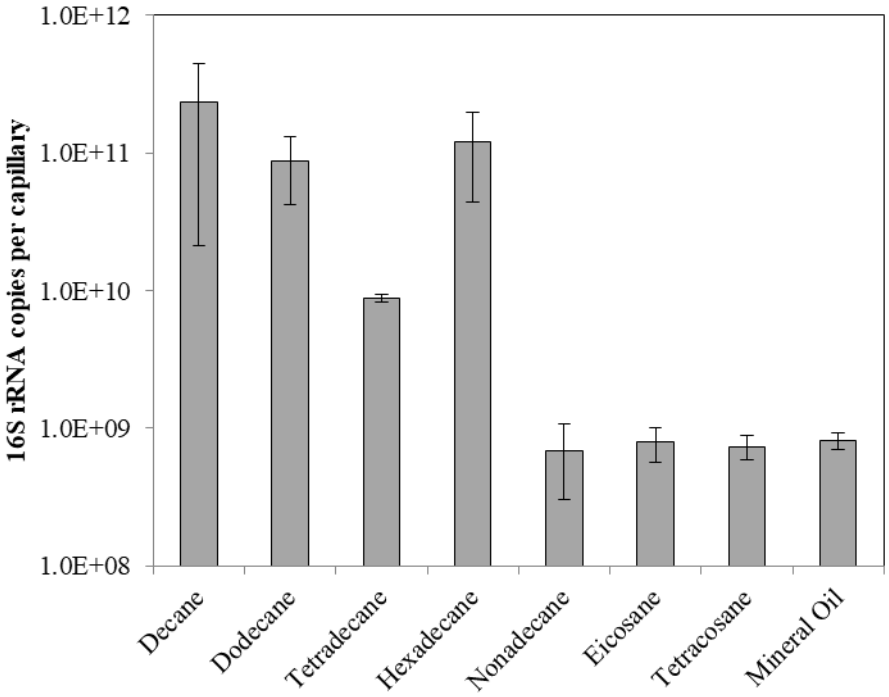

Figure S1. Chemotaxis of *A. baylyi* towards decane, dodecane, tetradecane, hexadecane, nonadecane, eicosane, tetracosane, and mineral oil *via* the capillary assay

Chapter 4

Interrogating the Selectivity of Bacterial Chemotaxis-Driven Affinity and Accumulation of Carbonaceous Substances *via* Raman Microspectroscopy

Hanbing Li, Francis L. Martin, Dayi Zhang

Manuscript for submission

Contribution:

- I prepared the samples required for the project;
- I processed and acquired all spectral data and carried out computational analysis;
- I prepared the first draft and figures of manuscript.

Interrogating the transient selectivity of bacterial chemotaxis-driven affinity and accumulation of carbonaceous substances *via* Raman microspectroscopy

Hanbing Li[a], Francis L Martin[b], Dayi Zhang[c,a,*]

[a] Lancaster Environment Centre, Lancaster University, Lancaster LA1 4YQ, UK

[b] School of Pharmacy and Biomedical Sciences, University of Central Lancashire, Preston PR1 2HE, UK

[c] School of Environment, Tsinghua University, Beijing, 100084, PR China

***Corresponding author**

Dr Dayi Zhang

School of Environment, Tsinghua University, Beijing, 100084, PR China

Lancaster Environment Centre, Lancaster University, Lancaster LA1 4YQ, UK

Tel.: +86(0)62773232; Fax: +86(0)62785687; Email: zhangdayi@tsinghua.org.cn

Abstract

Carbonaceous substances are fundamental organic nutrients for microbial metabolism and catabolism in natural habitats. Microbial abilities to sense, accumulate and utilize organic carbonaceous substances in the complex nutrient environment are important for their growth and ecological functions. Bacterial chemotaxis is an effective mechanism for microbial utilization of carbonaceous substances under nutrient depletion conditions. Although bacterial accumulation and utilization to individual carbonaceous substance in long-term cultivation has been well studied, their selective affinity of mixed carbonaceous substances remains to be investigated, primarily because of technical limitations of conventional methods. Herein, we applied Raman microspectroscopy to identify chemotaxis-driven affinity and accumulation of four organic carbonaceous substances (glucose, succinate, acetate and salicylate) by three bacterial strains (*Acinetobacter baylyi*, *Pseudomonas fluorescence* and *Escherichia coli*). *A. baylyi* exhibited strong binding affinity towards glucose and succinate, whereas *P. fluorescence* and *E. coli* were preferentially responsive to glucose and acetate. For the first time, bacterial transient selectivity of carbonaceous substances was studied *via* interrogating Raman spectral alterations. Post-exposure to carbonaceous-substance mixtures, the three bacterial strains showed distinct selective behaviors. Stronger selective affinity enhanced the chemotaxis-related signal transduction in *A. baylyi* cells, whereas the carbonaceous substance signal transduction in *E. coli* was decreased by higher selective affinity. In *P. fluorescence*, there was no specific effect of selective affinity on signal transduction. Our study suggests that Raman microspectroscopy can successfully investigate and distinguish different scenarios of bacterial competitive and transient unitization of organic carbonaceous substances.

Keywords: *Acinetobacter baylyi*; *Pseudomonas fluorescence*; *Escherichia coli*; Chemotaxis; Transient selectivity; Raman microspectroscopy

Introduction

Bacteria can employ diverse mechanisms to sense and accumulate chemical molecules in their natural environment (Adler, 1966; Sourjik and Wingreen, 2012). The bacterial chemotaxis system is a well-developed chemical gradient sensor, and motile chemotactic bacterial cells are able to follow concentration gradients of chemo-attractants, such as nutrients and other environmental stimuli, to select and accumulate them on cell membrane (Sourjik and Wingreen, 2012). Attractant nutrients include organic carbonaceous substances, organic nitrogen and other essential inorganic elements. Organic carbonaceous substances, *e.g.*, sugar, organic acids and polyols, are fundamental nutrients for bacterial growth. Bacteria show positive and selective responses towards some specific carbonaceous substance molecules present in medium (Adler, 1966; Kirby, 2009; Sampedro et al., 2015; Singh and Arora, 2001; Sourjik, 2004). Glucose is a major carbonaceous substance exhibiting high attraction to microbes (Hazelbauer et al., 1969; Singh and Arora, 2001; Weert et al., 2002), and carbonaceous acids such as succinate and acetate can be used as chemo-attractant in bacterial chemotaxis assays (Dailey and Berg, 1993; Oku et al., 2014; Sampedro et al., 2015). Microbial chemotaxis-related affinity towards carbonaceous substances is vital for their survival in natural habitats as it assists them in accessing carbonaceous nutrients, and determines the accumulation and utilization of carbonaceous nutrients in bacterial cells.

Bacterial chemotactic responses to carbonaceous substances are regulated by specific proteins. In *Pseudomonas*, methyl-accepting proteins (MCPs) are believed to determine the specificity of the chemotactic response (Ferrández et al., 2002). MCP comprises the periplasmic ligand-binding region and the cytosolic methyl-accepting domain that allows sense and transfer of the chemical signal to bacterial cells (Alexander and Zhulin, 2007; Ferrández et al., 2002). The chemotaxis protein McpS in *Pseudomonas putida* KT2440 is the chemoreceptor for sensing tricarboxylic acid (TCA) cycle intermediate (e.g. succinate, fumarate, oxaloacetate, citrate and isocitrate), as well as acetate and butyrate (Lacal et al., 2011), and the glucose-specific binding protein GLTB is characterized in *P. aeruginosa* (Sly et al., 1993). *E. coli* is a model strain for chemotaxis study (Sourjik, 2004; Sourjik and Wingreen, 2012), in which the CheA and CheW combine as a ternary complex to facilitate chemotactic responses to carbonaceous substances such as glucose and acetate (Maddock and

Shapiro, 1993; Sourjik and Berg, 2000). The CheW performs as an adaptor protein assits the linkage of MCPs with cytoplasmic histidine protein CheA. It is reported that *mcp*, *cheR* and *chew-2* genes in *Acinetobacter* are responsible for chemoreceptor cluster formation (Wang and Shao, 2014). The flagella on the *Acinetobacter* cell membrane facilitate the movement towards carbonaceous molecules (Foster, 1962). However, mechanisms of glucose or succinate chemotaxis in *Acinetobacter* remain unknown.

Approaches used to study bacterial chemotaxis include swarm plates (Henrichsen, 1972), capillary assays (Berg and Turner, 1990), temporal stimulation of tethered cells (Block et al., 1983), and automated tracking of swimming cells (Kearns, 2010; Shi et al., 2006). These approaches are versatile in testing bacterial chemotaxis towards specific individual chemicals. They can successfully describe the movement of bacterial cells to a certain carbonaceous substance; however, they fail in distinguishing which molecule is chemotactically sensed and accumulated by bacterial cells in a mixture of substances. In contrast, Raman microspectroscopy can provide the vibrational information on chemicals acquired by bacteria (Li et al., 2017). It is a fast, reproducible and non-destructive approach, and widely applied in biological studies (Efrima and Zeiri, 2009). The effects of the co-existence of carbonaceous substances on bacterial sensing and accumulation require further investigation, because it represents a real-world scenario of carbonaceous substance utilization by bacteria and explains the microbial ecological functions in complicated natural habitats.

Well-developed to determine cell-molecule interactions and the microbial response to the environment (Efrima and Bronk, 1998; Guzelian et al., 2002; Wang et al., 2011; Zhou et al., 2015; Jin et al., 2017b), Raman microspectroscopy has been applied to investigate nanotoxicity in bacterial cells (Cui et al., 2013) and to determine using heavy water labeling the minimum inhibitory concentrations of antibiotics (Tao et al., 2017). Recently, the alkane chemotactic affinity of *A. baylyi* is studied *via* Raman spectral alterations to illustrate the intracellular bioaccumulation in these cells (Li et al., 2017). Although it is well-documented that Raman spectroscopy is sophisticated in discriminating spectral alterations of bacterial cells after long-term cultivation with different carbon sources (Maquelin et al., 2000; Schuster et al., 2000), the study of bacterial transient affinity and uptake of diverse carbonaceous substances *via* Raman

spectra remains covered. The fast and non-destructive manners of biospectroscopy allow the measurement of binding affinity and accumulation of molecules on/inside bacterial cells, hinting at the possibility of characterizing the fingerprints of carbonaceous substances bioaccumulated by bacteria and to distinguish their transient and selective responses. To our knowledge, there is no such study exploring Raman spectral alterations in bacterial transient affinity towards and selective uptake from a mixture of organic carbonaceous substances.

Based on our recently developed Raman spectroscopic method for determining chemotactic affinity and accumulation of alkane molecules in *A. baylyi* cells (Li et al., 2017), this work further distinguishes the Raman spectral alterations and quantifies the bacterial transient affinity and accumulation of hydrophilic carbonaceous substances (glucose, succinate, acetate and salicylate) after short-time exposure (30 min). By interrogating the selective affinity and accumulation in *Acinetobacter baylyi*, *Pseudomonas fluorescence* and *Escherichia coli* towards individual carbonaceous substance and their mixtures *via* Raman spectra, we found the selective behavior of bacterial cells after transient exposure to carbonaceous substance mixtures. Additionally, Raman spectral alterations revealed the distinct mechanisms of chemotaxis-related signal transduction in the three bacterial strains. Signal transduction was enhanced or weakened by attractant binding affinity in *A. baylyi* or *E. coli*, respectively, whereas no significant effect of attractant binding affinity on the signal transduction was observed for *P. fluorescence*. Our results provide a novel and non-destructive Raman spectroscopic technique in distinguishing bacterial selective affinity and accumulation of various nutrients *in situ*, potentially feasible in characterizing bacterial metabolic and catabolic behavior in their natural habitats.

Materials and Methods

Bacteria strains and growth conditions

The bacterial strains used in this study included *Acinetobacter baylyi* ADP1, *Pseudomonas fluorescence* and *Escherichia coli* JM109 (Jin et al., 2017a). They were grown in minimal medium (MM) with 20 mM sodium succinate as the sole carbon source, shaking at 150 rpm and 30 ℃ for 16 h. To prepare mineral medium, 1.0 g of

$(NH_4)_2SO_4$, 2.5 g of KH_2PO_4, 0.1 g of $MgSO_4 \cdot 7H_2O$, 0.005 g of $FeSO_4 \cdot 7H_2O$, 0.25 g of nitrilotriacetic acid, 0.55 g of NaOH and 1 mL of Bauchop and Elsden solution were mixed well in 1.0 L deionized water and autoclaved (Jia et al., 2016). Bacterial cells were harvested by centrifugation at 4,000 rpm for 4 min and washed three times using sterile deionized water. Finally, the cell pellets were separately suspended in MM without any carbon source for further experiments. Unless specified otherwise, all chemicals used in this study were of analytical grade and purchased from Sigma-Aldrich (UK).

Exposure to carbonaceous substances

The four studied carbonaceous substances included three organic acid salts (sodium succinate, sodium acetate and sodium salicylate) and one carbohydrate (glucose). They were dissolved in MM to prepare the 1 M stock solution required. Bacterial suspensions were mixed with each carbonaceous substance stock solution to obtain a final concentration of 10 mM. From the dose-response affinity in Figure 4, the optimized concentration for carbonaceous substances used in this study was 10 mM. The transient exposure was 30 min at 30 ℃ for all treatments. From our previous study, all the three strains stayed in the lag phase at the concentration of about 10^7 CFU/mL for at least 2 hours after re-cultivated in MM with different carbon sources and exhibited distinct spectral fingerprints comparing to those after the long-term cultivation (usually 12-16 hours) (Jin et al., 2018). Their Raman spectral alterations, after transient exposure, were therefore entirely different from the alterations of bacterial cells after long-term cultivation with different carbon sources. Bacterial suspensions post-exposure to carbonaceous substances were centrifuged at 5,000 rpm for 5 min to remove the medium, and the cell pellets were washed once with sterile deionized water prior to Raman spectral acquisition.

The dose response of carbonaceous substance binding affinity and accumulation was measured by exposing bacterial suspensions to the carbonaceous substance with high binding affinity: succinate/glucose for *A. baylyi* and acetate/glucose for *P. fluorescence* and *E. coli*. After adding different volumes of carbonaceous substance stock solution to 1 mL bacterial suspensions to reach the final concentrations of 0, 1, 5 and 10 mM, the mixture was incubated for 30 min at 30 ℃, centrifuged at 5,000 rpm for 5 min and washed once with sterile deionized water prior to Raman spectra

acquisition.

To evaluate the transient and selective affinity response of each bacterial strain, the carbonaceous substance mixtures were prepared by mixing two carbonaceous substances, succinate/glucose for *A. baylyi* and acetate/glucose for *P. fluorescence* as well *E. coli*; their final concentration was 10-mM:10-mM and 5-mM:10-mM, respectively. Bacterial cells were exposed to carbonaceous mixtures for 30 min at 30 ℃, followed by the same centrifugation and washing protocol as described above.

Chemotaxis capillary assay

To evidence bacterial chemotactic propensity towards each carbonaceous substance, the conventional capillary assay was performed, as previously described (Adler, 1973; Li et al., 2017). The capillary tube (internal diameter of 0.2 mm and length of 10 cm) was first plunged into the carbonaceous substance stock solution for 5 min until the liquid was drawn up to approximately 1 cm in the tube. The tube was then inserted into the bacterial suspension for 30 min at 30 ℃. In order to measure the carbonaceous substance affinity of different bacterial strains, quantitative polymerase chain reaction (qPCR) was used to quantify the 16S rRNA copy numbers of chemotactic bacteria on each capillary in triplicates. The 1-cm exterior from the open end of the capillary tube was plunged into qPCR buffer as the DNA template. The 10 μL qPCR buffer contained 1 μL of primer 341F (5'-CCTACGGGNGGCWGCAG-3'), 1 μL of primer 802R (5'- TACNVGGGTATCTAATCC-3'), 3 μL of molecular water and 5 μL of iTaq™ Universal SYBR® Green Supermix (BioRad, USA). The thermo cycling program was: initial denaturation at 94 ℃ for 3 min; 34 amplification cycles of 94 ℃ for 45 s, 52 ℃ for 45 s, 72 ℃ for 45 s, and fluorescence data acquisition at 80 ℃ for 15 s. The qPCR standard curves were obtained with serial dilutions of quantified plasmid DNA containing the fragment of 16S rRNA genes.

Raman spectral acquisition

An InVia confocal micro-Raman system (Renishaw, Gloucestershire, UK) equipped with a 100 mW 785 nm excitation laser was employed for sample detection and Raman spectral acquisition, with a charged couple detector (CCD) and an attached microscope (Leica Microsystems, Milton Keynes, UK). The Raman system was calibrated using a Renishaw silicon calibration source before sample analysis. Ten microliter of washed cells were positioned onto a glass slide covered by aluminum

foil and air-dried before Raman spectral acquisition (Cui et al., 2016). Twenty spectra per sample were randomly acquired using the 50 μm spectrometer entrance slit combined with a 1200 lines per mm diffraction grating (1 cm^{-1} spatial resolution), ×50 objective (0.75 numerical aperture; approximately 1 μm spatial resolution), 50% laser power (13 mW at samples), 10 sec acquisition time and one accumulation within a spectral range from 500 to 2000 cm^{-1}.

Computational analysis

Unless specifically stated otherwise, Raman spectra were pre-processed using baseline correction and vector normalization prior to principal component analysis (PCA) and linear discriminant analysis (LDA) using the IRootLab toolbox based on Matlab (version R2013b, MathWorks, USA) (Trevisan et al., 2013). PCA was carried out to visualize the natural variance within the dataset and reduce the dimensionality of the multivariate data (Trevisan et al., 2013). The separation of individual spectral categories from negative control and pure carbonaceous substance classes was measured by exporting PCA-derived data. To attain inter-class separation and minimize intra-class differences, LDA was employed to extract inter-category discriminating features (Butler et al., 2015; Martin et al., 2007). Post-exposure to different concentrations of carbonaceous substances, the dispersion of individual Raman spectra to that of negative controls (carbonaceous substance concentration = 0 mM) and pure carbonaceous substance was calculated based on principal component (PC)1 and PC2, and visualized as dispersion indicator (D_I) score plots (Li et al., 2017). In a D_I score plot, the increasing D_I value between two categorizes is proportional to dissimilarity (Ami et al., 2013; Li et al., 2017).

Results and Discussion

Bacterial chemotaxis towards carbonaceous substance *via* capillary assay

The chemotaxis capillary assay of organic carbonaceous substance proved the different chemotactic sensitivities and binding affinities of *A. baylyi*, *P. fluorescence* and *E. coli* towards glucose, acetate, succinate and salicylate, respectively. From the results of the capillary assay, *A. baylyi* exhibited a highly sensitive chemotactic response towards glucose and succinate. The accumulation of *A. baylyi* 16S rRNA

genes was 6.38×10^7 and 6.75×10^7 copies/capillary for glucose and succinate, respectively, significantly higher than those in acetate and salicylate treatments [see Electronic Supporting Information (ESI) Figure S1]. In carbonaceous substance capillary assays, glucose, compared with other carbonaceous substances used in this study, was a strong chemo-attractant for *P. fluorescence*, achieving 2.13×10^7 copies/capillary 16S rRNA genes (see ESI Figure S1). *P. fluorescence* cells could also chemotactically sense acetate (1.18×10^7 copies/capillary) or succinate (7.54×10^6 copies/capillary), whereas only a small number of *P. fluorescence* cells accumulated in the salicylate capillary (1.29×10^6 copies/capillary), indicating the weak chemotaxis of *P. fluorescence* towards salicylate. The chemotactic behavior of *E. coli* was entirely different from that of *A. baylyi* and *P. fluorescence*, consistent with previous studies (De Gelder et al., 2007; Kirby, 2009; Sampedro et al., 2015; Singh and Arora, 2001; Sourjik and Wingreen, 2012). *E. coli* showed weak chemotaxis-related affinity to succinate, and the 16S rRNA copy numbers post-exposure to the succinate were approximately 50-fold or 100-fold lower than that of *A. baylyi* or *P. fluorescence* (see ESI Figure S1). Alternatively, the highest accumulation was achieved when post-exposure to acetate (1.57×10^6 copies/capillary), whereas the accumulation was only 2.26 copies/capillary 16S rRNA genes in salicylate assay, showing the extremely weak salicylate attraction to *E. coli*. Salicylate represses the synthesis of porin and induces antibiotic resistant in *E. coli* (Cohen et al., 1993; Sawai et al., 1987), which results in the adverse effects on bacterial affinity.

Raman spectral characterization of bacterial transient affinity to carbonaceous substances

Raman spectral alterations of the three bacterial strains post-exposure to four carbonaceous substances profile their transient binding affinity and cellular accumulation (Figure 1). Figure 2 further illustrates the PCA differentiation of the transient affinity and accumulation in *A. baylyi*, *P. fluorescence* and *E. coli* for each organic carbonaceous substance. To visualize the differences in the binding affinity of bacterial cells towards each carbonaceous substance, we use different colours to highlight the PCA score plots. The three different color gradients of light-, medium- and dark-red in PCA score plots represent weak, moderate and strong levels of bacterial binding affinity towards different organic carbonaceous substances, respectively. After transient exposure (30 min) to the four carbon sources, distinct

Raman spectra were identified for *A. baylyi*. Table 1 lists the predominant peaks in the Raman spectra of the pure *A. baylyi*, including 723 cm^{-1} and 777 cm^{-1} (nucleic acids) (De Gelder et al., 2007), 1002 cm^{-1} (phenylalanine) (Li et al., 2017), 1238 cm^{-1} and 1311 cm^{-1} (amino acids) (De Gelder et al., 2007), 1441 cm^{-1} (glycine) (Cui et al., 2013) and 1663 cm^{-1} (protein) (Li et al., 2017). Post-exposure to acetate or salicylate, the Raman spectra of *A. baylyi* remain unchanged, and the PCA of Raman spectra are indistinctive in comparison to the pure strains (Figure 1A and 2A). The PCA score plot indicates the obvious Raman alterations post-exposure to succinate (Figure 1A). The specific bands at 738 cm^{-1}, 1332 cm^{-1} and 1446 cm^{-1} observed in the Raman spectra are attributed to C-H wag, sodium deformation and C-H bend in succinate, confirming the transient affinity and accumulation of succinate molecules in *A. baylyi* cells (Figure 2A) (Dhanya et al., 2011; Frost and Kloprogge, 2000). The PCA category comprising *A. baylyi* post-exposure to glucose is close to pure glucose, significantly different from the group of pure *A. baylyi* cells (Figure 1A). In Figure 2A, the glucose affinity and accumulation of *A. baylyi* contributes to the Raman spectral alterations, especially at 1338 cm^{-1} (-CH_2 deformation), 1379 cm^{-1} (C-H bending and O-H bending) and 1454 cm^{-1} (-CH_2 bending) (Araujo-Andrade et al., 2005; Vasko et al., 1972). These results are consistent with those of capillary assays, highlighting that *A. baylyi* has moderate chemotactic accumulation of succinate and glucose. The ability of *A. baylyi* that grow on glucose as sole carbon source may cause the high glucose binding affinity (Barbe et al., 2004b). *A. baylyi* possesses the intact genes coding of the enzymes for TCA including succinate, suggesting that the positive utilization may enhance the succinate affinity and accumulation. It is worth noting that, compared to salicylate, the Raman spectral PCA categorization of *A. baylyi* post-exposure to acetate is closer to pure bacterial cells, whereas the capillary assays showed the opposite result that acetate attraction to *A. baylyi* was weaker than salicylate (see ESI Figure S1 and S2). The difference between the two approaches implies that the conventional capillary assay only evaluates the movement and accumulation of bacterial cells towards capillary, different from the detection of chemotaxis-driven accumulation and utilization of organic carbonaceous substances on/inside bacterial cells *via* Raman microspectroscopy. It hints at the applicability of employing Raman microspectroscopy to distinguish the vibrational fingerprints of organic carbonaceous substances on bacteria and further characterize the mechanisms

of bacterial chemotaxis in complex environment.

Table 1. Assignments of Raman bands of three bacteria strains pre- and post-exposure to four carbonaceous substances.

	Band (cm^{-1})	Tentative bands assignment	*A. baylyi*					*E. coli*					*P. fluorescence*				
			NC	Glu	Suc	Ace	Sal	NC	Glu	Suc	Ace	Sal	NC	Glu	Suc	Ace	Sal
Bacteria	723	Nucleic acids	●	●	●	●	●	●	●	●	●	●	●	●	●	●	●
	777	Nucleic acids	●	●	●	●	●	●	●	●	●	●	●	●	●	●	●
	1002	Phenylalanine	●	●	●	●	●	●	●	●	●	●	●	●	●	●	●
	1238	Amino acids	●	●	●	●	●	●	●	●	●	●	●	●	●	●	●
	1311	Amino acids	●	●	●	●	●	●	●	●	●	●	●	●	●	●	●
	1441	Glycine	●	●	●	●	●	●	●	●	●	●	●	●	●	●	●
	1663	Protein	●	●	●	●	●	●	●	●	●	●	●	●	●	●	●
Glucose	838	C-H deformation	-	●	-	-	-	-	-	-	-	-	-	●	-	-	-
	914	C-H and C-O-H deformation	-	●	-	-	-	-	-	-	-	-	-	●	-	-	-
	1054	C-H deformation	-	-	-	-	-	-	-	-	-	-	-	●	-	-	-
	1116	C-H and C-O-H deformation	-	●	-	-	-	-	-	-	-	-	-	●	-	-	-
	1125	C-H and C-O-H deformation	-	-	-	-	-	-	-	-	-	-	-	●	-	-	-
	1338	$-CH_2$ deformation	-	●	-	-	-	-	●	-	-	-	-	●	-	-	-
	1379	C-H bend and O-H bend	-	●	-	-	-	-	-	-	-	-	-	-	-	-	-
	1454	$-CH_2$ deformation	-	●	-	-	-	-	-	-	-	-	-	-	-	-	-
Succinate	738	C-H wag	-	-	●	-	-	-	-	-	-	-	-	-	-	-	-
	939	C-C symmetric stretch	-	-	●	-	-	-	-	-	-	-	-	-	-	-	-
	1332	Sodium deformation	-	-	●	-	-	-	-	-	-	-	-	-	-	-	-
	1446	C-H bend	-	-	●	-	-	-	-	-	-	-	-	-	-	-	-
Acetate	652	-COO deformation	-	-	-	-	-	-	-	-	-	-	-	-	-	●	-
	928	C-C stretch	-	-	-	-	-	-	-	-	-	-	-	-	-	●	-
	1350	Metal deformation	-	-	-	-	-	-	-	-	●	-	-	-	-	●	-

●, ●, ● and ● indicate the peak identified in corresponding Raman spectra of pure bacterial cells, glucose, succinate and acetate, respectively.

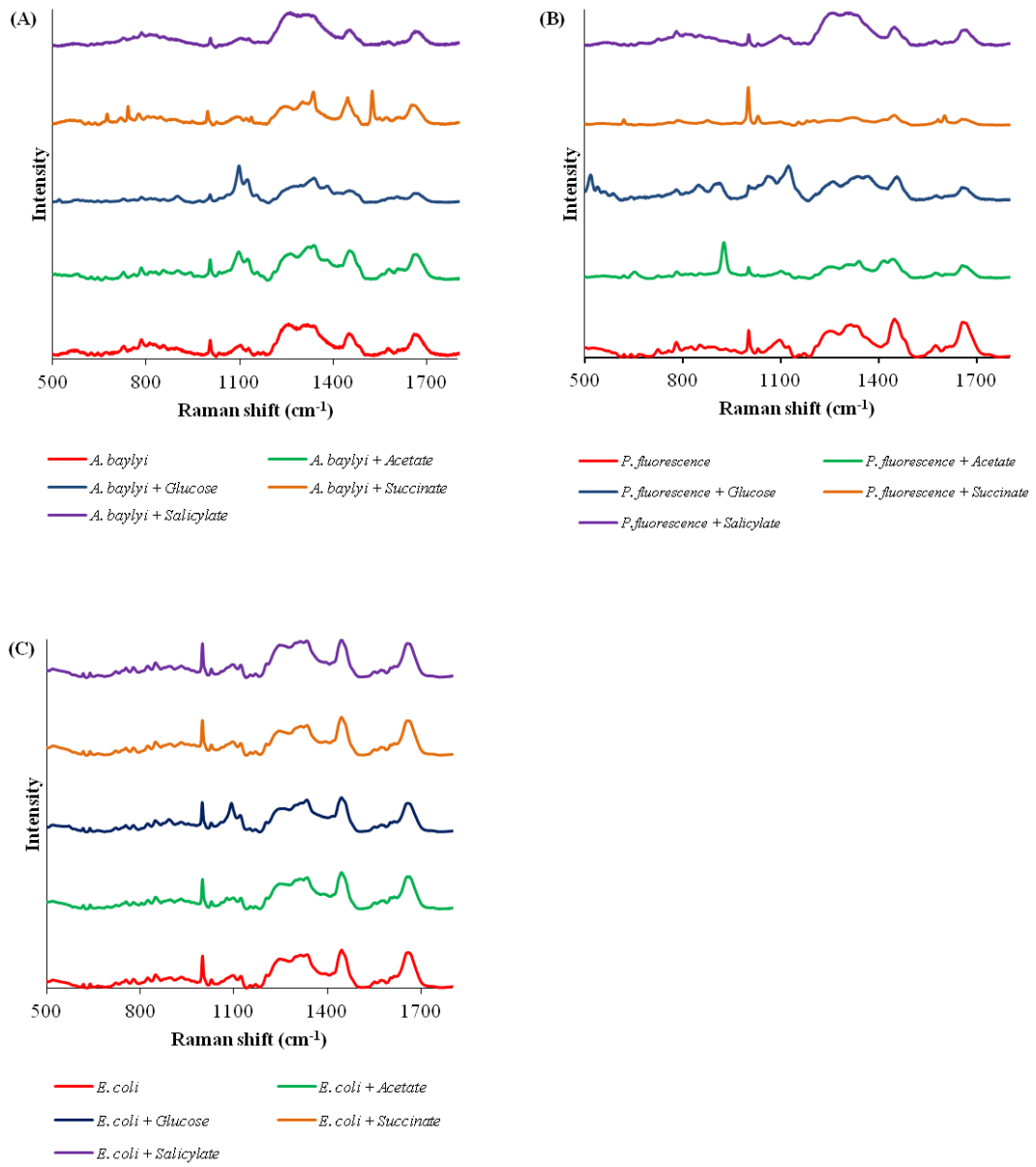

Figure 1. Raman spectra of *A. baylyi* (A), *P. fluorescence* (B) and *E. coli* (C), pre- and post-exposure to 10 mM acetate (green), glucose (blue), succinate (brown) and salicylate (purple). Twenty Raman spectra were randomly obtained per treatment.

Owing to the close genomic and proteomic relationship to the order *Pseudomonadales* between *A. baylyi* and *P. fluorescence*, the Raman spectra of these two bacterial strains are similar (Barbe et al., 2004a; Vaneechoutte et al., 2006; Young et al., 2005). However, the transient response of *P. fluorescence* towards four carbonaceous substances is different from *A. baylyi*. Significant alterations are found in *P. fluorescence* post-exposure to acetate and glucose (Table 1). Post-exposure to glucose (Figure 1B), Raman band of 1338 cm^{-1} attributed to -CH_2 deformation is dominant. Additionally, three glucose peaks are detected, occurring at 1125 cm^{-1} (C-H and C-O-H deformations), 1054 cm^{-1} (C-H deformation) and 914 cm^{-1} (C-H and C-O-H deformations).(Araujo-Andrade et al., 2005; Vasko et al., 1972) The remarkable difference Raman spectral PCA score plots of *P. fluorescence* between pre- and post-exposure to glucose also proves the high glucose binding affinity of this bacterial strain (Figure 2B). In acetate treatment, the specific 1350 cm^{-1} band is attributed to sodium deformation (Figure 1B) (Frost and Kloprogge, 2000), and the bands 928 cm^{-1} (C-C stretch) and 652 cm^{-1} (-COO deformation) are also apparent (Figure 1B) (Bickley et al., 1990). Figure 2B illustrates the close distance of Raman spectral PCA groups between pure acetate and *P. fluorescence* post-exposure to acetate, demonstrating the moderate acetate affinity and accumulation. In contrast, no specific Raman spectral biomarker was observed in *P. fluorescence* post-exposure to salicylate and the PCA score plots suggest a weak attraction of salicylate (Figure 1B and 2B). The transient exposure of *P. fluorescence* towards succinate contributes to higher binding affinity than towards acetate in Raman spectra (Figure 2B). However, from the results of capillary assay, the succinate affinity is lower than acetate (see ESI S1). We speculated that the faster movement speed of *P. fluorescence* towards acetate molecules in capillary tube increases the 16S rRNA copies, while the higher succinate binding affinity and accumulation in *P. fluorescence* leads to the strong Raman characterization.

Similar to the carbonaceous substances affinity and accumulation in *P. fluorescence*, *E. coli* exhibits positive affinity towards glucose and acetate. Some Raman spectral peaks of pure *E. coli* are identical to those of *A. baylyi* and *P. fluorescence*, including 1002 cm^{-1} (symmetric ring breathing of phenylalanine) (Li et al., 2017; Wang et al., 2011), 1238 cm^{-1} and 1331 cm^{-1} (amino acid) (De Gelder et al., 2007), 1441 cm^{-1} (-CH_2 deformation in glycine) and 1663 cm^{-1} (C=C stretching of bacterial proteins)

(Figure 1C) (De Gelder et al., 2007; Li et al., 2017). The strong glucose affinity of *E. coli* is highlighted in the PCA score plots, and the -CH_2 deformation Raman band at 1338 cm^{-1} indicates the accumulation of glucose molecules on/inside *E. coli* cells (Figure 1C, Table 1). Post-exposure to acetate, PCA scores of *E. coli* are close to that of pure acetate, demonstrating a strong acetate affinity (Figure 2C). In succinate or salicylate treatments, no Raman spectral alteration was found for *E. coli*, a consequence of weak affinity and accumulation of succinate or salicylate on *E. coli*, similar to the in capillary assay.

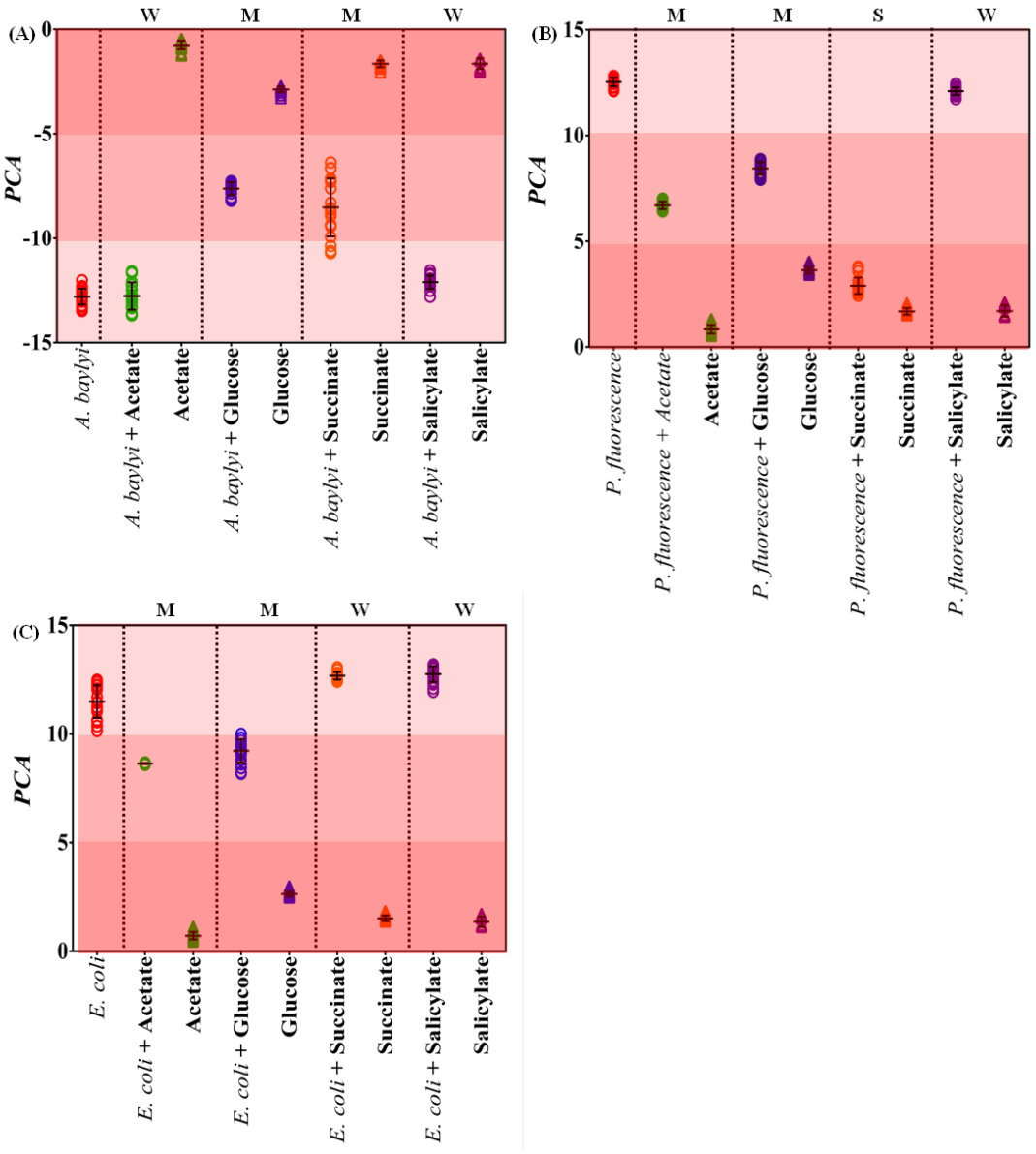

Figure 2. PCA score plots of *A. baylyi* (A), *P. fluorescence* (B) and *E. coli* (C) post-exposure to different organic carbonaceous substances including acetate (green), glucose (blue), succinate (orange) and salicylate (purple). In each plot, color gradients illustrate the level of bacterial binding affinity towards the four carbonaceous substances. Light-red indicates weak affinity (W), medium-red represents moderate affinity (M), and dark-red refers to strong affinity (S). Twenty Raman spectra were randomly obtained per treatment.

Because PCA is the unsupervised data analysis technique, it is only responsible for multi-variance in a whole dataset, but not for among-group identification (Kelly et al., 2011). Additionally, this method can give different scale bars to irrelevant Raman spectral group. Hence, to quantify the binding affinity and accumulation of different organic carbonaceous substances on/inside bacterial cells *via* Raman spectra, Dispersion indicator (D_I) is employed in this study to represent the dissimilarity between different treatments. Post-exposure to glucose, all the bacterial strains (*A. baylyi*, *P. fluorescence* and *E. coli*) exhibit positive affinity. The D_I values of *A. baylyi*, *P. fluorescence* and *E. coli* are 0.51, 0.72 and 0.22, respectively (see ESI Figure S2). The results indicate moderate to strong binding affinity and cellular accumulation of glucose by all the strains. The Raman spectral D_I values are 0.36 and 0.43 for *A. baylyi* and *P. fluorescence* post-exposure to succinate respectively, both higher than that of *E. coli* (see ESI Figure S2). It suggests weak bacterial attraction of succinate towards *E. coli*. Post-exposure to acetate, the D_I values of *P. fluorescence* and *E. coli* are both higher than 0.5, indicating their strong acetate affinity. The weak acetate binding affinity of *A. baylyi* results in the D_I value of 0.07. In salicylate treatment, all the D_I values of *A. baylyi*, *P. fluorescence* and *E. coli* are all lower than 0.30 and hint at weak salicylate affinity.

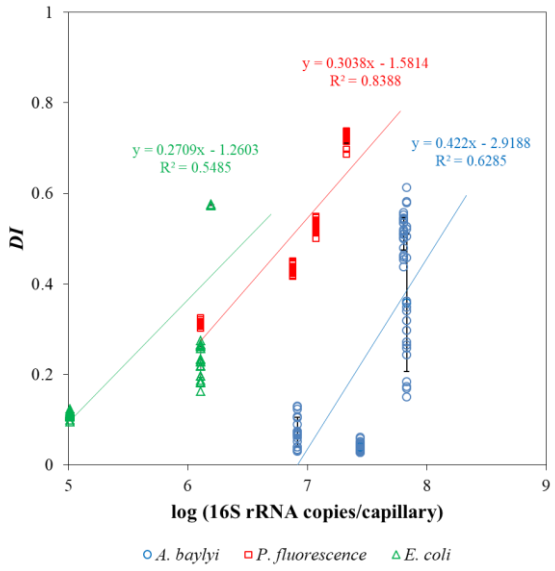

Figure 3. Semi-log linear regression of 16S rRNA copies per capillary and dispersion indicators (D_I) of *A. baylyi*, *P. fluorescence* and *E. coli* post-exposure to different organic carbonaceous substances. R^2 indicates the consistency of regression of D_I and 16S rRNA copies per capillary.

Raman microspectroscopy and capillary assay are different approaches to evaluate bacterial chemotaxis-driven affinity towards organic carbonaceous substances, using the distinct chemotactic indicators of D_I and 16S rRNA copies per capillary, respectively. The capillary assay quantifies the chemotaxis-driven movement and accumulation of bacterial strains to carbonaceous substances, whereas Raman spectral alterations illustrates the vibrational fingerprints of carbonaceous substances on/inside bacterial cells caused by binding affinity and accumulation (Li et al., 2017). We therefore generated a semi-log linear regression relationship between D_I scores in Raman spectral alterations and 16S rRNA copies in the capillary assay (Figure 3). The semi-log regression coefficient follows the order: *A. baylyi* (0.422) > *P. fluorescence* (0.308) > *E. coli* (0.271), indicating stronger chemotactic sensing and accumulation in *A. baylyi* and *P. fluorescence* than in *E. coli*. The R^2 coefficient of determination is 0.5485 for *E. coli*, 0.6285 for *A. baylyi* and 0.8388 for *P. fluorescence*, showing good agreements between D_I and 16S rRNA copies/capillary, acquired from Raman spectral alteration and capillary assay, respectively. These results validate the D_I model in predicting bacterial chemotactic behavior, and D_I is a feasible indicator to quantify carbonaceous substance chemotaxis-related affinity and accumulation on/inside bacterial cells.

Dose-responsive affinity and accumulation of carbonaceous substances

The strong Raman spectral alterations of *A. baylyi*, *P. fluorescence* and *E. coli* after transient exposure to carbonaceous substances allow one to quantify the binding affinity and cellular accumulation of organic carbonaceous molecules on/inside bacterial cells. The Raman spectra of bacteria towards 10 mM carbonaceous substances in ESI S3 are identical to those in Figure 1, and peak assignments are illustrated in Table 1. For the exposure of bacteria towards carbonaceous substances at the concentrations lower than 10 mM, the peak intensity of carbonaceous molecules can be reduced due to the less amount of molecules accumulated on/in bacterial cells. The changes in peak intensity are proceeded in following discussion, and all peaks are involved in Table 1. The targeted carbonaceous substances are succinate and glucose for *A. baylyi*, and acetate and glucose for *P. fluorescence* and *E. coli*. Glucose had moderate to strong affinity and accumulation in the cells of all three strains. Thus, the intensity of characteristic peaks increased with glucose concentrations in all the treatments. The band at 1338 cm^{-1} (methylene deformation) was found in all the

Raman spectra of *A. baylyi* post-exposure to glucose (see ESI Figure S3 and Table 1). The Raman band of C-H and C-O-H deformation at 1116 cm^{-1} was positively correlated to the concentration of glucose in *A. baylyi* and *P. fluorescence*. Raman bands at 914 cm^{-1} and 838 cm^{-1} bands assigned to C-H deformation were found in *A. baylyi* or *P. fluorescence* cells after transient exposure to 10-mM glucose. The D_I score plots (Figure 4A, 4C and 4E) illustrate a significant discrimination between the groups of *A. baylyi*, *P. fluorescence* or *E. coli* post-exposure to 1, 5 or 10 mM glucose. For all the three strains, the group of 1 mM glucose was significantly segregated from the negative control (0 mM glocuse). The D_I of *E. coli* post-exopsure to 5 mM glucose was 0.073, of no difference with the 10 mM glucose treatment (p>0.05). The results indicate a sensitive response of *E. coli* towards glucose, but the affinity and accumulation was weak at higher concentrations. It is hypothesized that *E. coli* is likely to capture and accumulate glucose molecules when the concentration is smaller than 5 mM, and higher glucose concentration may enhance the utilization and decrease the binding affinity of these molecules in bacterial cells. In contrast, the D_I values of *A. baylyi* or *P. fluorescence* post-exposure to glucose constantly increased with glucose concentrations (Figure 4A and 4C), owing to the increasing glucose molecules accumulated on or inside *A. baylyi* or *P. fluorescence* cells. As a classic chemo-attractant, glucose-binding affinity to MCPs is well-documented (Hazelbauer et al., 1969; Singh and Arora, 2001; Weert et al., 2002). Bacterial chemotaxis is a significant step for binding affinity and cellular accumulation of glucose molecules. MCPs mediate the sensitivity of chemotaxis-driven affinity *via* a two-component regulatory system comprising a sensor kinase CheA and a response regulator CheY (Sourjik, 2004; Weert et al., 2002). As the transmembrane signal transducers triggered by the concentrations of extracellular glucose, MCPs are responsible for glucose recognition and accumulation on bacterial cells (Aizawa et al., 2000; Weert et al., 2002). Increasing Raman spectral alterations are therefore measurable at higher concentration of glucose and quantified by D_I scores.

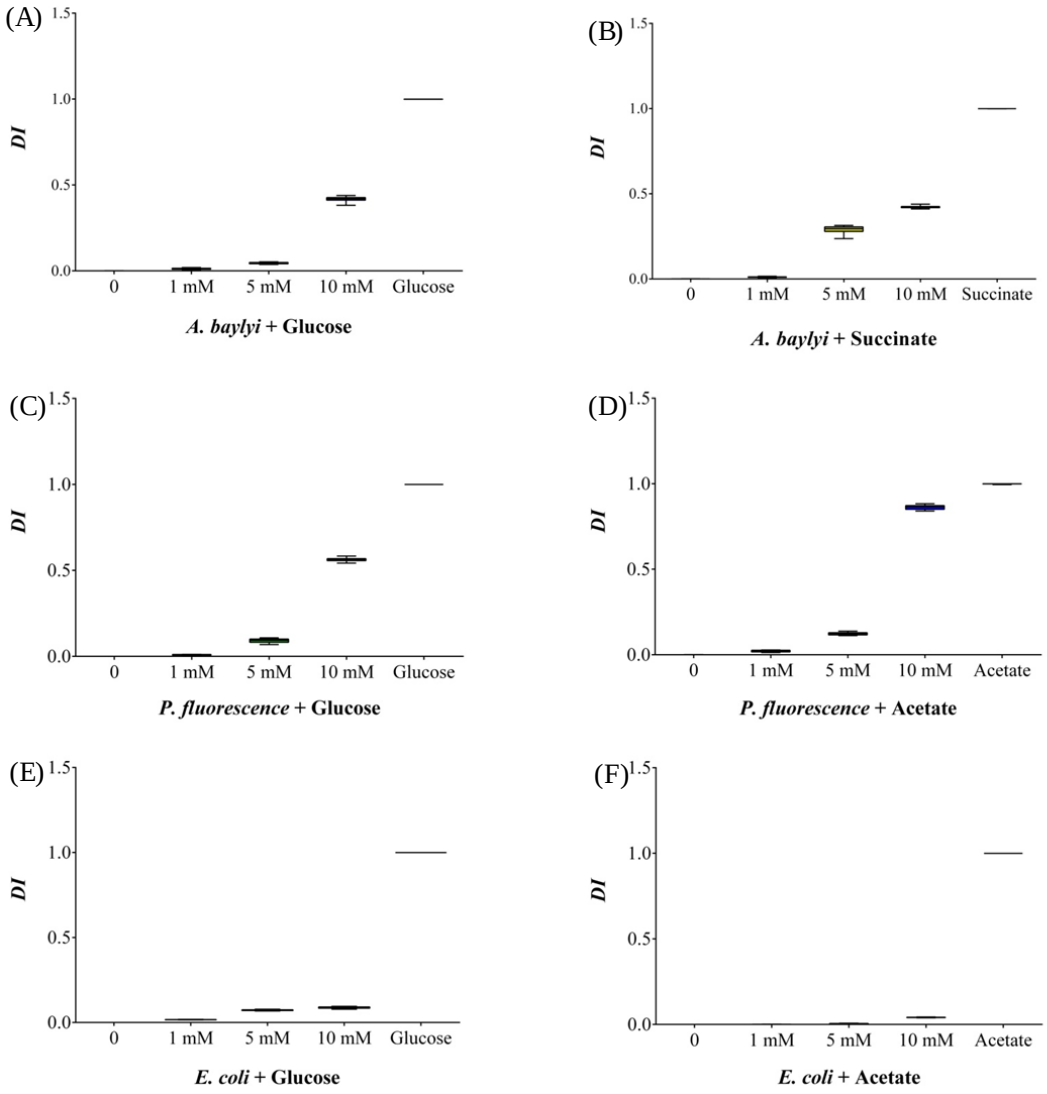

Figure 4. D_I score plots of bacterial Raman spectra after transient exposure to different concentrations of organic carbonaceous substances. (A) and (B) for D_I of *A. baylyi* cells post-exposure to glucose and succinate; (C) and (D) for D_I of *P. fluorescence* post-exposure to glucose and acetate; (E) and (F) for D_I of *E. coli* post-exposure to glucose and acetate. Twenty Raman spectra were randomly obtained per treatment.

For *A. baylyi* cells, we also observed the high binding affinity and cellular accumulation of succinate *via* Raman spectral alterations. The increasing concentrations of succinate raised the sodium deformation band at 1332 cm^{-1}, and the Raman band of C-C symmetric stretch at 939 cm^{-1} was detectable when succinate concentration was >1 mM (see ESI Figure S3). The 738 cm^{-1} band in *A. baylyi* post-exposure to 10 mM succinate was assigned to C-H wag. The D_I score plot illustrates that the group of *A. baylyi* post-exposure to 1 mM succinate were separated from negative control group (0 mM), confirming their highly sensitive affinity and accumulation of succinate (Figure 4B). Additionally, the D_I value of *A. baylyi* post-exposure to 5 mM succinate reached 0.29, significantly higher than that in 5 mM glucose treatment. It is reported that *A. baylyi* cells preferentially sense and accumulate straight chain dicarboxylic carbonaceous substances like succinate (Baumann et al., 1968; Parke et al., 2001). Therefore, succinate exhibits a higher attraction to *A. baylyi* especially at higher concentrations.

Post-exposed to acetate, Raman spectral alteration was detectable at 928 cm^{-1} (C-C stretch) in *P. fluorescence* and *E. coli*. The Raman bands at 652 cm^{-1} (sodium deformation) and 1350 cm^{-1} (carboxylic deformation) dominated the spectra of *P. fluorescence* post-exposure to 5 mM or 10 mM acetate (ESI Figure S3). Figure 4D illustrates the increasing D_I values with acetate concentrations, from 0.021 (1 mM) to 0.862 (10 mM). It indicates the strong response and binding affinity of *P. fluorescence* to acetate. The D_I value of *P. fluorescence* post-exposure 10 mM acetate was much higher than that in 10 mM glucose (Figure 4D), although there was no significant difference between the categories of 5 mM acetate (0.09) and glucose (0.12). In addition, the D_I group of *P. fluorescence* in 1 mM acetate treatment was entirely discriminated from that of the negative control (Figure 4D), but not for *E. coli* (Figure 4F). Only 10 mM acetate exhibits obvious attraction to *E. coli* from the D_I score plot. The results suggest that *P. fluorescence* could recognize and accumulate 1 mM acetate, but the response sensitivity of *E. coli* towards acetate was 5 mM. Some previous studies have reported the strong acetate binding affinity in *P. fluorescence*, and the weak sensing and accumulation of acetate molecules in *E. coli* is attributed to the prolonged physiological adaptation in mineral medium (Paliy et al., 2003; Paliy and

Gunasekera, 2007). Due to the low concentration of bivalent iron in mineral medium, the synthesis of enzymes is insufficient for acetate accumulation and uptake in *E. coli*.

Selective affinity and accumulation towards carbonaceous substance mixtures

Different to conventional capillary assay, which evaluates the movement and accumulation of bacterial cells towards carbonaceous substances, Raman microspectroscopy characterizes the chemotaxis-driven affinity, accumulation and utilization of organic carbonaceous substances on/inside bacterial cells *via* biospectral fingerprints. It allows one to distinguish which carbonaceous substance is selectively sensed and accumulated by bacterial cells and to discriminate the bacterial competitive affinity towards the mixtures of various carbonaceous substances. Figure 5 illustrates the LDA score plots of bacterial Raman spectra after transient exposure to individual and multiple carbonaceous substances, successfully evaluating the bacterial selective affinity and accumulation of individual carbonaceous substance in complicated nutrient environments.

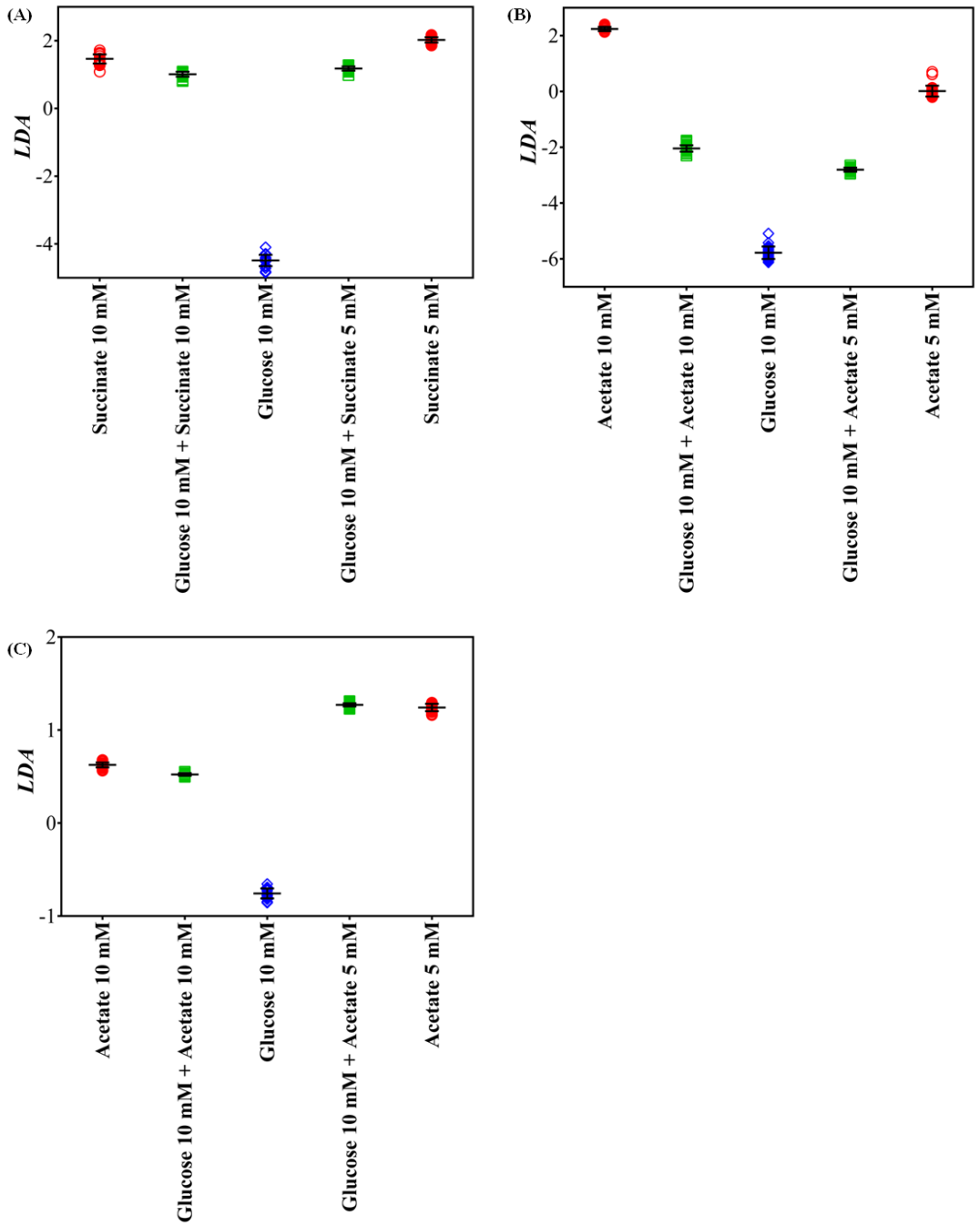

Figure 5. LDA score plots of *A. baylyi*, *P. fluorescence* and *E. coli* after transient exposure to individual and multiple carbonaceous substances. (A) *A. baylyi* post-exposure to 10 mM succinate, 5 mM succinate, 10 mM glucose, and glucose-succinate (10 mM + 5 mM and 10 mM + 10 mM); (B) *P. fluorescence* post-exposure to 10 mM acetate, 5 mM acetate, 10 mM glucose, and glucose-acetate (10 mM + 5 mM and 10 mM + 10 mM); (C) *E. coli* post-exposure to 10 mM acetate, 5 mM acetate, 10 mM glucose, and glucose-acetate (10 mM + 5 mM and 10 mM + 10 mM).

Post-exposure to the glucose-succinate mixture (10 mM + 5 mM and 10 mM + 10 mM), the LDA categorization of *A. baylyi* cells is close to the groups of the same succinate concentration but markedly separated from the group of 10 mM glucose (Figure 5A). The results of dose-response affinity in Figure 4A and 4B show that the binding affinity of *A. baylyi* towards 10 mM glucose is similar towards 10 mM succinate, but higher than towards 5 mM succinate. The 10 mM glucose was subsequently mixed with 5 mM succinate to investigate if the binding affinity of *A. baylyi* towards these two types of molecules in the mixture is consistent with that in the individual exposure. The difference in LDA position between LDA scores of multiple and individual carbonaceous substance treatments illustrates that only a small proportion of glucose molecules are sensed and accumulated on *A. baylyi* cells in the presence of both glucose and succinate (Figure 5A). Despite the decreasing concentration of succinate from 10 mM to 5 mM in the mixture, *A. baylyi* retains high binding affinity and accumulation of succinate. Namely, the molar ratio of succinate to glucose does not affect bacterial selectivity and the majority of *A. baylyi* cells have stronger binding affinity towards succinate. This result is consistent with the DI values of *A. baylyi* post-exposure to individual glucose or succinate. *A. baylyi* cells show noticeable affinity towards 5 mM succinate (Figure 4B), whereas the significant attraction of glucose is only detectable at 10 mM (Figure 4A). It hints a stronger succinate binding affinity than glucose, and succinate is selectively sensed and accumulated in *A. baylyi* in succinate-glucose regardless of the occurrence of glucose. Although the MCPs of *A. baylyi* can recognize and bind glucose molecules, they are reported to have stronger binding affinity towards succinate (Juni, 1978; Wang et al., 2013; Young et al., 2005). The higher succinate binding affinity up-regulates the chemotaxis signal transduction and promotes the activities of CheA autophosphorylation (Garrity and Ordal, 1997). As a result, the movement of *A. baylyi* cells is more positively promoted towards succinate than glucose, leading to the increasing and predominant affinity and accumulation of succinate.

From the LDA plots of *P. fluorescence* post-exposure to acetate or/and glucose (Figure 5B), LDA categorization of the glucose-acetate mixture groups, either 10 mM + 5 mM or 10 mM + 10 mM treatment, are both located with the same distance between the groups of individual acetate and glucose. Meanwhile, higher acetate concentration (10 mM) in the mixture does not significantly increase the selective

affinity and accumulation of *P. fluorescence* towards acetate (Figure 5B). The results demonstrate a neutral competitive affinity and accumulation towards acetate and glucose by *P. fluorescence*. Compared to the results in D_I score plots (Figure 4C and 4D) that the chemotactic behaviors of *P. fluorescence* are similar post-exposure to 5 mM acetate or glucose but significantly stronger for 10 mM acetate than 10 mM glucose, the neutral selectivity suggests different chemoreceptors for acetate and glucose in *P. fluorescence*. Previous studies report that *Pseudomonas* sp. have diverse MCP-like proteins and are strongly chemotactic towards a variety of attractants (Ramos, 2004). The chemoreceptor for acetate in *Pseudomonas* strains is McpS, a cluster II ligand binding region for TCA cycle intermediates and acetate (Lacal et al., 2011; Pineda-Molina et al., 2012; Sampedro et al., 2015). The ligand-binding protein McpS is found to bind with acetate to initiate the chemotaxis pathways, but this protein shows no binding affinity towards glucose in *Pseudomonas* (Sampedro et al., 2015; Sly et al., 1993). This acetate chemotaxis protein is different from that for glucose, but following the same downstream signal transduction pathway in *P. fluorescence* (Sampedro et al., 2015; Weert et al., 2002). Thus, post-exposure to acetate-glucose mixture, different MCPs exhibit limited effects on the chemotaxis signal transduction of other chemo-attractants.

Post-exposure to glucose or acetate, Raman spectral alterations show almost the same binding affinity and accumulation of these two carbonaceous molecules on *E. coli* cells from D_I score plots (Figure 4E and 4F). We therefore speculate a similar LDA categorization of *E. coli* in glucose-acetate mixture comparing to that of *P. fluorescence*. However, Raman spectra LDA score plots illustrate that groups of *E. coli* treated with two acetate-glucose mixtures are remarkably close to those in individual acetate treatments (5 mM and 10 mM, Figure 5C), indicating a strong selection towards acetate rather than glucose. Additionally, the concentration of acetate does not affect the selective affinity, and there is a significant difference in Raman spectral LDA score plot for the two groups between acetate-glucose mixtures with 5 mM and 10 mM acetate. It is obvious that, post-exposure to glucose-acetate mixtures, *E. coli* exhibits a more sensitive response to acetate than glucose. The difference between individual and multiple exposure illustrates the distinct selective behaviors of *E. coli* cells in a complex carbonaceous substance circumstance. Namely, although *E. coli* has moderate chemotaxis-driven affinity and accumulation of glucose,

similar as acetate, the glucose sensing is strongly inhibited by the presence of acetate. In *E. coli* cells, strong binding affinity decreases CheA autophosphorylation and weakens the chemotaxis signal transduction (Borkovich et al., 1989). In contrast, acetate can activate CheY phosphorylation *via* acetylation and promote *E. coli* chemotaxis (Dailey and Berg, 1993). Although acetylation is not essential for chemotaxis, it can offset the negative effects of CheA autophosphorylation in acetate-glucose mixture, and as a result, encourages acetate affinity and accumulation. Thus, increasing Raman spectral biomarkers of acetate on *E. coli* cells are identified post-exposure to acetate-glucose mixture, and our work for the first time successfully observes the significantly selective chemotaxis-driven affinity and accumulation between two carbonaceous substances with similar chemotactic behavior.

Raman spectra can measure bacterial binding affinity to individual carbonaceous substance and can also identify which molecule is sensed and accumulated on bacterial cells in a carbonaceous substance mixture. Our results suggest that Raman microspectroscopy is an effective tool in discriminating biospectral fingerprints and revealing the mechanisms of bacterial selective affinity and accumulation in complex nutrient environments. To our knowledge, and compare with the results of capillary assay, we believe the selective affinity and accumulation of bacteria towards the mixture of carbonaceous substances is related to the chemotactic regulatory mechanism. Comparing the different behaviors of the three bacterial strains towards individual or carbonaceous substance mixtures, we find three different types of chemo-attractants with distinct roles in MCPs recognition and signal transduction. When the signal transduction is not regulated by MCPs recognition and affinity, *P. fluorescence* towards glucose and acetate (neutral-chemo-attractant) as an example, there is no significant difference between individual and multiple carbonaceous substances. In the case of up-regulating chemotaxis signal transduction by MCPs recognition and affinity (succinate as active-chemo-attractant for *A. baylyi*), bacterial cells have strong selectivity and preferentially swim towards and accumulate active-chemo-attractant post-exposure to multiple carbonaceous substances. Conversely, if MCPs recognition and affinity down-regulates the signal transduction, like *E. coli* towards glucose as an inactive-chemo-attractant, bacterial binding affinity will prefer other types of chemo-attractants and less inactive-chemo-attractant is sensed. Bacterial chemotaxis is a complex biological behavior in seeking out and

accessing chemical stimuli, and both chemo-attractant sensing and signal transduction play important roles in chemotactic behavior. As the chemoreceptor protein, MCPs are able to recognize the periplasmic cognate ligands and deliver the adaptive response through methylation and demethylation (Ferrández et al., 2002). The signal is subsequently transmitted to regulate CheA kinase, CheW scaffolding protein and CheY signal transmission protein to control flagellar motor response (Mukherjee et al., 2016; Wadhams and Armitage, 2004). Some mechanisms of chemotaxis signal transduction pathways have been discussed for several bacterial strains (Borkovich et al., 1989; Garrity and Ordal, 1997; Mukherjee et al., 2016; Sampedro et al., 2015). CheA autophosphorylation and CheY phosphorylation regulate flagella rotation, leading to the change in swimming direction or a tumble (Toker and Macnab, 1997; Wadhams and Armitage, 2004; Welch et al., 1993). Our results from Raman spectral alterations and multivariate analysis suggest diverse mechanisms of bacterial chemotactic selectivity, varying across bacterial species and carbonaceous substances. Post-exposure to multiple carbonaceous substances, the chemo-affinity and chemotaxis signal transduction both play remarkable roles in the bacterial chemotactic behavior (Sampedro et al., 2015). Raman microspectroscopy allows one to elucidate the possible mechanisms of cell-molecule interaction *via* distinguishing specific molecular biomarkers, especially in a complex nutrient environment.

Conclusion

In the present study, we applied Raman microspectroscopy to investigate the transient binding affinity and accumulation of organic carbonaceous substances on/inside bacterial cells after extremely short-term exposure (30 min). To the best of our knowledge, this is the first study successfully discriminating the vibrational fingerprints of carbonaceous substances on/inside bacterial cells and revealing the different mechanisms of selective accumulation and utilization *via* Raman spectra coupled with multivariate analysis. After transient exposure to carbonaceous substance, Raman spectral alterations can visualize the molecular biomarkers in biospectra and quantify the selective affinity and accumulation of carbonaceous molecules. Furthermore, the selective behaviors uncovered by Raman microspectroscopy provide deeper insights into the complicated association of MCPs

recognition and chemotaxis signal transduction in different bacterial strains. The selective affinity and accumulation is important for bacterial access to adequate nutrients in their natural habitats, in which multiple carbonaceous substances co-exist. Our work suggests that Raman microspectroscopy is a robust and non-destructive tool, with great potential in diagnosing bacteria-molecule interaction *in situ* at single cell level. Discriminating bacterial selective access to carbonaceous molecules in real world scenario, particularly for those uncultivable microbes, also helps our deeper understanding on microbial functions in natural environment.

Acknowledgements

The authors would like to thank National Natural Science Foundation of China (No. 41301331) and Lancaster University FST research grant for financial support. H.L. is supported by China Scholarship Council (CSC).

Supporting Information

Chemotaxis of *A. baylyi*, *P. fluorescence* and *E. coli* towards glucose, acetate, succinate and salicylate *via* capillary assay (Figure S1); Dispersion indicator (D_I) of bacterial Raman spectra postexposure to glucose, acetate, succinate and salicylate (Figure S2); Bacterial Raman spectra post-exposure to different concentrations of organic carbonaceous substances (Figure S3).

References

Adler, J. 1966. Chemotaxis in Bacteria. *Science,* 153**,** 708-716.

Adler, J. 1973. A method for measuring chemotaxis and use of the method to determine optimum conditions for chemotaxis by Escherichia coli. *Microbiology,* 74**,** 77-91.

Aizawa, S.-I., Harwood, C. S. & Kadner, R. J. 2000. Signaling components in bacterial locomotion and sensory reception. *Journal of bacteriology,* 182**,** 1459-1471.

Alexander, R. P. & Zhulin, I. B. 2007. Evolutionary genomics reveals conserved structural determinants of signaling and adaptation in microbial chemoreceptors. *Proceedings of the National Academy of Sciences,* 104**,** 2885-2890.

Ami, D., Mereghetti, P. & Doglia, S. M. 2013. Multivariate analysis for Fourier Transform Infrared Spectra of complex biological systems and processes. *Multivariate Analysis in Management, Engineering and the Sciences.* InTech.

Araujo-Andrade, C., Ruiz, F., Mart ́nez-Mendoza, J. R. & Terrones, H. 2005. Infrared and Raman spectra, conformational stability, ab initio calculations of structure, and vibrational assignment of α and β glucose. *Journal of Molecular Structure: THEOCHEM,* 714**,** 143-146.

Barbe, V., Vallenet, D., Fonknechten, N., Kreimeyer, A., Oztas, S., Labarre, L., Cruveiller, S., Robert, C., Duprat, S. & Wincker, P. 2004a. Unique features revealed by the genome sequence of Acinetobacter sp. ADP1, a versatile and naturally transformation competent bacterium. *Nucleic Acids Research,* 32**,** 5766-5779.

Barbe, V., Vallenet, D., Fonknechten, N., Kreimeyer, A., Oztas, S., Labarre, L., Cruveiller, S., Robert, C., Duprat, S., Wincker, P., Ornston, L. N., Weissenbach, J., Marliere, P., Cohen, G. N. & Medigue, C. 2004b. Unique features revealed by the genome sequence of Acinetobacter sp. ADP1, a versatile and naturally transformation competent bacterium. *Nucleic Acids Res,* 32**,** 5766-79.

Baumann, P., Doudoroff, M. & Stanier, R. 1968. A study of the Moraxella group II. Oxidative-negative species (genus Acinetobacter). *Journal of bacteriology,* 95**,** 1520-1541.

Berg, H. C. & Turner, L. 1990. Chemotaxis of bacteria in glass capillary arrays. Escherichia coli, motility, microchannel plate, and light scattering. *Biophysical Journal,* 58**,** 919-930.

Bickley, R., Edwards, H., Rose, S. & Gustar, R. 1990. A Raman spectroscopic study of nickel (II) acetate, Ni (CH3COO) 2 and its aqueous and methanolic solutions. *Journal of Molecular Structure,* 238**,** 15-26.

Block, S. M., Segall, J. E. & Berg, H. C. 1983. Adaptation kinetics in bacterial chemotaxis. *Journal of bacteriology,* 154**,** 312-323.

Borkovich, K. A., Kaplan, N., Hess, J. F. & Simon, M. I. 1989. Transmembrane signal transduction in bacterial chemotaxis involves ligand-dependent activation of phosphate group transfer. *Proceedings of the National Academy of Sciences,*

86**,** 1208-1212.

Butler, H. J., Mcainsh, M. R., Adams, S. & Martin, F. L. 2015. Application of vibrational spectroscopy techniques to non-destructively monitor plant health and development. *Analytical Methods,* 7**,** 4059-4070.

Cohen, S. P., Levy, S. B., Foulds, J. & Rosner, J. L. 1993. Salicylate induction of antibiotic resistance in Escherichia coli: activation of the mar operon and a mar-independent pathway. *Journal of bacteriology,* 175**,** 7856-7862.

Cui, L., Butler, H. J., Martin-Hirsch, P. L. & Martin, F. L. 2016. Aluminium foil as a potential substrate for ATR-FTIR, transflection FTIR or Raman spectrochemical analysis of biological specimens. *Analytical Methods,* 8**,** 481-487.

Cui, L., Chen, P., Chen, S., Yuan, Z., Yu, C., Ren, B. & Zhang, K. 2013. In situ study of the antibacterial activity and mechanism of action of silver nanoparticles by surface-enhanced Raman spectroscopy. *Anal Chem,* 85**,** 5436-43.

Dailey, F. E. & Berg, H. C. 1993. Change in direction of flagellar rotation in Escherichia coli mediated by acetate kinase. *Journal of bacteriology,* 175**,** 3236-3239.

De Gelder, J., De Gussem, K., Vandenabeele, P. & Moens, L. 2007. Reference database of Raman spectra of biological molecules. *Journal of Raman Spectroscopy,* 38**,** 1133-1147.

Dhanya, V. S., Sudarsanakumar, M. R., Suma, S., Prasanna, S., Rajendra Babu, K., Suresh Kumar, B. & Roy, S. M. 2011. Growth and characterization of a new polymorph of lead succinate: A promising NLO material. *Journal of Crystal Growth,* 319**,** 96-101.

Efrima, S. & Bronk, B. 1998. Silver colloids impregnating or coating bacteria. *The Journal of Physical Chemistry B,* 102**,** 5947-5950.

Efrima, S. & Zeiri, L. 2009. Understanding SERS of bacteria. *Journal of Raman Spectroscopy,* 40**,** 277-288.

Ferrández, A., Hawkins, A. C., Summerfield, D. T. & Harwood, C. S. 2002. Cluster II che genes from Pseudomonas aeruginosa are required for an optimal chemotactic response. *Journal of bacteriology,* 184**,** 4374-4383.

Foster, J. 1962. Bacterial oxidation of hydrocarbons. *Oxygenases. Academic, New York***,** 241-261.

Frost, R. & Kloprogge, J. 2000. Raman spectroscopy of the acetates of sodium, potassium and magnesium at liquid nitrogen temperature. *Journal of Molecular Structure,* 526**,** 131-141.

Garrity, L. F. & Ordal, G. W. 1997. Activation of the CheA kinase by asparagine in Bacillus subtilis chemotaxis. *Microbiology,* 143**,** 2945-2951.

Guzelian, A. A., Sylvia, J. M., Janni, J. A., Clauson, S. L. & Spencer, K. M. SERS of whole-cell bacteria and trace levels of biological molecules. Environmental and Industrial Sensing, 2002. International Society for Optics and Photonics, 182-192.

Hazelbauer, G. L., Mesibov, R. E. & Adler, J. 1969. Escherichia coli mutants defective in chemotaxis toward specific chemicals. *Proceedings of the*

National Academy of Sciences, 64**,** 1300-1307.

Henrichsen, J. 1972. Bacterial surface translocation: a survey and a classification. *Bacteriological reviews,* 36**,** 478.

Jia, J., Li, H., Zong, S., Jiang, B., Li, G., Ejenavi, O., Zhu, J. & Zhang, D. 2016. Magnet bioreporter device for ecological toxicity assessment on heavy metal contamination of coal cinder sites. *Sensors and Actuators B: Chemical,* 222**,** 290-299.

Jin, N., Paraskevaidi, M., Semple, K. T., Martin, F. L. & Zhang, D. Y. 2017a. Infrared Spectroscopy Coupled with a Dispersion Model for Quantifying the Real-Time Dynamics of Kanamycin Resistance in Artificial Microbiota. *Analytical Chemistry,* 89**,** 9814-9821.

Jin, N., Semple, K. T., Jiang, L., Luo, C., Martin, F. L. & Zhang, D. 2018. Spectrochemical determination of unique bacterial responses following long-term low-level exposure to antimicrobials. *Analytical Methods***,** DOI: 10.1039/C8AY00011E.

Jin, N., Zhang, D. & Martin, F. L. 2017b. Fingerprinting microbiomes towards screening for microbial antibiotic resistance. *Integrative Biology*.

Juni, E. 1978. Genetics and physiology of Acinetobacter. *Annual Reviews in Microbiology,* 32**,** 349-371.

Kearns, D. B. 2010. A field guide to bacterial swarming motility. *Nat Rev Microbiol,* 8**,** 634-44.

Kelly, J. G., Trevisan, J., Scott, A. D., Carmichael, P. L., Pollock, H. M., Martin-Hirsch, P. L. & Martin, F. L. 2011. Biospectroscopy to metabolically profile biomolecular structure: a multistage approach linking computational analysis with biomarkers. *Journal of proteome research,* 10**,** 1437-1448.

Kirby, J. R. 2009. Chemotaxis-like regulatory systems: unique roles in diverse bacteria. *Annu Rev Microbiol,* 63**,** 45-59.

Lacal, J., Muñoz-Martínez, F., Reyes-Darías, J. A., Duque, E., Matilla, M., Segura, A., Calvo, J.-J. O., Jímenez-Sánchez, C., Krell, T. & Ramos, J. L. 2011. Bacterial chemotaxis towards aromatic hydrocarbons in Pseudomonas. *Environmental microbiology,* 13**,** 1733-1744.

Li, H., Martin, F. L. & Zhang, D. 2017. Quantification of Chemotaxis-Related Alkane Accumulation in Acinetobacter baylyi Using Raman Microspectroscopy. *Anal Chem,* 89**,** 3909-3918.

Maddock, J. R. & Shapiro, L. 1993. Polar location of the chemoreceptor complex in the Escherichia coli cell. *Science,* 259**,** 1717-1717.

Maquelin, K., Choo-Smith, L.-P. I., Van Vreeswijk, T., Endtz, H. P., Smith, B., Bennett, R., Bruining, H. A. & Puppels, G. J. 2000. Raman spectroscopic method for identification of clinically relevant microorganisms growing on solid culture medium. *Analytical Chemistry,* 72**,** 12-19.

Martin, F. L., German, M. J., Wit, E., Fearn, T., Ragavan, N. & Pollock, H. M. 2007. Identifying variables responsible for clustering in discriminant analysis of data from infrared microspectroscopy of a biological sample. *Journal of Computational biology,* 14**,** 1176-1184.

Mukherjee, T., Kumar, D., Burriss, N., Xie, Z. & Alexandre, G. 2016. Azospirillum brasilense chemotaxis depends on two signaling pathways regulating distinct motility parameters. *Journal of bacteriology,* 198**,** 1764-1772.

Oku, S., Komatsu, A., Nakashimada, Y., Tajima, T. & Kato, J. 2014. Identification of Pseudomonas fluorescens chemotaxis sensory proteins for malate, succinate, and fumarate, and their involvement in root colonization. *Microbes Environ,* 29**,** 413-9.

Paliy, O., Bloor, D., Brockwell, D., Gilbert, P. & Barber, J. 2003. Improved methods of cultivation and production of deuteriated proteins from E. coli strains grown on fully deuteriated minimal medium. *Journal of applied microbiology,* 94**,** 580-586.

Paliy, O. & Gunasekera, T. S. 2007. Growth of E. coli BL21 in minimal media with different gluconeogenic carbon sources and salt contents. *Appl Microbiol Biotechnol,* 73**,** 1169-72.

Parke, D., Garcia, M. & Ornston, L. 2001. Cloning and genetic characterization of dca genes required for β-oxidation of straight-chain dicarboxylic acids in Acinetobacter sp. strain ADP1. *Applied and environmental microbiology,* 67**,** 4817-4827.

Pineda-Molina, E., Reyes-Darias, J.-A., Lacal, J., Ramos, J. L., Garc á-Ruiz, J. M., Gavira, J. A. & Krell, T. 2012. Evidence for chemoreceptors with bimodular ligand-binding regions harboring two signal-binding sites. *Proceedings of the National Academy of Sciences,* 109**,** 18926-18931.

Ramos, J. 2004. Pseudomonas, vol 1. Genomics, life style and molecular architecture. Kluwer Academic Publishers, New York, NY.

Sampedro, I., Parales, R. E., Krell, T. & Hill, J. E. 2015. Pseudomonas chemotaxis. *FEMS Microbiol Rev,* 39**,** 17-46.

Sawai, T., Hirano, S. & Yamaguchi, A. 1987. Repression of porin synthesis by salicylate in Escherichia coli, Klebsiella pneumoniae and Serratia marcescens. *FEMS microbiology letters,* 40**,** 233-237.

Schuster, K. C., Urlaub, E. & Gapes, J. 2000. Single-cell analysis of bacteria by Raman microscopy: spectral information on the chemical composition of cells and on the heterogeneity in a culture. *Journal of Microbiological Methods,* 42**,** 29-38.

Shi, L. Z., Nascimento, J., Chandsawangbhuwana, C., Berns, M. W. & Botvinick, E. L. 2006. Real-time automated tracking and trapping system for sperm. *Microsc Res Tech,* 69**,** 894-902.

Singh, T. & Arora, D. K. 2001. Motility and chemotactic response of Pseudomonas fluorescens toward chemoattractants present in the exudate of Macrophomina phaseolina. *Microbiol Res,* 156**,** 343-51.

Sly, L. M., Worobec, E. A., Perkins, R. E. & Phibbs Jr, P. V. 1993. Reconstitution of glucose uptake and chemotaxis in Pseudomonas aeruginosa glucose transport defective mutants. *Canadian journal of microbiology,* 39**,** 1079-1083.

Sourjik, V. 2004. Receptor clustering and signal processing in E. coli chemotaxis. *Trends Microbiol,* 12**,** 569-76.

Sourjik, V. & Berg, H. C. 2000. Localization of components of the chemotaxis machinery of Escherichia coli using fluorescent protein fusions. *Molecular microbiology,* 37**,** 740-751.

Sourjik, V. & Wingreen, N. S. 2012. Responding to chemical gradients: bacterial chemotaxis. *Current Opinion in Cell Biology,* 24**,** 262-268.

Tao, Y., Wang, Y., Huang, S., Zhu, P., Huang, W. E., Ling, J. & Xu, J. 2017. Metabolic-Activity-Based Assessment of Antimicrobial Effects by D2O-Labeled Single-Cell Raman Microspectroscopy. *Anal Chem,* 89**,** 4108-4115.

Toker, A. S. & Macnab, R. M. 1997. Distinct regions of bacterial flagellar switch protein FliM interact with FliG, FliN and CheY. *Journal of molecular biology,* 273**,** 623-634.

Trevisan, J., Angelov, P. P., Scott, A. D., Carmichael, P. L. & Martin, F. L. 2013. IRootLab: a free and open-source MATLAB toolbox for vibrational biospectroscopy data analysis. *Bioinformatics***,** btt084.

Vaneechoutte, M., Young, D. M., Ornston, L. N., De Baere, T., Nemec, A., Van Der Reijden, T., Carr, E., Tjernberg, I. & Dijkshoorn, L. 2006. Naturally transformable Acinetobacter sp. strain ADP1 belongs to the newly described species Acinetobacter baylyi. *Applied and environmental microbiology,* 72**,** 932-936.

Vasko, P., Blackwell, J. & Koenig, J. 1972. Infrared and raman spectroscopy of carbohydrates.: Part II: Normal coordinate analysis of α-D-glucose. *Carbohydrate Research,* 23**,** 407-416.

Wadhams, G. H. & Armitage, J. P. 2004. Making sense of it all: bacterial chemotaxis. *Nature Reviews Molecular Cell Biology,* 5**,** 1024-1037.

Wang, W. & Shao, Z. 2014. The long-chain alkane metabolism network of Alcanivorax dieselolei. *Nat Commun,* 5**,** 5755.

Wang, X. B., Nie, Y., Tang, Y. Q., Wu, G. & Wu, X. L. 2013. n-Alkane chain length alters Dietzia sp. strain DQ12-45-1b biosurfactant production and cell surface activity. *Appl Environ Microbiol,* 79**,** 400-2.

Wang, Y., Ravindranath, S. & Irudayaraj, J. 2011. Separation and detection of multiple pathogens in a food matrix by magnetic SERS nanoprobes. *Analytical and bioanalytical chemistry,* 399**,** 1271-1278.

Weert, S. D., Vermeiren, H., Mulders, I. H. M., Kuiper, I., Hendrickx, N., Bloemberg, G. V., Vanderleyden, J., Mot, R. D. & Lugtenberg, B. J. J. 2002. Flagella-Driven Chemotaxis Towards Exudate Components Is an Important Trait for Tomato Root Colonization by Pseudomonas fluorescens. *Molecular Plant-Microbe Interactions,* 15**,** 1173-1180.

Welch, M., Oosawa, K., Aizawa, S.-L. & Eisenbach, M. 1993. Phosphorylation-dependent binding of a signal molecule to the flagellar switch of bacteria. *Proceedings of the National Academy of Sciences,* 90**,** 8787-8791.

Young, D. M., Parke, D. & Ornston, L. N. 2005. Opportunities for genetic investigation afforded by Acinetobacter baylyi, a nutritionally versatile bacterial species that is highly competent for natural transformation. *Annu. Rev.*

Microbiol., 59**,** 519-551.

Zhou, H., Yang, D., Ivleva, N. P., Mircescu, N. E., Schubert, S. R., Niessner, R., Wieser, A. & Haisch, C. 2015. Label-free in situ discrimination of live and dead bacteria by surface-enhanced Raman scattering. *Analytical chemistry,* 87**,** 6553-6561.

Electronic Supporting Information

Interrogating the selectivity of bacterial chemotaxis-driven affinity and accumulation of carbonaceous substances via Raman microspectroscopy

Hanbing Li[a], Francis L. Martin[b], Dayi Zhang [c,a,*]

[a] Lancaster Environment Centre, Lancaster University, Lancaster, LA1 4YQ, UK

[b] School of Pharmacy and Biomedical Sciences, University of Central Lancashire, Preston PR1 2HE, UK

[c] School of Environment, Tsinghua University, Beijing, 100086, PR China

***Corresponding author**

Dr Dayi Zhang

School of Environment, Tsinghua University, Beijing, 100086, PR China

Lancaster Environment Centre, Lancaster University, Lancaster, LA1 4YQ, UK

Tel.: +44(0)1524510288; Fax: +44(0)1524510082; Email: d.zhang@lancaster.ac.uk

No. of Pages = 4

No. of Figures = 3

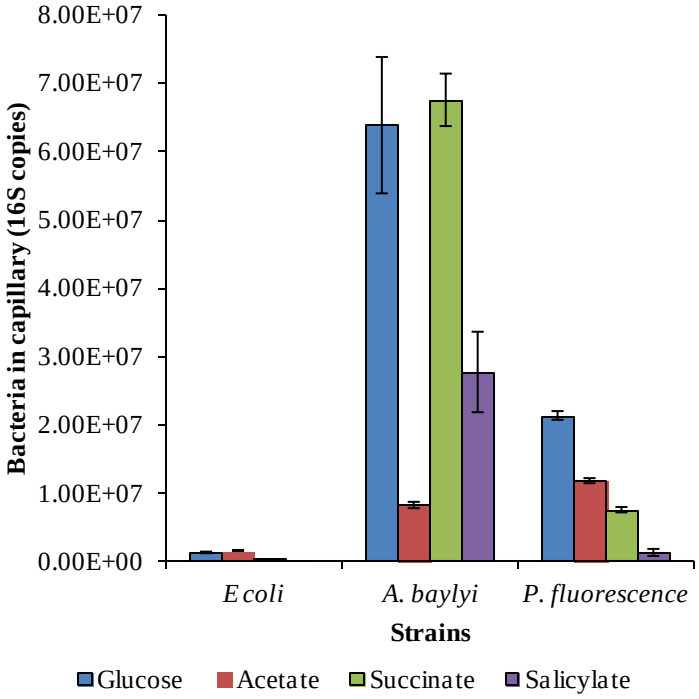

Figure S1. Chemotaxis of *A. baylyi*, *P. fluorescence* and *E. coli* towards glucose, acetate, succinate and salicylate *via* the capillary assay.

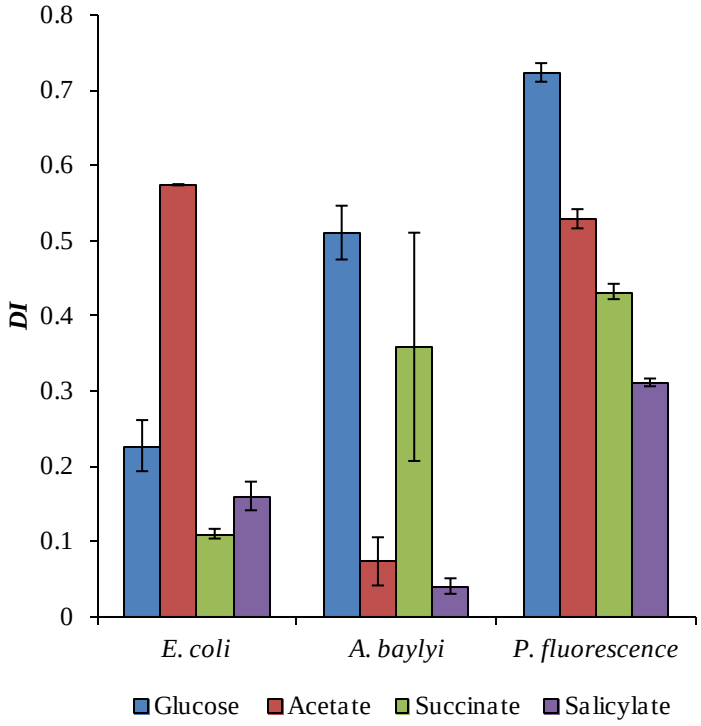

Figure S2. Dispersion indicator (D_I) of bacterial Raman spectra post-exposure to glucose, acetate, succinate and salicylate.

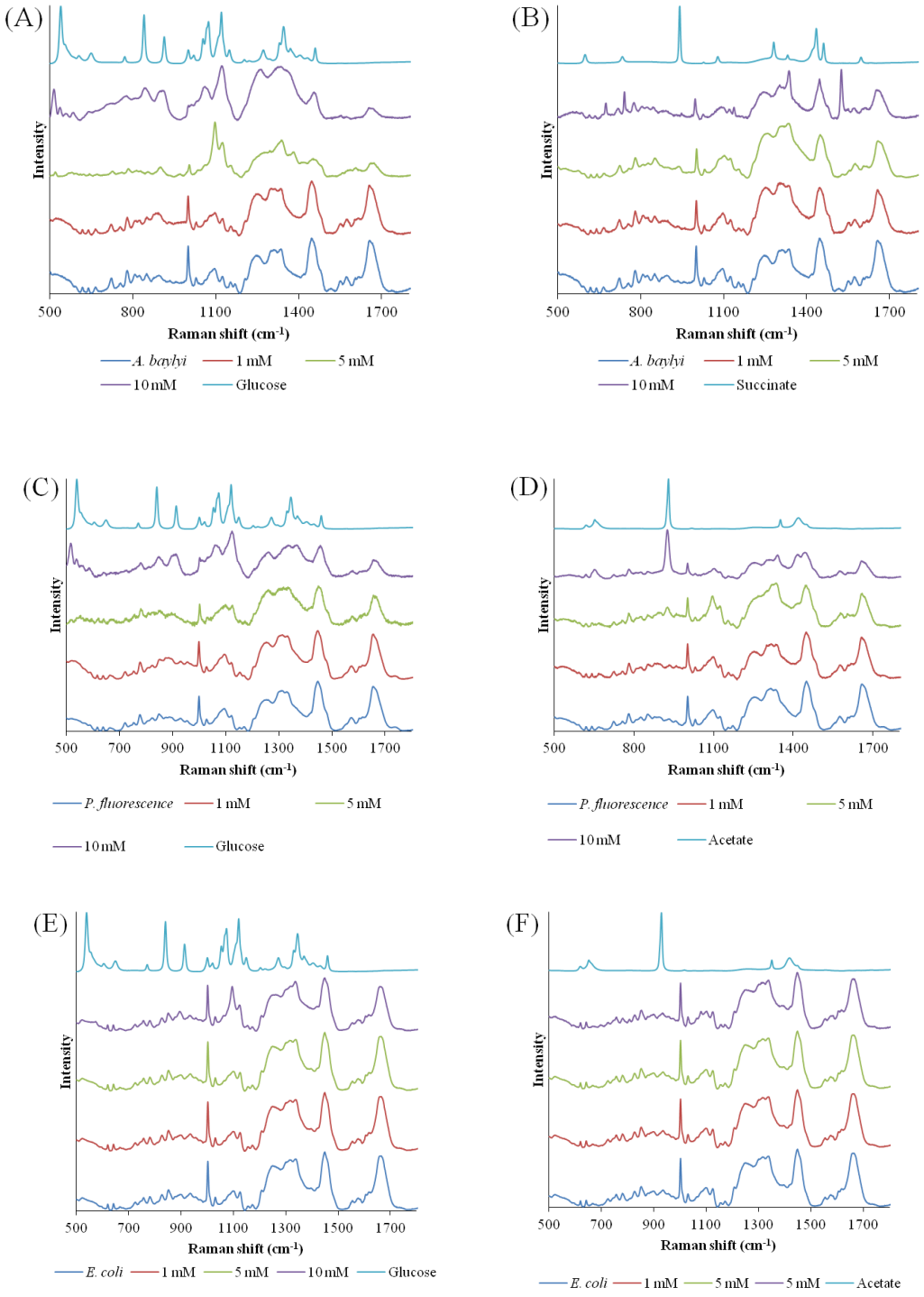

Figure S3. Bacterial Raman spectra post-exposure to different concentrations of organic carbonaceous substances. (A) and (B): *A. baylyi* post-exposure to glucose and succinate; (C) and (D): *P. fluorescence* post-exposure to glucose and acetate; (E) and (F): *E. coli* post-exposure to glucose and acetate. Twenty Raman spectra were randomly obtained per treatment.

Chapter 5 General Conclusion

1. Raman characterization of cell-molecule interaction

Owing to the heterogeneous nature of biological components in bacteria, the Raman spectral data derived from bacterial samples are complex and diverse (Cui et al., 2013; Wang et al., 2016; Zhou et al., 2014). This is suggested that tiny differences in these data may contain critical information, which means the difficulties in the information interpretation from the acquired spectral data. To solve these intricacies and have a deep insight into spectral data, a new and automated method was applied in this thesis for the analysis of Raman spectra (Cui et al., 2016; Trevisan et al., 2013). Data pre-processing is important step in workflow of spectral analysis. This step is independent and indispensable part involving specific processing for raw spectral data. A proper pre-processing is the basis for a better performance of Raman characterization and for further classification models. In Raman spectra, the fluorescence background is intense so that may affect Raman scattering (Mosier-Boss et al., 1995). Therefore, software based methods have been developed to provide polynomial baseline fitting for fluorescence background correction (Trevisan et al., 2013). The usual order for polynomial baseline fitting needs to be tuned up in a range of 4 to 6 for satisfied complexity reduction and over-fitting avoidance (Zhao et al., 2007). Normalization is essential and effective for comparing classification analysis of Raman spectra from heterogeneous sets of samples. Normalization can be introduced after baseline fitting to minimize the impacts of varying pathlength on Raman spectra. Therefore, Polynomial baseline fitting and normalization is applied in this thesis to characterize the interaction of bacterial cell with different molecules.

The silver coated magnetic nanoparticles (Ag@MNPs) can increase the Raman intensity of bacteria they interact with. Different from conventional SERS detection

(Feng et al., 2000; Liu et al., 2017; Mura et al., 2015), the magnetic property of this nanomaterial enables the rapid screening of bacteria in aquatic phase. Magnetic nanoparticle has high bacteria capturing efficiency for its affinity to biological molecules (Huang et al., 2010). The silver coating does not affect the magnetism of Ag@MNPs. Therefore, with Raman microspectroscopy, the specific binding of nanoparticles with bio-molecules in bacteria can be described. Due to the perfect core-shell structure, this nanomaterial exhibit minimal influences on iron on SERS spectra. The differences in the spectra of normal Raman and SERS characterize the favourable bindings of nanoparticle to cellular molecules, suggesting the possible interaction of bacteria with nanomaterials (Li et al., 2017a). The main SERS peaks explain that nanoparticles are likely to unite with adenine, guanine and aromatic amino acids in bacteria.

Raman spectral characterization can determine the chemotaxis-related affinity of bacteria towards specific carbonaceous substances including hydrocarbons, carbohydrates and organic acids. Different from conventional chemotaxis assays (Berg and Turner, 1990; Block et al., 1983; Henrichsen, 1972), Raman spectra provide the detailed information of molecules that interact with bacterial cells. Post-exposed to alkane molecules, the Raman spectra of alkane chemotactic bacteria generate significant alterations, whereas the spectra of negative chemotactic bacteria remain unchanged. Positive chemotaxis bacteria detect and accumulate alkane molecules, thereby exhibiting specific alkane alterations on the Raman spectra of bacteria. In addition to alkanes, carbohydrates and organic acids accumulated by bacteria are detectable through Raman spectroscopy due to their chemotactic attractions to them. Raman characterizations of cell-molecule interaction not only

show the specific affinity, but also prove the directed movement during the accumulation process.

2. Quantified interaction of bacteria with different molecules

Multivariate data analysis methods have been employed to extract the feature of Raman spectra. The feature extraction is the procedure to produce a small number of variables that keep the key information for the original wavenumber variables. The information extracted from the spectral data is necessary to quantify the interaction of bacteria with nanoparticles and carbonaceous substances. Principle component analysis (PCA) is an unsupervised data analysis method for dimensional reduction and data visualization (Kelly et al., 2011). PCA is a statistical technique that based on evaluating the total variances within a dataset via Eigen analysis. However, due to the fact that it is an unsupervised method, PCA is not capable of identifying within- and among-group variance (Wang and Mizaikoff, 2008). Therefore, the supervised technique linear discriminant analysis (LDA) is used to form linear combinations of variables dependent on differences between the classes in the data set (Kelly et al., 2011). In LDA method, each observation has fewer variables. Meantime, observations in the same class will form clusters and each cluster is clearly differentiated from the other. LDA is necessary for the data categorization. The combination model of PCA and LDA (PCA-LDA) improves the efficiency of classification of crucial features. This model is employed to attain inter-class separation and minimize intra-class differences. Dispersion indicator (D_I) is a method that based on LDA scores to visualize the dispersion of individual group to negative control and pure molecules group (Li et al., 2017b). This method provides key information for the quantification of bacteria-cell interactions.

Raman spectral alterations allow the evaluation of the sensitivity of alkane affinity in bacterial cells and quantification of alkane concentrations in the aquatic phase. D_I scores indicate the limit of detection through Raman microspectroscopy is 5 mg/L for dodecane and 1 mg/L for tetradecane. Similar observation was found for alkane mixtures. Above the limit of detection, all the alkanes or alkane mixtures increase as a semilog linear regression relationship with D_I. The alkane affinity and accumulation of bacteria is consistent with the values of semilog linear slopes, in which high slope value means strong selective affinity. Post-exposed to glucose and organic acids, the strong Raman alterations enable the quantification of the concentration of those organic carbonaceous chemicals. The intensity of characteristic peaks arose from molecules in the spectra of bacteria results in D_I scores increased with concentration of carbonaceous substances. Furthermore, the chemotactic affinity of bacteria towards hydrophilic organic carbon molecules is measured by D_I method.

3. Insights into the selective affinity of bacteria

In the complex environment, it is essential for bacteria to respond to the mixture of different nutrient molecules around them (Roszak and Colwell, 1987). Therefore, the investigation of bacterial selections towards the mixture nutrients is required. Conventional methods evaluate the movement and accumulation of bacterial cells (Berg and Turner, 1990; Block et al., 1983), but cannot provide the detailed information of molecules selected by bacterial cells. The statistical analysis of Raman spectra demonstrates that the bacterial selection towards alkane molecules in alkane mixture is dependent on the carbon chain length. Additionally, different extra nutrient cations such as sodium, potassium, magnesium and calcium affect the bacterial to select different alkane molecules in alkane mixture. The differentiated bacterial

selection influenced by various cations may lead to the changes in alkane degradation in hydrocarbon contaminated sites.

The selective affinity of bacteria in the mixture of hydrophilic organic substances is uncovered by analysing Raman spectra. Three different chemotactic responses from three different bacterial species are studied through Raman microspectroscopy. The chemotaxis signal transduction can be enhanced by stronger binding affinity, whereas the signal transduction is decreased in some bacterial strains by higher molecule affinity. Several bacteria develop different proteins for binding molecules, therefore no specific impacts of selective affinity on signal transduction. This is suggested that Raman microspectroscopy can successfully investigate and distinguish different scenarios of bacterial competitive selective affinity towards the mixture of organic carbonaceous substances.

4. Current limitations and future prospects

Raman spectroscopy is a promising tool to reveal the interaction of bacterial cells with molecules. The fast and non-destructive properties allow *in situ* detection of molecular variations on bacteria cells, and identification of changes in biochemical substances in bacteria. By interrogating Raman spectroscopy, toxic effects of nanomaterials on bacterial cells are evident, which is significant for the protection of ecological system (Tripathi et al., 2016). The enhancement of Au or Ag NPs on Raman signals of bacteria provides the possibilities of fast detection and identification of pathogenic bacteria in food and drinking water (Liu et al., 2017). To uncover the nutrients acquirements by bacteria, Raman spectroscopy has been applied for the study of bacterial behaviours including chemotaxis, accumulation and utilization towards molecules (Premasiri et al., 2016; Samek et al., 2016; Li et al., 2017b). In addition, the cell-cell communication for the formation of biofilm and quorum sensing,

and the bacterial response to the environmental stress is visualized via Raman spectra (David et al., 2016; Tao et al., 2017). There are still several challenges regarding Raman spectroscopy studies in cell-molecule interactions.

First of all, it is necessary to identify biomarker assignments of bacteria. In Raman spectra, biomarkers are critical label of biochemical components in bacterial cells, and changes in biomarker indicates significant bacterial activities interact with different molecules. Presently, limited studies have provided detailed information of biomarkers because of the complicated chemical components in bacterial cells. Strong or weak variations in Raman spectra are often compared with standard pure chemical molecules to predict possible chemical bonds representing relative biomarkers. However, pure chemicals cannot show the changes in biomarkers after interacted with molecules. Therefore, identifications of biomarker are of great importance for the study of cell-molecule interaction. The establishment of biomarker database is required to clarify the altered biochemical components in bacteria and can be recognized as an authoritative reference to improve the application of Raman spectroscopy in environment monitoring.

Secondly, due to instrumental variations, Raman spectra collected from different Raman facilities are not exactly identical, which might lead to the misreading of Raman shift. Different machine models, different calibration systems and different normalization of Raman peaks can either result in the differentiations in Raman shifts. The great number of various isolation and identification strategies highlighted that it is possible to find a solution for variations in Raman measurements. With miniaturization and automation of Raman based detection system, considerable collections of Raman spectra in a short time is achieved. To improve the accuracy of Raman measurement, the implementation of a standard detection procedure would be

a useful tool. Furthrermore, the construction of standard reference of Raman shift for spectral calibration and verification is helpful to make Raman spectroscopy a reliable technique.

Finally, the combination of Raman spectroscopy with other techniques including SIP, FISH and gene expression assay, is possible to further improve the application of Raman spectra in the study of cell-molecule interactions (Pahlow et al., 2015; Wang et al., 2016). With SIP-FISH, single bacterial cell can be sorted out in complex bacteria communities, and special carbon metabolic pathways are possible to be uncovered during Raman detection. Raman spectroscopy coupled with gene expression assay provides the genetic alterations which may attribute to the biochemical changes in bacterial components. In combination with chemometrics, it enables the identification of bacteria at strain level to obtain valuable cell information in Raman spectrum. Instrumental and methodological developments are important breakthroughs for the use of Raman spectroscopy in the investigation of bacteria-molecules interaction.

From this review, it is obvious that significant progress have been made for the application of Raman spectroscopy in bacterial interactions with nanomaterials, nutrient molecules, cell signal molecules and environment stress. Among these molecules, the number of studies in chemotactic utilization of bacteria towards different organic compounds is relatively low. Owing to the rapid development of Raman spectroscopy, it is not difficult to study the dynamic of bacterial movement in complex surrounding environment with various available nutrient molecules. Furthermore, Raman spectroscopy is supposed to cooperate with genetic approaches to reveal the basic reason for changes in Raman alterations.

References

Berg, H. C. & Turner, L. 1990. Chemotaxis of bacteria in glass capillary arrays. Escherichia coli, motility, microchannel plate, and light scattering. *Biophysical Journal,* 58**,** 919-930.

Block, S. M., Segall, J. E. & Berg, H. C. 1983. Adaptation kinetics in bacterial chemotaxis. *Journal of bacteriology,* 154**,** 312-323.

Cui, L., Chen, P., Chen, S., Yuan, Z., Yu, C., Ren, B. & Zhang, K. 2013. In situ study of the antibacterial activity and mechanism of action of silver nanoparticles by surface-enhanced Raman spectroscopy. *Analytical chemistry,* 85**,** 5436-5443.

Cui, L., Zhang, Y. J., Huang, W. E., Zhang, B. F., Martin, F. L., Li, J. Y., Zhang, K. S. & Zhu, Y. G. 2016. Surface-Enhanced Raman Spectroscopy for Identification of Heavy Metal Arsenic(V)-Mediated Enhancing Effect on Antibiotic Resistance. *Anal Chem,* 88**,** 3164-70.

David, M., Krishna, P. M. & Sangeetha, J. 2016. Elucidation of impact of heavy metal pollution on soil bacterial growth and extracellular polymeric substances flexibility. *3 Biotech,* 6**,** 172.

Feng, Q. L., Wu, J., Chen, G., Cui, F., Kim, T. & Kim, J. 2000. A mechanistic study of the antibacterial effect of silver ions on Escherichia coli and Staphylococcus aureus. *Journal of biomedical materials research,* 52**,** 662-668.

Henrichsen, J. 1972. Bacterial surface translocation: a survey and a classification. *Bacteriological reviews,* 36**,** 478.

Huang, Y.-F., Wang, Y.-F. & Yan, X.-P. 2010. Amine-functionalized magnetic nanoparticles for rapid capture and removal of bacterial pathogens. *Environmental science & technology,* 44**,** 7908-7913.

Kelly, J. G., Trevisan, J., Scott, A. D., Carmichael, P. L., Pollock, H. M., Martin-Hirsch, P. L. & Martin, F. L. 2011. Biospectroscopy to metabolically profile biomolecular structure: a multistage approach linking computational analysis with biomarkers. *Journal of proteome research,* 10**,** 1437-1448.

Li, H., Li, C., Martin, F. L. & Zhang, D. 2017a. Diagnose Pathogens in Drinking Water via Magnetic Surface-Enhanced Raman Scattering (SERS) Assay. *Materials Today: Proceedings,* 4**,** 25-31.

Li, H., Martin, F. L. & Zhang, D. 2017b. Quantification of chemotaxis-related alkane accumulation in Acinetobacter baylyi using Raman microspectroscopy. *Analytical Chemistry,* 89**,** 3909-3918.

Liu, Y., Zhou, H., Hu, Z., Yu, G., Yang, D. & Zhao, J. 2017. Label and label-free based surface-enhanced Raman scattering for pathogen bacteria detection: A review. *Biosensors and Bioelectronics*.

Mosier-Boss, P., Lieberman, S. & Newbery, R. 1995. Fluorescence rejection in Raman spectroscopy by shifted-spectra, edge detection, and FFT filtering techniques. *Applied Spectroscopy,* 49**,** 630-638.

Mura, S., Greppi, G. & Irudayaraj, J. 2015. Latest developments of nanotoxicology in plants. *Nanotechnology and Plant Sciences.* Springer.

Pahlow, S., Meisel, S., Cialla-May, D., Weber, K., Rosch, P. & Popp, J. 2015.

Isolation and identification of bacteria by means of Raman spectroscopy. *Adv Drug Deliv Rev,* 89**,** 105-20.

Premasiri, W. R., Lee, J. C., Sauer-Budge, A., Théberge, R., Costello, C. E. & Ziegler, L. D. 2016. The biochemical origins of the surface-enhanced Raman spectra of bacteria: a metabolomics profiling by SERS. *Analytical and bioanalytical chemistry,* 408**,** 4631-4647.

Roszak, D. & Colwell, R. 1987. Survival strategies of bacteria in the natural environment. *Microbiological reviews,* 51**,** 365.

Samek, O., Obruča, S., Šiler, M., Sedláček, P., Benešová, P., Kučera, D., Márova, I., Ježek, J., Bernatová, S. & Zemánek, P. 2016. Quantitative raman spectroscopy analysis of polyhydroxyalkanoates produced by Cupriavidus necator H16. *Sensors,* 16**,** 1808.

Tao, Y., Wang, Y., Huang, S., Zhu, P., Huang, W. E., Ling, J. & Xu, J. 2017. Metabolic-activity-based assessment of antimicrobial effects by D2O-labeled single-cell raman microspectroscopy. *Analytical Chemistry,* 89**,** 4108-4115.

Trevisan, J., Angelov, P. P., Scott, A. D., Carmichael, P. L. & Martin, F. L. 2013. IRootLab: a free and open-source MATLAB toolbox for vibrational biospectroscopy data analysis. *Bioinformatics***,** btt084.

Tripathi, D. K., Singh, S., Singh, S., Dubey, N. K. & Chauhan, D. K. 2016. Impact of nanoparticles on photosynthesis: challenges and opportunities. *Materials Focus,* 5**,** 405-411.

Wang, L. & Mizaikoff, B. 2008. Application of multivariate data-analysis techniques to biomedical diagnostics based on mid-infrared spectroscopy. *Analytical and bioanalytical chemistry,* 391**,** 1641-1654.

Wang, Y., Huang, W. E., Cui, L. & Wagner, M. 2016. Single cell stable isotope probing in microbiology using Raman microspectroscopy. *Curr Opin Biotechnol,* 41**,** 34-42.

Zhao, J., Lui, H., Mclean, D. I. & Zeng, H. 2007. Automated autofluorescence background subtraction algorithm for biomedical Raman spectroscopy. *Applied spectroscopy,* 61**,** 1225-1232.

Zhou, H., Yang, D., Ivleva, N. P., Mircescu, N. E., Niessner, R. & Haisch, C. 2014. SERS detection of bacteria in water by in situ coating with Ag nanoparticles. *Analytical chemistry,* 86**,** 1525-1533.

Appendix 1

Magnet Bioreporter Device for Ecological Toxicity Assessment on Heavy Metal Contamination of Coal Cinder Sites

Jianli Jia, **Hanbing Li,** Shuang Zong, Bo Jiang, Guanghe Li, Odafe Ejenavi, Jingrong Zhu, Dayi Zhang

Sensor and Actuators B: Chemical, 2016, 222, 290-299

Contribution:

- I prepared the biorepoter samples required for the project;
- I processed and acquired all bioluminescence data and carried out computational analysis;
- I prepared methods in the first draft of manuscript.

Sensors and Actuators B 222 (2016) 290–299

Contents lists available at ScienceDirect

Sensors and Actuators B: Chemical

journal homepage: www.elsevier.com/locate/snb

Magnet bioreporter device for ecological toxicity assessment on heavy metal contamination of coal cinder sites

Jianli Jia[a], Hanbing Li[b], Shuang Zong[a], Bo Jiang[c], Guanghe Li[c], Odafe Ejenavi[b], Jingrong Zhu[b], Dayi Zhang[b,*]

[a] School of Chemical and Environmental Engineering, China University of Mining & Technology (Beijing), Beijing 100083, PR China
[b] Lancaster Environment Centre, Lancaster University, Lancaster LA1 2YQ, UK
[c] School of Environment, Tsinghua University, Beijing 100084, PR China

ARTICLE INFO

Article history:
Available online 28 August 2015

Keywords:
Whole-cell bioreporter
Magnetic nanoparticles (MNPs)
Magnet bioreporter device
Heavy metal
Toxicity

ABSTRACT

A novel magnet bioreporter device was developed in this research for soil toxicity assessment, *via* magnetic nanoparticles functionalized whole-cell bioreporters. The whole-cell bioreporter ADPWH_recA kept response capability to DNA damage after magnetic nanoparticles (MNPs) functionalization, and could be harvested from soil samples by permanent magnet to reduce the soil particle disturbance. Compared to conventional treatments applying bioreporter directly in soil–water mixture (SW-M treatment) or supernatant (SW-S treatment), MNPs functionalized bioreporter *via* the magnet device (MFB) treatment achieved high sensitivity to evaluate the toxicity and bioavailability of chromium contamination in soils from 10 mg/kg to 5000 mg/kg soil dry weight. The MNPs functionalized bioreporter also achieved high reproducibility with pH value from 5.0 to 9.0, salinity from 0% to 3% and temperature from 20 °C to 37 °C. A case study was carried out on the ecological toxicity assessment of heavy metal contamination at the coal cinder site *via* the magnet bioreporter device. The heavy metal toxicity declined with the increasing distance to the coal cinder point, and a significant accumulation of heavy metal toxicity was observed along the vertical distribution. No direct link was found between the pollution load index (*PLI*) and heavy metal toxicity, and the results suggested the bioreporter test monitored the toxicity of heavy metals in soils and was an important approach for ecological risk assessment. Magnet bioreporter device also offered the high throughput biological measurement and was feasible for *in situ* monitoring.

1. Introduction

Heavy metals are the key anthropogenic environmental contaminants, mainly caused by industrial activities [1,2]. All around the world and particularly in China, numerous heavy metal contaminated sited are found due to the improper disposal of various chemical wastes [3], including coal cinders [4], and the key pollutants include chromium, mercury, arsenic, lead, cadmium, manganese, cobalt, copper, nickel and zinc. They have high mobility through the leachate and further contaminate the biospheric soils [5,6], with respective carcinogenic, teratogenic and mutagenic effects [7]. The high level of heavy metal in soils threatens the ecological system [8], poses potential risks to human health [9] and draws attention on early warning for potential cancer induction [10]. Due to the complex composition and synergetic effects in soils, traditional chemical and physical analysis only provides the amount information [3], but the toxicity and bioavailability of heavy metal contamination from coal cinder are hard to be evaluated.

Recently, whole-cell bioreporter has become initiative and legislative tool for environmental monitoring, with capability to sense the bioavailability and toxicity of contaminated water and soil samples [11]. With genetically engineered bacteria, yeast, fungi, or animal cells, the biological signals of whole-cell bioreporter are initiated by phenotypic colour (*lacZ*), fluorescent (*gfp*/*yfp*) or bioluminescent (*luc*/*lux*) genes [12–14]. It offers highly sensitive, rapidly analytic, easy operation and cost-effective feasibility for *in situ* pollutants assessment [15]. Some whole-cell bioreporter specifically senses the heavy metal molecules [16,17] or their cytotoxicity/genotoxicity [18].

Though the application of whole-cell bioreporter in water sample is successful, it suffers from the heterogeneous features of soils [19]. Exposed to whole-cell bioreporter, the soil particles will

* Corresponding author at: B27, LEC3, Lancaster Environment Centre, Lancaster University, Lancaster LA1 2YQ, UK.
E-mail address: d.zhang@lancaster.ac.uk (D. Zhang).

http://dx.doi.org/10.1016/j.snb.2015.08.110
0925-4005/

absorb the bioluminescent signal (*lux* or *luc*) or give strong fluorescent interference (*gfp*). Some recent work has assessed the bioavailability and toxicity of copper [20], cobalt and nickel [21] *via* direct exposing the whole-cell bioreporter to the soils [22], but the biological sensitivity and specificity are significantly reduced. Some pre-treatments, like water extraction or ultrasonication, are therefore applied to transfer contaminants into aqueous phase for biological analysis [23]. Particularly for heavy metal, the aqueous extraction has been used for whole-cell bioreporters to sense the bioavailability of chromium [24], mercury [16], lead and cadmium [25,26] in soils. Nevertheless, the main drawback is the neglect of the real occurrence of pollutants in the porous soil [17]. Technically, a new type of bioreporter device is required to sense the soil contaminants *in situ* and effectively separate the living reporter cells from the soil particles for biological signal detection. Magnetic nanoparticles (MNPs) functionalization offers the feasibility of magnetic remote control and is biocompatible for whole cell bioreporter [27]. Its equipping and portability for *in situ* monitoring is still under development and requires further research.

In this work, a novel magnet bioreporter device was developed and optimized for effective monitoring and assessment of coal cinder contaminated soils. With whole-cell *Acinetobacter* ADPWH_recA bioreporter [28], the magnet device effectively reduced the impacts of soil particles and improved the sensitivity and reproducibility, comparing to the direct exposure of bioreporters to the soils. The MNPs functionalized bioreporter was able to evaluate the ecological toxicity of heavy metal contamination, *via* the high throughput and easy operation magnet device. This work showed the feasibility and potential of *in situ* environmental risk assessment *via* whole-cell bioreporter for the coal contaminated sites.

2. Material and methods

2.1. Bioreporter strain and incubation

In this research, the *Acinetobacter baylyi* ADPWH_recA whole-cell bioreporter was introduced for environmental ecological toxicity evaluation [28,29]. Compared to other plasmid based or *Escherichia coli* hosted toxicity bioreporter, the reporter gene was located on the chromosome with high stability and *Acinetobacter* was soil bacterium to tolerate the ambient soil environment and achieve high sensitivity. After cultivation in Luria-Bertani (LB) medium overnight at 30 °C, the 10.0 mL ADPWH_recA cells were harvested by 3000 rpm centrifugation for 10 min. The bioreporter pellets were further washed by deionized water and resuspended in 10 mL deionized water for magnetic nanoparticles functionalization or 10 mL fresh MMS medium for toxicity measurement. The 1.0 L MMS medium contained 1.0 g $(NH_4)_2SO_4$, 2.5 g KH_2PO_4, 0.1 g $MgSO_4{\cdot}7H_2O$, 0.005 g $FeSO_4{\cdot}7H_2O$, 0.25 g nitrilotriacetic acid (NTA), 0.55 g NaOH, 3.24 g sodium succinate (20 mM) and 1 mL Bauchop and Elsden solution.

2.2. Direct toxicity measurement on soil samples

The direct toxicity measurement of soil samples was conducted for the supernatant of soil/water mixtures (SW-S) and the bulk soil/water mixtures (SW-M) respectively. For SW-S treatment, the 100 mg soil sample was suspended in 1 mL deionized water and homologized by 150 rpm shaking for 10 min. The 20 μL supernatant and 180 μL bioreporter suspensions were added into each well of a black clear-bottom 96-well microplate. For SW-M treatment, the 1.0 mL bioreporter suspensions were added into 100 mg soil sample, and the mixture was directly transferred into the microplate. The incubation and induction was conducted at 30 °C for 4 h, in the Spectra M5 Plate Reader (Molecular Devices, USA). Three biological replicates were carried out for each sample and the bioluminescent signal was measured every 10 min with 5 s shaking before each reading.

2.3. Magnetic nanoparticles synthesis and functionalization

All the chemicals in this study were analytical grade and purchased from Sigma Aldrich (UK) without specific statement. Magnetic nanoparticles synthesis followed chemical deposition method [27]. The 12.5 mL NaOH (1.5 M) was added dropwisely into the mixture of 1.0 mL $FeCl_3$ (2 M in 2 M HCl) and 0.5 mL $FeCl_2$ (1 M in 2 M HCl) with 40k Hz ultrasonic homologization, until the appearance of dark iron oxide precipitates. The precipitates were further separated by permanent magnet and washed with deionized water until the supernatant reached pH = 7.0.

For bioreporter functionalization, 10 mL bioreporter suspensions (in deionized water) were mixed with 1 mL MNPs suspension, incubated at room temperature for 10 min with 150 rpm shaking. The MNPs-bioreporter was subsequently harvested by a permanent magnet and washed twice by deionized water. The magnetized bioreporter was finally suspended in 10 mL MMS medium for soil toxicity assessment *via* the magnet bioreporter device.

2.4. Magnet bioreporter device and operation

The magnet bioreporter device contained the magnet probe assay and plastic cover for bioreporter strain transfer, as illustrated in Fig. 1(a). The magnet probe assay was assembled by 96 magnet probes (1 cm length and 3 mm id), fixed on the plastic base and patterned (20.66 mm distance between each magnet probe) for the high throughput bioreporter measurement on the 96-well microplate. For MNPs functionalized bioreporter *via* the magnet device (MFB treatment), the 1.0 mL bioreporter suspension was mixed with 100 mg soil samples and transferred into each well of the 96-well microplate (Fig. 1(b-1)). For the determination of the best cultivation time before magnetic separation, the bioreporter cells were magnetically harvest at 0, 15, 30, 45, 60, 75, 90, 105 and 120 min. The recovered MNPs functionalized bioreporter was counted by plate count and the bioluminescent response was also measured.

After incubation at 30 °C for 1 h as the optimal cultivation condition, the magnet probe assay (with plastic cover) was emerged into the reaction system for 30 s (Fig. 1(b-2)). The bioreporter cells were then separated from the soil suspension and attached on the plastic cover by magnetic field. The magnet device was transferred and emerged in another 96-well microplate, supplemented with 200 μL fresh MMS medium (Fig. 1(b-3)). Removing the magnet probe, the plastic cover and microplate was incubated at 30 °C for 5 min with 150 rpm shaking (Fig. 1(b-4)). The bioreporter cells were resuspended in the fresh MMS medium and the bioluminescence was further measured on the Spectra M5 Plate Reader (Molecular Devices, USA). The detection and data analysis followed the same instruction for the direct toxicity measurement on soil samples.

For reproducibility test, MNPs-bioreporter was applied to sense the toxicity of 100 mg/kg chromium contaminated soils in the medium with different pH values and salt contents. The pH value in the induction medium was adjusted by 1.0 M HCl or 1.0 M NaOH solution as 4.0, 5.0, 6.0, 7.0, 8.0, 9.0 and 10.0. The series of salty medium was prepared by adding NaCl into the MMS medium with the final concentration of 1%, 2%, 3%, 4%, 5% and 10%. As for the temperature influence, the temperature during induction period was controlled by the Spectra M5 Plate Reader at 10 °C, 15 °C, 20 °C, 30 °C, 37 °C, 40 °C and 45 °C. To evaluate the life-time of MNPs-bioreporters, the bioreporter suspension was stored at 4 °C and taken out for direct toxicity measurement without any pre-treatment.

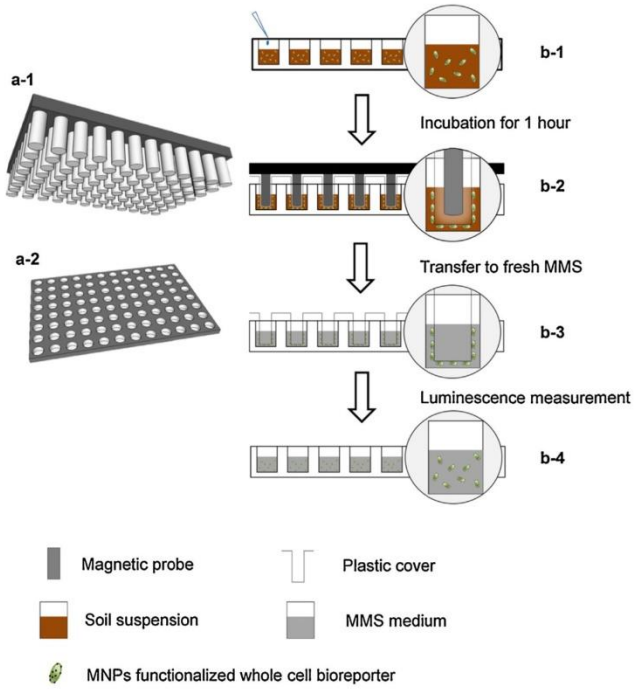

Fig. 1. Schematic instruction for magnet bioreporter device. (a-1) and (a-2) for magnetic probe assay and the 96-well microplate respectively. (b-1) The 1.0 mL MNPs functionalized bioreporter was mixed with soil samples and further incubated at 30 °C for 1 h; (b-2) separation from soil suspensions *via* magnetic probe. (b-3) Resuspension in fresh MMS medium; (b-4) incubation and bioluminescence measurement at 30 °C for 3 h.

2.5. Toxicity model for heavy metal contaminated soils

For the calibration of heavy metal toxicity in soils, chromium was chosen at the target analyte since it was the main heavy metal contamination at the coal cinder site. The artificial chromium contaminated soils were prepared by mixing 1.0 g uncontaminated soil with 1 mL potassium bichromate solution with the concentration of 0, 0.1, 0.2, 0.5, 1, 2, 5, 10, 20, 50, 100, 200, 500, 1000, 2000 and 5000 mg/L. The soil slurry was air dried in the laminar hood. The chromium contamination in soils was 0, 0.1, 0.2, 0.5, 1, 2, 5, 10, 20, 50, 100, 200, 500, 1000, 2000 and 5000 mg/kg soil dry weight, respectively.

The genotoxicity of hexavalent chromium in soil was identified as several mechanistic processes, including mutagenic effects on DNA and direct inductive immunological responses [30]. Such genotoxic effects consequently caused the accumulation of single stranded DNA (ssDNA) and the activation of SOS response for damaged DNA repair. The SOS response (bioluminescent response of ADPWH_recA) is the function of LexA-like SOS repressor (*LSR*, $cell^{-1}$) and can be simulated by the previous gene expression model [31,32], as shown in Eq. (1).

$$SOS_{r,s} = 1 + \left(\frac{k_{dSLR}}{2 \cdot (1 + k_{ssDNA})} \cdot [LSR]\right) \cdot \frac{[Cr]}{(K_{mLSR} \cdot K_{Cr} \cdot k_{ssDNA} \cdot k_{Cr})^{-1} + [Cr]} \quad (1)$$

Here, $SOS_{r,s}$ (SOS response ratio) is dependent on the hexavalent chromium contamination level in soils ([*Cr*], mg/kg). K_{Cr} is the isotherm equilibrium of chromium-DNA adduct (DNA phosphodiester backbone with chromium) and k_{Cr} represents ssDNA generation constant from the chromium-DNA adduct (L/(cell·g) chromium). k_{dSLR} represents the equilibrium coefficient of *LSR* dimer (*dSLR*, $cell^{-1}$) and monomer (*mLSR*, $cell^{-1}$) and k_{ssDNA} represents the cleavage reaction constant of *LSR* dimer. K_{mLSR} is the dynamic gene expression (SOS response) level activated by *LSR* monomer.

2.6. Sites description

A total of 16 soil samples were taken from the methanol plant of Yulin Energy and Chemical Industry, Yanzhou Coal Corporation, China (Fig. 2). The site (698,000 m^2) was located in Yulin Shaanxi Province (N38°34′41.9″, E109°55′50.4″), in the junction of Maowusu Sandy Land and the Loess Plateau. The annual coal consumption was 31,200 tonnes and the soils have been seriously contaminated by the coal with high heavy metal content. The sampling sites were designed along the leeward direction of the cinder heap, with the distance of 0, 10, 50, 80 and 150 m. The uncontaminated soil sample was collected in the living area of the plant, 500 m away from the heap. At each point, the soils were sampled at different depth of 0–20 cm (surface soil), 20–35 cm (middle soil) and 35–50 cm (bottom soil) to evaluate the toxicity profiles caused by the trace metal transportation.

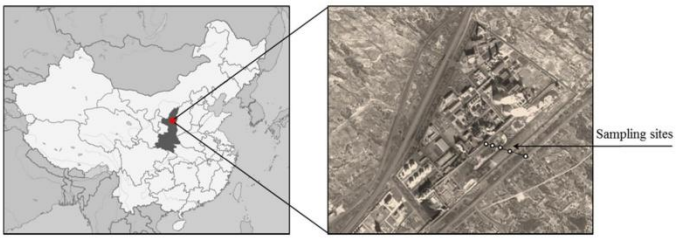

Fig. 2. Location of research area in Yulin and the sampling sites.

2.7. Chemical analysis

Before chemical analysis, all of soil samples were seized by 200 mesh. Mercury was determined by DMA-80 Hg analyzer (Milestone S.r.L., Italy). For other trace elements, the samples were digested in an UltraCLAVE microwave high pressure reactor (Milestone S.r.L., Italy), containing 330 mL distilled H_2O, 30 mL 30% H_2O_2 and 2 mL 98% H_2SO_4 as the digestion solution [33]. With 50 bars initial nitrogen pressure, the microwave digestion programme was listed in Table S1. Further digestion for 50 mg soil sample was conducted in 5 mL 40% HF, 2 mL 65% HNO_3, and 1 mL 30% H_2O_2 [34]. The inductively coupled plasma mass spectrometry (ICP-MS, X series II, Thermo Fischer Scientific, USA) was used for the determination of the trace elements in a pulse counting mode (three points per peak). In this study, the multi-element standards (Inorganic Ventures, CCS-1, CCS-4, CCS-5, and CCS-6) were referenced for the calibration of trace element concentrations. As and Se were determined by ICP-MS with collision cell technology (CCT) due to their volatility [35]. Polyfluoroalkoxy volumetric flasks were used without drying on electric hot plate to avoid As/Se volatile loss. With the 1 μg/L tuning solution, the torch position and ion lenses were optimized before real sample measurement. The optimal parameters of the ICP-CCT-MS and calibration curves of As/Se were listed in Tables S2 and S3.

2.8. Data analysis

The bioluminescence response was calculated by averaging the bioluminescent signal from the 7 time points between 180 and 240 min for each well. The relative bioluminescence response ratio was the specific value of the bioluminescence response of contaminated soil samples to that of the uncontaminated soils. The heavy metal profiles in soil samples were statistically analyzed by SPSS software (version 15.0 for Windows) *via* Principal Component Analysis (PCA). The equality and normality of data were tested by Brown–Forsythe and Shapiro–Wilk test respectively, and the null hypothesis was rejected for $p < 0.05$.

Contamination factor (*CF*) is defined as the ratio of the heavy metal concentration in the sample soil to the baseline concentration in background soil, as shown in Eq. (2) [36]. Pollution load index (*PLI*) is determined as the *n*th root of the *n* CF in Equation (3) [36]. The *CF* and *PLI* are empirical indices to evaluate the level of heavy metal contamination, and the higher values indicate heavier contamination of individual and multiple heavy metals respectively.

$$CF = \frac{[\text{Heavy metal in sample soils}]}{[\text{Heavy metal in background soils}]} \quad (2)$$

$$PLI = (CF_1 \times CF_2 \times \cdots \times CF_n)^{1/n} \quad (3)$$

Table 1
Analytical characteristics of magnetic ADPWH_recA whole-cell bioreporter.

Characteristics	Description
Limit of detection	1 mg/kg chromium(VI) in dry soil
Linear range	1–100 mg/kg chromium(VI) in dry soil
Pre-incubation time	1 h
Detection time	4 h
Reproducibility	High reproducible when pH value is from 5.0 to 9.0, salinity ranges from 0% to 3%, and temperature is from 20 °C to 37 °C
Storage time	30 days

3. Results and discussions

3.1. Higher sensitivity and reproducibility of magnet bioreporter device

The MNPs functionalized bioreporter could be magnetic remote controlled for effectively separation from the soil particles. The MNPs were biocompatible, and the viability and bioluminescent signal of whole-cell bioreporter remained over 99% comparing to the native bioreporter cells [27]. With the strong electrostatic attraction between the negative iron oxide (Fe—OO^-) and positive amino-groups (—NH_3^+) on bacterial membrane, the separation effectiveness by magnetic field was above 99.6% and the synthesized MNPs had neither cytotoxicity nor genotoxicity on bacterial bioreporter cells [37]. MNPs functionalized whole-cell bioreporter therefore had the feasibility to sense the toxicity of soil samples *in situ* and subsequently isolated for bioluminescent signal measurement.

Due to the cell division, the MNPs functionalized bioreporter gradually lost their magnetic capacity [38]. Though longer incubation with soil samples could improve the chemical uptake by bioreporter cells for higher responsive ratio, the less recovery rate consequently resulted in lower bioluminescent signal and lower sensitivity. Fig. 3 illustrated that, within 45 min incubation, over 90% living bioreporter cells were isolated from the soil/water mixture based on plate count. The results fitted with previous study that about 12% free bioreporter cells were observed after 120 min cultivation in rich medium [27]. As for the bioluminescence and relative response ratios, the bioluminescent signals were stable from 3600 RLU to 3800 RLU when the incubation time was less than 75 min, and the response ratio ranged from 1.90 to 2.00. The results suggested a highly reliable responsive period between 30 and 70 min. The optimal incubation time for sufficient bioreporter cell recovery and high response sensitivity was identified as 60 min, and it was further applied in the following work on calibration curve and real soil sample assessment.

The summarized features of the magnetic ADPWH_recA whole-cell bioreporter were listed in Table 1 from the reproducibility test. After 1 h pre-incubation of the MNPs functionalized bioreporter,

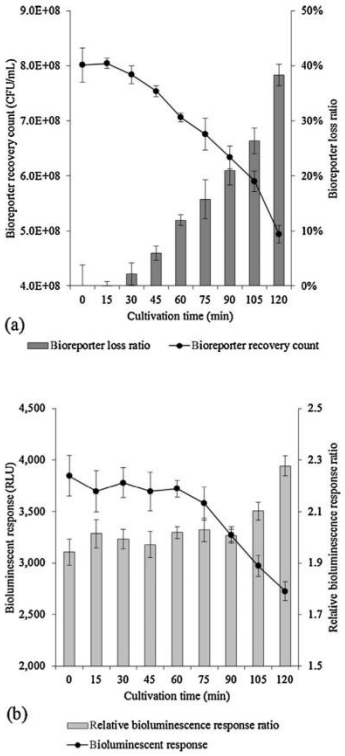

Fig. 3. The cell recovery rate (a) and bioluminescent response (b) of whole-cell bioreporter against the incubation time with soils. Over 90% of living bioreporter cells were successfully harvested from the soil/water mixture within 45 min incubation. The relative bioluminescence response ratio ranged between 1.90 and 2.00 when the incubation time was less than 75 min. The 60-min incubation was identified as the optimal time for sufficient bioreporter cell recovery and high response sensitivity.

the cells were captured by permanent magnet and resuspended in fresh medium without soil disturbance for another 4 h. As a soil bacterium, ADPWH_recA had strong tolerance to the environmental variations and maintained high reproducibility under different pH, salinity and temperature condition. The relative bioluminescent response ratio maintained stable (1.44–1.51) when pH value ranged from 5.0 to 9.0, dramatically dropping to 1.25 at pH = 4.0 and 1.12 at pH = 10.0 (Fig. 4(a)). The results were similar to previous research on the pH influence on *A. baylyi* ADP1 that *Acinetobacter* based bioreporter could tolerate large pH variation [39]. Fig. 4(b) also illustrated the good responsive performance of MNPs functionalized ADPWH_recA at 20 °C (relative bioluminescent response ratio = 1.47), 30 °C (relative bioluminescent response ratio = 1.50) and 37 °C (relative bioluminescent response ratio = 1.49). The tiny reduction of bioluminescent response at 15 °C and 40 °C attributed to the less bacterial activities at inappropriate temperatures, and the response was very weak under even lower (10 °C) or higher (45 °C) temperature conditions. Salinity did not significantly affect the reproducibility of ADPWH_recA and the relative bioluminescent response ratios were above 1.45 when the salinity was no higher than 3%, but were gradually suppressed at higher salinity level (Fig. 4(c)). Therefore, the MNPs functionalized bioreporters had high reproducibility under the normal pH value, salinity and temperature conditions of natural soils and no specific pre-treatment was required for real soil sample assessment. High activity and responsive sensitivity of MNPs functionalized whole-cell bioreporters was also observed after 30 days storage at 4 °C (Fig. 4(d)). Without any pre-treatment, the stored bioreporter cells could be directly applied for soil assessment and the relative bioluminescent response ratio was above 1.45 for chromium contaminated soils of 100 mg/kg soil dry weight. The life-time of MNPs functionalized bioreporter was the same to the original *Acinetobacter* based bioreporters [28,40], indicating that MNPs functionalization had minimal impacts on the bacterial activities and was an appropriate approach to expand its application in soil contamination assessment.

From the calibration curve of soil/water supernatant (SW-S), soil/water mixture (SW-M) and MNPs functionalized bioreporter (MFB) (Fig. 5), magnet device had the highest responsive sensitivity and illustrated the chromium bioavailability in contaminated soils. In SW-S and SW-M treatments, ADPWH_recA bioreporter did not show any positive response to the chromium due to the strong light adsorption by soil particles. The negative bioluminescent response was observed when chromium concentration was above 100 mg/kg soil dry weight for both treatments. Significant positive response was only found in MFB treatment and the limit of detection was 1 mg/kg soil dry weight (Fig. 5 and Table 1). From 1 mg/kg to 100 mg/kg chromium contamination in dry soils, the relative bioluminescence response ratio showed a linear relationship to quantify the toxicity and bioavailability of chromium in soil samples, ranging from 1.05 to 1.60. Above 500 mg/kg soil dry weight, chromium predominantly behaved the cytoxicity effects and all the three treatments had similar inhibited bioluminescent signal. From the whole-cell bioreporter growth curve (Fig. S1), there was no significant growth difference when the chromium concentration was less than 500 mg/kg soil dry weight, in which range that the relative bioluminescent response ratio was positively correlated with chromium. It therefore explained the decreasing bioluminescent response ratio at higher chromium level that strong cytoxicity of chromium inhibited bioreporter growth and activities.

Given the model simulation of bioreporter's response to chromium with different bioavailability in aqueous phase in Fig. 5 [41], the results further revealed the bacteria-contaminant interaction within the porous soils and its impacts on bioreporter response. With lower chromium bioavailability, the calibration curve shifted towards higher chromium values. The SOS response coefficient ($K_{sLSR} \cdot K_{Cr} \cdot k_{ssDNA} \cdot k_{MO}$, 3.8) and genotoxicity coefficient ($(k_{dsSLR}/2 \cdot (1 + k_{ssDNA})) \cdot [LSR]_{total}$, 1.724 L/mg) kept stable, similar to previous research [41]. Referring to the synergetic efficiency through the SOS repair process (including genotoxin DNA damage, ssDNA recognition and SOS box activation), the similar SOS response coefficients indicated the same SOS mechanism of bioreporter's responsive to chromium genotoxicity and cytotoxicity in the soils *via* the magnet bioreporter device [32]. Since the bioluminescent signal of ADPWH_recA was regulated by the SOS process, all the carcinogens causing DNA damage would activate its response, including mitomycin C, UV light, ethidium bromide and H_2O_2 [22]. The bioreporter therefore did not respond to a particular heavy metal (like chromium), but evaluated the synergistic toxicity of all the carcinogens in environmental samples.

From the parabolic curve of MNPs functionalized bioreporter to hexavalent chromium, both the relative bioluminescent response ratio and growth curve (Fig. S1) were considered to evaluate the toxicity of unknown environmental samples. In absence of growth inhibition, the sample had low cytoxicity and its bioluminescent

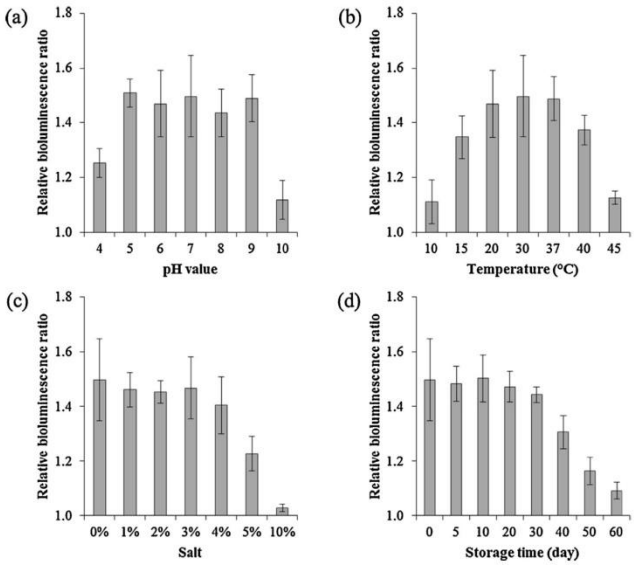

Fig. 4. The impacts of pH (a), temperature (b), salt (c) and storage time (d) on magnetic bioreporter's response to artificial chromium contaminated soils. The chromium concentration was 100 mg/kg soil dry weight.

response belonged to the positive relationship range, oppositely in presence of growth inhibition. Only the MFB treatment had the positive bioluminescence response when chromium concentration was less than 200 mg/kg soil dry weight, and the response ratio fitted well with the model prediction of 10% chromium bioavailability when chromium concentration was above 100 mg/kg soil dry weight. At lower chromium contamination level, chromium bioavailability changed due to the complex adsorption effects of soil particles and the irregular bioluminescent response ratio represented the changing bioavailable fraction. Given heavy chromium contamination level (>500 mg/kg soil dry weight), MFB and SW-M treatments had similar responsive results, significantly higher than SW-S treatment. Since the whole-cell bioreporter only sensed the water soluble chromium in the supernatant of soil-water mixture in SW-S treatment, it measured the chromium toxicity in the unbound water phase. The dominant fraction of chromium existed in the bound water or was absorbed on the soil particles, and their carcinogenic effects were only assessable by the direct-contact bioreporter assay [24]. The results indicated magnetic functionalized bioreporter could effectively evaluate the real toxic effects of chromium in soils, by directly contacting soil particles and seeking for chromium in unbound/bound water or adsorbed on particle surface. The portable magnet bioreporter device provided the ready-to-use and nature-inspired technique for soil *in situ* measurement by optimizing the operation procedure and enhancing the bioluminescent signal [42].

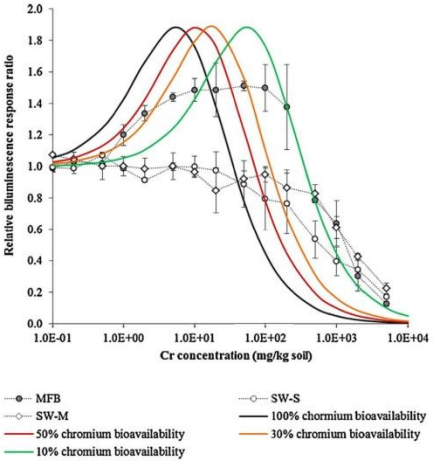

Fig. 5. The calibration curve for toxicity assessment on artificial chromium contaminated soils. Grey circle refers to magnet bioreporter device (MFB); white circle represents direct measurement of soil/water supernatant (SW-S); white diamond is the direct measurement of soil/water mixture (SW-M). The black line represents the simulation of whole-cell bioreporter's response to chromium toxicity with 100% bioavailability, and a significant bioluminescent response curve shift was found for 50% (red line), 30% (yellow line) and 10% (green line) chromium bioavailability respectively.

3.2. Heavy metal contamination profiles in soils

The heavy metal profiles of the 16 investigated soil samples and the coal cinder were listed in Table 2. The chromium was 23 times enriched in the rough cinder (from 38.18 mg/kg to 920.82 mg/kg),

Table 2
Heavy metal contamination in coal/cinder (mg/kg coal or cinder dry weight) and coal cinder contaminated sites (mg/kg soil dry weight).

Samples	Be	Cr	Ni	Cu	Zn	As	Se	Cd	Pb	U	Hg
Raw coal	0.27	38.18	4.93	6.62	8.55	2.26	0.23	0.05	3.43	0.48	0.006
Rough cinder	0.83	920.82	26.89	22.66	9.01	4.14	0.84	0.12	7.44	1.42	0.001
Background soil	1.33	398.94	30.99	16.22	37.91	6.36	0.87	0.26	21.62	1.20	0.008
0 m											
0–20 cm	1.07	745.15	23.11	17.92	28.78	4.71	0.75	0.25	18.19	1.29	0.003
20–35 cm	1.19	552.97	17.61	10.55	27.72	3.18	0.43	0.22	20.26	0.64	0.005
35–50 cm	1.27	505.60	14.68	10.25	20.97	3.10	0.44	0.16	20.36	0.64	0.003
10 m											
0–20 cm	1.55	802.77	29.38	21.67	23.05	5.26	1.00	0.22	18.05	1.48	0.002
20–35 cm	1.58	620.79	21.71	16.52	29.26	5.60	1.19	0.24	30.31	1.20	0.001
35–50 cm	1.26	525.79	15.80	9.74	17.53	3.00	0.29	0.15	21.44	0.56	0.001
50 m											
0–20 cm	1.16	508.43	13.80	8.93	28.10	3.66	0.36	0.14	20.08	0.54	0.033
20–35 cm	1.12	482.68	12.29	8.09	16.19	2.62	0.41	0.13	19.88	0.45	0.001
35–50 cm	1.12	628.89	15.03	9.35	18.22	3.08	0.46	0.14	20.17	0.53	0.001
80 m											
0–20 cm	1.15	483.48	13.26	9.03	18.61	3.22	0.30	0.16	20.01	0.53	0.001
20–35 cm	1.19	502.34	13.84	9.31	19.76	3.35	0.45	0.18	21.03	0.57	0.001
35–50 cm	1.29	613.57	19.76	15.32	29.44	4.01	0.43	0.25	21.28	0.86	0.001
150 m											
0–20 cm	1.10	494.60	13.56	8.90	19.03	3.24	0.58	0.15	19.99	0.56	0.001
20–35 cm	1.24	474.09	16.46	10.87	24.61	4.48	0.43	0.22	20.51	0.76	0.001
35–50 cm	1.25	448.66	18.50	13.00	28.81	5.08	0.41	0.22	21.70	0.90	0.001

Note: the analytical instrument is Hg analyzer (DMA-80) for Hg and ICP-MS (X series II) for other elements.

followed by nickel (5.5 times enrichment). The enrichment of other heavy metals ranged from 1.8 to 3.7 times, except for zinc (no significant change) and mercury (loss due to volatile during the combustion process) [43]. Similar to previous research on coal combustion residues [44,45], chromium and nickel were mostly found concentrated in bottom ash or cinder as the dominant toxic heavy metal residues, due to their low volatility and high stability.

As for heavy metal contamination in soils, the investigated soils only showed significant contamination of chromium from 448.66 mg/kg to 802.77 mg/kg soil dry weight, with the *CF* values from 1.12 to 2.01 (398.94 mg/kg soil dry weight in background). The levels of the other heavy metals were similar to the background soils (p-value > 0.05), as the *CF* value of beryllium ranged from 0.80 to 1.19, nickel from 0.40 to 0.95, copper from 0.50 to 1.34, zinc from 0.43 to 0.78, arsenic from 0.41 to 0.88, selenium from 0.33 to 1.37, cadmium from 0.50 to 0.96, lead from 0.83 to 1.40, uranium from 0.38 to 1.28 and mercury from 0.13 to 4.13. The results indicated that the key ecological toxicity was attributed to chromium, same as revealed by many previous research on mutagens in heavy metal contaminated soils [46], and its toxicity in soils could be effectively evaluated by various biological assays [47,48]. The magnet bioreporter device in this study was therefore feasible to enhance the toxicity test sensitive by directly exposing MNPs-functionalized whole-cell bioreporter cells and diagnosing their bioluminescent response signal.

For soils nearer to the coal cinder point (0 m and 10 m), there was higher heavy metal contamination in the upper layer soil. The chromium contamination declined from 745.15 mg/kg (0–20 cm, 0 m) to 505.60 mg/kg (35–50 cm, 0 m), and from 802.77 mg/kg (0–20 cm, 10 m) to 525.79 mg/kg (35–50 cm, 10 m), respectively. Except for Be, Pb and Hg, all the other heavy metal elements (Ni, Cu, Zn, As, Se, Cd, and U) have the same vertical decreasing distribution. Comparing to the heavy metal composition in the cinders, chromium was also the key carcinogenic heavy metal in soils. Given the sequence of the exchangeable fractions of heavy metals as Cd > Zn > Cu > Ni > Pb > Cr [5], chromium was further concentrated in top soils with less mobility. The results further suggested that the main source of heavy metal contamination in soils was the leachates from the cinders and their residues were dependant on the transportation process in soils.

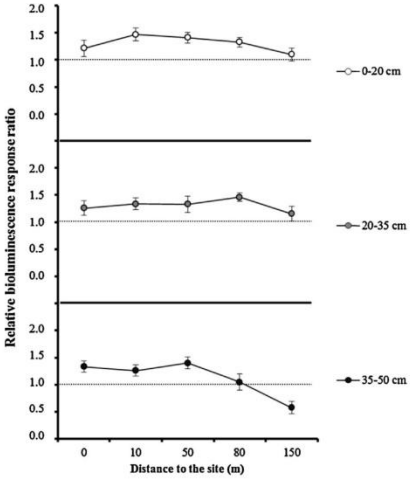

Fig. 6. Ecological toxicity assessment of heavy metal contaminated soils *via* magnetic bioreporter device.

3.3. Ecological risk profiles of heavy metal contaminated soils

In the ecological toxicity evaluation by directly applying whole-cell bioreporters to the soil (SW-M, Fig. S2 in Supplementary Materials) and soil–water supernatant (SW-S, Fig. S3 in Supplementary Materials), ADPWH_recA only behaved negative (relative bioluminescence response ratio < 1.0) or neutral signal (relative bioluminescence response ratio = 1.0) and was not suitable to quantify the toxicity impacts of heavy metal contamination *in situ*. Fig. 6 illustrated the ecological toxicity profiles of the soil samples by the magnetic bioreporter device (MFB treatment), and the toxicity of heavy metals declined with the increasing distance to the coal cinder point. From the whole-cell bioreporter growth curve for the

soil samples (Fig. S4), all the heavy metal contaminated soils did not show inhibition effects on bacterial growth, indicating all the bioluminescent signals were within the linear response range and the relative bioluminescence response ratio had positive relationship with the ecological toxicity in soils. Except for 0 m point, the relative bioluminescence response ratio dropped from 1.47 (10 m) to 1.10 (150 m) in the surface soil, 1.34 (10 m) to 1.16 (150 m) in the middle soil, and 1.26 (0 m) to 0.58 (150 m) in the bottom soil. At the 0 m point, the low bioluminescence signal of surface soil was caused by the high cytotoxicity effects of chromium (745.15 mg/kg soil dry weigh) and the growth of ADPWH_recA bioreporter was inhibited. The soil sample at 0 m point was therefore characterized with the highest ecological risk.

From the toxicity vertical distribution, the ecological risks had a significant decline in deeper soils. Attributing to the heavy metals leachates from the coal cinders, the ecological risk distribution fitted well with chemical analysis and previous studies. The high ecological risk at the surface soils than bottom soils suggested the leakage and vertical transportation chromium in soils [49]. Comparing to the horizontal ecological risk distribution, the results further identified the main toxicity sources as the heavy metals from the coal cinders.

3.4. Correlation between soil heavy metal profiles and ecological risk

The Principle Component Analysis (PCA) illustrated the main factors causing the ecological risks in soil samples (Fig. S5a). More precisely, the principle component 1 (PC1) was the heavy metal contamination level, accounting for 60.5% of the total variance. At the sampling points nearer to the coal cinder site (0 m and 10 m), the surface and middle soils were heavily contaminated and therefore recognized as isolated square (red) and circle (blue) to the higher value of PC1-axis. For the rest soils, they gathered due to similar contamination level (*PLI*). PC1 was therefore derived from the external heavy metal sources, leaching from the coal cinder for the surface soil (0–20 cm) and heavy metal vertical transportation for middle soil (20–35 cm). The soil depth was the principle component 2 (PC2), contributing to 13.3% of the total variance. Heavy metals distribution and mobility were reported to depend on soil properties and depth [50], and their spatial distribution in different depths of soils also affected the mobility and bioavailability [51]. Nevertheless, the soil ecological risks (illustrated as the area of each symbol) were associated with neither the load of PC1 nor PC2, suggesting that they were complicatedly affected by both heavy metal profiles and soil features.

There was also no significant correlation between heavy metal pollution load index (*PLI*) and ecological risk (p-value > 0.05) (Fig. S5b). Higher *PLI* indicated high heavy metal contamination level, but did not fit with the ecological risk distribution. Previous research had shown the positive correlation between heavy metal content and ecological toxicity at the contaminated sites with individual heavy metal pollutant, like chromium residues [24] or copper contaminated agricultural soils [52]. The ecological toxicity was only affected by the individual *CF* value and bioavailability in soil. At the coal cinder contaminated sites, we found the existence of multiple heavy metals and their synergic/antagonistic effects consequently resulted in complicated ecological toxicity [53]. Many evidences had revealed that the toxicity of individual or multiple heavy metals behaved antagonistic or additive effects, dependent on the composition and soil features, like organic matters or pH value [54,55]. In this case, *PLI* was an empirical indicator evaluating the multiple heavy metal contamination level, but suffered from identifying and characterizing the interaction between various heavy metal molecules and their association with soil particles. From the mechanisms of ADPWH_recA to sense all the carcinogens activating SOS process, the response of whole-cell bioreporter effectively represented the synergic/antagonistic effects of multiple heavy metals. By directly exposing the living bioreporter cells to the contaminated samples *in situ*, the MNPs functionalized bioreporter had its feasibility as an important approach, supplementary to chemical analysis, in ecological risk assessment and environmental risk management.

4. Conclusion

This work developed a novel magnet bioreporter device for soil toxicity assessment, *via* magnetic nanoparticles functionalized whole-cell bioreporters. The living magnetic bioreporter cells could sense the carcinogenic chemicals in the soil and were effectively separated from the soil-water slurry in the bioluminescence detection step to avoid the disturbance of soil particles. Comparing to the conventional treatments directly applying bioreporter in soil–water mixture or supernatant, the magnet bioreporter device achieved high sensitivity and reproducibility under soil pH, salinity and temperature conditions. The dose–toxicity calibration curve revealed the impacts of chromium bioavailability on its ecological risk in soils, where strong genotoxicity was identified when chromium concentration was from 1 mg/kg to 500 mg/kg soil dry weight and the cytotoxic inhibition was found at chromium over 500 mg/kg soil dry weight. For the first time, the ecological toxicity of heavy metal contaminated soils was evaluated by the whole-cell bioreporter at the coal cinder site. Though the existence of heavy metal contamination contributed to the main ecological risks at the site, the pollution load index (*PLI*) had no significantly relationship with the ecological toxicity distribution. The synergic and antagonistic effects of soil multiple heavy metal contamination brought the challenges for environmental risk assessment by chemical analysis. The magnetic bioreporter device behaved as an alternative approach for the high throughput biological measurement and was feasible for *in situ* monitoring.

Acknowledgements

The authors would like to thank National Basic Research Program of China (973 Program, No. 2014CB238906) and National Natural Science Foundation of China (No. 41301331) for financial support. Prof. Shifeng Dai (China University of Mining & Technology, Beijing) helped in ICP-MS analysis of heavy metal components in the soil samples.

Appendix A. Supplementary data

Supplementary data associated with this article can be found, in the online version, at http://dx.doi.org/10.1016/j.snb.2015.08.110.

References

[1] X.D. Li, O.W.H. Wai, Y.S. Li, B.J. Coles, M.H. Ramsey, I. Thornton, Heavy metal distribution in sediment profiles of the Pearl River estuary, South China, Appl. Geochem. 15 (2000) 567–581.
[2] K. Loska, D. Wiechula, I. Korus, Metal contamination of farming soils affected by industry, Environ. Int. 30 (2004) 159–165.
[3] S.R. Smith, A critical review of the bioavailability and impacts of heavy metals in municipal solid waste composts compared to sewage sludge, Environ. Int. 35 (2009) 142–156.
[4] H. Alizai, D. Preston, S.S. Meng, M. Kolkas, Heavy metal contamination in the coastal sediments of the Lower New York Bay, Northeast. Geol. Environ. Sci. 25 (2003) 226–231.
[5] P.J. He, Z. Xiao, L.M. Shao, J.Y. Yu, D.J. Lee, In situ distributions and characteristics of heavy metals in full-scale landfill layers, J. Hazard. Mater. 137 (2006) 1385–1394.
[6] Z. Dang, C.Q. Liu, M.J. Haigh, Mobility of heavy metals associated with the natural weathering of coal mine spoils, Environ. Pollut. 118 (2002) 419–426.
[7] M. Valko, H. Morris, M.T.D. Cronin, Metals, toxicity and oxidative stress, Curr. Med. Chem. 12 (2005) 1161–1208.

[8] K.E. Giller, E. Witter, S.P. McGrath, Toxicity of heavy metals to microorganisms and microbial processes in agricultural soils: a review, Soil Biol. Biochem. 30 (1998) 1389–1414.
[9] L. Jarup, Hazards of heavy metal contamination, Br. Med. Bull. 68 (2003) 167–182.
[10] M.L. Farre, R. Brix, D. Barcelo, Screening water for pollutants using biological techniques under European Union funding during the last 10 years, Trends Anal. Chem. 24 (2005) 532–545.
[11] S. Belkin, Microbial whole-cell sensing systems of environmental pollutants, Curr. Opin. Microbiol. 6 (2003) 206–212.
[12] T.K. Van Dyk, E.J. DeRose, G.E. Gonye, LuxArray, a high-density, genomewide transcription analysis of *Escherichia coli* using bioluminescent reporter strains, J. Bacteriol. 183 (2001) 5496–5505.
[13] E.A. Meighen, Genetics of bacterial bioluminescence, Annu. Rev. Genet. 28 (1994) 117–139.
[14] J. Sanseverino, R.K. Gupta, A.C. Layton, S.S. Patterson, S.A. Ripp, L. Saidak, et al., Use of *Saccharomyces cerevisiae* BLYES expressing bacterial bioluminescence for rapid, sensitive detection of estrogenic compounds, Appl. Environ. Microbiol. 71 (2005) 4455–4460.
[15] S.F. D'Souza, Microbial sensors, Biosens. Bioelectron. 16 (2001) 337–353.
[16] L.D. Rasmussen, S.J. Sorensen, R.R. Turner, T. Barkay, Application of a mer-lux biosensor for estimating bioavailable mercury in soil, Soil Biol. Biochem. 32 (2000) 639–646.
[17] A. Ivaska, M. Virtab, A. Kahrua, Construction and use of specific luminescent recombinant bacterial sensors for the assessment of bioavailable fraction of cadmium, zinc, mercury and chromium in the soil, Soil Biol. Biochem. 34 (2002) 1439–1447.
[18] S. Rodriguez-Mozaz, M.J. Lopez de Alda, D. Barcelo, Biosensors as useful tools for environmental analysis and monitoring, Anal. Bioanal. Chem. 386 (2006) 1025–1041.
[19] J.R. van der Meer, S. Belkin, Where microbiology meets microengineering: design and applications of reporter bacteria, Nat. Rev. Microbiol. 8 (2010) 511–522.
[20] P. Corbisier, E. Thiry, L. Diels, Bacterial biosensors for the toxicity assessment of solid wastes, Environ. Toxicol. Water Qual. 11 (1996) 171–177.
[21] C. Tibazarwa, P. Corbisier, M. Mench, A. Bossus, P. Solda, M. Mergeay, et al., A microbial biosensor to predict bioavailable nickel and its transfer to plants, Environ. Pollut. 113 (2001) 19–26.
[22] Y. Song, B. Jiang, S. Tian, H. Tang, Z. Liu, C. Li, et al., A whole-cell bioreporter approach for the genotoxicity assessment of bioavailability of toxic compounds in contaminated soil in China, Environ. Pollut. 195C (2014) 178–184.
[23] V.H.C. Liao, M.T. Chien, Y.Y. Tseng, K.L. Ou, Assessment of heavy metal bioavailability in contaminated sediments and soils using green fluorescent protein-based bacterial biosensors, Environ. Pollut. 142 (2006) 17–23.
[24] B. Jiang, D. Zhu, Y. Song, D. Zhang, Z. Liu, X. Zhang, et al., Use of a whole-cell bioreporter *Acinetobacter baylyi*, to estimate the genotoxicity and bioavailability of chromium(VI)-contaminated soils, Biotechnol. Lett. 37 (2015) 343–348.
[25] R. Turpeinen, J. Salminen, T. Kairesalo, Mobility and bioavailability of lead in contaminated boreal forest soil, Environ. Sci. Technol. 34 (2000) 5152–5156.
[26] H. Fritze, J. Perikomaki, T. Petanen, T. Pennanen, M. Romantschuk, M. Karp, et al., A microcosms study on the effects of Cd containing wood ash on the coniferous humus fungal community and the Cd bioavailability, Soils Sediments 1 (2001) 146–150.
[27] D. Zhang, R.F. Fakhrullin, M. Özmen, H. Wang, J. Wang, V.N. Paunov, et al., Functionalization of whole-cell bacterial reporters with magnetic nanoparticles, Microbiol. Biotech. 4 (2011) 89–97.
[28] Y.Z. Song, G.H. Li, S.F. Thornton, I.P. Thompson, S.A. Banwart, D.N. Lerner, et al., Optimization of bacterial whole cell bioreporters for toxicity assay of environmental samples, Environ. Sci. Technol. 43 (2009) 7931–7938.
[29] D. Zhang, A. Ding, S. Cui, C. Hu, S.F. Thornton, J. Dou, et al., Whole cell bioreporter application for rapid detection and evaluation of crude oil spill in seawater caused by Dalian oil tank explosion, Water Res. 47 (2013) 1191–1200.
[30] K.P. Nickens, S.R. Patierno, S. Ceryak, Chromium genotoxicity: a double-edged sword, Chem. Biol. Interact. 188 (2010) 276–288.
[31] A.A. Al-Anizi, M.T. Hellyer, D. Zhang, Toxicity assessment and modeling of *Moringa oleifera* seeds in water purification by whole cell bioreporter, Water Res. 56 (2014) 77–87.
[32] D. Zhang, Y. Zhao, Y. He, Y. Wang, Y. Zhao, Y. Zheng, et al., Characterization and modeling of transcriptional cross-regulation in *Acinetobacter baylyi* ADP1, ACS Synth. Biol. 1 (2012) 274–283.
[33] S. Dai, X. Wang, Y. Zhou, J.C. Hower, D. Li, W. Chen, et al., Chemical and mineralogical compositions of silicic, mafic, and alkali tonsteins in the late Permian coals from the Songzao Coalfield, Chongqing, Southwest China, Chem. Geol. 282 (2011) 29–44.
[34] S. Dai, X. Wang, V.V. Seredin, J.C. Hower, C.R. Ward, J.M.K. O'Keefe, et al., Petrology, mineralogy, and geochemistry of the Ge-rich coal from the Wulantuga Ge ore deposit Inner Mongolia, China: new data and genetic implications, Int. J. Coal Geol. 90 (2012) 72–99.
[35] X. Li, S. Dai, W. Zhang, T. Li, X. Zheng, W. Chen, Determination of As and Se in coal and coal combustion products using closed vessel microwave digestion and collision/reaction cell technology (CCT) of inductively coupled plasma mass spectrometry (ICP-MS), Int. J. Coal Geol. 124 (2014) 1–4.
[36] M.A.H. Bhuiyan, L. Parvez, M.A. Islam, S.B. Dampare, S. Suzuki, Heavy metal pollution of coal mine-affected agricultural soils in the northern part of Bangladesh, J. Hazard. Mater. 173 (2010) 384–392.
[37] C. Chen, D. Zhang, S.F. Thornton, M. Duan, Y. Luo, A. Ding, et al., Functionalization and immobilization of whole cell bioreporters for the detection of environmental contamination, Environ. Eng. Manag. J. 12 (2013) 1417–1422.
[38] D. Zhang, J.P. Berry, D. Zhu, Y. Wang, Y. Chen, B. Jiang, et al., Magnetic nanoparticle-mediated isolation of functional bacteria in a complex microbial community, ISME J. 9 (2015) 603–614.
[39] C. Li, H. Wang, L. Zhou, Y. Zhang, F. Song, J. Zhang, Quantitative measurement of pH influence on SalR regulated gene expression in *Acinetobacter baylyi* ADP1, J. Microbiol. Methods 79 (2009) 8–12.
[40] D. Zhang, Y. He, Y. Wang, H. Wang, L. Wu, E. Aries, et al., Whole-cell bacterial bioreporter for actively searching and sensing of alkanes and oil spills, Microbiol. Biotech. 5 (2012) 87–97.
[41] Y. Xu, J. Zhu, H. Li, Y. Du, D. Zhang, Removal and immobilization of hexavalent chromium contaminated water by magnetic nanoparticles, Environ. Sci. Technol. (2015) (under review).
[42] E. Michelini, L. Cevenini, M.M. Calabretta, S. Spinozzi, C. Camborata, A. Roda, Field-deployable whole-cell bioluminescent biosensors: so near and yet so far, Anal. Bioanal. Chem. 405 (2013) 6155–6163.
[43] R. Meij, L.H.J. Vredenbregt, H.T. Winkel, The fate and behavior of mercury in coal-fired power plants, J. Air Waste Manag. Assoc. 52 (2002) 912–917.
[44] F. Goodarzi, F.E. Huggins, H. Sanei, Assessment of elements, speciation of As, Cr, Ni and emitted Hg for a Canadian power plant burning bituminous coal, Int. J. Coal Geol. 74 (2008) 1–12.
[45] F. Goodarzi, Assessment of elemental content of milled coal, combustion residues, and stack emitted materials: Possible environmental effects for a Canadian pulverized coal-fired power plant, Int. J. Coal Geol. 65 (2006) 17–25.
[46] P.A. White, L.D. Claxton, Mutagens in contaminated soil: a review, Mutat. Res. – Rev. 567 (2004) 227–345.
[47] H.Q. Wang, Clastogenicity of chromium contaminated soil samples evaluated by Vicia root-micronucleus assay, Mutat. Res. – Fundam. Mol. Mech. Mutagen. 426 (1999) 147–149.
[48] J.C. Codina, C. Pereztorrente, A. Perezgarcia, F.M. Cazorla, A. Devicente, Comparison of microbial tests for the detection of heavy metal genotoxicity, Arch. Environ. Contam. Toxicol. 29 (1995) 260–265.
[49] X. Ma, Z. Lu, J. Cheng, Ecological risk assessment of open coal mine area, Environ. Monit. Assess. 147 (2008) 471–481.
[50] L. Hernandez, A. Probst, J.L. Probst, E. Ulrich, Heavy metal distribution in some French forest soils: evidence for atmospheric contamination, Sci. Total Environ. 312 (2003) 195–219.
[51] K. Nemati, N.K. Abu Bakar, M.R. Abas, E. Sobhanzadeh, Speciation of heavy metals by modified BCR sequential extraction procedure in different depths of sediments from Sungai Buloh, Selangor, Malaysia, J. Hazard. Mater. 192 (2011) 402–410.
[52] K.K. Brandt, P.E. Holm, O. Nybroe, Bioavailability and toxicity of soil particle-associated copper as determined by two bioluminescent *Pseudomonas fluorescens* biosensor strains, Environ. Toxicol. Chem. 25 (2006) 1738–1741.
[53] M. Holmstrup, A.M. Bindesbol, G.J. Oostingh, A. Duschl, V. Scheil, H.R. Kohler, et al., Interactions between effects of environmental chemicals and natural stressors: a review, Sci. Total Environ. 408 (2010) 3746–3762.
[54] C.A.M. VanGestel, P.J. Hensbergen, Interaction of Cd and Zn toxicity for *Folsomia candida* Willem (Collembola:Isotomidae) in relation to bioavailability in soil, Environ. Toxicol. Chem. 16 (1997) 1177–1186.
[55] S. Preston, N. Coad, J. Townend, K. Killham, G.I. Paton, Biosensing the acute toxicity of metal interactions: are they additive, synergistic, or antagonistic? Environ. Toxicol. Chem. 19 (2000) 775–780.

Biographies

Jianli Jia received her Ph.D. degree in environmental science and engineering from Tsinghua University in 2005. Currently, she is an associate professor at the School of Chemical and Environmental Engineering, China University of Mining & Technology (Beijing), China. Her main research area is bioremediation of contaminated land, particularly the heavy metal contaminated sites.

Hanbing Li received his B.Sc. degree in environmental engineering in 2014 from Beijing University of Technology, China. He is currently a Ph.D. research student at Lancaster University, UK. His research topic is the application of magnetic nanoparticles in environmental monitoring and remediation.

Shuang Zong received her B.Sc. degree in environmental engineering in 2014 from China University of Mining & Technology (Beijing), China. She is currently an M.Sc. student at China University of Mining & Technology (Beijing), China. Her research topic is ecological risk assessment at the coal cinder sites.

Bo Jiang received her Ph.D. degree in environmental science and engineering from Tsinghua University in 2015. Her Ph.D. research topic is the construction and application of whole-cell bioreporter in environmental monitoring.

Guanghe Li received his Ph.D. degree in 1992 from China University of Geosciences. He is currently a professor at the School of Environment, Tsinghua University, China.

As the senior researcher in contaminated site and groundwater management in China, his specialists are risk assessment and remediation of contaminated land, ecotoxicological characterization of contaminated sites and theories/technologies for water pollution control.

Odafe Ejenavi received his M.Sc. degree in geology in 1999 from University of Benin, Nigeria. He is currently a Ph.D. research student at Lancaster University, UK. His research topic is the impact of crude oil exploration on the fortunes of the Niger Delta and his interests are the application of whole-cell bioreporters for crude oil contamination *in situ* monitoring.

Jingrong Zhu received her M.Sc. degree in environmental science in 2014 from Lancaster University, UK. Her research topic is removal and immobilization of hexavalent chromium contaminated water by magnetic nanoparticles, and her main research interests include magnetic nanoparticles synthesis and functionalization.

Dayi Zhang received his Ph.D. degree in environmental science and engineering from Tsinghua University in 2009. Currently, he is a lecturer of environmental science and technology at Lancaster University, UK. His main research interests are whole-cell bioreporter in environmental monitoring, environmental microbiology, synthetic biology, and gene regulation mechanisms.

Appendix 2

Preparing and Characterizing Fe_3O_4@Cellulose Nanocomposites for Effective Isolation of Cellulose-Decomposing Microorganisms

Xiaohui Zhao, **Hanbing Li,** Aihong Ding, Guizhong Zhou, Yujiao Sun, , Dayi Zhang

Materials letters, 2016, 163, 154-157

Contribution:

- I prepared the samples required for Raman detection;
- I processed and acquired all Raman spectra data and carried out computational analysis;

Materials Letters 163 (2016) 154–157

Contents lists available at ScienceDirect

Materials Letters

journal homepage: www.elsevier.com/locate/matlet

Preparing and characterizing Fe_3O_4@cellulose nanocomposites for effective isolation of cellulose-decomposing microorganisms

Xiaohui Zhao [a,b], Hanbing Li [b], Aihong Ding [a], Guizhong Zhou [c], Yujiao Sun [a], Dayi Zhang [b,*]

[a] College of Water Sciences, Beijing Normal University, Beijing 100875, PR China
[b] Lancaster Environment Centre, Lancaster University, Lancaster LA1 4YQ, UK
[c] College of Environment and Safety Engineering, Qingdao University of Science and Technology, Qingdao 266042, PR China

ARTICLE INFO

Article history:
Received 22 August 2015
Received in revised form
9 October 2015
Accepted 14 October 2015
Available online 23 October 2015

Keywords:
Magnetic nanoparticles
Cellulose
Uncultivable microorganisms
Cellulose-decomposing

ABSTRACT

This study developed Fe_3O_4@cellulose nanocomposites by co-precipitation synthesis for bacteria capture and isolation. By surface modification with cellulose, the Fe_3O_4@cellulose nanocomposites have 20 nm average particle size and 3.3–24.9 emu/g saturation magnetization. Living bacteria could be captured by the Fe_3O_4@cellulose nanocomposites and harvested by magnetic field, with high efficiency (95.1%) and stability (> 99.99%). By metabolizing cellulose and destroying the Fe_3O_4@cellulose@bacteria complex, cellulose-decomposing microorganisms lost the magnetism. They were therefore able to be isolated from the inert microbial community and the separation efficiency achieved over 99.2%. This research opened a door to cultivate the uncultivable cellulose-decomposing microorganisms *in situ* and further characterize their ecological functions in natural environment.

1. Introduction

With the capability of remote control by magnetic field, magnetic nanoparticles (MNPs) introduce many possibilities in biochemical processes as a novel tool in microbial biotechnology [1]. MNPs surface modification is widely investigated to improve their stability and biocompatibility. Antigen functionalized MNPs achieve high throughput bacteria or cell separation by flow cytometry [2], and chitosan functionalization allows accurate and targeting gene/drug delivery via MNPs by the tagging biological entities [3]. In environmental engineering, MNPs are functionalized with poly-allylamine-hydrochloride to improve biosensor sensitivity [4,5], and remove pathogens for drinking water purification [6,7].

Uncultivable microorganisms account for over 99% of all the species and their functions are important for ecological system [8]. Particularly, cellulose metabolism is a key component of carbon cycle on the planet [9], but the majority of cellulose-decomposing microorganisms remain uncultivable and unknown. The recent progress to cultivate the uncultivable microorganisms with MNPs is the cutting edge for environmental ecology [10], opening a door to reveal the physiological behavior and ecological functions of uncultivable bacteria from complex microbial community. Nevertheless, the macromolecular poly-allylamine-hydrochloride reduces the accessibility of cellulose-decomposing microorganisms to cellulose. New surface functionalization technique can broaden its applicable potential in assessing the fate of various polymers in natural environment.

We developed a novel cellulose functionalization method and prepared the biocompatible Fe_3O_4@cellulose nanocomposites. Two different bacterial strains, *Acinetobacter baylyi* and *Aeromonas veronii* (cellulose-decomposing bacterium), were functionalized by Fe_3O_4@cellulose nanocomposites and investigated for their magnetism change after cultivation. The successful isolation of *A. veronii* from *Acinetobacter–Aeromonas* community proved the feasibility to cultivate the functional cellulose-decomposing bacteria *in situ*.

2. Experimental section

2.1. Synthesis of Fe_3O_4@cellulose nanocomposites

All the chemicals were analytical grade from Sigma-Aldrich (UK) without specific statement. Cellulose suspension was prepared by dissolving 0.4 g cellulose in 20 mL alkaline solution (NaOH:urea:H_2O=7:12:81), mixed well and standing at 4 °C overnight [11]. MNPs were synthesized by co-precipitation method [4]. The Fe_3O_4@cellulose nanocomposites was subsequently synthesized by gently mixing the MNPs and cellulose suspension (with ratios of 0.60, 0.55, 0.50, 0.45, 0.43, 0.36, 0.30, 0.24, 0.18, 0.12 and 0.06, m/m) for 5 min, captured by permanent magnet for

* Corresponding author.
E-mail address: d.zhang@lancaster.ac.uk (D. Zhang).

http://dx.doi.org/10.1016/j.matlet.2015.10.061
0167-577X/

5 min, and finally washed by deionized water 2 to 3 times until the pH value was 7.0.

2.2. Cellulose-decomposing microorganisms isolation from microbial community

Acinetobacter baylyi (no cellulose-decomposing capacity) and *Aeromonas veronii* (cellulose-decomposing bacterium) were used in this study. The artificial microbial community was made by mixing *A. baylyi* and *A. veronii* in water (1:1). To isolate the cellulose-decomposing microorganism from *A. baylyi*, *A. veronii* and microbiota, a hundred microliter of each bacterial suspension (diluted to 1.0×10^8 CFU/mL) was mixed with 900 μL Fe_3O_4@cellulose suspension. After successful functionalization and cultivation for 5 days, the targeting cellulose-decomposing bacteria were harvested from the supernatant (Graphic abstract, details see Supplementary material).

2.3. Measurements and data analysis

The morphology of MNPs and Fe_3O_4@cellulose nanocomposites were analyzed by transmission electron microscopy (TEM, JEM-2100, 100 kV, Japan). Phase identification was carried out by X-ray diffraction (XRD, D8-Advance, Bruker, UK). The magnetic properties were measured by a vibrating sample magnetometer (VSM, Lake Shore, 7304, USA) at 25 °C and in a magnetic field varying from −1.7 T to +1.7 T. The nanoparticle fingerprint was obtained by InVia Raman microscopy (Renishaw, UK) with a 785-nm excitation laser and 10 s acquisition time. The number of magnetic-free bacteria was determined by quantitative polymerase chain reaction (qPCR, Supplementary material) [12,13].

3. Results and discussion

From the TEM morphology (Fig. 1A), raw MNPs showed a round shape and had strong self-aggregation attributing to the large surface-to-volume ratio and the expressed surface energy [14]. The XRD pattern (Fig. 1C) identified the diffraction peaks of MNPs as $2\theta = 30.0°$, 35.4°, 43.2°, 53.6°, 57.1° and 62.7°, indexed to (220), (311), (400), (422), (511) and (440) lattice planes [15]. The mean size of MNPs was calculated as 8 nm by Scherer equation ($D = \kappa\lambda / \beta\cos\theta$). Fe_3O_4@cellulose nanocomposites had bigger size (20 nm, Fig. 1B) but with less aggregation since polymer functionalization could improve their stability by steric repulsion [4].

The Raman spectra (Fig. 1D) showed that the characteristic peaks of Fe_3O_4@cellulose nanocomposites fitted well with those of MNPs (magnetite at 678 cm^{-1}) and cellulose (υ(C–O–C) asym at 1094 cm^{-1} and 1120 cm^{-1}, υ(C–O–C) at 906 cm^{-1}, δ(CH_3) at 1380 cm^{-1} and δ(CH_3) asym at 1460 cm^{-1}) [16]. All the magnetization curves behaved S shape, and raw MNPs had the highest the saturation magnetization (43.4 emu/g, Fig. 1E). The saturation magnetization of Fe_3O_4@cellulose was positively related to the ratio of MNPs to cellulose, as 24.9 emu/g for 0.6:1 (MNPs:cellulose), 11.4 emu/g for 0.4:1 and 3.3 emu/g for 0.12:1, respectively.

Fe_3O_4@cellulose nanocomposites could effectively capture bacteria via electrostatic adsorption. The ratio of MNPs to cellulose affected the bacteria capture efficiency (Fig. 2A). When the MNPs: cellulose ratio was above 0.1, the bacteria capture efficiency was above 90%, whereas it declined to 84.3% at the ratio of 0.06. The optimized ratio was set as 0.4 to achieve both high capture efficiency and sufficient cellulose for bacterial growth.

The capture efficiency was above 90% when the bacterial amount was less than 4.0×10^{14} CFU/g Fe_3O_4@cellulose (Fig. 2B). Langmuir isotherm equation (Eq. (1)) can describe the adsorption isotherm of Fe_3O_4@cellulose nanocomposites and fitted well with the experimental data (Fig. 2B).

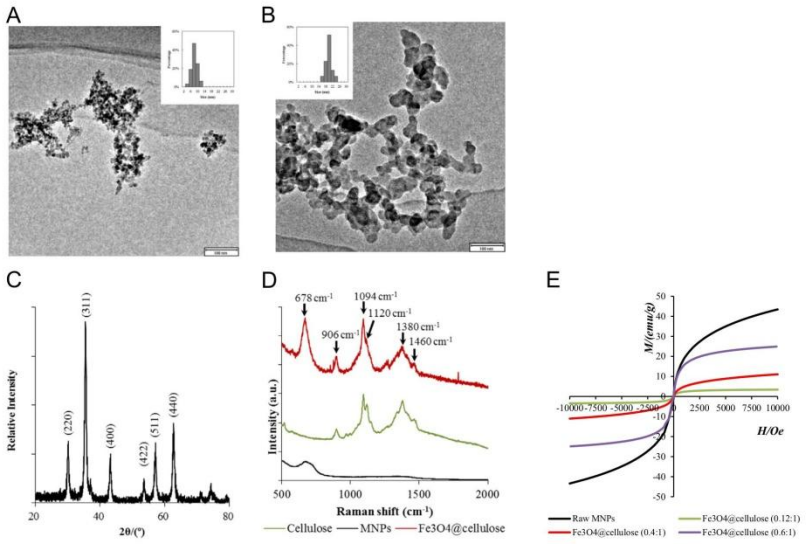

Fig. 1. TEM images of MNPs (A) and Fe_3O_4@cellulose nanocomposites (B). The XRD pattern of Fe_3O_4@cellulose nanocomposites (C). Raman microscopy of cellulose, MNPs and Fe_3O_4@cellulose (D). The magnetization curve of synthesized MNPs and Fe_3O_4@cellulose (E).

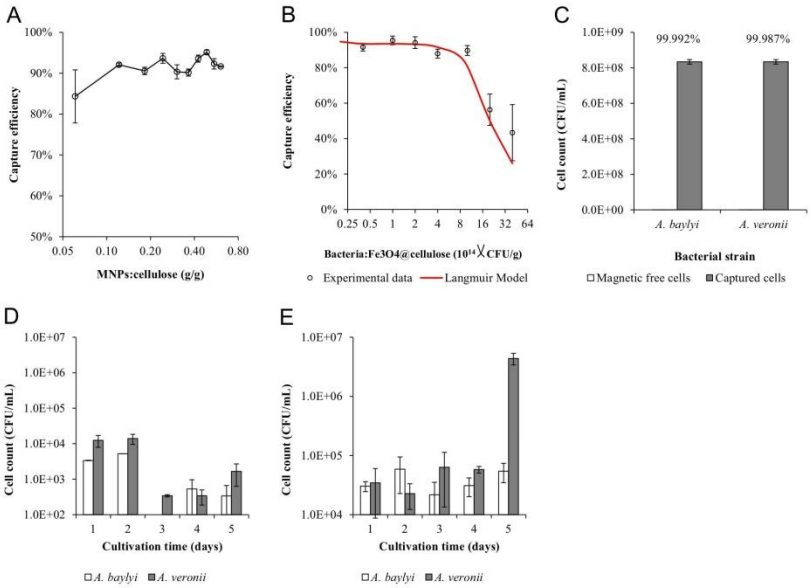

Fig. 2. (A) Bacteria capture efficiency against the ratio of MNPs to cellulose during synthesis process. (B) Bacteria capture efficiency against the ratio of bacteria amount to MNPs weight. (C) Bacteria functionalization stability of *A. baylyi* and *A. veronii*. (D) Long-term (5 days) stability of Fe_3O_4@cellulose@bacteria complex in water. (E) The isolation efficiency of Fe_3O_4@cellulose@bacteria complex after 5 days cultivation in M9 medium.

$$Q_e = Q_{max}\frac{K_L C_e}{1 + K_L C_e} \quad (1)$$

Here, Q_e (CFU/g Fe_3O_4@cellulose) refers to the captured bacterial cells on the Fe_3O_4@cellulose surface, and C_e (CFU/mL) represents the equilibrium bacterial amount in the suspension. Q_{max} (CFU/g Fe_3O_4@cellulose) is the maximum adsorption capacity for monolayer adsorption in Langmuir isotherm model, and K_L (mL/CFU) is the Langmuir constant associated with adsorption energy. In this study, Q_{max} is 17.57×10^{14} CFU/g Fe_3O_4@cellulose, and K_L is 187.56×10^{-14} mL/CFU. The results described the monolayer adsorption equilibrium of the adsorbed bacterial cells on Fe_3O_4@cellulose nanocomposites. Given the larger particle size of Fe_3O_4@cellulose nanocomposites than raw MNPs, a significant less specific surface area was found for the bacteria captured by Fe_3O_4@cellulose than cyanobacteria harvesting by raw MNPs [17]. Nevertheless, the high K_L value indicated the high binding affinity of bacteria to Fe_3O_4@cellulose nanocomposites. Since the electrostatic mechanism is the ion exchange interaction between carboxyl (–COOH) or thiol (–SH) functional groups on bacterial membrane and the positively charged position on Fe_3O_4@cellulose nanocomposites [7], the electrostatic adsorption of living bacteria is therefore non-selective. This feature secures to magnetize all the bacteria via Fe_3O_4@cellulose nanocomposites in the environmental microbiota.

Fe_3O_4@cellulose@bacteria complex had high stability and bacteria maintained their magnetism even after long period storage. Resuspended in deionized water, the majority of both *A. baylyi* and *A. veronii* remained effective attachment on Fe_3O_4@cellulose nanocomposites (Fig. 2C), and the released magnetic-free bacteria were less than 2×10^5 CFU/mL. The short-term stability was 99.992% for *A. baylyi* and 99.987% for *A. veronii* respectively. Stored in deionized water, only less than 1.5×10^4 CFU/mL cells of *A. baylyi* or *A. veronii* were detected in the supernatant after 5 days (Fig. 2D), and the long-term Fe_3O_4@cellulose@bacteria stability was over 99.99%. Cultivated in M9 medium, *A. baylyi* could not metabolize cellulose, remaining inert and captured by the Fe_3O_4@cellulose with less than 6.0×10^4 CFU/mL in the supernatant ($< 0.007\%$ of the total bacteria amount, Fig. 2E). As for cellulose-decomposing *A. veronii*, the Fe_3O_4@cellulose@bacteria complex was destroyed due to cellulose consumption and *A. veronii* were then released from the magnetic pellet into the supernatant. The enriched *A. veronii* raised from 3.4×10^4 CFU/mL (Day 1) to 4.4×10^6 CFU/mL (Day 5).

After 5 days cultivation of the artificial microbial community of *A. veronii* and *A. baylyi*, Fe_3O_4@cellulose nanocomposites successfully isolated the cellulose-decomposing *A. veronii* from the complex microbiota (Fig. 3). Without Fe_3O_4@cellulose functionalization (direct cultivation), *A. veronii* ranged from 32.8% to 61.7% of the whole microbial community after 5 days cultivation, not significantly dominant and hard to be isolated (Fig. 3). In Fe_3O_4@cellulose treatment, the targeting *A. veronii* became dominant on Day 4 (65.3%) and Day 5 (99.2%). Thus, the cellulose-decomposing *A. veronii* was enriched and isolated in the supernatant from the artificial microbiota. The results prove that Fe_3O_4@cellulose nanocomposite is an effective tool to identify and isolate living cellulose-decomposing bacteria from environmental microbiota and the magnetic-free fraction is suitable for further analysis of cellulose degradation genes and pathways.

4. Conclusions

By co-precipitation synthesis and surface functionalization with cellulose, living bacteria were successfully captured and

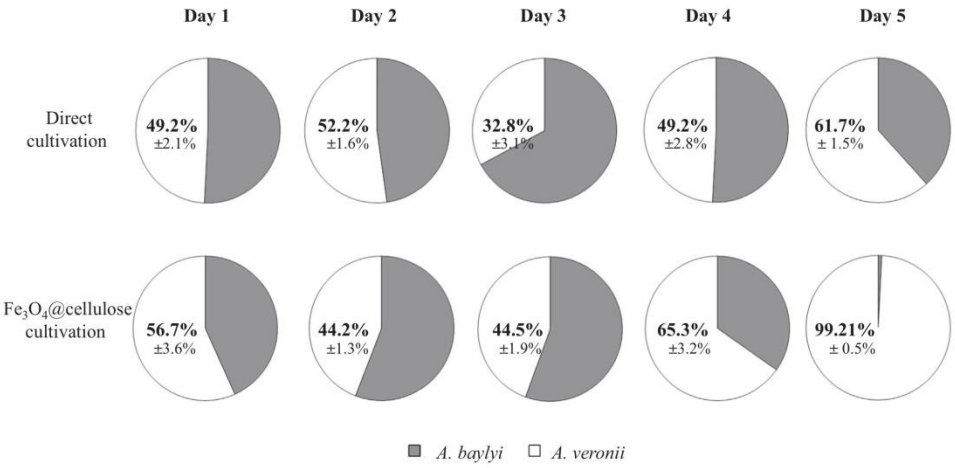

Fig. 3. Cellulose-decomposing bacteria isolation from artificial *Acinetobacter–Aeromonas* microbial community by direct cultivation and Fe_3O_4@cellulose cultivation.

harvested by Fe_3O_4@cellulose nanocomposites with high efficiency (95.1%) and stability (> 99.99%). The Fe_3O_4@cellulose nanocomposites achieved 99.2% isolation efficiency of cellulose-decomposing bacteria from artificial microbial community. With the novel Fe_3O_4@cellulose nanocomposites functionalization method, uncultivable and unknown cellulose-decomposing bacteria are able to be effectively isolated from complex microbiota to investigate the potential new cellulose-decomposing functional genes and reveal their ecological roles in natural environment.

Acknowledgment

The authors would like to thank National Natural Science Foundation of China (No. 41301331) for financial support.

Appendix A. Supplementary material

Supplementary data associated with this article can be found in the online version at http://dx.doi.org/10.1016/j.matlet.2015.10.061.

References

[1] J. Gao, H. Gu, B. Xu, Acc. Chem. Res. 42 (2009) 1097–1107.
[2] T.P. Lagus, J.F. Edd, J. Phys. D: Appl. Phys. 46 (2013).
[3] Q.A. Pankhurst, J. Connolly, S.K. Jones, J. Dobson, J. Phys. D: Appl. Phys. 36 (2003) R167–R181.
[4] D. Zhang, R.F. Fakhrullin, M. Ozmen, H. Wang, J. Wang, V.N. Paunov, et al., Microb. Biotechnol. 4 (2011) 89–97.
[5] J. Jia, H. Li, S. Zong, B. Jiang, G. Li, O. Ejenavi, et al., Sens. Actuators B 222 (2015) 290–299.
[6] Y.-F. Huang, Y.-F. Wang, X.-P. Yan, Environ. Sci. Technol. 44 (2010) 7908–7913.
[7] Y. Xu, C. Li, X. Zhu, W.E. Huang, D. Zhang, Environ. Eng. Manag. J. 13 (2014) 2023–2029.
[8] T. Kaeberlein, K. Lewis, S.S. Epstein, Science 296 (2002) 1127–1129.
[9] P. Beguin, J.P. Aubert, FEMS Microbiol. Rev. 13 (1994) 25–58.
[10] D. Zhang, J.P. Berry, D. Zhu, Y. Wang, Y. Chen, B. Jiang, et al., ISME J. 9 (2015) 603–614.
[11] X. Luo, L. Zhang, J. Hazard. Mater. 171 (2009) 340–347.
[12] D.P.R. Herlemann, M. Labrenz, K. Juergens, S. Bertilsson, J.J. Waniek, A. F. Andersson, ISME J. 5 (2011) 1571–1579.
[13] D. Zhang, Y. He, Y. Wang, H. Wang, L. Wu, E. Aries, et al., Microb. Biotechnol. 5 (2012) 87–97.
[14] R.F. Fakhrullin, J. Garcia-Alonso, V.N. Paunov, Soft Matter 6 (2010) 391–397.
[15] H. Cui, D. Li, Z. Zhang, Mater. Lett. 143 (2015) 38–40.
[16] J. De Gelder, K. De Gussem, P. Vandenabeele, L. Moens, J. Raman Spectrosc. 38 (2007) 1133–1147.
[17] Z. Lin, Y. Xu, Z. Zhen, Y. Fu, Y. Liu, W. Li, et al., Bioresour. Technol. 190 (2015) 82–88.